Springer Theses
Recognizing Outstanding Ph.D. Research

Janet T. F. Lau

Towards Dual and Targeted Cancer Therapy with Novel Phthalocyanine-based Photosensitizers

Springer

Springer Theses

Recognizing Outstanding Ph.D. Research

For further volumes:
http://www.springer.com/series/8790

Aims and Scope

The series "Springer Theses" brings together a selection of the very best Ph.D. theses from around the world and across the physical sciences. Nominated and endorsed by two recognized specialists, each published volume has been selected for its scientific excellence and the high impact of its contents for the pertinent field of research. For greater accessibility to non-specialists, the published versions include an extended introduction, as well as a foreword by the student's supervisor explaining the special relevance of the work for the field. As a whole, the series will provide a valuable resource both for newcomers to the research fields described, and for other scientists seeking detailed background information on special questions. Finally, it provides an accredited documentation of the valuable contributions made by today's younger generation of scientists.

Theses are accepted into the series by invited nomination only and must fulfill all of the following criteria

- They must be written in good English.
- The topic should fall within the confines of Chemistry, Physics, Earth Sciences, Engineering and related interdisciplinary fields such as Materials, Nanoscience, Chemical Engineering, Complex Systems and Biophysics.
- The work reported in the thesis must represent a significant scientific advance.
- If the thesis includes previously published material, permission to reproduce this must be gained from the respective copyright holder.
- They must have been examined and passed during the 12 months prior to nomination.
- Each thesis should include a foreword by the supervisor outlining the significance of its content.
- The theses should have a clearly defined structure including an introduction accessible to scientists not expert in that particular field.

Janet T. F. Lau

Towards Dual and Targeted Cancer Therapy with Novel Phthalocyanine-based Photosensitizers

Doctoral Thesis accepted by
The Chinese University of Hong Kong, Shatin,
People's Republic of China

Springer

Author
Dr. Janet T. F. Lau
Department of Chemistry
The Chinese University of Hong Kong
Shatin
People's Republic of China

Supervisor
Prof. Dennis K. P. Ng
Department of Chemistry
The Chinese University of Hong Kong
Shatin
People's Republic of China

ISSN 2190-5053 ISSN 2190-5061 (electronic)
ISBN 978-3-319-00707-6 ISBN 978-3-319-00708-3 (eBook)
DOI 10.1007/978-3-319-00708-3
Springer Cham Heidelberg New York Dordrecht London

Library of Congress Control Number: 2013940440

Printed on acid-free paper

Springer is part of Springer Science+Business Media (www.springer.com)

Parts of this thesis have been published in the following journal articles:

"A Zinc(II) Phthalocyanine Conjugated with an Oxaliplatin Derivative for Dual Chemo- and Photodynamic Therapy."

Janet T. F. Lau, Pui-Chi Lo,* Wing-Ping Fong, and Dennis K. P. Ng

Journal of Medicinal Chemistry **2012,** *55,* 5446–5454.

"A Disulfide-Linked Conjugate of Ferrocenyl Chalcone and Silicon(IV) Phthalocyanine as an Activatable Photosenzitiser"

Janet T. F. Lau, Xiong-Jie Jiang, Dennis K. P. Ng,* and Pui-Chi Lo*

Chemical Communications **2013**, *49*, 4274–4276.

This Thesis is Dedicated to
Prof. Dennis K. P. Ng, Prof. Gigi P. C. Lo,
My Family, George, and Lily

In Memory of My Grandfather
Mr. Ping Wu
1926–2012

Supervisor's Foreword

Light has long been used for medicinal purposes. By combining the action of this source of energy, a photosensitive drug and molecular oxygen, a new therapeutic modality, namely photodynamic therapy (PDT), has been developed. This can be used for the treatment of some localized and superficial cancers, as well as certain non-cancerous conditions. Compared with the traditional therapies in oncology, photodynamic therapy is relatively non-invasive and has fewer side effects, higher tolerance of repeated doses, and higher specificity that can be achieved through precise delivery of light with modern fiber optic systems and various types of endoscopy. Although positive therapeutic outcomes have been reported, only a few photosensitive drugs have been clinically approved so far and they still suffer from a number of deficiencies, such as weak absorption in the tissue-penetrating near-infrared region, sustained skin photosensitivity, low initial selectivity, and long drug-to-light intervals. As a result, considerable efforts have been expended in the development of more efficient photosensitizers toward targeted PDT and that can conjugate with chemotherapeutic agents to achieve dual cancer therapy. This multi-disciplinary field of study has received much current attention.

This thesis describes a series of novel phthalocyanine-based photosensitizers, including their molecular design, synthesis, spectroscopic and photophysical properties, in vitro photodynamic activity, and potential of being used for combined chemo- and photodynamic therapy and targeted PDT. After a general overview of the background and current status in this research area given in Chap. 1, the details of the studies are presented in the following chapters for conjugates with a chemotherapeutic oxaliplatin derivative, a polyamine ligand with a view to targeting the polyamine transporters over-expressed in tumor cells, and a ferrocene-based quencher that can inhibit their photodynamic activity, yet can be removed under a tumor-associated environment, such as low pH and high thiol concentration, thereby restoring their photocytotoxicity. A dual activatable photosensitizer has also been reported for the first time. The activation effects have been well demonstrated both in solution and at the cellular level. The studies

reported in the thesis are original and significant, and can stimulate further investigations in this important research field. We imagine that "smarter" photosensitizers that can respond selectively at tumors could be developed in the near future, which could advance further this promising treatment modality.

Hong Kong, May 2013 Dennis K. P. Ng

Acknowledgments

Professor Dennis K. P. Ng, my supervisor, deserves the utmost gratitude for admitting me as one of his postgraduate students, which is the greatest honor in my life. Throughout my postgraduate studies, not only does he impart a host of chemistry knowledge to me, he also spends lots of effort on nourishing and cultivating me with the ability of critical thinking, a proactive and responsible attitude toward my work, and the qualities to be a good scientific researcher. His genuine and refined teaching has paved a concrete foundation toward my future development. I am extremely thankful to him for giving me ample opportunities to participate in international conferences, seminars, and manuscripts preparation. Without his continuous tolerance, trust, and inspiration, I may not be confident enough to overcome obstacles encountered during my research. To him, I owe my heartfelt thanks.

Sincere thanks should also go to Prof. Gigi P. C. Lo, my co-supervisor, for her willingness to entrust so much on my judgment toward my research. She is certainly a heavyweight throughout my five-year postgraduate research life. I probably would not be writing my doctoral dissertation if she did not introduce me to Prof. Ng's lab seven years ago. I would like to express my deepest gratitude to her for her patience, selfless teaching, and guidance throughout my study. Apart from sharing her valuable experience in her field of expertise with me, she has also established a harmonious atmosphere in our lab through frequent communication and participating in different gatherings and functions with us. She is a fine and delicate supervisor who always tries her very best to take care and support every one of us in every way she can.

Being in Prof. Ng's lab for five years, I am delighted to be able to befriend with many colleagues with various cultural and research background. Every one of them has played a very important role during my research. I am indebted to Dr. Xue-Bing Leng, Dr. Ming Bai, Dr. Bill C. F. Choi, Dr. Hu Xu, Dr. Jian-Yong Liu, Dr. Xiong-Jie Jiang, Dr. Hui He, Dr. Qun-Ling Fang, Venus Y. S. Huang, Mei-Rong Ke, Wen-Jing Shi, Liang Qu, and Esther S. L. Yeung. It is also my great honor to be able to associate with four summer research students, Cheok-Lam Wong, Chi-Him Lai, Kin-Lung Chui, and Yun-Sang Chow. I am grateful to them for bringing lots of fun and cutie little gadgets to our lab.

Particular acknowledgements are to be addressed to Prof. Wing-Ping Fong of the School of Life Sciences for allowing me to access his apparatuses, instruments, and other necessary reagents for all my in vitro studies. My research would not have been possible without his persistent and generous support. I would also like to thank Pui-Wah Choi, Chi-Lung Chan, and Victor H. Y. Yeung for teaching and sharing their experience with me in performing cell culture and various kinds of biochemical assays. It is my pleasure to be able to work with these excellent biochemists!

I would also like to express my deepest gratitude to Prof. Chi Wu for giving me his greatest support in my in vitro studies especially when the cell culture facilities with the School of Life Sciences are temporary suspended. I would have never completed my biochemical assays without his understanding and kind offer. I would also like to thank Zhuo-Jun Dai, Jin-Ge Cai, Qian-Jin Chen, Shu Diao, Xiang-Jun Gong, Yong-Zheng Ma, Jian-Qi Wang, Yanan Yue, and Hong Zhao for their patience, assistance, and teachings.

I am heartily thankful to Prof. Hung-Kay Lee for giving me lots of advice toward my future career. I am exceptionally obliged to him for granting me the opportunity to work in the Hong Kong Government Laboratory. Not only do I gain hand on experience in operating a vast number of analytical instruments, he has also indirectly brought me to Dr. Boris Y. T. Wong, Miss Twinnie S. C. Tso, and Mr. Hubert P. O. Tang who are three excellent government chemists, bosses, and friends. I really appreciate their unfailing support, enlightenment, and guidance throughout my work and study.

Special thanks are also due to Miss Sara H. Y. Ng and Mr. Chun-Wah Lin for performing all the mass spectroscopic measurements and tackling all unexpected NMR problems. I am particularly thankful to Mr. Ka-Fai Woo and Dr. Chui-Man Lo for their continuous encouragement and affable support during my postgraduate studies.

I would also like to thank my family (especially to my grandfather who has passed away during the preparation of this thesis) who have always stood by me and dealt with all of my absence from morning tea, dinner, and family gatherings with a smile. In addition, I have to extend my gratefulness to my fiancé, George, for his unconditional love, support, and encouragement.

Lastly, I offer my regards and blessings to all of those who supported me in any respect during my study.

Contents

Abbreviations

General

Ac	Acetyl
Anal.	Analytical
Ar	Aromatic
Boc	*tert*-Butoxycarbonyl
ca.	Coarse approximation
calcd	Calculated
conc.	Concentrated
equiv.	Equivalent
Et	Ethyl
Fc	Ferrocenyl
IC_{50}	Dye concentration required to kill 50 % of the cells
Me	Methyl
Ms	Methanesulfonyl
n.d.	Not determined
NIR	Near-infrared
Pc(s)	Phthalocyanine(s)
PDT	Photodynamic therapy
PET	Photoinduced electron transfer
Ph	Phenyl
r.t.	Room temperature
R_f	Retention factor
ROS	Reactive oxygen species
S.D.	Standard deviation
S.E.M.	Standard error of the mean
THP	Tetrahydropyranyl
TLC	Thin layer chromatography
Ts	Tosyl
UV	Ultraviolet
Vis	Visible
v/v	Volume-to-volume ratio

w/v	Weight per volume
w/w	Weight-to-weight ratio

Units of Measurement

cm	Centimeter(s)
°C	Degree Celsius
g	Gram(s)
h	Hour(s)
Hz	Hertz
J	Joule
kJ	Kilojoule
M	Molarity
mg	Milligram(s)
MHz	Megahertz
min	Minute(s)
mL	Milliliter(s)
μm	Micromolar
μm	Micrometer(s)
μL	Microliter(s)
μs	Microsecond(s)
mm	Millimeter(s)
mM	Millimolar
mol	Mole(s)
mmol	Millimole(s)
mW	Milliwatt
nm	Nanometer(s)
nM	Nanomolar
rpm	Revolutions per minute
s	Second(s)
W	Watt

Chemicals and Solvents

DBU	1,8-Diazabicyclo[5.4.0]undec-7ene
DCC	*N*,*N*′-Dicyclohexylcarbodiimide
DCFDA	2',7′-Dichlorodihydrofluorescein diacetate
DMAP	4-(Dimethylamino)pyridine
DMEM	Dulbecco's modified Eagle's medium
DMF	*N*,*N*-Dimethylformamide
DMSO	Dimethylsulfoxide
DPBF	1,3-Diphenylisobenzofuran
DTT	Dithiothreitol
EDTA	Ethylenediaminetetraacetic acid

GFP	Green fluorescent protein
HEPES	4-(2-Hydroxyethyl)-1-piperazineethanesulfonic acid
HOBt	1-Hydroxybenzotriazole
MTT	3-(4,5-Dimethyl-2-thiazolyl)-2,5-diphenyl-2*H*-tetrazolium bromide
PBS	Phosphate buffered saline
PI	Propidium iodide
RPMI	Roswell Park Memorial Institute
TFA	Trifluoroacetic acid
THF	Tetrahydrofuran
SDS	Sodium dodecyl sulfate
ZnPc	Unsubstituted zinc(II) phthalocyanine

Photophysical Data

λ	Wavelength in nm
λ_{max}	Absorption maximum
λ_{em}	Emission maximum
λ_{ex}	Excitation wavelength
ε	Molar extinction coefficient
Φ_F	Fluorescence quantum yield
$^1O_2$	Singlet oxygen
Φ_Δ	Singlet oxygen quantum yield

Nuclear Magnetic Resonance (NMR) Data

COSY	Correlation spectroscopy
$\{^1H\}$	Proton decouple
δ	Chemical shift in ppm
H	Proton
C	Carbon
J	Coupling constant in Hz
ppm	Parts per million
s	Singlet
d	Doublet
t	Triplet
q	Quartet
p	Pentat
vt	Virtual triplet
dd	Doublet of doublet
dq	Doublet of quartet
m	Multiplet
br s	Broad signal

Mass Spectrometric (MS) Data

M^+	Molecular ion
m/z	Mass-to-charge ratio
ESI	Electrospray ionization
HRMS	High-resolution mass spectroscopy

Chapter 1
Introduction

1.1 Introduction

Photodynamic therapy (PDT) involves the administration of a non-toxic drug known as photosensitizer systemically, locally, or topically to a patient bearing a lesion, which is frequently, but not always cancer [1, 2]. After an incubation period, the lesion is illuminated by red visible light (620–690 nm). In the presence of oxygen, it leads to the generation of cytotoxic reactive oxygen species (ROS) and consequently to cell death and tissue destruction [3, 4]. The use of PDT as a cancer therapy is particularly attractive because of its potential specificity. This is due to the fact that the photosensitizer can localize in the malignant tissue. When the light is directly focused on the lesion, the ROS that generated during photosensitization results in cellular destruction in that particular region. In recent years, PDT has become a subject of intense investigation as a possible treatment modality for various forms of cancer [4–6].

1.1.1 History of Photodynamic Therapy

The use of light in the treatment of disease can be traced back over 4,000 years [7–9]. Ancient Egyptian, Indian, and Chinese civilizations used light to treat various diseases including psoriasis, rickets, vitiligo, and skin cancer [10]. Reports of contemporary PDT first appeared during the investigations led by Finsen in the late nineteenth century [11]. He found that exposure of red light can prevent the formation and discharge of smallpox pustules [11]. He also successfully demonstrated phototherapy by employing heat-filtered light from a carbon-arc lamp in the treatment of cutaneous tuberculosis, for which he won the Nobel Prize in Physiology and Medicine in 1903 [12]. In 1900, Raab, a German medical student discovered that a combination of acridine red and light can kill a species of *paramecium* [13]. He reported that the combined cytotoxic effect was greater than that of the individual components. In the same year, Prime, a French neurologist,

J. T. F. Lau, *Towards Dual and Targeted Cancer Therapy with Novel Phthalocyanine-based Photosensitizers*, Springer Theses,
DOI: 10.1007/978-3-319-00708-3_1, © Springer International Publishing Switzerland 2013

used eosin (a brominated derivative of fluorescein) orally in the treatment of epilepsy, but discovered that this treatment induced dermatitis in sun-exposed areas of skin [14]. This discovery led to the first therapeutic medical application of a combination of photosensitizer and light in the treatment of skin cancer [15]. This process was described as "photodynamic action" [16]. The more recent era of PDT was initiated by Lipson in the 1960s when he discovered a mixture of chemicals, termed hematoporphyrin derivative (HpD), which had tumor-localizing properties [17]. It was also found that this mixture could be activated with red light, resulting in the PDT effect. A timeline starting from the ancient development to the recent milestones in the evolution of PDT is presented in Fig. 1.1.

The therapeutic application of PDT to patients with cancer took a long time to develop until a significant breakthrough occurred in 1975 when Dougherty et al. reported that the administration of HpD and red light could completely eradicate mammary tumor growth in mice [18]. In the same year, Kelly also reported that light activation of HpD could also eliminate bladder carcinoma in mice [19]. The first approval of PDT by a regulatory authority occurred in 1993 in Canada using a purer and better characterized derivative of HpD called Photofrin® for the treatment of bladder cancer [20]. The first approval of using Photofrin® for PDT by the Food and Drug Administration (FDA) in the United States was obtained in 1995 for palliation of obstructive esophageal cancer [20]. The success of treatments and subsequent approvals of using Photofrin® generated worldwide interest in this treatment modality. To date, more selective and potent photosensitizers have been developed, and are now under investigation in clinical trials (Table 1.1).

1.1.2 Basic Principles of Photodynamic Therapy

1.1.2.1 Photophysical Mechanisms

The photophysical processes involved in PDT are illustrated in Fig. 1.2. The ground electronic state of the photosensitizer is a singlet state (S_0). Upon absorption of light of appropriate wavelengths (**1**), the photosensitizer is excited to the short-lived first excited state (S_1). The photosensitizer can return to the S_0 state by emitting the absorbed energy as fluorescence (**2**) or by internal conversion (**3**). Alternatively, the S_1 photosensitizer can convert to the first excited triplet state (T_1) by intersystem crossing (**4**). The S_1 state is rather short-lived, with typical values for singlet state lifetimes (τ_s) being in nanoseconds, while triplet state lifetimes (τ_T) are in the microsecond to millisecond range. In general, the T_1 state is longer lived than the S_1 state, and hence the biologically relevant photochemistry is often mediated by this state [21, 22]. The T_1 photosensitizer can also return to the S_0 state by emitting phosphorescence (**5**).

There are two types of photodynamic reactions [21, 22]. In Type I mechanism, the excited photosensitizer interacts with biomolecules resulting in hydrogen atom or electron transfer that leads to the production of ROS such as superoxide,

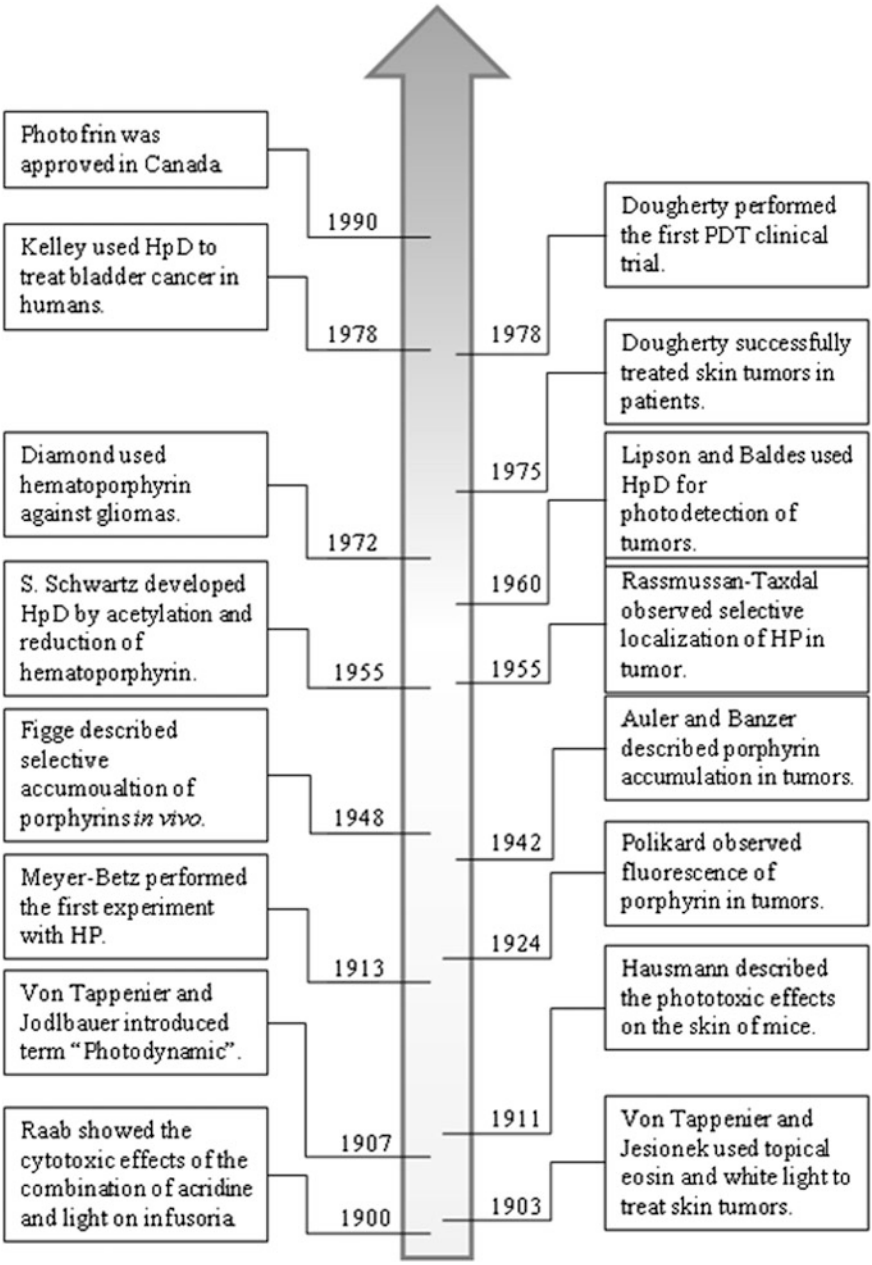

Fig. 1.1 Timeline of historical milestones in development of PDT

Table 1.1 Photosensitizers for malignant diseases [108]

Photosensitizers	Trade name	Potential indications
HpD, porfimer sodium	Photofrin®	Cervical, endobronchial, esophageal, bladder, and gastric cancers
Benzoporphyrin derivative monoacid ring A	Veteporfin	Basal cell carcinoma
meta-tetrahydroxyphenylchlorin	Foscan	Head, neck, prostate, and pancreatic cancers
5-Aminolevulinic acid	Levulan	Basal cell carcinoma, head and neck, and gynecological tumors
Boronated protoporphyrin	BOPP	Brain tumors
Lutetium texaphyrin	Lutex	Cervical, prostate, and brain tumors
Phthalocyanine 4	Pc4	Cutaneous/subcutaneous lesions from diverse solid tumor origins
Taporfin sodium	Talaporfin	Solid tumors from diverse origins

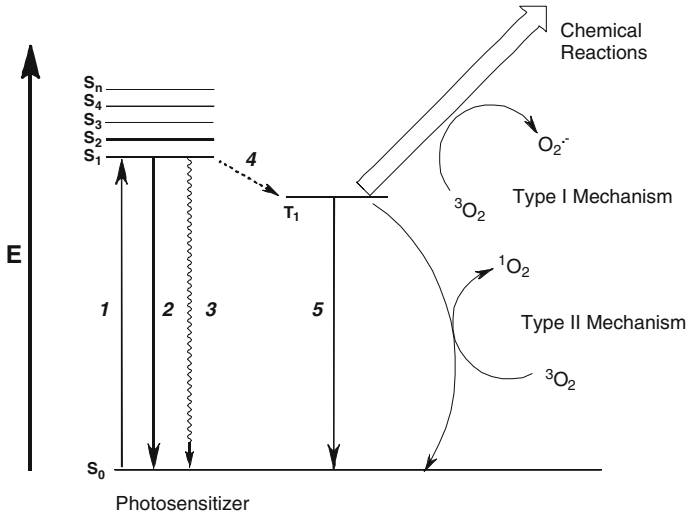

Fig. 1.2 Modified Jablonski diagram showing various photophysical processes (***1:*** absorption; ***2:*** fluorescence; ***3:*** internal conversion; ***4:*** intersystem crossing; ***5:*** phosphorescence) of an excited photosensitizer

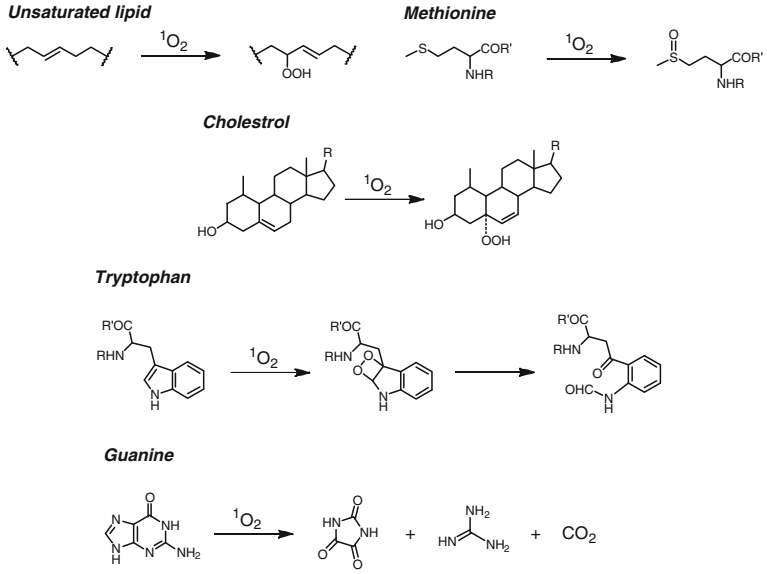

Fig. 1.3 Typical reactions of singlet oxygen with selected biomolecules

hydroperoxyl and hydroxyl radicals, and hydrogen peroxide. Alternatively, the photosensitizer in T_1 state can undergo an energy transfer with oxygen to form cytotoxic singlet oxygen ($^1O_2$). This process is classified as Type II mechanism. $^1O_2$ is regarded as the main mediator of phototoxicity in PDT. Both Type I and Type II mechanisms cause oxidative damage within the target tissues which lead to cell death and tumor destruction. However, it is generally accepted that the generation of $^1O_2$ from Type II mechanism predominates during PDT. Figure 1.3 illustrates how different kinds of biomolecules react readily with this highly reactive molecule [23].

1.1.2.2 Biological Mechanisms

It is now known that there are three main biological mechanisms emanating from photodynamic treatment [24]. PDT can generally induce tumor destruction in vivo in three different ways, namely direct tumor cell destruction, vascular destruction, and elicitation of an antitumor immune response. These three mechanisms can influence each other and the combination of all these components is required for long-term tumor control. In the following subsections, these three mechanisms are briefly discussed.

Direct Damage and Cell Death

The ROS generated during PDT can kill tumor cells directly. Tumor cells being directly eliminated by PDT undergo at least two types of cell death: necrosis or apoptosis [3, 25, 26]. Necrosis is a violent and quick form of degeneration that results from extensive cellular damage. It is characterized by the destruction of organelles and disruption of the plasma membrane leading to the release of intracellular contents into the extracellular compartment. In contrast, apoptosis is a mechanism of genetically programmed death of old cells in both physiological and pathological conditions of a living organism. It is characterized by a common sequence of morphological and biochemical changes including condensation of chromatin and formation of apoptotic bodies. In vivo PDT of tumors has been shown to reduce a number of clonogenic tumor cells through direct photodamage [27].

Vascular Damage

The viability of tumor cells depends on the amount of nutrients supplied by blood vessels. Over the last two decades, there have been a number of reports of PDT-induced damage to tumor microvasculature leading to persistent post-PDT tumor hypoxia/anoxia and nutrient deficiency, which in turn is lethal to the tumor [21, 25, 28]. The mechanism underlying the vascular occlusion includes vessel constriction/collapse, macromolecular leakage, leukocyte adhesion, blood flow stasis, and thrombus formation.

Inflammatory and Immune Response

Photodynamically induced changes in the plasma membrane and the membrane cell organelles can trigger multiple signal transduction pathways. These include a variety of protein kinase signaling cascades which elicit an inflammatory or immune response leading to cell death [24, 29]. In fact, studies in the late 1980s and early 1990s have reported the infiltration of lymphocytes, leukocytes, and macrophages into PDT-treated tissue which indicates an activation of the immune response [30, 31]. The differences in the nature and intensity of the inflammatory response between normal and cancerous tissues may contribute to the selectivity of PDT-induced damage [24, 32].

1.2 Photosensitizers of Photodynamic Therapy

Photosensitizers are compounds that are capable of absorbing light of a specific wavelength and transforming it into other forms of energy. Although photosensitizing compounds such as methylene blue, rose bengal, and acridine (Fig. 1.4)

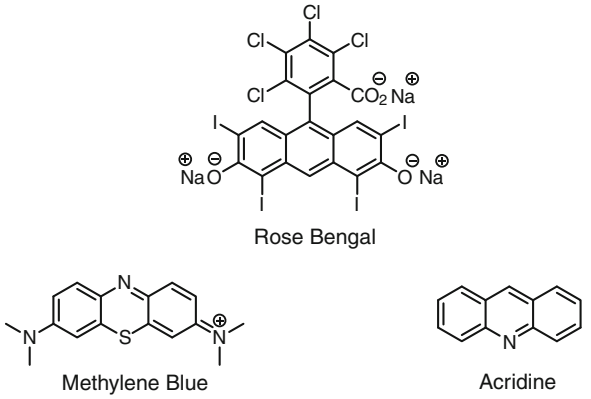

Fig. 1.4 Examples of non-porphyrinic photosensitizers

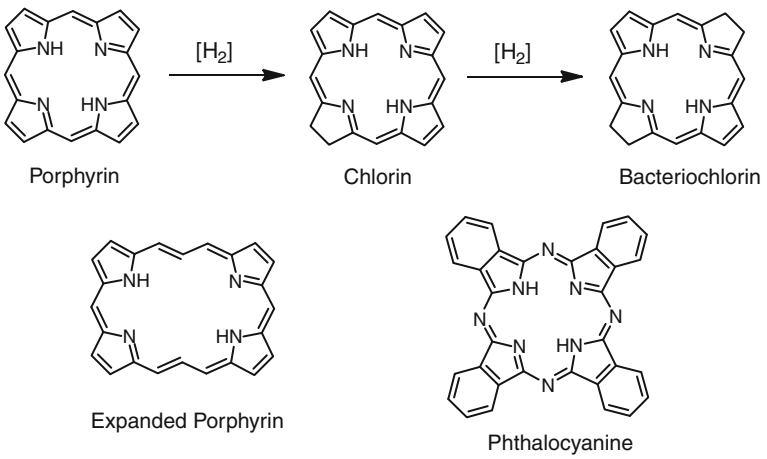

Fig. 1.5 Structures of porphyrinic photosensitizers

are potential PDT agents, the majority of the photosensitizers are cyclic tetrapyrroles and their analogues, such as porphyrins, chlorins, bacteriochlorins, expanded porphyrins, and phthalocyanines (Fig. 1.5).

1.2.1 Characteristics of Ideal Photosensitizers

Photosensitizers play a crucial role in PDT. The key characteristic of a photosensitizer is its ability to preferentially accumulate in diseased tissue and, via the generation of cytotoxic species, induce a desired biological effect. In order to

develop novel photosensitizers with high potency and selectivity, the characteristics of efficient photosensitizers must first be known [33–35].

A good photosensitizer is preferably a single and well-characterized compound with a known and constant composition. The synthetic route should be short and efficient. The compound should have minimum dark toxicity and negligible cytotoxicity in the absence of light. It should exhibit greater retention in diseased/target tissue over healthy tissue, and be eliminated from the body readily to avoid generalized skin photosensitization. Its triplet quantum yield (Φ_t) should be high and the triplet state energy (ΔE_t) should be larger than the energy of singlet oxygen ($\Delta E_\Delta = 94$ kJ mol^{-1}) so that energy transfer can occur to generate $^1O_2$. It should not significantly self-aggregate in the body because aggregation decreases Φ_t and singlet oxygen quantum yield (Φ_Δ) [36]. It should have strong absorption in the red/near-infrared region of the electromagnetic spectrum (650–850 nm) so that the light penetration can be as deep as possible [37, 38]. However, the absorption wavelength should not be too long. Otherwise, the energy would not be sufficient to trigger the formation of $^1O_2$ [33, 39]. In addition, the photostability of a compound often decreases when its absorption wavelength increases [39, 40]. Preferably, the photosensitizer would not strongly absorb in the region of 400–600 nm to minimize the risk of generalized photosensitivity caused by sunlight.

1.2.2 First-Generation Photosensitizers

Photofrin®

The first photosensitizer being approved for clinical use by governmental regulatory agencies is the first-generation hematoporphyrin derivatives. The most typical and well-known example is Photofrin®. It is a mixture of dimers and oligomers of hematoporphyrin in which the porphyrin units are linked by ether and/or ester linkages (Fig. 1.6). It has been approved for clinical use against early- and late-stage lung cancer, esophageal cancer, bladder cancer, and malignant, nonmalignant, and early-stage cervical cancer in the worldwide. Despite the clinical success achieved using Photofrin®, this drug has several serious limitations. First, the high degree of chemical heterogeneity makes it difficult to control its behavior in vivo, both in terms of the photosensitizing properties and the distribution between the tumor and the normal tissues. Since the composition of these oligomers may vary in different preparations and storage times, it is difficult to study the structure–activity relationship [33]. Secondly, Photofrin® absorbs weakly at the therapeutic wavelength of ca. 630 nm (Fig. 1.7). This restricts the treatment to a tumor depth of no more than 5 mm [41]. In addition, the small extinction coefficient at 630 nm ($\varepsilon = 3 \times 10^3$ M^{-1} cm^{-1}) lowers the probability of photoexcitation, thus requiring the administration of a relatively large amount

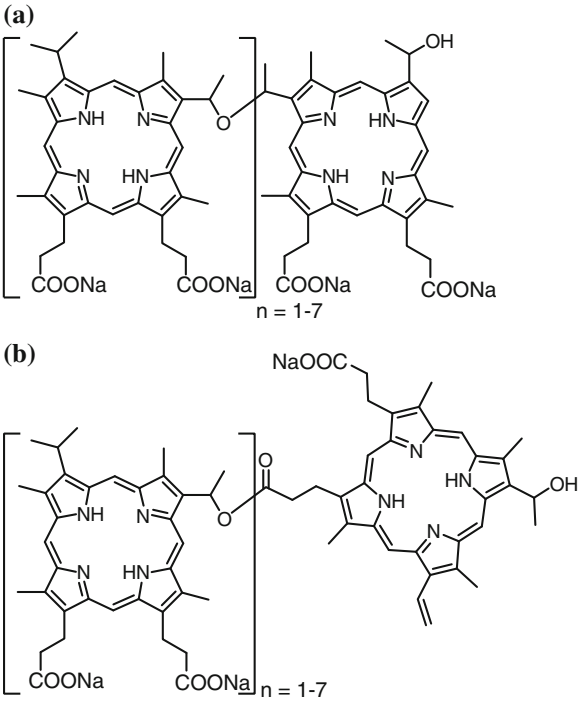

Fig. 1.6 Structures of **(a)** ether-linked and **(b)** ester-linked oligomeric porphyrins found in Photofrin®

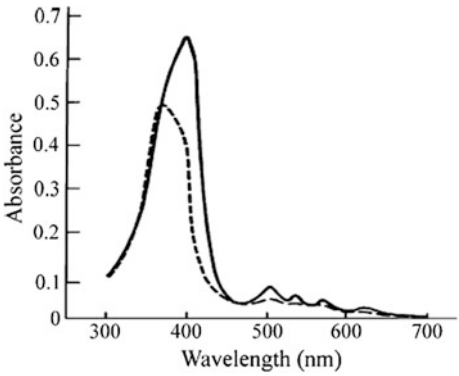

Fig. 1.7 Electronic absorption spectra of HpD (5 μg mL^{-1}) in saline (- - - -) and saline with 10 % fetal calf serum (—)

of dye (2–5 mg kg^{-1} body weight) in order to obtain a satisfactory phototherapeutic response. Thirdly, Photofrin® has been proved to be ineffective for cancers such as pigmented melanoma due to the overlapping absorption spectra of the photosensitizer and melanin in the malignant tissue [42]. More importantly, this drug exhibits extended retention in cutaneous tissue for up to 10 weeks post-injection [43].

Table 1.2 Absorption characteristics for several classes of second-generation photosensitizers

Compound type	λ_{max} (nm)	ε (M^{-1} cm^{-1})
Porphyrins	620–640	3,500
meso-substituted porphyrins	650	18,000
Chlorins	680	40,000
Phthalocyanines	700	200,000
Naphthalocyanines	780	350,000
Bacteriochlorins	780	150,000

1.2.3 Second-Generation Photosensitizers

The limitations on the use of Photofrin® in PDT have led to the development of new and more effective photosensitizers. The investigations to identify these new "second-generation" photosensitizers are mainly directed toward porphyrin analogues which absorb in the far-red spectral region. The absorption characteristics for several classes of second-generation photosensitizers are presented in Table 1.2. In the following subsections, some important classes of second-generation photosensitizers are highlighted.

Porphyrins

meso-Tetraphenylporphyrin (TPP) (see **1.1** in Fig. 1.8) was the first porphyrin as a single compound to be evaluated as a photosensitizer. TPP has an absorption maximum of 630 nm and is an efficient generator of $^1O_2$ but has limited solubility in water. To enhance the hydrophilicity of TPP, suitable substituents have been added to its periphery. Sulfonation of TPP gives *meso*-tetra(4-sulfonatophenyl)porphyrin (*p*-$TPPS_4$) (see **1.2** in Fig. 1.8), which is an excellent producer of $^1O_2$ ($\Phi_\Delta = 0.71$) [43] and has excellent water solubility, and was viewed as a promising photosensitizer for PDT [44]. Due to its hydrophilicity, it does not require a carrier to avoid self-aggregation in the plasma which will decrease its Φ_Δ [45–47]. In addition, it is membrane permeable, displays lysosomal accumulation in tumor cells, and is effective both in vitro and in vivo. However, clinical trials with *p*-$TPPS_4$ were ceased after neurotoxicity was reported in mice being exposed to high doses of *p*-$TPPS_4$ [48, 49].

Recently, dendritic porphyrin derivatives have been prepared in which a porphyrin chromophore is buried inside a hydrophobic shell. Surface modifications on the periphery have provided a cationic or anionic surface for a zinc porphyrin core with up to 32 charged terminal groups. These compounds have been found to be effective photosensitizers in vitro (see **1.3a–b** in Fig. 1.9) [50]. In addition, a series of tetraphenylporphyrin derivatives bearing amino acids, peptides, or diamines (see **1.4a–f** in Fig. 1.9) have also been prepared which are also potential photosensitizers [51].

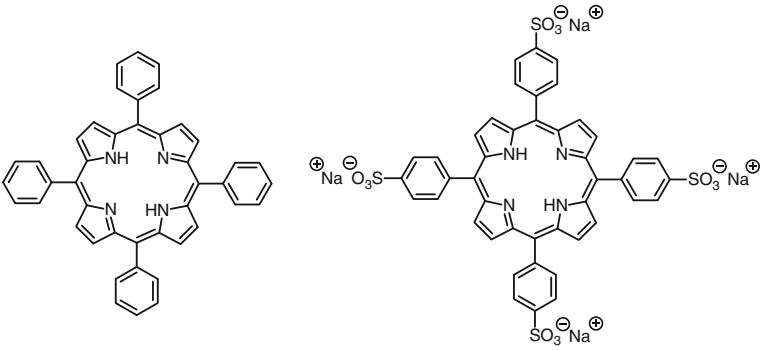

Fig. 1.8 *meso*-Substituted porphyrins **1.1** and **1.2** that have been developed as potential photosensitizers for PDT

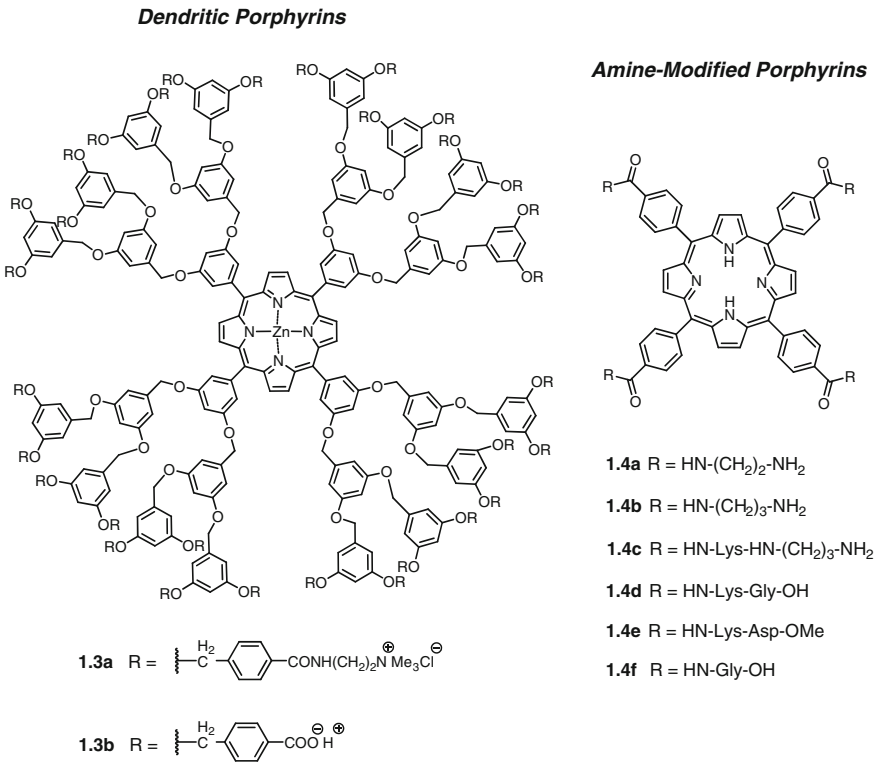

Fig. 1.9 Structures of third-generation ionic dendritic porphyrins **1.3a–b** and amine-modified porphyrins **1.4a–f**

Chlorins and Bacteriochlorins

Porphyrins generally have a strong absorption at around 400 nm, which is called the Soret band (or B-band). Unfortunately, the short-wavelength absorption of this band does not allow deep penetration into tissue. These compounds exhibit weak absorptions at around 630 nm. By contrast, their derivatives chlorins and bacteriochlorins have strong absorption maxima around 680 and 780 nm, respectively (Table 1.2). Figure 1.5 shows the structures of a general porphyrin, chlorin, and bacteriochlorin. Reduction of a peripheral double bond of porphyrins shifts the λ_{max} to the red. The dihydroporphyrins obtained are called chlorins. In bacteriochlorins, two double bonds on the opposite sides of the macrocycle are reduced, which further moves their absorption to the red.

meta-Tetrahydroxyphenylchlorin (*m*-THPC) is probably the most useful chlorin-based photosensitizer (see **1.5** in Fig. 1.10). *m*-THPC (also called Foscan or Temoporfin) shows a strong absorption at 652 nm. It has been approved in Europe for the palliative treatment of head and neck cancer, and additional indications have been filed for prostate and pancreatic tumors [32, 52, 53]. It has also been used effectively in recurrent breast cancer for chest wall lesions [54]. However, it shows long-term skin photosensitization of up to 6 weeks, which is one drawback to its use.

Naturally occurring chlorin e_6 (see **1.6a** in Fig. 1.10), derived from oxidation of chlorophyll *a*, has an absorption maximum at 654 nm with a value of ε of ca. $4 \times 10^4\ M^{-1}\ cm^{-1}$. However, it also exhibits long-term skin photosensitization and requires high doses [55]. Alkyl esters of chlorin e_6 and other derivatives such as mono-*L*-aspartyl chlorin e_6 (see **1.6b** in Fig. 1.10) have been found to be more bioavailable and effective at lower doses and are being evaluated for topical delivery [56].

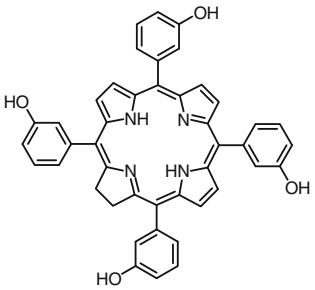

1.5 *m*-THPC

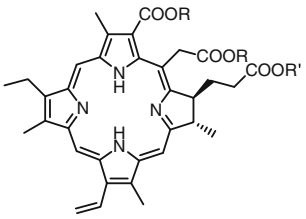

1.6a Chlorin e_6, R = R' = H

1.6b Mono-*L*-aspartyl chlorin e_6, R = H, R' = (*L*)-NHCH(CO_2H)CH_2CO_2H

Fig. 1.10 Structures of *meta*-tetrahydroxyphenylchlorin (**1.5**), chlorin e_6 (**1.6a**), and mono-*L*-aspartyl chlorin e_6 (**1.6b**)

1.2.4 Phthalocyanine-Based Photosensitizers

Phthalocyanines (Pcs) have been extensively studied as second-generation photosensitizers for PDT (see structure in Fig. 1.5) [57–60]. Due to the four additional peripheral benzene rings, they have absorptions at longer wavelengths compared with porphyrins (Table 1.2). These absorptions, normally in the red visible region, allow a deeper light penetration into tissues. In addition to the bathochromic shift of the Q-band absorption maxima, Pcs have higher molar extinction coefficients by two orders of magnitude over that of the longest Q-band absorption of HpD (Pc: $\varepsilon \sim 10^5\ M^{-1}\ cm^{-1}$; HpD: $\varepsilon \sim 10^3\ M^{-1}\ cm^{-1}$). Hence, Pcs have desirable photophysical and photochemical properties. Very often, these properties can be altered through rational modification of the substituents either on the periphery of the macrocycle or at the axial positions linked to the metal center. However, Pcs tend to aggregate which shortens the singlet excited state lifetime and hence decreases the singlet oxygen quantum yield by dissipating energy through internal conversions [61]. This problem can be overcome by incorporating large substituents or using emulsifying agents, such as Cremophor EL to create a micro-heterogeneous environment [62, 63]. In addition, the central metal ions of Pcs also play influential roles on their photophysical properties. Normally, Pcs containing a closed *d* shell and diamagnetic metal center, such as Zn^{2+}, Al^{3+}, and Ga^{3+} have higher triplet state quantum yields ($\Phi_t > 0.4$) and longer lifetimes ($\tau_T > 200\ \mu s$) [64]. The triplet state of these compounds varies in energy from 110 to 126 kJ mol^{-1}, which is sufficient to generate singlet oxygen (94.5 kJ mol^{-1}) with high quantum yields (0.3–0.5) [65].

In the following subsections, selected examples of phthalocyanines that were studied as second-generation photosensitizers for PDT are discussed.

Zinc Phthalocyanines

The preparation of unsubstituted zinc(II) phthalocyanine (ZnPc) involves a straightforward and one-step condensation reaction of phthalonitrile in the presence of zinc acetate [66, 67]. This compound is highly insoluble in almost all organic solvents and aqueous media, and hence it needs to be formulated as emulsions or conjugated with proteins for biological uses. Unlike silicon(IV) phthalocyanines (SiPcs), aggregation is a very common phenomenon for ZnPcs, especially in aqueous media, since Zn^{2+} ion does not support two axial ligands as SiPcs do. As mentioned earlier, aggregation tends to reduce the photosensitizing efficiency, and thus numerous efforts have been put on synthesizing hydrophilic and non-aggregated Phthalocyanines in order to inhibit molecular aggregation in aqueous media.

Ng et al. reported two hexadeca-carboxy phthalocyanines which exhibited a considerable water solubility in the presence of NaOH (see **1.7** and **1.8** in Fig. 1.11) [68]. Both compounds (in their deprotonated forms) were not significantly aggregated in aqueous media when pH > 7, probably due to the inherent repulsion of the

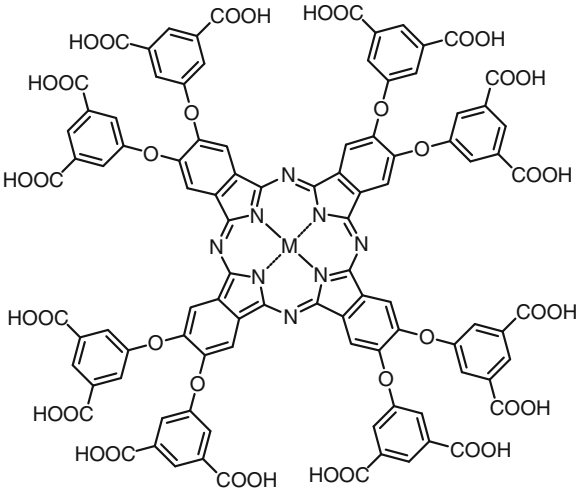

Fig. 1.11 Structures of hexadeca-carboxy phthalocyanines **1.7** and **1.8**

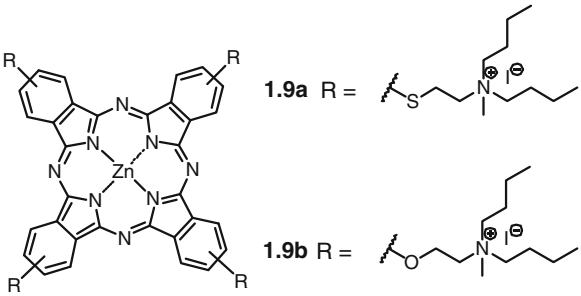

Fig. 1.12 Structures of isosteric alkyl substituted zinc phthalocyanines **1.9a–b**

highly negatively charged molecules. The in vitro photodynamic activities of both compounds (in their deprotonated forms) were investigated against two different cell lines, namely murine macrophage J774 and human hepatocarcinoma HepG2. It was found that the zinc(II) analogue **1.8** exhibited a high and selective photocytotoxicity against J774 cells due to the expression of class-A scavenger receptors in J774 cells but not in HepG2 cells [69, 70]. The conclusion was supported by a polyinosinic acid competitive assay.

Awruch et al. reported two novel isosteric cationic zinc(II) phthalocyanines (see **1.9a–b** in Fig. 1.12) [71]. The photodynamic effect and the cellular uptake of both phthalocyanines were evaluated on human nasopharynx KB carcinoma cells. Upon exposure to light (4.7 J cm^{-2}, 1.96 mW cm^{-2}), phthalocyanine **1.9a** showed a higher cytotoxicity than **1.9b** with IC_{50} values (defined as the dye concentration to kill 50 % of the cells) of 1.45 μM for the former and 10.5 μM for the latter phthalocyanine. In addition, **1.9a** showed a relatively higher cellular uptake and

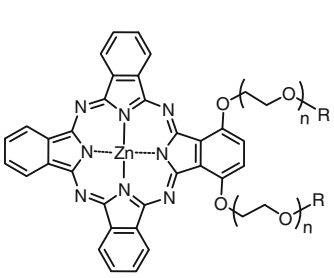

1.10a	n = 2	R = CH_3
1.10b	n = 4	R = CH_3
1.10c	n ~ 12	R = CH_3
1.10d	n = 4	R = H
1.10e	n = 6	R = CH_3
1.10f	n = 8	R = CH_3
1.10g	n = 3	R = H
1.10h	n = 3	R = CH_3

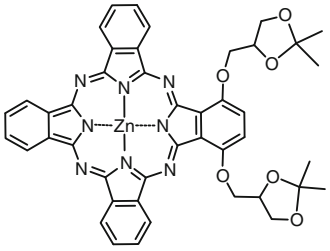

1.11

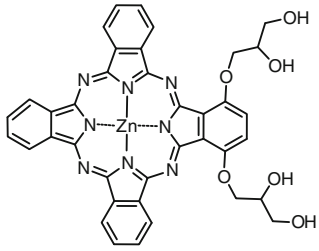

1.12

Fig. 1.13 Structures of 1,4-di-α-substituted zinc phthalocyanines **1.10–1.12**

more efficient ROS generation. It also tended to accumulate in the lysosomes of the KB cells.

Ng et al. further reported a series of 1,4-di-α-substituted zinc phthalocyanines **1.10–1.12** (see structures in Fig. 1.13) [72, 73]. These phthalocyanines are highly soluble and remain non-aggregated in *N*,*N*-dimethylformamide (DMF). Compared with the unsubstituted ZnPc, these 1,4-di-α-substituted analogues exhibit a red-shifted Q-band (689–701 nm). Upon illumination (48 J cm^{-2}, 40 mW cm^{-2}), these phthalocyanines are highly cytotoxic toward human colon adenocarcinoma HT29 and human hepatocarcinoma HepG2 cells, with IC_{50} values as low as 0.02 μM. The high photodynamic activity of these compounds can be attributed to their high cellular uptake, low aggregation tendency in the biological media, and high efficiency in generating ROS.

Silicon Phthalocyanines

Another class of phthalocyanines that receives a great deal of attention is silicon(IV) phthalocyanines. Axial ligation of hydrophilic or amphiphilic groups in silicon(IV) phthalocyanines can tune the properties of the macrocycles such as the solubility in biological media, aggregation behavior, and targeting properties.

The silicon(IV) phthalocyanine Pc4 (**1.13**) developed by Kenney et al. is perhaps the most representative example. Scheme 1.1 shows the synthetic route used to prepare this compound [74]. Owing to the high photodynamic activities,

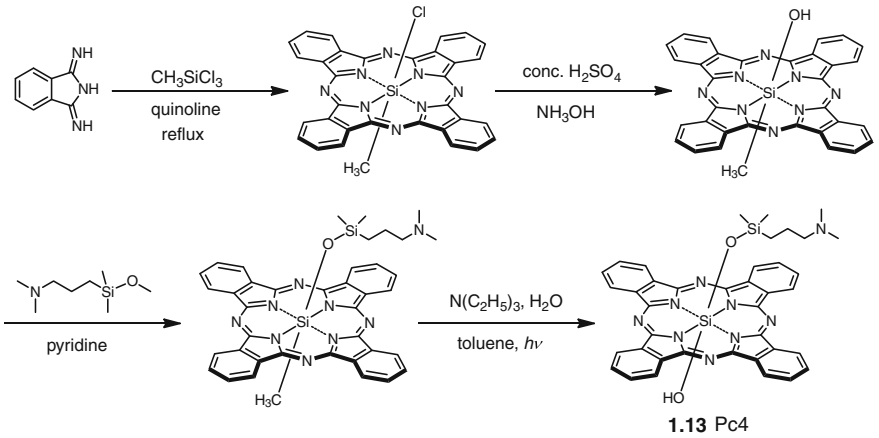

Scheme 1.1 Synthesis of silicon(IV) phthalocyanine Pc4 (**1.13**)

Pc4 has been studied extensively. It is highly effective in causing regression of the RIF-1 tumor at low drug dosage with little cutaneous photosensitivity. It is also effective in killing HIV and blood-borne parasites, rendering this compound to be used in the photosterilization of red blood cells and platelets concentrates [75].

Based on the fact that positively charged rhodamine B (Rh B) accumulates specifically in the mitochondria of living cells, Wong et al. have recently designed two axially ligated silicon(IV) phthalocyanine-rhodamine B conjugates **1.14a–b** (see structures in Fig. 1.14) [60]. Their linear and two-photon photophysical properties, subcellular localization, and photocytotoxicity have been studied. These conjugates localize almost exclusively in the mitochondria in human nasopharyngeal carcinoma HK-1 cells and human cervical carcinoma HeLa cells. In addition, they demonstrate substantial PDT activities via two-photon excitation

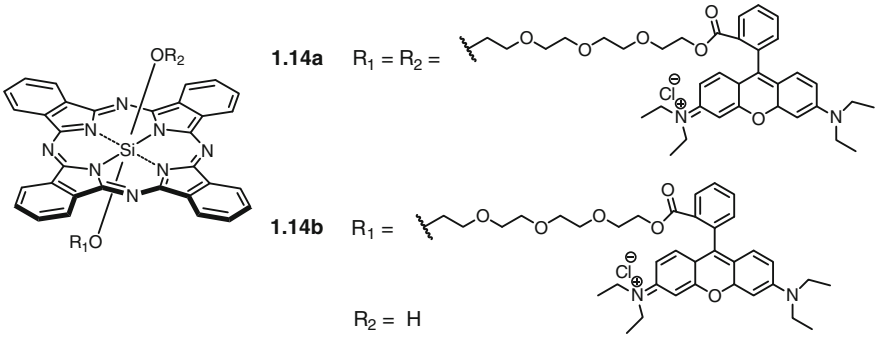

Fig. 1.14 Structures of silicon(IV) phthalocyanine-rhodamine B conjugates **1.14 a–b**

of the Rh B chromophore. As revealed by nuclei-staining method and flow cytometric DNA content analysis, apoptotic cell death was induced by these conjugates upon photoactivation.

1.3 Toward Targeted Photodynamic Therapy

Although some photosensitizers used in PDT can exhibit a certain degree of tumor selectivity, it is desirable to have further control of their photodynamic action. Various strategies have been developed to improve the drug specificity for diseased tissue and to achieve targeted PDT [76]. In the following sections, two key strategies are briefly discussed, including (1) the utilization of site-specific delivery agents to carry the photosensitizers to target tissue (e.g. antibodies, peptides, or folic acid) [77–79] and (2) the development of smart PDT agents that can be activated upon interaction with tumor-associated stimuli [80].

1.3.1 Site-Specific Delivery of Photosensitizers

1.3.1.1 Conjugation to Monoclonal Antibodies

A major challenge in PDT is to improve the tumor selectivity of the photosensitizers. One of the strategies is through the conjugation with monoclonal antibodies (MAbs) which have high affinity toward tumor-associated antigens. Since the expression of these antigens on normal tissues is limited, it is anticipated that these tissues will be relatively free from these MAb-conjugated photosensitizers.

Vrouenraets et al. investigated the photodynamic activities of the MAb conjugate of tetrasulfonated aluminum(III) phthalocyanine **1.15** ($AlPcS_4$-MAb) and *meso*-tetra(hydroxyphenyl)chlorin **1.16** (*m*-THPC-MAb) (see structures in Fig. 1.15) [81, 82]. Preliminary in vitro data showed that the $AlPcS_4$-MAb conjugate was highly toxic to A431 cells. This conjugate was 7500 times more toxic than the free compound (IC_{50}: 0.12 vs. 900 nM), and about 60 times more toxic than *m*-THPC-MAb. In an extended in vitro evaluation, $AlPcS_4$- and *m*-THPC-MAb conjugates were studied using five different squamous cell carcinoma (SCC) cell lines as target and three different MAbs (BIWA 4, E48, and 425) for targeting. In contrast to free $AlPcS_4$ ($IC_{50} > 700$ nM), MAb-conjugated $AlPcS_4$ was found to be highly photocytotoxic in all the five cell lines. $AlPcS_4$-BIWA 4 was most consistently effective with IC_{50} values ranging from 0.06 to 5.4 nM. However, *m*-THPC-MAb conjugates were ineffective. These results showed that $AlPcS_4$-MAb conjugates have a higher potential than *m*-THPC-MAb conjugates for use in PDT.

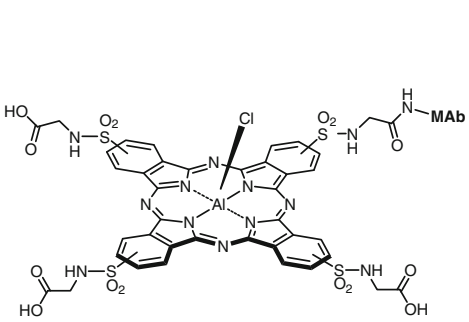

1.15 $AlPcS_4$-MAb

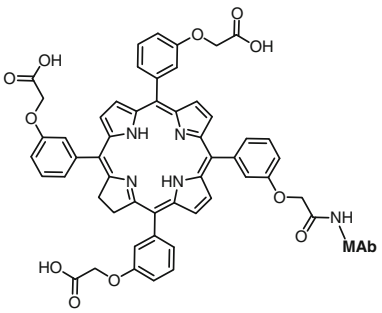

1.16 *m*-THPC-MAb

Fig. 1.15 Structures of aluminum(III) phthalocyanine tetrasulfonate- and *meso*-tetra(hydroxyphenyl)chlorin-monoclonal antibody conjugates

1.3.1.2 Conjugation to Tumor Vessel-Targeted Peptides

Endothelial cells are crucial in angiogenesis, the process of new blood vessel formation associated with tumor growth and metastasis [83]. By specifically targeting tumor endothelial cells, it is possible to induce vascular shutdown and enhance treatment efficacy. $\alpha_v\beta_3$-Integrin, a heterodimeric transmembrane glycoprotein receptor, is overexpressed in proliferating endothelial cells in and around tumor tissues [84]. This integrin may therefore represent a promising target for the delivery of photosensitizers. Owing to the fact that cyclic peptides containing an arginine-glycine-aspartic acid (RGD) motif show high affinity for this integrin, conjugation of photosensitizers to cyclic RGD may potentiate the vascular effect of PDT that is thought to play a major role in tumor eradication. Vernon et al. synthesized a protoporphyrin IX-cyclic RGD conjugate **1.17** (PpIX:cRGD) (see structure in Fig. 1.16) [85]. Pharmacokinetic analysis of this PpIX:cRGD-treated

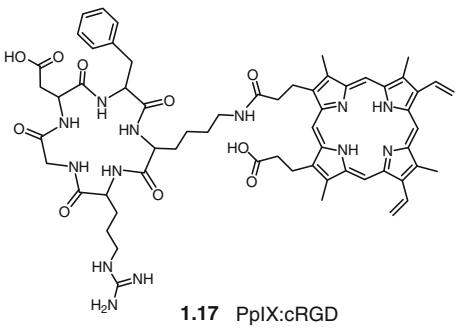

1.17 PpIX:cRGD

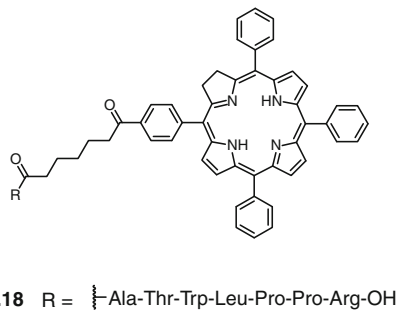

1.18 R = Ala-Thr-Trp-Leu-Pro-Pro-Arg-OH

Fig. 1.16 Structures of protoporphyrin IX-cyclic RGD conjugate **1.17** and 5-(4-carboxyphenyl)-10,15,20-triphenylchlorin-ATWLPPR conjugate **1.18**

mice showed significant drug retention and accumulation in tumor tissue with higher tumor : normal tissue ratios than the free photosensitizer.

Receptors for growth factors are overexpressed on cancer cells, which are also excellent targets for specific photosensitizer delivery system. Vascular endothelial growth factor (VEGF) is considered to be a key mediator of angiogenesis in cancer. Therefore, after conjugation with photosensitizer, it can also trigger the vascular effect of PDT. Barberi-Heyob et al. conjugated 5-(4-carboxyphenyl)-10,15,20-triphenylchlorin (TPC) to a VEGF receptor-specific heptapeptide (ATWLPPR) (see **1.18** in Fig. 1.16) [86]. Its uptake by human umbilical vein endothelial (HUVEC) cells was up to 25-fold higher than that of free TPC. In nude mice xenografted with U87 human malignant glioma cells expressing VEGF receptors, the conjugated photosensitizer could target angiogenic endothelial cells as well as tumor cells.

1.3.1.3 Conjugation to Folic Acid

Folic acid is a vitamin which has a high affinity for folate receptor, a glycosyl-phosphatidylinositol-anchored cell surface receptor that is overexpressed in many human tumors but absent in most normal tissues [87]. Although the precise mechanism of folate receptor transport of folic acid into cells remains unresolved, folate conjugates are taken up non-destructively by mammalian cells via receptor-mediated endocytosis [88]. Schneider et al. reported the first conjugation of TPP with folic acid (see **1.19** and **1.20** in Fig. 1.17) and studied their targeted delivery to human nasopharynx KB carcinoma cells, which overexpress folate receptors [89].

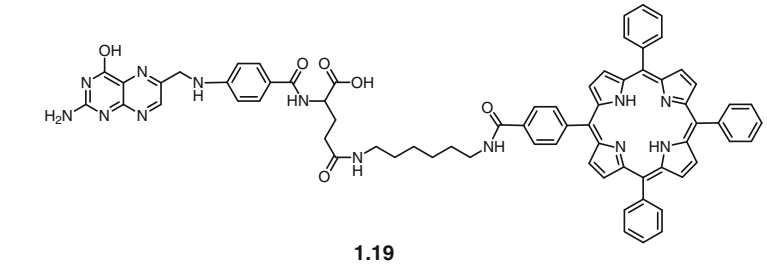

1.19

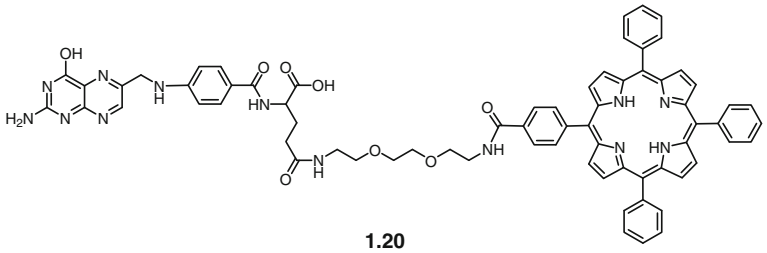

1.20

Fig. 1.17 Structures of tetraphenylporphyrin-folic acid conjugates **1.19–1.20**

After 24 h incubation, the cellular uptake of these conjugates was on average 7-fold higher than that of TPP. Moreover, the cellular uptake kinetics suggested that these conjugates enter into the cells through an active transport via receptor-mediated endocytosis. The cellular uptake of **1.19** and **1.20** showed a reduction of 70 % in the presence of a competitive concentration of folic acid. While TPP displayed no photocytotoxicity, conjugates **1.19** and **1.20** showed 50 % growth inhibition at a light dose of 22.6 and 6.7 J cm^{-2}, respectively.

1.3.2 Activatable Photosensitizers

Activatable photosensitizers are a special class of photosensitizers that can be activated by a wide variety of molecular stimuli, resulting in increased cytotoxic singlet oxygen generation. This is often accomplished by maintaining the photosensitizers in a quenched state prior to activation. Förster resonance energy transfer (FRET), photoinduced electron transfer (PET), and self-quenching are potential quenching strategies in the design of activatable photosensitizers. Compared to conventional PDT which relies on specific light and photosensitizer delivery, activation by appropriate stimuli confers an additional control of the specificity of the PDT process.

1.3.2.1 Environmental Activatable Photosensitizers

Environmental activation is an important factor in controlling the singlet oxygen generation of photosensitizers. It was documented that the singlet oxygen production efficiency of photosensitizers is dependent on solvent properties including pH and hydrophobicity. As shown in Fig. 1.18, the common photosensitizer methylene blue (**1.21**) displays a 5-fold enhancement in singlet oxygen quantum yield as the pH increases from 5 to 9 under which the photosensitizer is

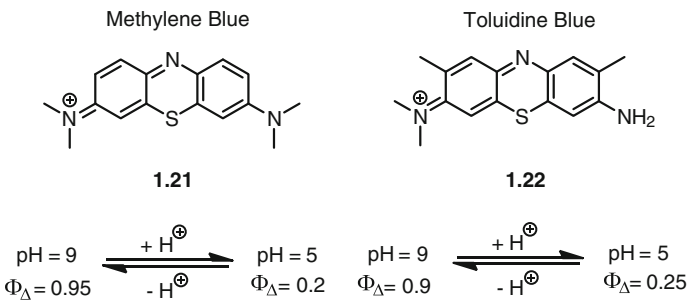

Fig. 1.18 pH-dependent changes in singlet oxygen quantum yields of methylene blue (**1.21**) and toluidine blue (**1.22**)

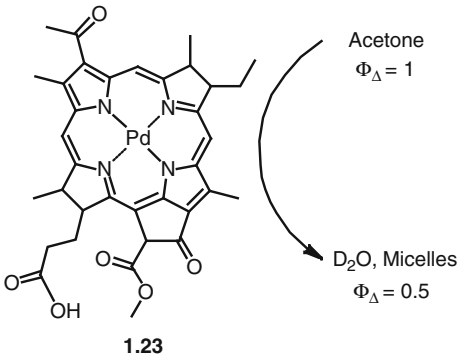

1.23

Fig. 1.19 Change in singlet oxygen quantum yields of palladium-bacteriopheophorbide *a* in solvents of different hydrophobicity

deprotonated [28]. The structurally related photosensitizer toluidine blue (**1.22**) shows a similar response upon deprotonation [90]. Solvent hydrophobicity also plays an important role in determining the photosensitizer efficiency. For example, palladium-bacteriopheophorbide *a* (**1.23**) undergoes an approximately 2-fold change in singlet oxygen quantum yield as the solvent changes from acetone to deuterated water (Fig. 1.19).

Although solvent and pH effects have long been recognized to affect singlet oxygen production, efforts have only been made recently to exploit these properties in the design of activatable photosensitizers. For example, by attaching a pH-sensitive moiety to photosensitizers, pH-activated photosensitizers can be formed that can function at a low pH environment. O'Shea et al. synthesized a novel series of amine-containing BF_2-chelated azadipyrromethenes. Their singlet oxygen production in DMF could be switched on and off through changing the pH environment (Fig. 1.20) [91]. Upon addition of HCl, the amino groups were protonated, which inhibited the PET process thereby promoting the production of singlet oxygen. These photosensitizers were demonstrated to effectively kill the MRC5-SV40 transformed fibroblast cells.

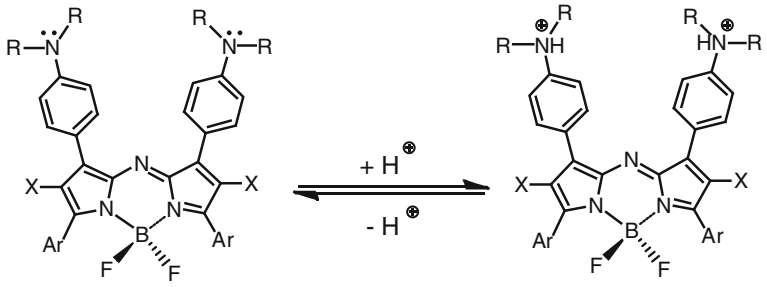

Fig. 1.20 A PET-based pH-activatable photosensitizer. The BF_2-chelated azadipyrromethene showed a higher singlet oxygen production efficiency when the amino moieties became protonated

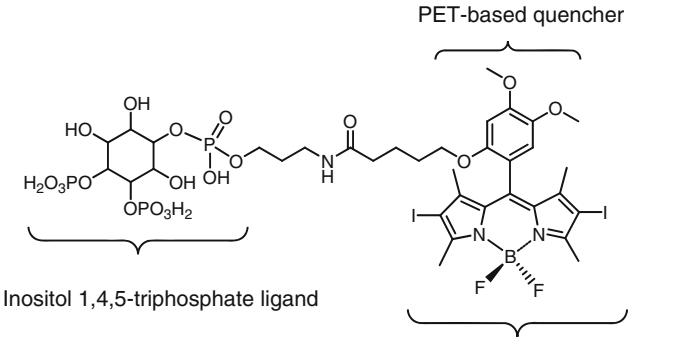

1.24

Fig. 1.21 Hydrophobically activatable photosensitizer with protein targeting ligand for chromophore-assisted light inactivation

This approach was extended to PET-based quenchers that are only active in a hydrophobic environment. Figure 1.21 shows an example of these activatable photosensitizers in which a boron dipyrromethene (BODIPY)-based photosensitizer is linked to a modulatable PET-based quencher and an inositol 1,4,5-triphosphate unit (a protein-targeting ligand) (**1.24**) that can deliver the photosensitizer to the IP3 receptors of cells [92], where it was activated by binding in a hydrophobic pocket and could then specifically damage that protein through singlet oxygen generation. This approach demonstrated the specific inactivation of specific proteins in live cells.

1.3.2.2 Photodynamic Molecular Beacons

Molecular beacons are FRET-based target-activatable probes. They offer a control of fluorescence emission in response to specific cancer targets, and thus are useful tools for in vivo cancer imaging. By combining the principles of molecular beacons and PDT, photodynamic molecular beacons (PMB) have recently been developed for controlling the photosensitizer's ability to generate singlet oxygen and, ultimately, for controlling its PDT activity. The PMB comprise a photosensitizer (PS), a quencher (Q), and a disease-specific linker, keeping them in close proximity so that the photosensitizer is quenched due to FRET. When the linker interacts with target molecules, such as tumor-associated enzymes or nucleic acids, the PS and Q are separated which abolishes the quenching effect by FRET, thereby restoring the photoactivity of the photosensitizer (Fig. 1.22).

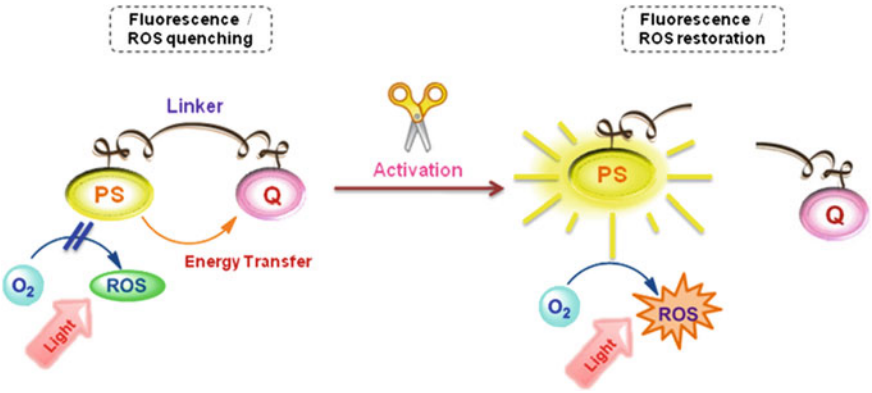

Fig. 1.22 Schematic diagram showing the general working principle of PMB

Enzyme-Activated PMB

Enzymes are biological catalysts and central to all facets of cellular functions. They are therefore excellent targets. In fact, overexpression of enzymes is often correlated with specific diseases. Activation of photosensitizer can be confined to the location where the enzyme is present, while in tissues not expressing the enzyme, the photosensitizer remains inactive.

Zheng et al. have developed an activatable photosensitizer that targets matrix metalloproteinase-7 (MMP-7), which plays a crucial role in the pathogenesis of cancer [93]. The system is composed of an enzyme-specific peptide sequence, a pyropheophorbide *a* photosensitizer, and a BHQ3 quencher (see **1.25** in Fig. 1.23).

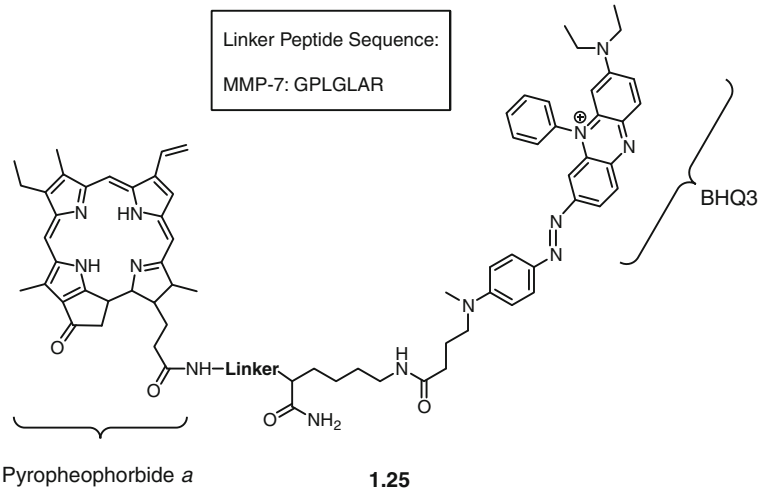

Fig. 1.23 Structure of a pyropheophorbide *a*-based activatable photosensitizer **1.25**. It is linked to a BHQ3 quencher via an MMP-7 enzyme-specific peptide sequence

Upon incubation of this photosensitizer with MMP-7, the production of singlet oxygen was greatly enhanced. Inhibition of the enzyme activity, the use of non-MMP-7-expressed cells, or modification of linker peptide sequence resulted in lowering the PDT activity.

Nucleic Acid-Activated PMB

Apart from enzymes, nucleic acids can also be used to regulate the activity of photosensitizers. Since gene mutations or altered gene expressions lie at the heart of almost all diseases, nucleic acid-based activatable photosensitizers could form the basis of PDT that removes unwanted cells expressing specific genes and discriminating even single-base mismatches.

Zheng et al. have reported a PMB of which the singlet oxygen production can be triggered by tumor-specific mRNA [94]. They have synthesized a *c-raf-1* mRNA-triggered PMB using pyropheophorbide *a* as the photosensitizer, carotenoid as the quencher, and *c-raf-1* mRNA-targeted antisense oligonucleotide as the loop sequence (see **1.26** in Fig. 1.24). The conformationally restricted hairpin (or stem-loop) structure forces the quencher to efficiently inhibit the photoreactivity of the photosensitizer. In the presence of tumor-specific *c-raf-1* mRNA, the hairpin opens and the photosensitizer emits fluorescence and generates cytotoxic $^1O_2$ upon irradiation. The $^1O_2$ production of pyropheophorbide *a* is quenched in its native state by 15-fold and is restored to 9-fold after addition of target RNA. In addition, upon incubation of *c-raf-1* expressing MDA-MB-231 cancer cells with the PMB, the PMB displays efficient cellular uptake and subsequently effective PDT activation in targeted cells.

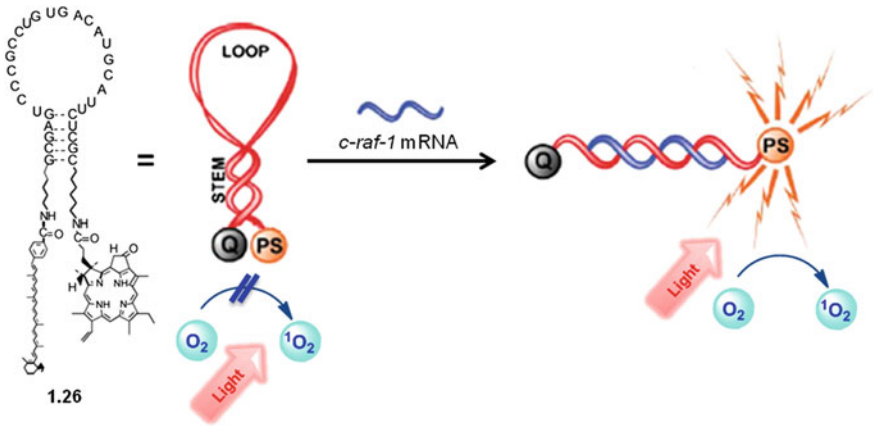

Fig. 1.24 Schematic diagram showing the working principle of mRNA-triggered photodynamic molecular beacon **1.26**

1.4 Dual Chemo- and Photodynamic Therapy

Degenerative diseases such as cancer usually involve more than one pathological process. As a result, attempts to combat such diseases with single therapeutic approaches may not always be efficient. For this reason, the use of combination therapy with modalities that target different disease pathways represents an alternative strategy. As mentioned in Sect. 1.1.2, in the presence of tissue oxygen, the photosensitizer triggers a series of photochemical and photobiological processes that may lead to direct cancer cell damage, tumor microvascular occlusion, and host immune response. Due to these multiple actions, PDT has been recently evaluated as a potential adjuvant for conventional cancer treatments such as radiotherapy, immunotherapy, and chemotherapy. In the following, the combination of PDT with chemotherapy is briefly reviewed. For dual PDT and chemotherapy, there are three general approaches, including the use of covalent conjugates, co-encapsulation of a photosensitizer and an anticancer drug in a polymeric nanocarrier, and sequential administration of these agents.

1.4.1 Covalent Conjugation

One approach in the context of combination treatments consists of the use of covalent conjugates of a photosensitizer and a chemotherapeutic drug. Brunner et al. developed a series of porphyrin-platinum complex conjugates in which a porphyrin derivative is covalently linked to a platinum complex [95]. The hypothesis for the use of such systems was based on the combined effect of PDT and cytostatic activity, as well as the porphyrin-mediated targeting of tumors. These porphyrin-platinum complex conjugates were prepared by complexation of the platinum complexes of a 1,2-diamine ligand with hematoporphyrin or 13,17-bis (2-carboxyethyl)-3,8-bis[1-(ethyleneglycolmonoethylether)oxyethyl]-2,7,12,18-tetramethylporphin (see **1.27**–**1.30** in Fig. 1.25). Their cytotoxicity was evaluated against MDA-MB-231 mammary carcinoma cells and compared to that of cisplatin and Photofrin® either alone or in combination [96]. Three of the tested conjugates were as active as or even more active than cisplatin in association with PDT.

Apart from these porphyrin-platinum complex conjugates, Guo et al. reported a molecular combo of silicon(IV) phthalocyanine and a cisplatin analogue (see **1.31** in Fig. 1.26) [97]. The cytotoxicity of the conjugate was evaluated toward human cervical cancer HeLa cells, both in the absence and presence of light. At a concentration of 100, the conjugate only achieved inhibition ratios of 45–55 %. However, the cytotoxic activities increased drastically after exposure to red light. At a concentration of 1 μM, the red light irradiation led from 7- to 25-fold enhancement in inhibitory efficiencies. In addition, both conjugates exhibited a nuclei-localization behavior and DNA binding ability, which may be due to the presence of the Pt(II) moieties. As a result, the use of DNA-targeting Pt(II)

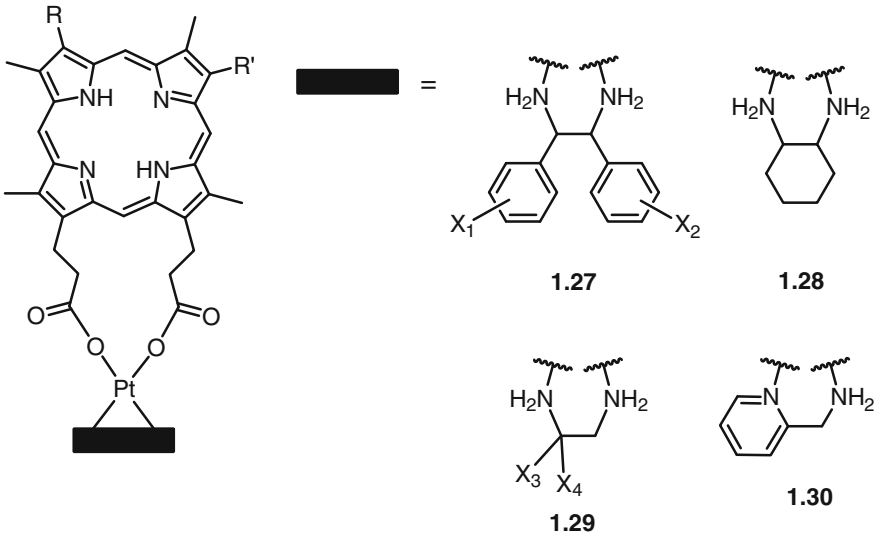

Fig. 1.25 Structures of porphyrin-platinum complex conjugates **1.27–1.30**. Refer to the original references for the structural details on the R, R', and X_1–X_4

Fig. 1.26 Structure of a silicon(IV) phthalocyanine-platinum complex conjugate **1.31**

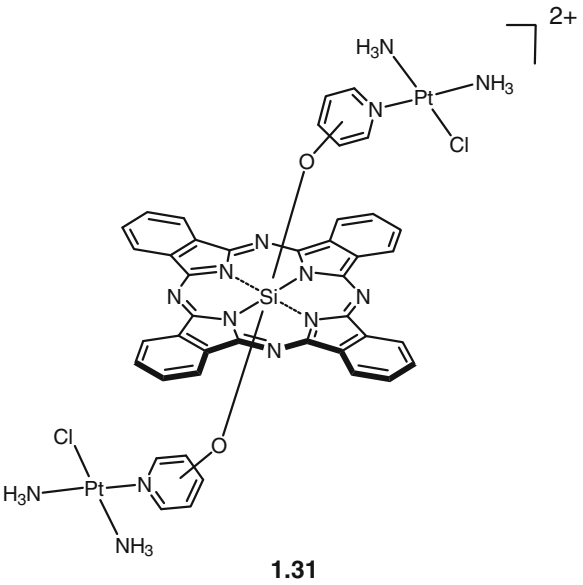

moieties allowed the photosensitizing unit to bind to DNA and induce oxidative damage to it. On the other hand, the incorporation of a photoactive SiPc moiety might allow the Pt(II) unit induce photochemical reactions, such as DNA platination.

1.4.2 Co-encapsulation in Polymeric Micelles

Recently, nanomaterials such as polymer-drug conjugates [98], liposomes [99], nanoparticles [100], and polymeric micelles[101, 102] have been considered as potential carriers for hydrophobic drugs. When photosensitizers are incorporated into polymeric micelles formed by amphiphilic block copolymers, they can actually act as nanosized photosensitizing agents for PDT. If another cytotoxic hydrophobic drug is also encapsulated into the micelles, this system may serve as a potential dual carrier for combined PDT and chemotherapy for the treatment of cancer.

Shieh et al. synthesized a chlorin-core star-shaped block copolymer (CSBC) based on methoxy poly(ethylene glycol) (mPEG) and poly(ε-caprolactone) (PCL). In the presence of paclitaxel (PTX), it assembled in aqueous media to form a micelle-like structure in which both the photosensitizer and PTX are entrapped inside (see **1.32** in Fig. 1.27) [103]. In the absence of PTX, the polymeric micelles exhibited phototoxicity against MCF-7 human breast cancer cells at a chlorin concentration of 125 μg mL^{-1} with 7 or 14 J cm^{-2} light irradiation (53 % or 38 % cell survival, respectively). The cell viability of PTX-loaded micelles was further evaluated with 7 J cm^{-2} light irradiation. The cell viability in the dark was inhibited by about 35 % by PTX alone and 33 % by the PTX-loaded micelles at the highest PTX concentration (20 μg mL^{-1}) for 24 h. After light irradiation,

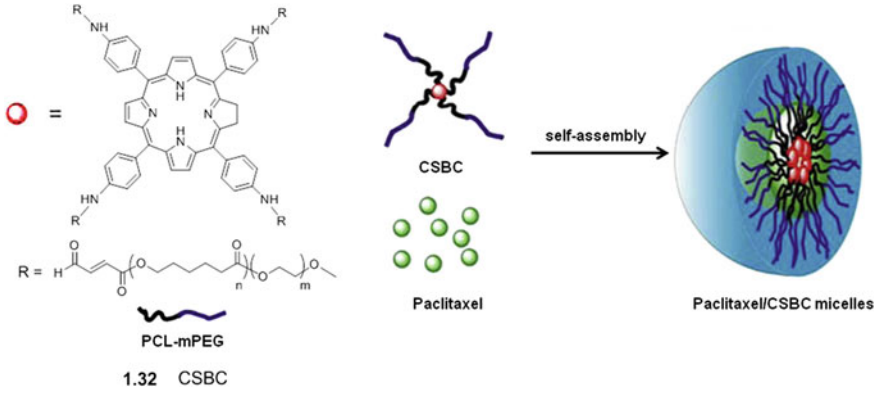

Fig. 1.27 Structure of chlorin-core star block copolymer **1.32** and schematic drawing of self-assembled paclitaxel/CSBC micelles

about a further 62 % of cells were killed by the micelles at 20 μg mL^{-1} PTX concentration, whereas there was no conspicuous difference with PTX alone. The significantly higher cytotoxicity after irradiation showed that there was a synergistic effect for the two components.

Apart from PTX, the same research group also encapsulated 7-ethyl-10-hydroxy-camptothecin (SN-38), which is an antitumor agent that targets the nuclear enzyme topoisomerase I (Top I) to CSBC [104]. The combined effects of SN-38/CSBC micelles were evaluated in an HT29 human colon cancer xenograft model. SN-38/CSBC-mediated PDT synergistically inhibited tumor growth, resulting in up to 60 % complete regression of well-established tumors after three treatments. These treatments also decreased the microvessel density and cell proliferation within the subcutaneous tumors.

1.4.3 Sequential Administration

The rationale behind the combination of PDT and chemotherapeutic drugs is the different modes of cytotoxic action. Light-activated photosensitizers generate ROS that oxidize various biomolecules in close proximity of the site of localization of the photosensitizers (Sect. 1.1.2.1). Meanwhile, chemotherapeutic drugs like cisplatin, doxorubicin, and mitomycin C (see structures in Fig. 1.28) kill cancer cells by binding to DNA and interfering with subsequent processes in cell replication. As a result, combination of PDT and chemotherapeutic drugs is likely to produce an additive or even synergistic effect from a clinical point of view. In fact, it is well-documented that the combination of these therapeutic modalities might improve the overall outcome of the treatment of cancer.

Nonaka et al. investigated the cytotoxic and apoptotic effects of a combination of Photofrin® and cisplatin on L5178Y mouse lymphoma cells [105]. PDT with Photofrin® (5 μg mL^{-1}) alone or chemotherapy with cisplatin (20 μg mL^{-1}) alone killed 41.5 ± 8.5 % or 42.9 ± 6.5 % of L5178Y cells, respectively, while a combination of these two treatments killed 99.7 ± 0.6 %. Apoptotic cell death

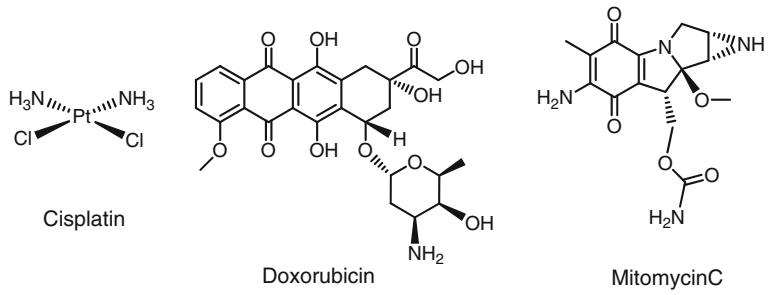

Fig. 1.28 Structures of cisplatin, doxorubicin, and mitomycin C

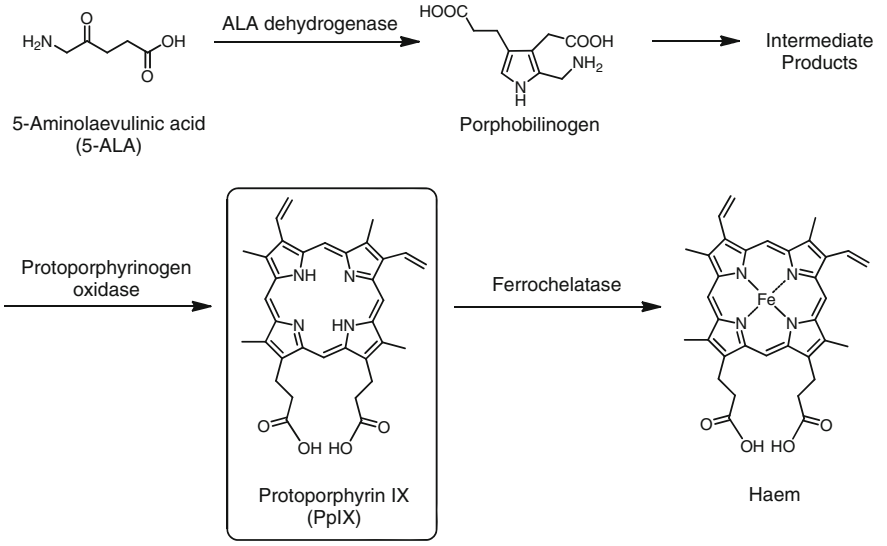

Scheme 1.2 Simplified biosynthesis of heme

after combination treatment also revealed to be 49.6 ± 7.8 % compared to 12.4 ± 3.4 % after PDT alone, and 18.8 ± 2.6 % after cisplatin treatment alone. The study demonstrated that combined treatment of PDT and cisplatin resulted in enhanced apoptotic cell death as well as a cytotoxic effect on L5178Y cells.

The sequence of the addition of the chemotherapeutic drug and the photosensitizer exerts a great influential effect on the overall therapeutic outcome. Kirveliene et al. observed that the antitumor activity was more pronounced when MH-22A murine hepatoma cells were subject to photodynamic treatment with *m*-THPC followed by the treatment with doxorubicin [106]. The difference in cytotoxicity between doxorubicin and the combined treatment with doxorubicin before PDT was approximately 40 %, while it exceeded 60 % when doxorubicin was added after PDT. The contribution of combination was evaluated by analysis of variance. The analysis revealed an antagonistic component when doxorubicin was given first. On the other hand, when doxorubicin was added after PDT, the combined action resulted in the addition of cytotoxicities of individual components. In vivo data showed that the antitumor activity of PDT 15 min before doxorubicin regimen was higher than that of doxorubicin 24 h before PDT. However, the statistical significance between these two sequences was not as high as it was observed in vitro.

Datta et al. studied the effect of 5-aminolaevulinic acid (5-ALA)-mediated photodynamic treatment in combination with mitomycin C on the J82 bladder cancer cells and a mitomycin C-resistant counterpart (J82/MMC) [107]. 5-ALA itself is not a photosensitizer, but a key precursor in the biosynthesis of the naturally occurring porphyrin, heme (Scheme 1.2). The immediate precursor to heme

is a pure endogenous porphyrin called protoporphyrin IX (PpIX), which is an effective photosensitizer. Cell viability assays demonstrated that the J82/MMC was not cross-resistant to PDT and suggested a higher sensitivity of J82/MMC to PDT than the parent cell line. For both cell lines, an enhanced effect was observed only when the cytostatic agent was given followed by a photodynamic treatment.

1.5 Objectives of this Study

The increasing number of drug resistance cases toward conventional chemotherapeutic drugs and the nonspecific toxicity of drugs on healthy tissues give impetus to the development of new therapeutic methods. One of the possible strategies to circumvent these growing problems is dual and targeted PDT. Since photosensitizers play a crucial role in controlling the therapeutic outcome, it is imperative to explore new photosensitizers that can accommodate the present imperfections. The objective of this thesis is to design and construct novel phthalocyanine-based photosensitizers toward dual and targeted PDT, with a view to improving their specific delivery to cancerous tissue and efficiency in PDT.

References

1. Kubler, A.C.: Med. Laser Appl. **20**, 37 (2005)
2. Mitra, A., Stables, G.I.: Photodiag. Photodyn. Ther. **3**, 116 (2006)
3. Castano, A.P., Demidova, T.N., Hamblin, M.R.: Photodiag. Photodyn. Ther. **2**, 1 (2005)
4. Schuitmaker, J.J., Bass, P., Van Leengoed, H.L.L.M., Van Der Meulen, F.W., Star, W.M., Zandwijk, N.J.: Photochem. Photobiol. B **34**, 3 (1994)
5. Brown, S.B., Brown, E.A., Walker, I.: Lancet Oncol. **5**, 497 (2004)
6. De Rosa, F.S., Bentley, M.V.L.B.: Pharm. Res. **17**, 1447 (2000)
7. Ackroyd, R., Kelty, C., Brown, N., Reed, M.: Photochem. Photobiol. **74**, 656 (2001)
8. Daniell, M.D., Hill, J.S.: Aust. NZ J. Surg. **61**, 340 (1991)
9. Edelson, M.F.: Sci. Am. **259**, 68 (1988)
10. Spikes, J.D.: In: Berghausen, R.V., Jori, G., Land, E.J., Truscott, T.H. (eds.) Primary photoprocesses in biology and medicine, pp. 209–227. Plenum Press, New York (1985)
11. Finsen, N.R.: Phototherapy. Arnold, E, London (1901)
12. Bonnett, R.: Chem. Soc. Rev. **24**, 19 (1995)
13. Raab, O.: Zeitung Biol. **39**, 524 (1900)
14. Prime, J.: Les accidents toxiques par l'eosinate de sodium. Jouve and Boyer, Paris (1900)
15. Von Tappeiner, H., Jesionek, A.: Muench Med. Wochenschr. **47**, 2042 (1903)
16. Von Tappeiner, H., Jodlbauer, A.: Die sensiblilisierende Wirkung fluoreszierender Substanzer Gesammte Untersuchungen uber die photodynamische Erscheinerung. Voger F. C, Leipzig (1907)
17. Lipson, R.L., Baldes, E.J., Olsen, A.M.J.: Natl. Cancer Inst. **26**, 1 (1961)
18. Dougherty, T.J., Grindey, G.B., Fiel, R., Weishaupt, K.R., Boyle, D.G.J.: Natl. Cancer Inst. **55**, 115 (1975)
19. Kelly, J.F., Snell, M.E.J.: J. Urol. **115**, 150 (1976)
20. Huang, Z.: Technol. Cancer Res. Treat. **4**, 283 (2005)

21. Celli, J.P., Spring, B.Q., Rizvi, I., Evans, C.L., Samkoe, K.S., Verma, S., Pogue, B.W., Hasan, T.: Chem. Rev. **110**, 2795 (2010)
22. Foote, C.S.: Photochem. Photobiol. **54**, 659 (1991)
23. Zuluaga, M.-F., Lange, N.: Curr. Med. Chem. **15**, 1655 (2008)
24. Dougherty, T.J., Gomer, C.J., Henderson, B.W., Jori, G., Kessel, D., Korbelik, M., Moan, J., Peng, Q.J.: Natl. Cancer Inst. **90**, 889 (1998)
25. Agostinis, P., Buytaert, E., Breyssens, H., Hendrickx, N.: Photochem. Photobiol. Sci. **3**, 729 (2004)
26. Macdonald, I.J., Dougherty, G.J.J.: Porphyrins Phthalocyanines **5**, 105 (2000)
27. Henderson, B.W., Waldow, S.M., Mang, T.S., Potter, W.R., Malone, P.B., Dougherty, T.J.: Cancer Res. **45**, 572 (1985)
28. Bonneau, R., Pottier, R., Bagno, O., Joussot-Dubien, J.: Photochem. Photobiol. **21**, 159 (1975)
29. Canti, G., De Simone, A., Korbelik, M.: Photochem. Photobiol. Sci. **1**, 79 (2002)
30. Henderson, B.W., Dougherty, T.J.: Photochem. Photobiol. **55**, 145 (1992)
31. Shumaker, B.P., Hetzel, F.W.: Photochem. Photobiol. **46**, 899 (1987)
32. Dolmans, D.E.J.G.J., Kadambi, A., Hill, J.S., Waters, C.A., Byron, C.R., Walker, J.P., Fukumura, D., Jain, R.K.: Cancer Res. **62**, 2151 (2002)
33. Brown, S.B., Truscott, T.G.: Chem. Br. **29**, 955 (1993)
34. Nyman, E.S., Hynninen, P.H.J.: Photochem. Photobiol. B **73**, 1 (2004)
35. Sternberg, E.D., Dolphin, D., Brückner, C.: Tetrahedron **54**, 4151 (1998)
36. MacRobert, A.J., Bown, S.G., Philips, D.: In: Bock, G., Harnett, S. (eds.) Photosensitizing compounds: Their chemistry, biology and clinical use, vol. 146, pp. 4–16. Wiley, Chichester (1989)
37. Jori, G.: EPA Newslett. **60**, 12 (1997)
38. Jori, G.J.: Photochem. Photobiol. A **62**, 371 (1992)
39. Milgrom, L., MacRobert, S.: Chem. Br. **34**, 45 (1998)
40. Hirth, A., Michelsen, U., Wöhrle, D.: Chem. unserer Zeit **33**, 84 (1999)
41. Wöhrle, D., Hirth, A., Bogdahn-Rao, T., Schnurpfeil, G., Shopova, M.: Russ. Chem. Bull. **47**, 807 (1998)
42. Peeva, M., Shopovan, M., Stoichkova, N., Michailov, N., Wöhrle, D., Müller, S.J.: Porphyrins Phthalocyanines **3**, 380 (1999)
43. Philips, D.: Prog. React. Kinetics **22**, 175 (1997)
44. Wilkinson, F., Helman, W.P., Ross, A.B.J.: Phys. Chem. Ref. Data **22**, 113 (1993)
45. Berg, K., Prydz, K., Moan, J.: Biochim. Biophys. Acta **1158**, 300 (1993)
46. Kessel, D., Thompson, P., Saatio, K., Nantwi, K.D.: Photochem. Photobiol. **45**, 787 (1987)
47. Kessel, D., Woodburn, K.: Int. J. Biochem. **25**, 1377 (1993)
48. Sema, A.A.F., Kennedy, J.C., Blakeslee, D., Robertson, D.M.: Can. J. Neurol. Sci. **8**, 105 (1981)
49. Winkelman, J.W., Collins, G.H.: Photochem. Photobiol. **46**, 801 (1987)
50. Nishiyama, N., Stapert, H.R., Zhang, G.-D., Takasu, D., Jiang, D.L., Nagano, T., Aida, T., Kataoka, K.: Bioconjugate Chem. **14**, 58 (2003)
51. Gradl, S.N., Felix, J.P., Isacoff, E.Y., Garcia, M.L., Trauner, D.J.: Am. Chem. Soc. **125**, 12668 (2003)
52. Fingar, V.H., Wieman, T.J., Haydon, P.S.: Photochem. Photobiol. **66**, 513 (1997)
53. Star, W.M., Marijnissen, H.P.A., van den Berg-Blok, A.E., Versteeg, J.A.C., Franken, K.A.P., Reinhold, H.S.: Cancer Res. **46**, 2532 (1986)
54. Wyss, P., Schwarz, V., Dobler-Girdziunaite, D., Hornung, R., Walt, H., Degen, A., Fehr, M.K.: Int. J. Cancer **93**, 720 (2001)
55. Sharman, W.M., Allen, C.M., van Lier, J.E.: Drug Discovery Today **4**, 507 (1999)
56. Wong, T.W., Aizawa, K., Sheyhedin, I., Wushur, C., Kato, H.J.: Pharmacol. Sci. **93**, 136 (2003)
57. Lau, J.T.F., Lo, P.-C., Fong, W.-P., Ng, D.K.P.: Chem. Eur. J. **17**, 7569 (2011)

58. Lau, J.T.F., Lo, P.-C., Tsang, Y.-M., Fong, W.-P., Ng, D.K.P.: Chem. Commun. **47**, 9657 (2011)
59. Liu, J.-Y., Lo, P.-C., Fong, W.-P., Ng, D.K.P.: Org. Biomol. Chem. **7**, 1583 (2009)
60. Zhao, Z.X., Chan, P.S., Li, H.G., Wong, K.L., Wong, R.N.S., Mak, N.K., Zhang, G., Tam, H.L., Wong, W.Y., Kwong, D.W.J., Wong, W.K.: Inorg. Chem. **51**, 812 (2012)
61. Howe, L., Zhang, J.Z.J.: Phys. Chem. A **101**, 3207 (1997)
62. Dhami, S., Cosa, J.J., Bishop, S.M., Philips, D.: Langmuir **12**, 293 (1996)
63. Li, X.-Y., Ng, A.C.H., Ng, D.K.P.: Macromolecules **33**, 2119 (2000)
64. Darwent, J.R., Douglas, P., Harroman, A., Porter, G., Richoux, M.C.: Coord. Chem. Rev. **44**, 83 (1982)
65. Wagner, J.R., Ali, H., Langlois, R., Brasseur, N., van Lier, J.E.: Photochem. Photobiol. **45**, 587 (1987)
66. McKeown, N.B. (ed.): Phthalocyanine materials: Synthesis, structure and function. Cambridge University Press, Cambridge (1998)
67. Lenzoff, C.C., Lever, A.B.P. (eds.): Phthalocyanines—properties and applications, Vol. 1–4. VCH, New York (1989–1996)
68. Choi, C.-F., Tsang, P.-T., Huang, J.-D., Chan, E.Y.M., Ko, W.-H., Fong, W.-P., Ng, D.K.P.: Chem. Commun. 2236 (2004)
69. Hamblin, M.R., Miller, J.L., Ortel, B.: Photochem. Photobiol. **72**, 533 (2000)
70. Rhainds, D., Falstrault, L., Tremblay, C., Brissette, L.: Eur. J. Biochem. **261**, 227 (1999)
71. Gauna, G.A., Marino, J., Vior, M.C.G., Roguin, L.P., Awruch, J.: Eur. J. Med. Chem. **46**, 5532 (2011)
72. Liu, J.-Y., Jiang, X.-J., Fong, W.-P., Ng, D.K.P.: Org. Biomol. Chem. **6**, 4560 (2008)
73. Liu, J.-Y., Lo, P.-C., Jiang, X.-J., Fong, W.-P., Ng, D.K.P.: Dalton Trans. **37**, 4129 (2009)
74. Oleinick, N.L., Antunez, A.R., Clay, M.E., Rihter, B.D., Kenney, M.E.: Photochem. Photobiol. **57**, 242 (1993)
75. Rywkin, R., Ben-Hur, E., Malik, Z., Prince, A.M., Li, Y.-S., Kenney, M.E., Oleinick, N.L., Horowitz, B.: Photochem. Photobiol. **67**, 332 (1998)
76. Jori, G.J.: Photochem. Photobiol. B **36**, 87 (1996)
77. Koo, Y.-E.L., Fan, W., Hah, H., Xu, H., Orringer, D., Ross, B., Rehemtulla, A., Phhilbert, M.A., Kopelman, R.: Appl. Opt. **46**, 1924 (2007)
78. McCarthy, J.R., Weissleder, R.: Adv. Drug Delivery Rev. **60**, 1241 (2008)
79. Verma, S., Watt, G.M., Mai, Z., Hasan, T.: Photochem. Photobiol. **83**, 996 (2007)
80. Stefflova, K., Chen, J., Zheng, G.: Front Biosci. **12**, 4709 (2007)
81. Vrouenraets, M.B., Visser, G.W.M., Stigter, M., Oppelaar, H., Snow, G.B., van Dongen, G.A.M.S.: Cancer Res. **61**, 1970 (2001)
82. Vrouenraets, M.B., Visser, G.W.M., Stigter, M., Oppelaar, H., Snow, G.B., van Dongen, G.A.M.S.: Int. J. Cancer **98**, 793 (2002)
83. Bamias, A., Dimopoulos, M.A.: Eur. J. Int. Med. **14**, 459 (2003)
84. Giancotti, F.G., Ruoslahti, E.: Science **285**, 1028 (1999)
85. Conway, C.L., Walker, I., Bell, A., Roberts, D.J.H., Brown, S.B., Vernon, D.I.: Photochem. Photobiol. Sci. **7**, 290 (2008)
86. Tirand, L., Frochot, C., Vanderesse, R., Thomas, N., Trinquet, E., Pinel, S., Viriot, M.-L., Guillemin, F., Barberi-Heyob, M.K.J.: Controlled Release **11**, 153 (2006)
87. Campbell, I.G., Jones, T.A., Foulkes, W.D., Trowsdale, J.: Cancer Res. **51**, 5329 (1991)
88. Jackman, A.L., Theti, D.S., Gibbs, D.D.: Adv. Drug Delivery Rev. **56**, 1111 (2004)
89. Schneider, R., Schmitt, F., Frochot, C., For, Y., Lourette, N., Guillemin, F., Müller, J., Barberi-Heyob, M.: Bioorg. Med. Chem. **13**, 2799 (2005)
90. Pottier, R., Bonneau, R., Joussot-Dubien, J.: Photochem. Photobiol. **22**, 59 (1975)
91. McDonnell, S.O., Hall, M.J., Allen, L.T., Byrne, A., Gallagher, W.M., O'Shea, D.F.J.: Am. Chem. Soc. **127**, 16360 (2005)
92. Yogo, T., Urano, Y., Mizushima, A., Sunahara, H., Inoue, T., Hirose, K., Iino, M., Kikuchi, K., Nagano, T.: Proc. Natl. Acad. Sci. U. S. A. **105**, 28 (2008)

93. Zheng, G., Chen, J., Stefflova, K., Jarvi, M., Li, H., Wilson, B.C.: Proc. Natl. Acad. Sci. U. S. A. **104**, 8989 (2007)
94. Chen, J., Lovell, J.F., Lo, P.-C., Stefflova, K., Niedre, M., Wilson, B.C., Zheng, G.: Photochem. Photobiol. Sci. **7**, 775 (2008)
95. Osterloh, J., Vicente, M.G.H.J.: Porphyrins Phthalocyanines **6**, 305 (2002)
96. Schellerer, K.-M., Brunner, H.: Inorg. Chim. Acta **350**, 39 (2003)
97. Mao JF; Zhang YM; Zhu JH; Zhang CL; Guo ZJ (2009) Chem. Commun. 908
98. Kopecek, J., Kopeckova, P., Minko, T., Lu, Z.R., Peterson, C.M.J.: Controlled Release **74**, 147 (2001)
99. Takeuchi, Y., Ichikawa, K., Yonezawa, S., Kurohane, K., Koishi, T., Nango, M.J.: Controlled Release **97**, 231 (2004)
100. Vargas, A., Pegaz, B., Debefve, E., Konan-Kouakou, Y., Lange, N., Ballini, J.P.: Int. J. Pharm. **286**, 131 (2004)
101. Ideta, R., Tasaka, F., Jang, W.D., Nishiyama, N., Zhang, G.D., Harada, A.: Nano Lett. **5**, 2426 (2005)
102. Jang, W.D., Nakagishi, N., Kawauchi, S., Morimoto, Y., Kikuchi, M.J.: Controlled Release **113**, 73 (2006)
103. Peng, C.-L., Shieh, M.-J., Tsai, M.-H., Chang, C–.C., Lai, P.-S.: Biomaterials **29**, 3599 (2007)
104. Peng, C.-L., Lai, P.-S., Lin, F.-H., Wu, S.Y.-H., Shieh, M.-J.: Biomaterials **30**, 3614 (2009)
105. Nonaka, M., Ikeda, H., Inokuchi, T.: Cancer Lett. **184**, 171 (2002)
106. Kirveliene, V., Grazeliene, G., Dabkeviciene, D., Micke, I., Kirvelis, D., Juodka, B., Didziapetriene, J.: Cancer Chemother. Pharm. **57**, 65 (2006)
107. Datta, S.N., Allman, W., Loh, C., Mason, M., Matthews, P.N.: Br. J. Cancer **76**, 312 (1997)
108. Serra, A., Pineiro, M., Pereira, N., Gonsalves, A.R., Laranjo, M., Abrantes, M., Botelho, F.: Oncol. Rev. **2**, 235 (2008)

Chapter 2
A Zinc(II) Phthalocyanine Conjugated with an Oxaliplatin Derivative for Dual Chemo- and Photodynamic Therapy

2.1 Introduction

As mentioned in Chap. 1, there has been considerable interest in combining photodynamic therapy (PDT) with other anticancer therapeutic methods. The combination of modalities that act on different disease pathways has shown several advantages, such as enhanced therapeutic efficacy, reduced side effects, and retarded drug-resistance problem [1]. For dual PDT and chemotherapy, there are generally three approaches, including sequential administration of a photosensitizer and an anticancer drug, the use of their covalent and non-covalent conjugates, and co-encapsulation of these agents in a polymeric nanocarrier. For some of the cases, additive or synergistic effects have been observed which can reduce the effective doses of anticancer drugs.

In light of the potential advantages of combined chemo- and PDT, we have been interested in studying phthalocyanine-based photosensitizers conjugated with platinum-based anticancer drugs. The latter have been widely used for the treatment of a variety of cancers through disruption of DNA in the nucleus [2, 3]. It is believed that the combination of these two components can embrace the advantages of the two very different therapeutic mechanisms and the resulting conjugates can exhibit synergistic anticancer effects. In this chapter, we report the preparation and in vitro photodynamic activities of such a conjugate, in which an oxaliplatin derivative is linked to a zinc(II) phthalocyanine core through a triethylene glycol spacer. The conjugate is highly potent of which the cytotoxicity is five-fold higher than that of the analogue without the platinum complex, demonstrating the cooperative effects of the two cytotoxic components.

J. T. F. Lau, *Towards Dual and Targeted Cancer Therapy with Novel Phthalocyanine-based Photosensitizers*, Springer Theses,
DOI: 10.1007/978-3-319-00708-3_2,

2.2 Results and Discussion

2.2.1 Molecular Design, Synthesis, and Characterization

In this conjugate, a zinc(II) phthalocyanine was employed as the photosensitizing unit due to its near-infrared fluorescence emission, high singlet oxygen generation efficiency, and high photostability [4–6]. Owing to the high therapeutic efficacy of oxaliplatin [2, 3, 7] a derivative of this drug was selected as the cytostatic part. The two components were linked with a triethylene glycol chain, which can enhance the amphiphilicity and biocompatibility of the system. Scheme 2.1 shows the synthetic route used to prepare this conjugate. Starting with the commercially available triethylene glycol (**2.1**), protection of one of the hydroxyl groups with 3,4-dihydropyran under an acidic condition afforded 2-[2-[2-(tetrahydropyranyl-oxy)ethoxy]ethoxy]-ethanol (**2.2**) [8]. This compound was then tosylated to give compound **2.3** [8], followed by substitution with sodium iodide in refluxing acetone to give 1-iodo-8-(tetrahydro-2*H*-pyran-2-yloxy)-3,6-dioxaoctane (**2.4**) [9]. It was then reacted with diethyl methylmalonate in the presence of NaH in *N*, *N*-dimethylformamide (DMF) to give compound **2.5**. The tetrahydropyranyl protecting group of **2.5** was then removed with concentrated sulfuric acid to give compound **2.6**. Nucleophilic aromatic substitution reaction of 4-nitrophthalonitrile with alcohol **2.6** afforded the substituted phthalonitrile **2.7**. This compound then underwent mixed cyclization with an excess of 1,2-dicyanobenzene in the presence of $Zn(OAc)_2{\cdot}2H_2O$ and 1,8-diazabicyclo [5.4.0] undec-7-ene (DBU) in *n*-pentanol to give the "3 + 1" unsymmetrical phthalocyanine **2.8** in 18 % yield. This compound was then hydrolyzed with NaOH in acetone to yield the carboxyl derivative **2.9**, which was further complexed with *trans*-(d,l)-1,2-diaminocyclohexanedinitratoplatinum(II) (**2.10**) [10] in an aqueous NaOH solution to give the phthalocyanine-platinum complex conjugate **2.11**. This compound was purified by flash column chromatography followed by recrystallization from a mixture of DMF and ethanol.

For comparison, two model compounds, phthalocyanine **2.14** and oxaliplatin analogue **2.17**, were also prepared. Scheme 2.2 shows the preparation of phthalocyanine **2.14**. Treatment of triethylene glycol monomethyl ether (**2.12**) with 4-nitrophthalonitrile in the presence of anhydrous potassium carbonate in DMF gave 4-(3,6,9-trioxadecyloxy)phthalonitrile (**2.13**) [11]. It was then treated with an excess of 1,2-dicyanobenzene and $Zn(OAc)_2{\cdot}2H_2O$ to afford the β-substituted phthalocyanine **2.14**. Scheme 2.3 shows the synthetic route for the preparation of oxaliplatin analogue **2.17**. *Trans*-(d,l)-1,2-diaminocyclohexane (**2.15**) underwent a ligand substitution reaction with potassium tetrachloroplatinate(II) in water to give dichloroplatinum(II) complex **2.16** in good yield. Silver nitrate was then used to precipitate the two chloro ligands to obtain dinitratoplatinum(II) complex **2.10**. *Trans*-(d,l)-1,2-diaminocyclohexane-malonatoplatinum(II) (**2.17**) was prepared by treating **2.10** with an aqueous solution of malonic acid and KOH [10]. All the new

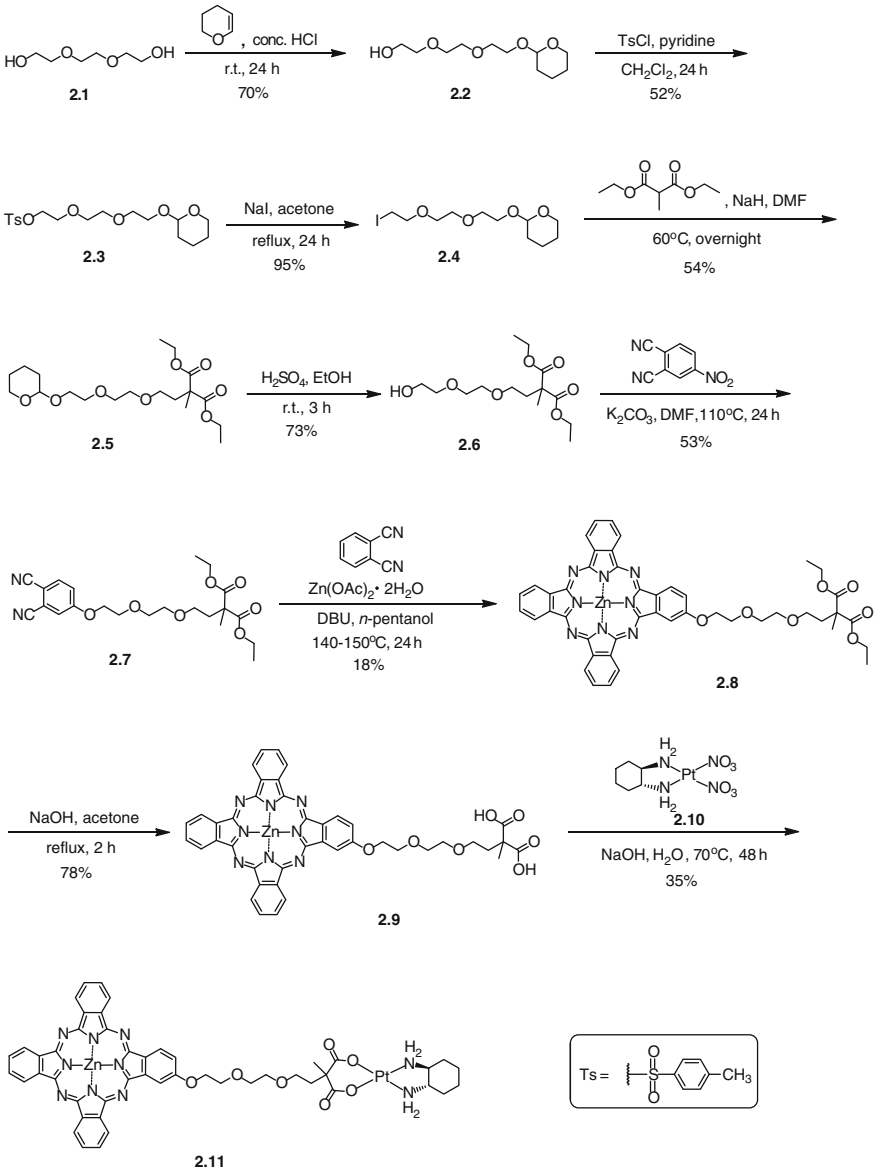

Scheme 2.1 Synthesis of phthalocyanine-platinum complex conjugate **2.11**

compounds were fully characterized with various spectroscopic methods and elemental analysis (for phthalocyanines **2.9**, **2.11**, and **2.14**) or accurate mass measurements (for phthalocyanine **2.8** and all the precursors).

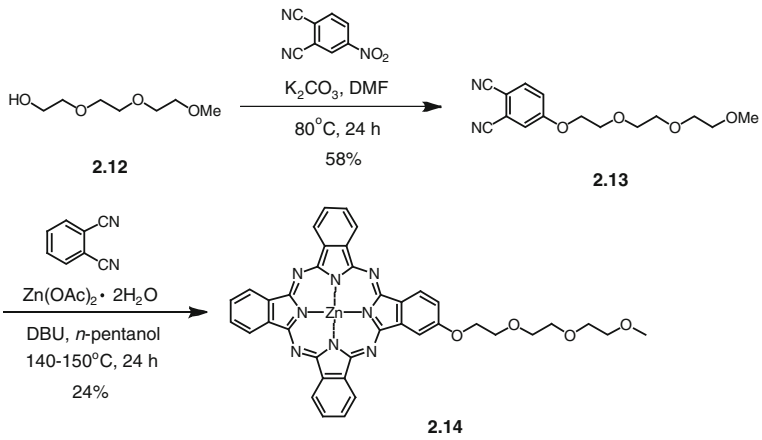

Scheme 2.2 Synthesis of phthalocyanine **2.14**

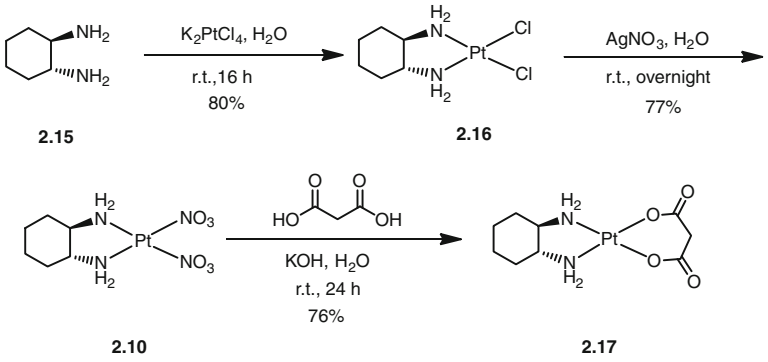

Scheme 2.3 Synthesis of *trans*-(d,l)-1,2-diaminocyclohexanemalonatoplatinum(II) (**2.17**)

2.2.2 Electronic Absorption and Photophysical Properties

The absorption spectrum of **2.11** in DMF was typical as the spectra for non-aggregated phthalocyanines (Fig. 2.1). It showed a B-band at 344 nm, two vibronic bands at 607 and 639 nm, and an intense and sharp Q-band at 672 nm, which strictly followed the Lambert–Beer's law. Upon excitation at 610 nm, the compound showed a fluorescence emission at 688 nm with a fluorescence quantum yield (Φ_F) of 0.22 relative to the unsubstituted zinc(II) phthalocyanine (ZnPc) ($\Phi_F = 0.28$) [12]. The spectral data of the reference compound **2.14** were very similar to those of **2.11**, except its slightly higher value of Φ_F (0.25) probably due to the absence of the heavy platinum complex (Fig. 2.2 and Table 2.1).

To evaluate the photosensitizing efficiency of these two compounds, their singlet oxygen quantum yields (Φ_Δ) were determined in DMF by a steady-state

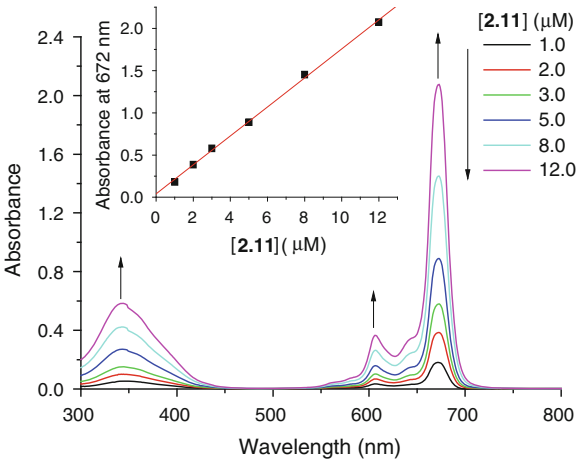

Fig. 2.1 Electronic absorption spectra of **2.11** in DMF in different concentrations. The inset plots the absorbance at 672 nm versus the concentration of **2.11**

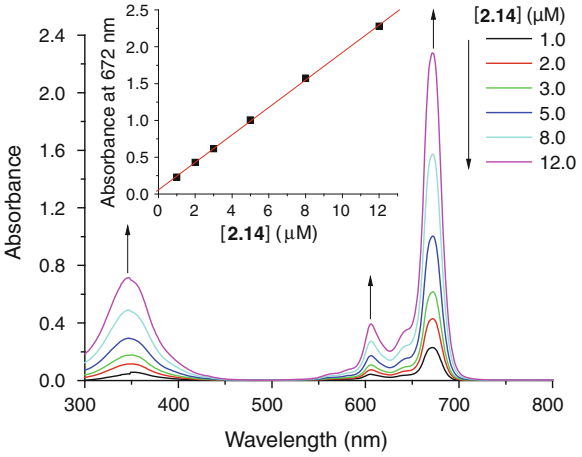

Fig. 2.2 Electronic absorption spectra of **2.14** in DMF in different concentrations. The inset plots the absorbance at 672 nm versus the concentration of **2.14**

Table 2.1 Electronicabsorption and photophysical data for **2.11** and **2.14** in DMF

Compound	λ_{max} (nm) (log ε)	λ_{em}(nm)[a]	Φ^{b}_{F}	Φ^{c}_{Δ}
2.11	344 (4.69), 607 (4.48), 639 (4.42), 672 (5.23)	688	0.22	0.56
2.14	347 (4.78), 606 (4.50), 639 (4.42), 672 (5.27)	688	0.25	0.57

[a] Excited at 610 nm
[b] Using ZnPc in DMF as the reference ($\Phi_F = 0.28$)
[c] Using ZnPc as the reference ($\Phi_\Delta = 0.56$ in DMF)

method with 1,3-diphenylisobenzofuran (DPBF) as the scavenger. The concentration of the quencher was monitored spectroscopically at 411 nm with time of irradiation (Fig. 2.3), from which the values of Φ_Δ could be determined by the

method described previously [13]. The results showed that both compounds are highly efficient singlet oxygen generators and the values of Φ_Δ were virtually identical to that of ZnPc ($\Phi_\Delta = 0.56$) (Table 2.1).

2.2.3 *In Vitro Photodynamic Activities*

The cytotoxic effects of conjugate **2.11** in a Cremophor EL emulsion were then investigated. The surfactant was added to solubilize the compound in water and reduce its aggregations. Since oxaliplatin is one of the most important chemotherapeutic drugs in colorectal cancer treatment [7], HT29 human colon adenocarcinoma cells were used for these studies. In order to reveal the photo- and chemo-cytotoxic effects of **2.11**, the antiproliferative properties of the two reference compounds **2.14** and **2.17** were also examined. Figure 2.4 shows the dose-dependent survival curves for these compounds. It can be seen in Fig. 2.4a that the non-platinum-containing phthalocyanine **2.14** does not show any dark toxicity up to 100 μM. However, upon illuminating with red light ($\lambda > 610$ nm), it shows substantial cytotoxicity with an IC_{50} value, defined as the dye concentration required to kill 50 % of the cells, of 0.55 μM (Fig. 2.4b, Table 2.2). The oxaliplatin analogue **2.17** exhibits cytostatic activity both in the absence and presence of light, and the corresponding IC_{50} values are 10.7 and 5.5 μM, respectively. It is interesting to note the enhanced cytotoxicity under illumination. The actual mechanism however remains elusive at this stage. Having a photosensitizer and a chemotherapeutic drug in the same molecule, conjugate **2.11** is highly photocytotoxic. The IC_{50} value is as low as 0.11 μM, which is five-fold lower than that of **2.14**. In fact, this conjugate is much more potent than the classical photosensitizer porfimer sodium, which has an IC_{50} value of 4.5 μg mL^{-1} under the same experimental conditions (vs. 0.12 μg mL^{-1} for **2.11**). Its cytotoxicity is also

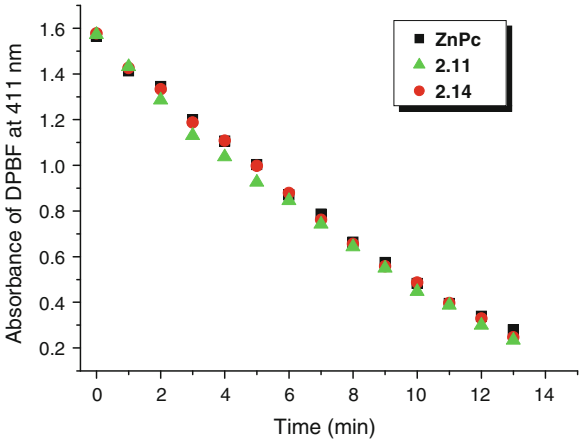

Fig. 2.3 Comparison of the rate of decay of DPBF (initial concentration = 70 μM) sensitized by **2.11**, **2.14**, or **ZnPc** (all at 3 μM) in DMF as shown by the decrease in the absorbance at 411 nm

significantly higher than that of oxaliplatin and some of its derivatives, of which the IC_{50} values are in the range of 2–30 μg mL^{-1} [14]. Conjugate **2.11** also exhibits some dark toxicity (IC_{50} = 78.5 μM), which can be attributed to the oxaliplatin moiety as **2.14** is nontoxic under these conditions. As a better control, the cytotoxicity of an equimolar mixture of **2.14** and **2.17** was also studied and compared with that of **2.11**. It can be seen in Fig. 2.4b and Table 2.2 that the mixture is relatively more potent than **2.14** alone (IC_{50} = 0.42 vs. 0.55 μM) probably due to the additional antitumor effect of the oxaliplatin derivative. However, its photocytotoxicity is still significantly lower than that of **2.11** (IC_{50} = 0.42 vs. 0.11 μM). The results clearly show that the two antitumor components in conjugate **2.11** work in a cooperative fashion.

Considering the fact that the aggregation state of photosensitizers is an important factor relating to their photodynamic activities,[4–6] the aggregation behavior of conjugate **2.11** and the reference compound **2.14**, formulated with Cremophor EL, in the Dulbecco's modified Eagle's medium (DMEM) was

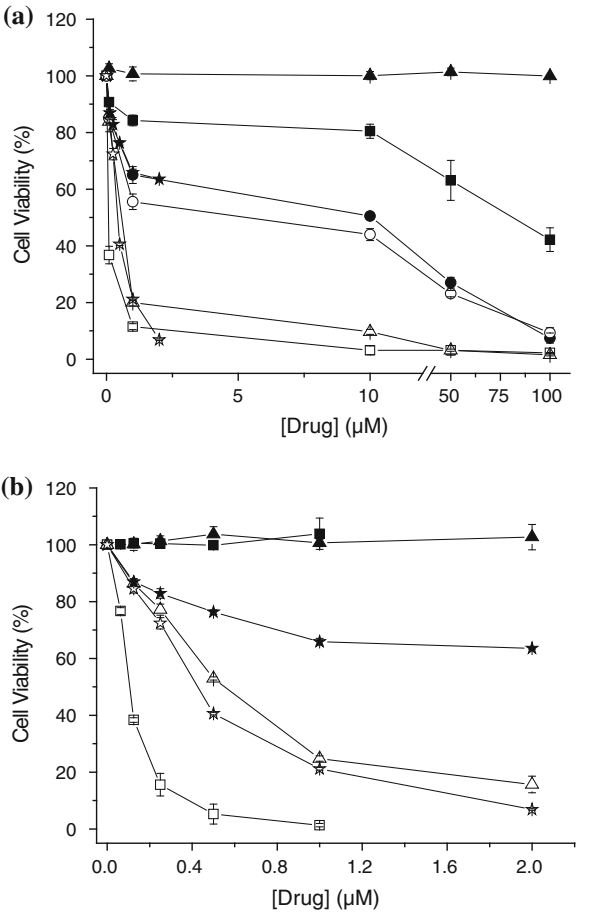

Fig. 2.4 **(a)** Comparison of the cytotoxic effects of **2.11** (*squares*), **2.14** (*triangles*), **2.17** (*circles*), and an equimolar mixture of **2.14** and **2.17** (*stars*) on HT29 cells in the absence (*closed symbols*) and presence (*open symbols*) of light ($\lambda > 610$ nm, 40 mW cm^{-2}, 48 J cm^{-2}). Data are expressed as mean value ± standard error of the mean (S.E.M.) of three independent experiments, each performed in quadruplicate. Figure **(b)** shows the data for **2.11** (*squares*), **2.14** (*triangles*), and an equimolar mixture of **2.14** and **2.17** (*stars*) in the range up to 2.0 μM. (*The conditions for the present experiments have been described in* Sects. 7.1.4 *and* 7.2.2. *Experimental details regarding all in vitro studies in this thesis can be found in* Chap. 7)

Table 2.2 IC_{50} values for **2.11**, **2.14**, **2.17**, and an equimolar mixture of **2.14** and **2.17** against HT29 cells

Compound	$IC^{d}_{50}(\mu M)$	
	In Dark	With Light
2.11	78.5	0.11
2.14	–[e]	0.55
2.17	10.7	5.5
1:1 mixture of **2.14** and **2.17**	–[f]	0.42

[d] Defined as the dye concentration required to kill 50 % of the cells
[e] Non-cytotoxic up to 100 μM
[f] Not determined

examined by absorption and fluorescence spectroscopic methods. As shown in Fig. 2.5, both compounds show a relatively sharp and intense Q-band, and a relatively strong fluorescence emission. The results suggest that both compounds are not significantly aggregated under these conditions, which seems to be in accord with their high photocytotoxicity.

To account for the different photocytotoxicity of these two compounds, their cellular uptake was examined by fluorescence microscopy and absorption spectroscopy. As shown by the images captured by confocal laser scanning microscopy (Fig. 2.6a), both compounds could enter into the cells causing intracellular fluorescence after incubation for 2 h. The average relative fluorescence intensity per cell of these compounds was also measured and compared in Fig. 2.6b. It can be seen that the intracellular fluorescence intensity of **2.11** is about five-fold lower than that of **2.14**. However, to take into account that these two compounds may have different efficiency in generating fluorescence inside the cells, an extraction method was also employed to quantify the cellular uptake. After incubation with these phthalocyanines, the cells were washed and DMF was used to lyse the cells and extract the dyes. The dye concentrations inside the cells were quantified by measuring their Q-band absorbance at 672 nm. The results are depicted in Fig. 2.6c, which shows that the cellular uptake of **2.11** is actually about seven-fold higher than that of **2.14**. The presence of the oxaliplatin derivative in **2.11** may enhance the amphiphilicity of the overall compound, thereby promoting the cellular uptake. The higher cellular uptake of **2.11** is in accord with its higher photocytotoxicity.

In addition, the intracellular production of ROS by these compounds was also studied using 2′,7′-dichlorodihydrofluorescein diacetate (DCFDA) as the quencher [15]. DCFDA (see structure in the next page) is a fluorescent probe for visualizing oxidative stress in living cells. When DCFDA is taken up by cells, it undergoes deacetylation by esterase enzymes. Oxidation of the deacetylated product by the nearby ROS leads to the formation of 2′,7′-dichlorofluorescein, which can be visualized with its strong emission at 525 nm when excited at 488 nm. There are two ways to produce intracellular ROS during the PDT process: (1) during PDT by the photosensitizer and (2) after PDT by the cells. In this study, by including DCFDA in the assay mixture during the illumination period, a direct production of

ROS by the drugs was demonstrated. As shown in Fig. 2.7, both **2.11** and **2.14** as well as the mixture of **2.14** and **2.17** can sensitize the production of ROS upon illumination. Conjugate **2.11** is the most efficient compound in producing intracellular ROS, which may be a result of its higher cellular uptake. Since the oxaliplatin derivative **2.17** is not a photosensitizer, it is expected that it does not produce any ROS even after illumination. The ROS production efficiencies of **2.14** and the mixture of **2.14** and **2.17** are therefore comparable to each other. All these results suggest that the higher photocytotoxicity of conjugate **2.11** can be attributed to its low aggregation tendency and higher cellular uptake and efficiency in generating intracellular ROS.

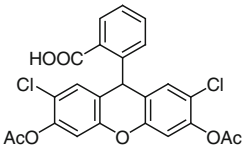

2',7'-dichlorodihydrofluorescein diacetate (DCFDA)

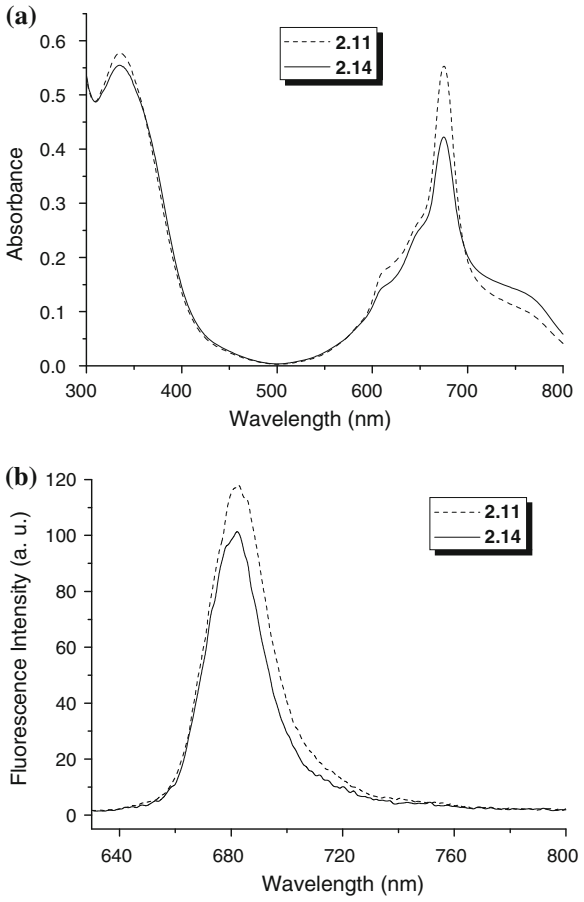

Fig. 2.5 **(a)** Electronic absorption and **(b)** fluorescence spectra ($\lambda_{ex} = 610$ nm) of **2.11** (*dashed line*) and **2.14** (*straight line*), formulated with Cremophor EL, in the DMEM (both at 8 μM)

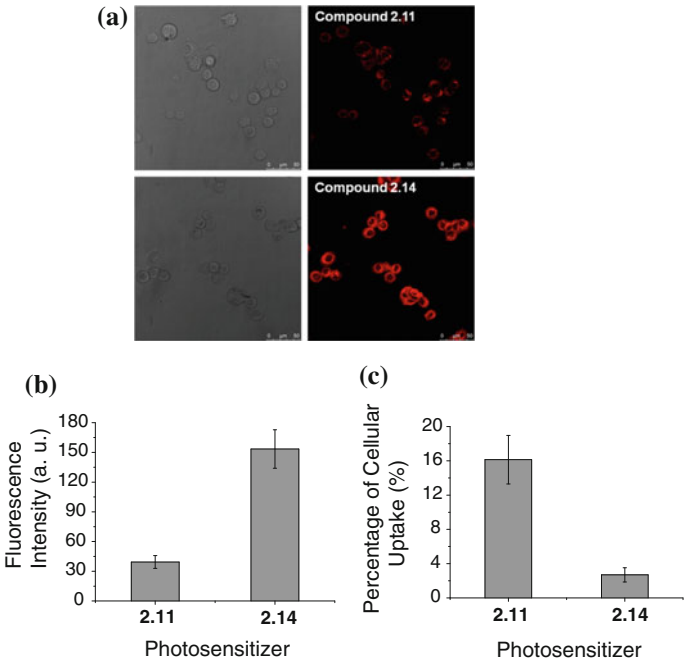

Fig. 2.6 **(a)** Confocal fluorescence images of HT29 cells after incubation with **2.11** or **2.14** for 2 h (both at 5 μM). The corresponding bright field images are given in the left column. **(b)** Comparison of the relative intracellular fluorescence intensity of **2.11** and **2.14** (number of cells = 30). **(c)** Comparison of the percentage of cellular uptake of **2.11** and **2.14** as determined by an extraction method. Data are expressed as mean value ± standard deviation (S.D.) of three independent experiments

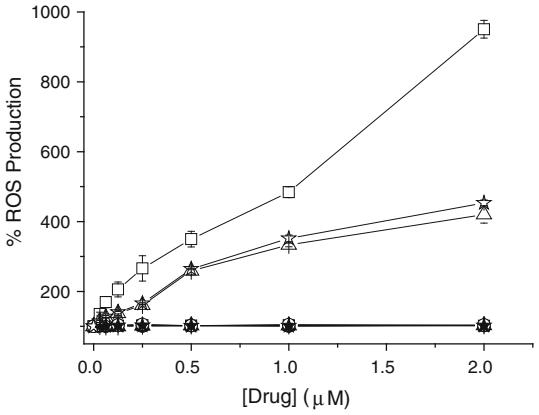

Fig. 2.7 ROS production induced by **2.11** (*squares*), **2.14** (*triangles*), **2.17** (*circles*), and an equimolar mixture of **2.14** and **2.17** (*stars*) in HT29 cells in the absence (*closed symbols*) and presence (*open symbols*) of light ($\lambda > 610$ nm, 40 mW cm^{-2}, 48 J cm^{-2}). Data are expressed as mean value ± S.E.M. of three independent experiments, each performed in quadruplicate

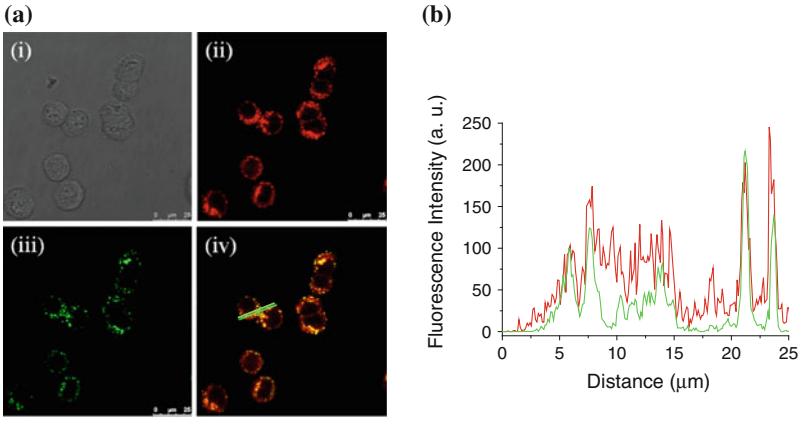

Fig. 2.8 **(a)** Visualization of (i) the bright field image, intracellular fluorescence of HT29 using filter sets specific for (ii) **2.11** (5 μM; in red) and (iii) LysoTracker (in green), and (iv) the corresponding superimposed image. Figure **(b)** shows the fluorescence intensity profiles of **2.11** (*red*) and LysoTracker (*green*) traced along the *green line* in Figure (**a**) (iv)

The subcellular localization of conjugate **2.11** was also investigated. The cells were first incubated with the compound in the culture medium for 2 h, then stained with LysoTracker Green DND-26, ER-Tracker Green, MitoTracker Green FM, or SYTO-16 (for 10–20 min), which are specific dyes for lysosomes, endoplasmic reticulum, mitochondria, and nucleus, respectively. As shown in Fig. 2.8, the fluorescence caused by the LysoTracker (excited at 488 nm, monitored at 510–570 nm) can superimpose with the fluorescence caused by **2.11** (excited at 633 nm, monitored at 650–750 nm). The very similar fluorescence intensity line profiles of **2.11** and LysoTracker traced along the green line in Fig. 2.8a (iv) also confirms that **2.11** can target the lysosomes of the cells. By contrast, the fluorescence images of **2.11** could not be merged with those of the ER-Tracker, MitoTracker, and SYTO-16 (excited at 488 nm, monitored at 510–570 nm) (Fig. 2.9), showing that **2.11** is not localized in the endoplasmic reticulum, mitochondria, and nucleus of the cells.

It has been reported that PDT is a strong inducer of apoptosis in many situations [16]. The earliest hallmark of apoptosis is the loss of plasma membrane asymmetry. In apoptotic cells, the membrane phospholipid phosphatidylserine is translocated from the inner to outer leaflet of the plasma membrane, thus exposing phosphatidylserine to the external cellular environment. Annexin V-green fluorescent protein (GFP) has high affinity for phosphatidylserine and therefore serves as a sensitive probe for identifying apoptotic cells [17]. Generally, annexin V-GFP is costained together with propidium iodide (PI), which is a fluorescent probe to distinguish viable cells from dead cells, as the former with intact membranes exclude PI. We studied the mode of cell death induced by **2.11** by examining the

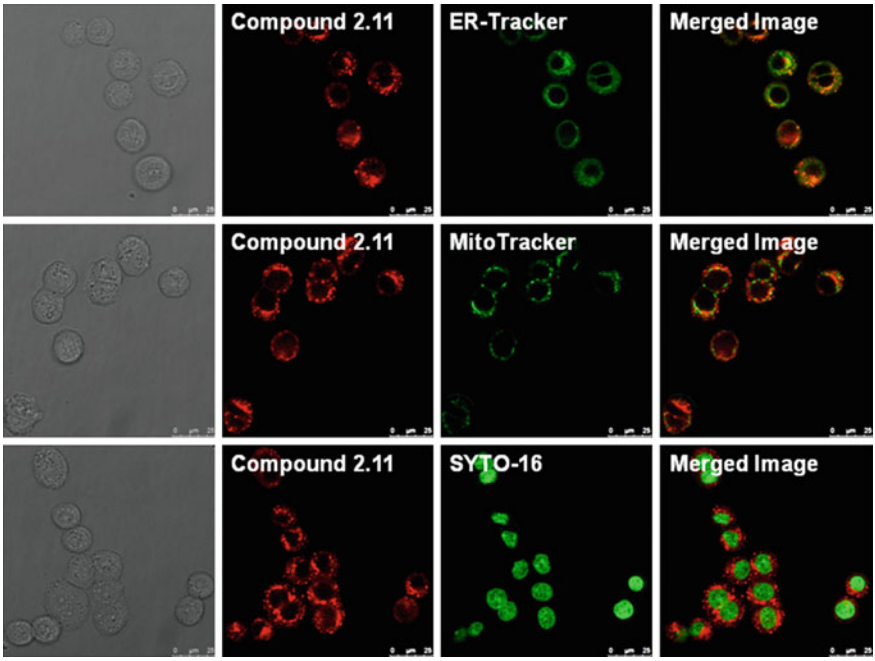

Fig. 2.9 Visualization of the bright field images (column 1), intracellular fluorescence of HT29 using filter sets specific for **2.11** (5 μM; column 2, in *red*) and ER-Tracker, MitoTracker, or SYTO-16 (column 3, in *green*), and the corresponding superimposed images (column 4)

dual fluorescence of annexin V-GFP/PI using flow cytometry. In order to find out whether the introduction of the oxaliplatin derivative will alter the cell death mechanism, the results for **2.14** and **2.17** were also compared. The cell populations in different phases of cell death, namely viable (annexin V-GFP$^-$/PI$^-$), early apoptotic (annexin V-GFP$^+$/PI$^-$), and necrotic or late-stage apoptotic (annexin V-GFP$^+$/PI$^+$) were examined at the respective IC_{50} values of the drugs. The only exception was for **2.14** in the dark for which the IC_{50} value could not be determined, a dye concentration of 100 μM was used for the measurements. As shown in Table 2.3, when the cells were treated with **2.11** or **2.14** in the presence of light, about 50 % of apoptotic cells and less than 10 % of necrotic cells were observed. Compound **2.11** also exhibited a significant dark toxicity, showing 41 % of apoptotic cells and 9 % of necrotic cells after the treatment due to the oxaliplatin derivative. For **2.14** in the dark, more than 95 % of the tumor cells remained viable even at 100 μM. The oxaliplatin derivative **2.17** could induce apoptotic as well as necrotic cells, both in the absence and presence of light. The results showed that apoptosis is the major pathway for the PDT action of **2.11** and the presence of the oxaliplatin derivative does not significantly affect the cell death pathways.

Table 2.3 Flow cytometric analysis of the cell death mechanism induced by **2.11**, **2.14**, and **2.17** at their respective IC_{50} values in the absence and presence of light ($\lambda > 610$ nm, 40 mW cm^{-2}, 48 J cm^{-2}) on HT29 cells. Data are expressed as mean value ± S.D. of three independent experiments

	Drug (μM)	Illumination	Cell population (%)		
			Viable	Early apoptotic	Late apoptotic/necrotic
Blank	0	–	95.0 ± 1.2	3.3 ± 0.5	1.2 ± 0.3
2.11	0.11	+	36.5 ± 1.1	54.2 ± 2.9	8.4 ± 1.6
	78	–	48.9 ± 1.5	41.0 ± 1.2	9.3 ± 0.7
2.14	0.55	+	44.9 ± 1.9	50.2 ± 1.9	4.4 ± 0.7
	100[g]	–	95.3 ± 1.8	2.2 ± 1.5	2.1 ± 1.2
2.17	5.5	+	45.2 ± 4.8	41.4 ± 1.8	13.0 ± 3.1
	10.7	–	53.8 ± 3.5	25.7 ± 3.0	19.9 ± 0.6

[g] The IC_{50} value could not be determined

2.3 Summary

In summary, we have synthesized and characterized a zinc(II) phthalocyanine-platinum complex conjugate and evaluated its in vitro photodynamic activities. This conjugate contains both photo- and chemotherapeutic agents which are covalently linked and function in a cooperative manner. The introduction of the oxaliplatin derivative can enhance the cellular uptake and intracellular ROS generation efficiency of the phthalocyanine unit, resulting in a higher cytotoxicity. The IC_{50} value of the conjugate is as low as 0.11 μM toward the HT29 cells, which is five-fold lower than that of the reference compound without the oxaliplatin derivative. The conjugate also shows preferential localization in the lysosomes of the cells and induces cell death mainly through apoptosis. The overall results show that this conjugate is a highly promising antitumor agent for dual chemo- and photodynamic therapy.

References

1. Zuluaga, M.-F., Lange, N.: Curr. Med. Chem. **15**, 1655 (2008)
2. Wong, E., Giandomenico, C.M.: Chem. Rev. **99**, 2451 (1999)
3. Kelland, L.: Nat. Rev. Cancer **7**, 573 (2007)
4. Liu, J.-Y., Lo, P.-C., Fong, W.-P., Ng, D.K.P.: Org. Biomol. Chem. **7**, 1583 (2009)
5. Liu, J.-Y., Jiang, X.-J., Fong, W.-P., Ng, D.K.P.: Org. Biomol. Chem. **6**, 4560 (2008)
6. Liu, J.-Y., Lo, P.-C., Jiang, X.-J., Fong, W.-P., Ng, D. K. P.: Dalton Trans. **2009**, 4129 (2009)
7. Stein, A., Arnold, D.: Expert Opin. Pharmacother. **13**, 125 (2012)
8. Richard, A., Bourel-Bonnet, L.: Chem. Eur. J. **11**, 7315 (2005)
9. Loiseau, F.A., Hill, A.M., Hii, K.K.: Tetrahedron **63**, 9947 (2007)
10. Wyrick, S.D., Chaney, S.G.J.: Labelled Compd. Radiopharm. **25**, 349 (1988)
11. Erdem, S.S., Nesterova, I.V., Soper, S.A., Hammer, R.P.J.: Org. Chem. **73**, 5003 (2008)
12. Scalise, I., Durantini, E.N.: Bioorg. Med. Chem. **13**, 3037 (2005)

13. Maree, M.D., Kuznetsova, N., Nyokong, T.: J Photochem. Photobiol. A **140**, 117 (2001)
14. Al-Allaf, T.A.K., Rashan, L.J., Ketler, G., Fiebig, H.-H., Al-Dujaili, A.H.: Appl. Organometal. Chem. **23**, 173 (2009)
15. Shen, H.M., Shi, C.Y., Shen, Y., Ong, C.N.: Free Radical Biol. Med. **21**, 139 (1996)
16. Oleinick, N.L., Morris, R.L., Belichenko, I.: Photochem. Photobiol. Sci. **1**, 1 (2002)
17. Vermes, I., Haanen, C., Steffens-Nakken, H., Reutelingsperger, C.J.: Immunol. Methods **184**, 39 (1995)

Chapter 3
Zinc(II) Phthalocyanine-Polyamine Conjugates as Efficient Photosensitizers for Photodynamic Therapy

3.1 Introduction

One of the major imperfections of photodynamic therapy (PDT) is the nonselective delivery of photosensitizers to both targeted tumor and healthy cells. It frequently leads to necrosis of surrounding healthy tissues along with a cutaneous photosensitivity that may last for several weeks after treatment. As a result, targeted delivery of photosensitizers to cancer cells appears to be a viable means to circumvent these problems. It could alleviate associated toxicity of the photosensitizers by reducing their uptake by healthy cells. In addition, it could increase efficiency of PDT by lowering the effective dosage required to kill the tumor cells. Over the past decade, various strategies have been explored to enhance the tumor selectivity of photosensitizers. These include encapsulation of photosensitizers in liposomes [1], polymeric micelles [2, 3], and silica-based nanoparticles [4], and bioconjugation of photosensitizers to various tumor-specific vehicles, such as epidermal growth factor, adenoviral proteins, and monoclonal antibodies [5, 6]. Photodynamic molecular beacons and activatable photosensitizers that can be activated by tumor-associated stimuli are also highly promising ways to achieve targeted PDT [7–9].

Polyamines, such as spermine, spermidine, and putrescine (see structures in Fig. 3.1) play crucial roles in a number of cell processes including cell proliferation and differentiation [10–12]. Rapidly dividing cells such as tumor cells require large amounts of polyamines to sustain rapid cell division. They can either be internally biosynthesized or imported from exogenous sources through specific polyamine transporters (PAT). In fact, a wide variety of tumor types ranging from neuroblastoma, melanoma, human lymphocytic leukemia to murine L1210 cells, have been shown to contain elevated polyamine levels and active PAT for importing exogenous polyamines [13]. Based on the high demand for these biological growth factors by the highly proliferating tumor cells, vectorization of chemotherapeutic and DNA-targeting drugs by polyamines will be another attractive approach for targeted delivery. To date, a substantial number of polyamine-containing cytotoxic drugs, such as chlorambucil [14, 15], nitroimidazole

J. T. F. Lau, *Towards Dual and Targeted Cancer Therapy with Novel Phthalocyanine-based Photosensitizers*, Springer Theses,
DOI: 10.1007/978-3-319-00708-3_3,

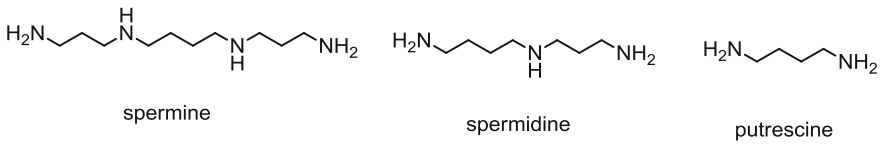

Fig. 3.1 Structures of naturally occurring polyamines

[16], aziridine [17, 18], acridine [19, 20], paclitaxel [21], and camptothecin [22, 23], have been synthesized with improved tumor selectivity and/or enhanced therapeutic efficacies. Several polyamine-appended porphyrin- and chlorin-based photosensitizers have also been prepared with their in vitro phototoxicity briefly examined [24–28].

By virtue of specific molecular recognition events occurred during the importation of exogenous polyamines through the PAT system, tethering polyamines to phthalocyanine-based photosensitizers will be a possible way toward targeted PDT. Recently, Ng et al. [29] have reported a series of silicon(IV) phthalocyanines substituted axially with a range of polyamines with different lengths and spacers between the nitrogen centers. All these compounds are highly photocytotoxic against human colon adenocarcinoma HT29 cells and Chinese hamster ovary (CHO) cells. Some of them can effectively inhibit the growth of the tumor of HT29 tumor-bearing nude mice. However, experiments show that the cellular uptake of these phthalocyanines may not involve the PAT of the cells. Early studies suggested that small structural changes could lead to dramatic differences in the transport behavior of polyamine analogues [19, 20]. In order to enhance the selectivity of the photosensitizers to PAT active tumor cells, we extend our study by introducing a new series of polyamine moieties with different lengths and spacers between the nitrogen centers to zinc(II) phthalocyanine. Unlike the polyamine analogues adopted in our previous study, these polyamine moieties do not contain any methyl groups at the nitrogen atoms and show stronger resemblance to the naturally occurring polyamines (Fig. 3.1). This chapter describes the synthesis, photophysical properties, and in vitro photodynamic activities of these zinc(II) phthalocyanine-polyamine conjugates.

3.2 Results and Discussion

3.2.1 Preparation and Characterization

The zinc(II) phthalocyanine-polyamine conjugates were synthesized starting from a series of *tert*-butoxycarbonyl (Boc) protected hydroxyamines (**3.2a–b** and **3.7a–b**). These compounds were prepared according to the synthetic strategies as described by Phanstiel and co-workers [30]. Scheme 3.1 shows the synthetic route for hydroxyamines **3.2a–b**. Treatment of the commercially available 2-aminoethanol

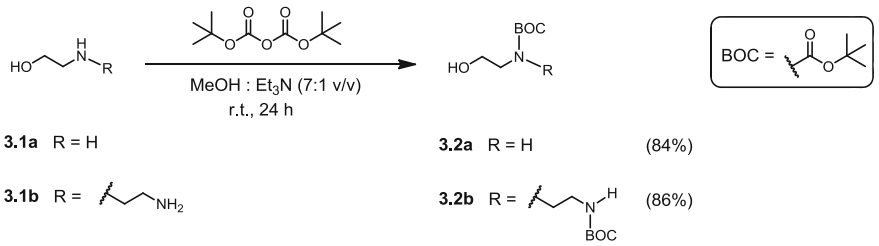

Scheme 3.1 Synthesis of *N*-Boc protected hydroxyamines **3.2a–b**

(**3.1a**) or 2-(2-aminoethylamino)ethanol (**3.1b**) with di-*tert*-butyl dicarbonate in a mixture of methanol and triethylamine (Et_3N) gave **3.2a–b**. The preparation of hydroxyamines **3.7a–b** involved a modular approach for the introduction of varying chain lengths between the nitrogen centers (Scheme 3.2). It was commenced with a typical *N*-Boc protection of 3-amino-1-propanol (**3.3a**) or 4-amino-1-butanol (**3.3b**) with di-*tert*-butyl dicarbonate to afford **3.4a–b**, followed by *O*-sulfonylation to obtain compounds **3.5a–b**. These compounds then underwent mesylate displacement reactions with **3.3a–b** to afford **3.6a–b**. Further *N*-Boc protection of the internal amino groups gave *N*-Boc protected hydroxyamines **3.7a–b** in satisfactory yields.

Zinc(II) phthalocyanines are promising second-generation photosensitizers for PDT because of their general robustness and desirable photophysical properties [31]. In addition, appropriate substituents could be grafted at their peripheral positions to adjust their amphiphilicity, reduce their aggregation tendency, and enhance tumor selectivity. We therefore conjugated the polyamines moieties to a zinc(II) phthalocyanine core. Scheme 3.3 shows the synthetic pathway for the

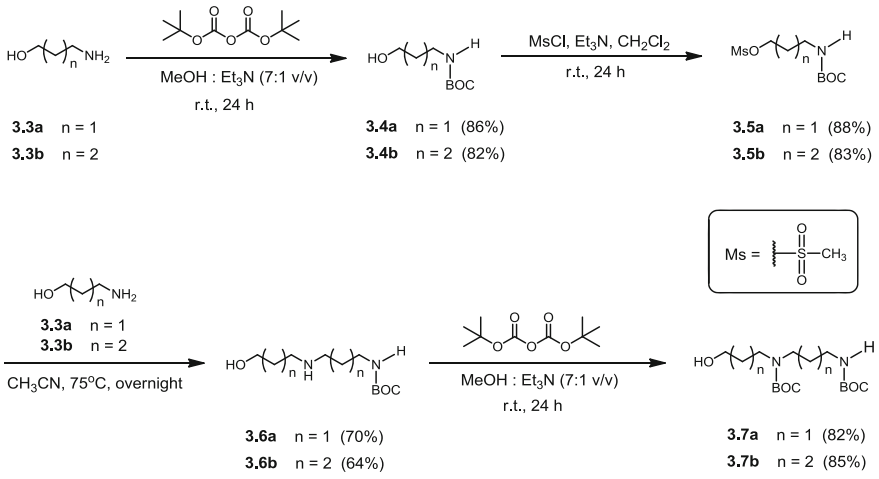

Scheme 3.2 Synthesis of *N*-Boc protected hydroxyamines **3.7a–b**

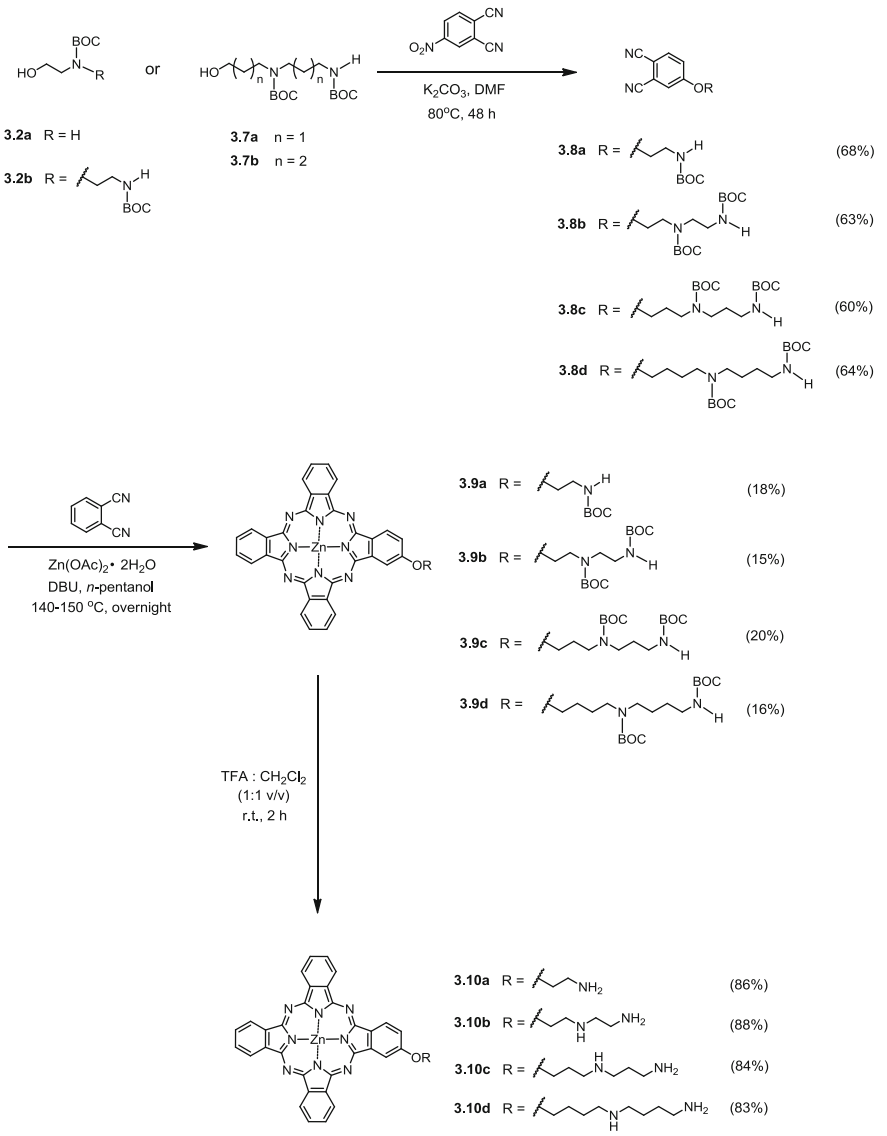

Scheme 3.3 Synthesis of phthalocyanine-polyamines conjugates **3.10a–d**

preparation of these phthalocyanine-polyamine conjugates. Nucleophilic aromatic substitution reaction of 4-nitrophthalonitrile with *N*-Boc protected hydroxyamines **3.2a**–**b** and **3.7a**–**b** in *N*,*N*-dimethylformamide (DMF) afforded the substituted phthalonitriles **3.8a–d**. These compounds then underwent mixed cyclization with an excess of 1,2-dicyanobenzene in the presence of $Zn(OAc)_2{\cdot}2H_2O$ and 1,8-diazabicyclo[5.4.0]undec-7-ene (DBU) in *n*-pentanol to give the "3 + 1"

unsymmetrical *N*-Boc protected phthalocyanines **3.9a–d**. These polyamine moieties could enhance the solubility and reduced the aggregation of these macrocycles, facilitating their separation from the other cyclized side products, particularly the unsubstituted zinc(II) phthalocyanine (ZnPc), which was found to be the major product. Hence, these β-substituted phthalocyanines could be isolated readily by silica-gel column chromatography followed by size exclusion chromatography in 16–20 % yield. Phthalocyanines **3.10a–d** were obtained subsequently after *N*-Boc deprotection with a mixture of trifluoroacetic acid (TFA) and dichloromethane.

All the zinc(II) phthalocyanines **3.9a–d** and **3.10a–d** were fully characterized with various spectroscopic methods. The ^{1}H NMR spectra of **3.9a–d** were recorded in $CDCl_3$ with a trace amount of pyridine-d_5 to reduce their aggregation. The spectra show signals at δ 8.82–9.32 (6H), 8.35–9.04 (1H), and 8.07–8.90 (1H) for the phthalocyanine α-ring protons together with signals resonated at δ 7.83–8.08 (6H) and 7.04–7.55 (1H) for the phthalocyanine β-ring protons. The methylene protons on the polyamine chains are widely spread from δ 1.61 to 4.58. The signals for the methyl protons of the *N*-Boc groups appear as one (for **3.9a**) or two (for **3.9b–d**) strong singlet(s) between δ 1.41–1.61. For the deprotected analogues **3.10a–d**, the ^{1}H NMR spectra were recorded in pyridine-d_5. The spectra are similar to those of **3.9a–d** in which the eight α- and seven β-ring protons of the phthalocyanine are resonated at δ 7.71–9.76, while the methylene protons on the polyamine chains are widely spread from δ 1.03 to 4.76. However, the signals for the methyl protons of the *N*-Boc moieties are absent, indicating that all the amino groups are deprotected completely.

The ESI mass spectra of all these phthalocyanines showed the molecular ion signals. Accurate mass measurements were also performed to confirm the identity of these compounds. The experimental values were in good agreement with the theoretical values for all the cases as shown in the Experimental Sect. 7.3).

3.2.2 Electronic Absorption and Photophysical Properties

The electronic absorption spectra of phthalocyanines **3.9a–d** and **3.10a–d** are very similar and typical for non-aggregated phthalocyanines. It is likely that DMF, being a coordinating solvent, binds axially to these zinc(II) phthalocyanines, reducing their aggregation tendency. Figure 3.2 shows the spectra of the *N*-Boc protected phthalocyanine **3.9d** and the deprotected analogue **3.10d** for exemplification. They show a broad B-band peaking at 344–349 nm, an intense and sharp Q-band at 672–673 nm, together with a vibronic band at 606–608 nm. The Q-band strictly follows the Lambert–Beer's law suggesting that aggregation of these compounds is not significant. The very similar spectral features of the *N*-Boc protected and the deprotected series indicate that the phthalocyanine π systems are not perturbed by the presence of the *N*-Boc groups. These data are summarized in Table 3.1.

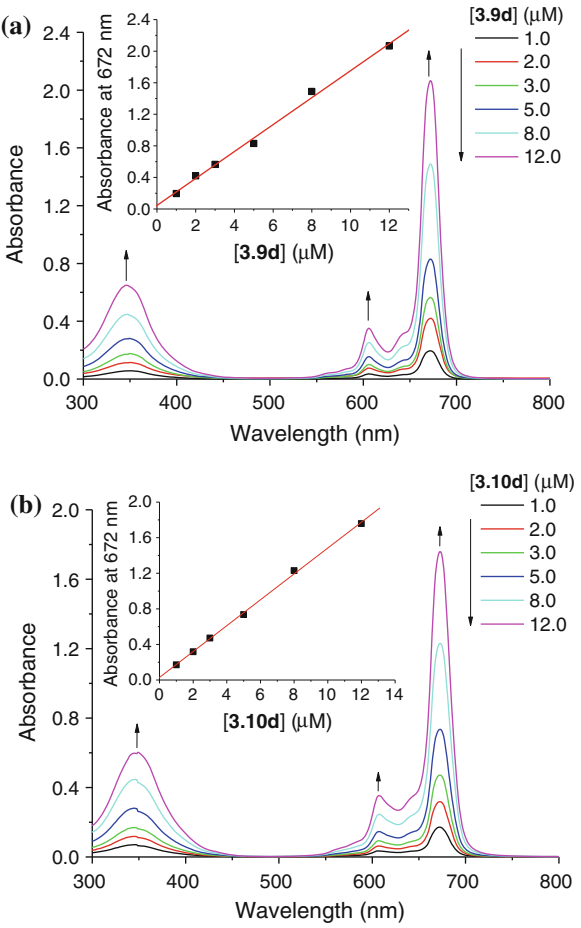

Fig. 3.2 Electronic absorption spectra of (**a**) **3.9d** and (**b**) **3.10d** in different concentrations in DMF. The inset plots the Q-band absorbance versus the concentration of the phthalocyanine, and the line represents the best-fitted straight line

Table 3.1 Electronic absorption and photophysical data for **3.9a–d** and **3.10a–d** in DMF

Compound	λ_{max} (nm) (log ε)	λ_{em}(nm)[a]	Φ^{b}_{F}	Φ^{c}_{Δ}
3.9a	346 (4.73), 606 (4.46), 672 (5.23)	683	0.25	0.54
3.9b	346 (4.75), 606 (4.49), 672 (5.25)	682	0.26	0.51
3.9c	346 (4.73), 606 (4.45), 672 (5.23)	686	0.24	0.58
3.9d	346 (4.72), 606 (4.46), 672 (5.23)	685	0.26	0.58
3.10a	346 (4.70), 606 (4.48), 672 (5.18)	684	0.19	0.32
3.10b	348 (4.71), 606 (4.47), 673 (5.17)	682	0.17	0.29
3.10c	349 (4.65), 608 (4.42), 672 (5.11)	684	0.16	0.34
3.10d	344 (4.69), 607 (4.47), 672 (5.16)	683	0.19	0.31

[a] Excited at 610 nm
[b] Using ZnPc in DMF as the reference ($\Phi_F = 0.28$)
[c] Using ZnPc as the reference ($\Phi_\Delta = 0.56$ in DMF)

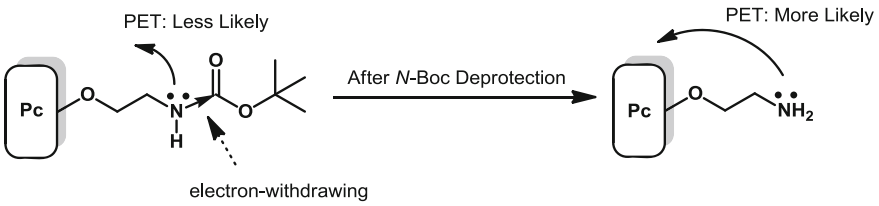

Fig. 3.3 Proposed mechanism of the quenching of the singlet excited state of the phthalocyanine core by the peripheral amino groups through PET before and after *N*-Boc deprotection

The fluorescence emission spectra of these compounds were also recorded in DMF. Upon excitation at 610 nm, these compounds showed a fluorescence emission at 682–686 nm with fluorescence quantum yield (Φ_F) of 0.16–0.26 relative to unsubstituted ZnPc ($\Phi_F = 0.28$) [32]. The fluorescence quantum yields of **3.10a–d** are relatively lower as compared to their corresponding *N*-Boc protected counterparts **3.9a–d**. When the Boc group is attached to the amino group, its electron-withdrawing nature tends to reduce the electron density of the nitrogen atoms and this renders a less effective quenching of the singlet excited state of the phthalocyanine core through intramolecular photoinduced electron transfer (PET) (Fig. 3.3). By contrast, the electron density of the amino moiety is higher after deprotection. As a result, the PET process is more likely to occur, and hence their Φ_F values are comparatively lower. In fact, reductive quenching of the singlet excited state of phthalocyanines by amino moieties has been reported earlier [33, 34].

To evaluate the photosensitizing efficiency of these compounds, their singlet oxygen quantum yields (Φ_Δ) were determined by a steady-state method using 1,3-diphenylisobenzofuran (DPBF) as the scavenger. The concentration of the quencher was monitored spectroscopically at 411 nm with time of irradiation (Fig. 3.4), from which the values of Φ_Δ could be determined. As shown in Table 3.1, all the phthalocyanines can generate singlet oxygen in DMF. The singlet oxygen generation efficiency of the *N*-Boc protected analogues **3.9a–d** is comparable to that of ZnPc. However, due to the PET process, the singlet oxygen generation efficiency is reduced after removal of the Boc groups [35–37].

To gain a better understanding of the aggregation behavior of these compounds in the biological environment, the electronic absorption and fluorescence spectra were also recorded in the Roswell Park Memorial Institute (RPMI) 1640 culture medium. All the compounds displayed two broad Q-bands (Fig. 3.5a). Upon excitation at 610 nm, these compounds did not show fluorescence (Fig. 3.5b), probably due to their aggregation in the culture medium. However, the Q-bands become sharpened and more intense (Fig. 3.5c) and a strong fluorescence was observed after the addition of 0.05 % Cremophor EL (Fig. 3.5d). These observations indicate that these compounds, particularly **3.10d**, are not extensively aggregated in the culture medium containing Cremophor EL. The non-aggregated nature of these compounds is highly desirable as aggregation almost inevitably

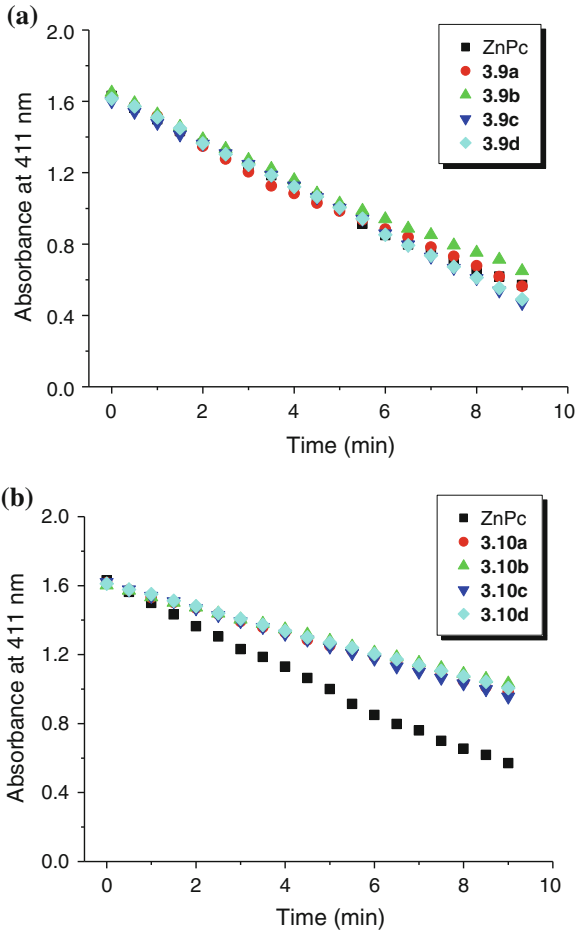

Fig. 3.4 Comparison of the rate of decay of DPBF (initial concentration = 70 μM) sensitized by (**a**) **3.9a–d** and (**b**) **3.10a–d** with ZnPc (all at 3 μM) in DMF as shown by the decrease in the absorbance at 411 nm

shortens the triplet lifetime of the dyes, resulting in a drastic reduction of the overall photosensitizing efficiency [38–40]

3.2.3 In Vitro Photodynamic Activities

The photodynamic activities of phthalocyanines **3.10a–d** were evaluated against two different cell lines, namely, B16 melanoma and CHO cells. Both cell lines are known to have high PAT activity [30, 41], Fig. 3.6 shows the cytotoxic effects of **3.10a–d** on B16 and CHO cells. All of these compounds are essentially non-cytotoxic in the absence of light but exhibit high photocytotoxicity. The IC_{50} values of these compounds against both cell lines are compiled in Table 3.2. Generally, all these compounds show higher photocytotoxicity toward the B16

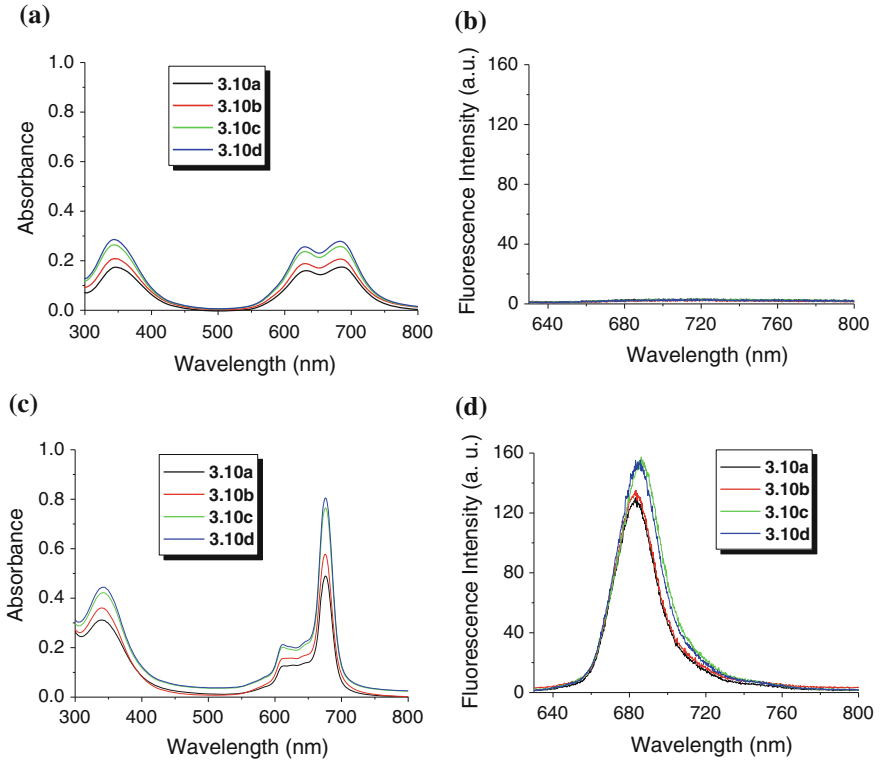

Fig. 3.5 Electronic absorption and fluorescence spectra ($\lambda_{ex} = 610$ nm) of **3.10a–d** in the absence [(**a**) and (**b**)] and presence of 0.05 % Cremophor EL [(**c**) and (**d**)] in the RPMI culture medium (all at 8 μM)

cells. The IC_{50} values for the B16 cells are about two- to three-fold lower than those for the CHO cells. Compound **3.10d**, which has the longest polyamine chain, in particular, exhibits the highest potency against both cell lines with IC_{50} values as low as 0.34 μM (for B16 cells) and 0.97 μM (for CHO cells).

In order to account for the different photodynamic activities, the intracellular production of reactive oxygen species (ROS) by **3.10a–d** was also studied by using 2′,7′-dichlorodihydrofluorescein diacetate (DCFDA) as the scavenger [42]. As depicted in Fig. 3.7, these compounds cannot generate ROS in the absence of light. However, they can sensitize the production of ROS upon illumination and the efficiency follows the order **3.10d** > **3.10c** > **3.10b** ≈ **3.10a**. The ROS generation efficiency of these compounds is comparatively higher toward the B16 cells. The trend in ROS production is generally in accordance with that observed for the photocytotoxicity toward both cell lines.

To have a better understanding on the role of the polyamine moieties, we performed a competitive experiment in which the cellular uptake of **3.10a–d** against B16 and CHO cells was studied in the presence of excess spermidine.

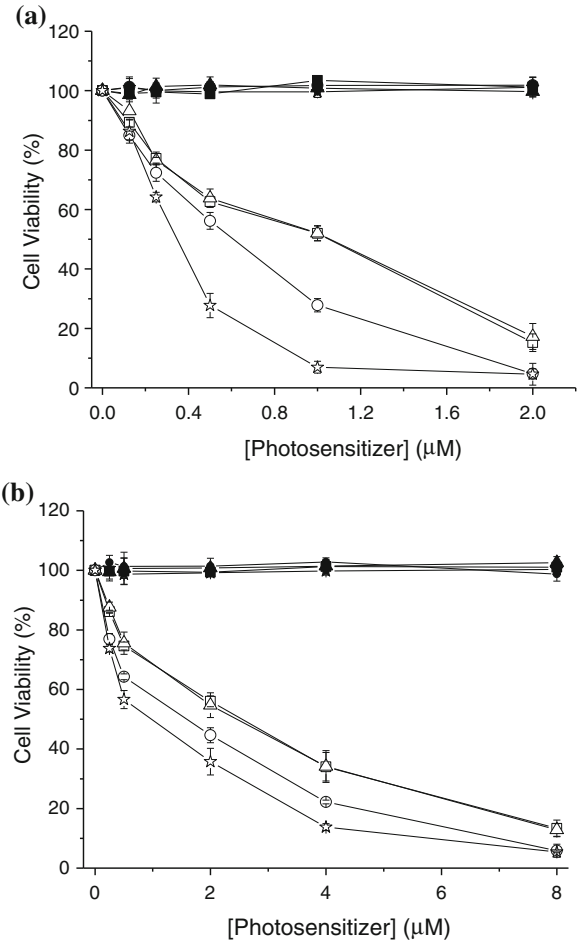

Fig. 3.6 Comparison of the cytotoxic effects of **3.10a** (*squares*), **3.10b** (*triangles*), **3.10c** (*circles*), and **3.10d** (*stars*) on (**a**) B16 and (**b**) CHO cells in the absence (*closed symbols*) and presence (*open symbols*) of light ($\lambda > 610$ nm, 40 mW cm^{-2}, 48 J cm^{-2}). Data are expressed as mean value ± standard error of the mean (S.E.M.) of three independent experiments, each performed in quadruplicate

Table 3.2 IC_{50} values for phthalocyanines **3.10a–d** against B16 and CHO cells

Compound	IC^{d}_{50} (μM)	
	B16	CHO
3.10a	1.05	2.53
3.10b	1.06	2.43
3.10c	0.61	1.57
3.10d	0.34	0.97

[d] Defined as the dye concentration required to kill 50 % of the cells

As an important control experiment, it was demonstrated that spermidine does not cause any cytotoxicity to both cells up to a concentration of 5 mM. Figure 3.8 shows the results for the B16 cells as an example. During the incubation of the

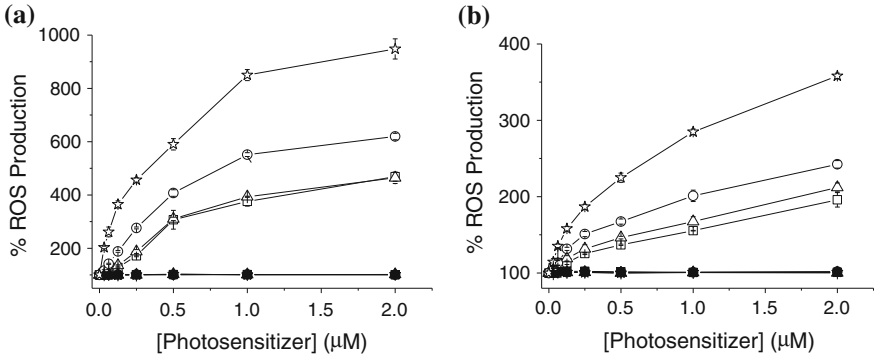

Fig. 3.7 ROS production induced by **3.10a** (*squares*), **3.10b** (*triangles*), **3.10c** (*circles*), and **3.10d** (*stars*) in (**a**) B16 and (**b**) CHO cells in the absence (*closed symbols*) and presence (*open symbols*) of light ($\lambda > 610$ nm, 40 mW cm^{-2}, 48 J cm^{-2}). Data are expressed as mean value ± S.E.M. of three independent experiments, each performed in quadruplicate

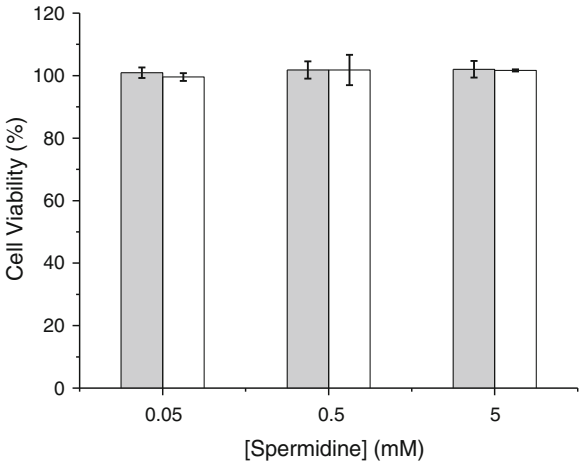

Fig. 3.8 Cytotoxic effect of spermidine on B16 cells in the absence (*gray bars*) and presence (*white bars*) of light ($\lambda > 610$ nm, 40 mW cm^{-2}, 48 J cm^{-2}). Data are expressed as mean value ± S.E.M. of three independent experiments, each performed in quadruplicate

phthalocyanines (8 μM), a solution of spermidine in medium (0.05–5 mM) was added. After 2 h incubation, the cells were lysed and the dye concentrations inside the cells were quantified by measuring their Q-band absorbance and the results are depicted in Fig. 3.9. For both of these cell lines, the cellular uptake of **3.10a–d** was found to be virtually identical with that in the absence of spermidine. The results suggested that the cellular uptake of these compounds may not involve the PAT of the cells and so the polyamine moieties do not play the related functional role in these compounds.

In addition to an extraction method, we also employed confocal laser scanning microscopy to investigate the cellular uptake of these compounds toward both cell lines. The confocal fluorescence images of these compounds against B16 cells are shown in Fig. 3.10a as an example. All the compounds could enter into the cells

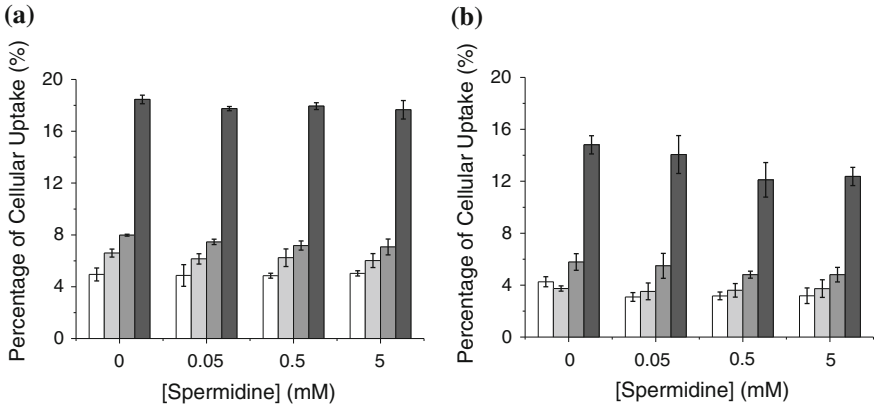

Fig. 3.9 Comparison of the percentage of cellular uptake of **3.10a** (*white*), **3.10b**, (*light gray*), **3.10c** (*gray*), and **3.10d** (*dark gray*) on (**a**) B16 and (**b**) CHO cells in the absence and presence of free spermidine (0.05–5 mM) as determined by an extraction method. Data are expressed as mean value ± standard deviation (S.D.) of three independent experiments

causing intracellular fluorescence after incubation for 2 h. The average relative fluorescence intensity per cell of these compounds against both cell lines was also measured and compared in Fig. 3.10b. It can be seen that the intracellular fluorescence intensity of **3.10d** is about six- to eight-fold higher than that of the other compounds for both cell lines. This result is in accord with the uptake experiment as determined by an extraction method in which **3.10d** exhibits the highest cellular uptake among the four compounds toward both cell lines (Fig. 3.9). Hence, the trend in photocytotoxicity can be explained by the difference in cellular uptake and ROS production efficiency.

Since phthalocyanine **3.10d** is the most potent compound toward both cell lines, the subcellular localization of this compound was also investigated by confocal microscopy. The cells were incubated with this compound together with LysoTracker Green DND-26, ER-Tracker Green, or MitoTracker Green FM, which are specific dyes for lysosomes, endoplasmic reticulum, and mitochondria, respectively. For the B16 cells, the fluorescence caused by MitoTracker (excited at 488 nm, monitored at 500–570 nm) could be well superimposed with the fluorescence caused by **3.10d** (excited at 633 nm, monitored at 650–750 nm) (Fig. 3.11). The very similar fluorescence intensity profile of **3.10d** and MitoTracker traced along the green line in this figure [Fig. 3.11a (iv)] also confirmed that this compound can target mitochondria of the cells, which is an important target for the initiation of apoptosis by PDT [43]. By contrast, the fluorescence images of **3.10d** and ER-Tracker or LysoTracker (excited at 488 nm, monitored at 500–570 nm) could not be superimposed, indicating that this compound is not localized in endoplasmic reticulum and lysosomes of the cells (data not shown).

For the CHO cells, the subcellular localization property of **3.10d** is different from that in B16 cells. As shown in Figs. 3.12 and 3.13, the fluorescence caused by

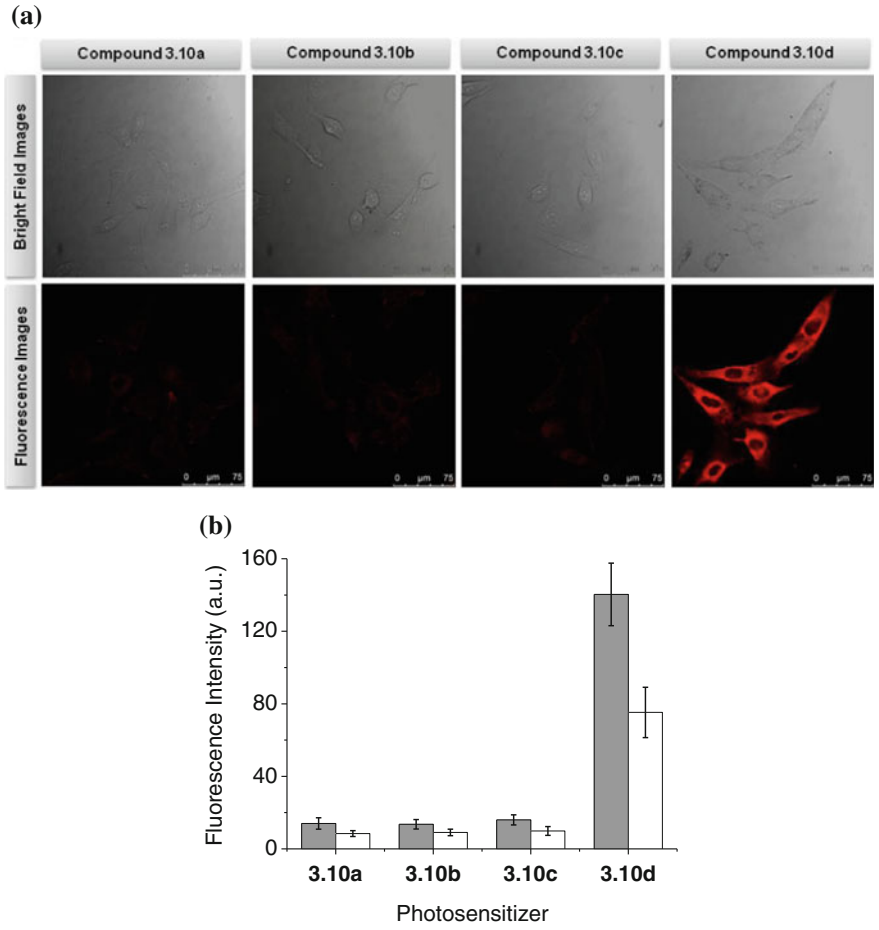

Fig. 3.10 **(a)** Confocal fluorescence images of B16 cells after incubation with **3.10a–d** for 2 h (all at 2 μM). The corresponding bright field images are given in the upper row. **(b)** Comparison of the relative intracellular fluorescence intensity of **3.10a–d** against B16 (*gray bars*) and CHO (*white bars*) cells (number of cells = 30). Data are expressed as mean value ± S.D. of three independent experiments

3.10d is well merged with the fluorescence caused by both the ER-Tracker and MitoTracker. The fluorescence intensity line profiles of **3.10d** and both the Trackers are also very similar. The results suggested that **3.10d** accumulates preferentially in both the endoplasmic reticulum and mitochondria. Endoplasmic reticulum is known to play a central role in lipid and protein biosynthesis and serve as an intracellular calcium store. It has been shown that accumulation of photosensitizers in this organelle also results in efficient triggering of cell death upon illumination [33, 34]. On the contrary, the fluorescence image of **3.10d** could not overlap with that of the LysoTracker, showing that this compound is not localized in the lysosomes of the cells (data not shown).

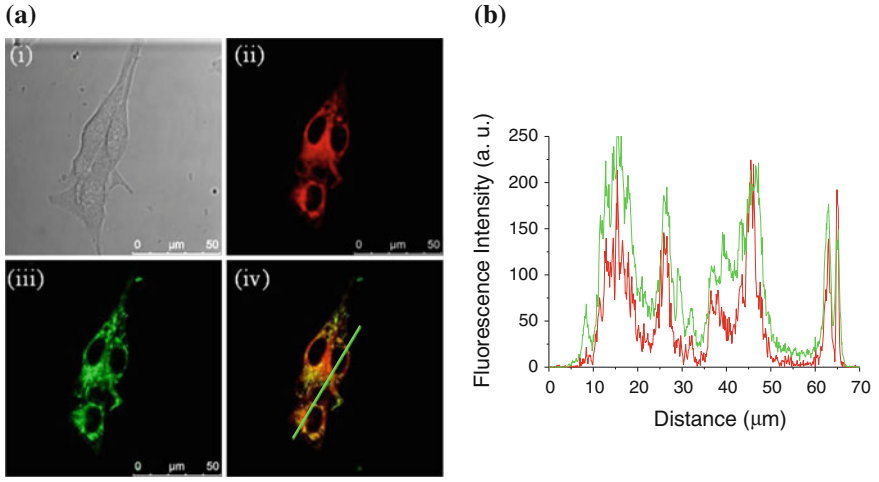

Fig. 3.11 **(a)** Visualization of (i) the bright field image, intracellular fluorescence of B16 cells using filter sets specific for (ii) **3.10d** (2 μM; in *red*) and (iii) MitoTracker (in *green*), and (iv) the corresponding superimposed image. Figure **(b)** shows the fluorescence intensity profiles of **3.10d** (*red*) and MitoTracker (*green*) traced along the *green line* in Figure **(a)** (iv)

To study the mode of cell death induced by **3.10d**, a flow cytometric assay of annexin V-green fluorescent protein (GFP) and propidium iodide (PI) costaining was employed [44]. The cell populations in different phases of cell death, namely

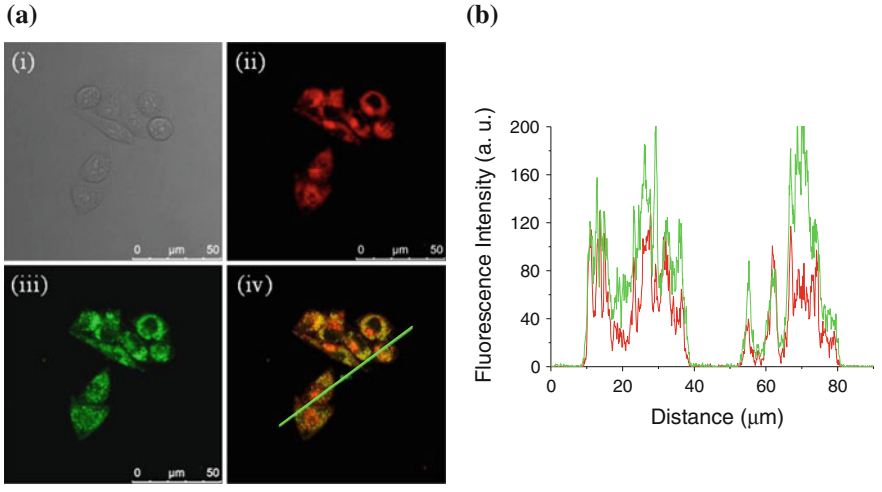

Fig. 3.12 **(a)** Visualization of (i) the bright field image, intracellular fluorescence of CHO cells using filter sets specific for (ii) **3.10d** (2 μM; in *red*) and (iii) ER-Tracker (in *green*), and (iv) the corresponding superimposed image. Figure **(b)** shows the fluorescence intensity profiles of **3.10d** (*red*) and ER-Tracker (*green*) traced along the *green line* in Figure **(a)** (iv)

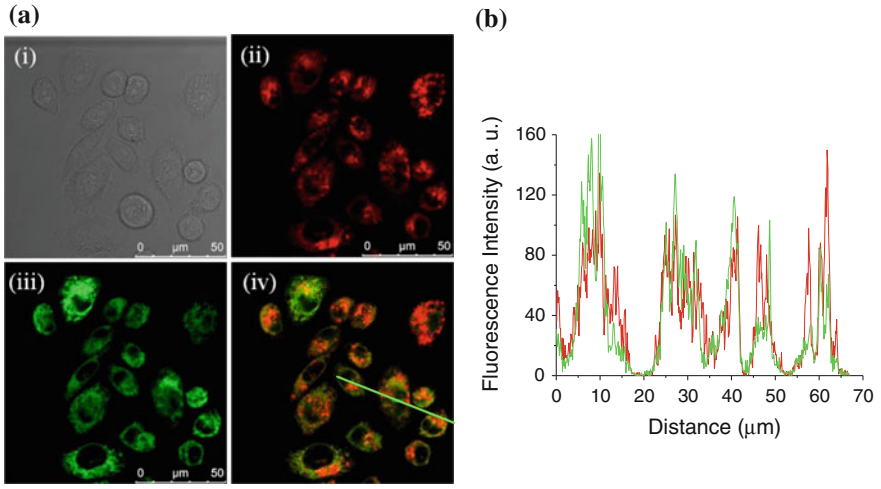

Fig. 3.13 **(a)** Visualization of (i) the bright field image, intracellular fluorescence of CHO cells using filter sets specific for (ii) **3.10d** (2 μM; in *red*) and (iii) MitoTracker (in *green*), and (iv) the corresponding superimposed image. Figure **(b)** shows the fluorescence intensity profiles of **3.10d** (*red*) and MitoTracker (*green*) traced along the *green line* in Figure **(a)** (iv)

viable (annexin V-GFP$^-$/PI$^-$), early apoptotic (annexin V-GFP$^+$/PI$^-$), and necrotic or late-stage apoptotic (annexin V-GFP$^+$/PI$^+$) were examined at different drug doses. As shown in Table 3.3, above 91 % of the B16 and CHO cells are negative for annexin V-GFP and PI after treatment with **3.10d** (1.36 μM for B16 and 3.88 μM for CHO cells) in the absence of light. This indicates that this compound

Table 3.3 Flow cytometric analysis of the cell death mechanism induced by **3.10d** in the absence and presence of light ($\lambda > 610$ nm, 40 mW cm^{-2}, 48 J cm^{-2}) on B16 and CHO cells. Data are expressed as mean value ± S.D. of three independent experiments

Drug (μM)	Illumination	Cell population (%)		
		Viable	Early apoptotic	Late apoptotic/necrotic
(a) B16 cells				
0	–	91.7 ± 1.4	3.4 ± 0.9	4.5 ± 2.0
1.36	–	91.0 ± 0.2	5.3 ± 0.8	2.7 ± 0.3
0.34	+	45.7 ± 4.3	41.3 ± 3.3	12.8 ± 0.8
0.68	+	14.0 ± 0.6	64.3 ± 2.0	21.5 ± 1.6
1.36	+	1.7 ± 1.5	70.4 ± 1.9	27.4 ± 2.5
(b) CHO cells				
0	–	94.6 ± 0.1	1.8 ± 0.9	3.1 ± 1.2
3.88	–	91.0 ± 1.4	5.4 ± 0.5	3.0 ± 1.1
0.97	+	49.1 ± 0.6	46.2 ± 1.1	4.7 ± 1.7
1.94	+	25.7 ± 2.4	53.6 ± 1.3	20.7 ± 1.2
3.88	+	10.8 ± 2.4	63.2 ± 2.3	25.4 ± 0.4

is essentially non-cytotoxic toward both cell lines in darkness. However, upon illumination, the percentage of cells in the early apoptotic stage increases from 41 % to 70 % for B16 and 46 % to 63 % for CHO cells as the concentration of **3.10d** increases. A significant amount of necrotic cells (less than 30 %) was also observed (in annexin V-GFP$^+$/PI$^+$ region) for both cell lines. These results suggested that apoptosis is a major pathway for the PDT action of this compound toward both cell lines.

3.3 Summary

In summary, we have prepared and characterized a series of novel zinc(II) phthalocyanines with polyamine moieties. The phthalocyanines **3.10a–d** exhibit relatively lower fluorescence and singlet oxygen quantum yields as compared with the *N*-Boc protected analogues as a result of the quenching effect by the amino moieties. Upon illumination, these compounds are highly photocytotoxic against B16 and CHO cells, particularly for the phthalocyanine which bears the longest polyamine chain (**3.10d**), of which the IC_{50} values are as low as 0.34 μM. The higher photodynamic activity of this compound can be attributed to its lower aggregation tendency in the biological media, higher ROS generation efficiency, and higher cellular uptake. Confocal microscopic studies of **3.10d** have shown that it localizes preferentially in the mitochondria of B16 and CHO cells. It also displays high affinity to the endoplasmic reticulum of the CHO cells. As revealed by flow cytometric studies, it can induce predominately apoptosis upon illumination toward both cell lines.

References

1. Derycke, A.S.L., de Witte, P.A.M.: Adv. Drug Delivery Rev. **56**, 17 (2004)
2. Bechet, D., Couleaud, P., Frochot, C., Viriot, M.-L., Guillemin, F., Barberi-Heyob, M.: Trends Biotechnol. **26**, 612 (2008)
3. Nishiyama, N., Morimoto, Y., Jang, W.-D., Kataoka, K.: Adv. Drug Delivery Rev. **61**, 327 (2009)
4. Couleaud, P., Morosini, V., Frochot, C., Richeter, S., Raehm, L., Durand, J.-O.: Nanoscale **1083**, 2 (2010)
5. Sharman, W.M., van Lier, L.E., Allen, C.M.: Adv. Drug Delivery Rev. **56**, 53 (2004)
6. Solban, N., Rizvi, I., Hasan, T.: Lasers Surg. Med. **38**, 522 (2006)
7. Lovell, J.F., Liu, T.W.B., Chen, J., Zheng, G.: Chem. Rev. **110**, 2839 (2010)
8. Verhille, M., Couleayd, P., Vanderesse, R., Brault, D., Barberi-Heyob, M., Frochot, C.: C. Curr. Med. Chem. **17**, 3925 (2010)
9. Liu, T.W.B., Chen, J., Zheng, G.: Amino Acids **41**, 1123 (2011)
10. Gerner, E.W., Meyskens Jr, F.L.: Nat. Rev. **4**, 871 (2004)
11. Agostinelli, E., Marques, M.P.M., Calheiros, R., Gil, F.P.S.C., Tempera, G., Viceconte, N., Battaglia, V., Grancara, S., Toninello, A.: Amino Acids **38**, 393 (2010)
12. Igarashi, K., Kashiwagi, K.: Int. J. Biochem. Cell Biol. **42**, 39 (2010)
13. Cullis, P.M., Green, R.E., Merson-Davies, L., Travis, N.: Chem. Biol. **6**, 717 (1999)

14. Holley, J.L., Mather, A., Wheelhouse, R.T., Cullis, P.M., Hartley, J.A., Bingham, J.P., Cohen, G.M.: Cancer Res. **52**, 4190 (1992)
15. Cullis, P.M., Green, R.E., Malone, M.E.: J. Chem. Soc. Perkin Trans. **2**, 1503 (1995)
16. Papadopoulou, M.V., Rosenzweig, H.S., Bloomer, W.D.: Bioorg. Med. Chem. Lett. **14**, 1519 (2004)
17. Yuan, Z.-M., Egorin, M.J., Rosen, D.M., Simon, M.A., Callery, P.S.: Cancer Res. **54**(742), 104–118 (1994)
18. Eiseman, J.L., Rogers, F.A., Guo, Y., Kauffman, J., Sentz, D.L., Klinger, M.F., Callery, P.S., Kyprianou, N.: Cancer Res. **58**, 4864 (1998)
19. Bergeron, R.J., Feng, Y., Weimar, W.R., McManis, J.S., Dimova, H., Porter, C., Raisler, B., Phanstiel, O.J.: Med. Chem. **40**, 1475 (1997)
20. Delcros, J.-G., Tomasi, S., Carrington, S., Martin, B., Renault, J., Blagbrough, I.S., Uriac, P.J.: Med. Chem. **45**, 5098 (2002)
21. Battaglia, A., Guerrini, A., Baldelli, E., Fontana, G., Varchi, G., Samorì, C., Bombardelli, E.: Tetrahedron Lett. **47**, 2667 (2006)
22. Dallavalle, S., Giannini, G., Alloatti, D., Casati, A., Marastoni, E., Musso, L., Merlini, L., Morini, G., Penco, S., Pisano, C., Tinelli, S., De Cesare, M., Beretta, G.L., Zunino, F.J.: Med. Chem. **49**, 5177 (2006)
23. Samor, C., Guerrini, A., Varchi, G., Beretta, G.L., Fontana, G., Bombardelli, E., Carenini, N., Zunino, F., Bertucci, C., Fiori, J., Battaglia, A.: Bioconjugate Chem. **19**, 2270 (2008)
24. Lamarche, F., Sol, V., Huang, Y.-M., Granet, R., Guilloton, M., Krausz, P.J.: Porphyrins Phthalocyanines **6**, 130 (2002)
25. Sol, V., Lamarche, F., Enache, M., Garcia, G., Granet, R., Guilloton, M., Blais, J.C., Krausz, P.: Bioorg. Med. Chem. **14**, 1364 (2006)
26. Garcia, G., Sol, V., Lamarche, F., Granet, R., Guilloton, M., Champavier, Y., Krausz, P.: Bioorg. Med. Chem. Lett. **16**, 3188 (2006)
27. Hahn, F., Schmitz, K., Balaban, T.S., Bräse, S., Schepers, U.: Chem Med Chem **3**, 1185 (2008)
28. Ménard, F., Sol, V., Ringot, C., Granet, R., Alves, S., Le Morvan, C., Queneau, Y., Ono, N., Krausz, P.: Bioorg. Med. Chem. **17**, 7647 (2009)
29. Jiang, X.-J., Yeung, S.-L., Lo, P.-C., Fong, W.-P., Ng, D.K.P.J.: Med. Chem. **54**, 320 (2011)
30. Kaur, N., Delcros, J.G., Martin, B., Phanstiel, O.J.: Med. Chem. **48**, 3832 (2005)
31. Ishii, K., Kobayashi, N.: The photophysical properties of phthalocyanines and related compounds. In: Kadish, K.M., Smith, K.M., Guilard, R. (eds.) The Porphyrin Handbook, p. 106. Academic Press, San Diego (2003)
32. Scalise, I., Durantini, E.N.: Bioorg. Med. Chem. **13**, 3037 (2005)
33. Teiten, M.-H., Bezdetnaya, L., Morlière, P., Santus, R., Guillemin, F.: Br. J. Cancer **88**, 146 (2003)
34. Gallagher, W.M., Allen, L.T., O'Shea, C., Kenna, T., Hall, M., Gorma, A., Killoran, J., O'Shea, D.F.: Br. J. Cancer **92**, 1702 (2005)
35. Lo, P.-C., Huang, J.-D., Cheng, D.Y.Y., Chan, E.Y.M., Fong, W.-P., Ko, W.-H., Ng, D.K.P.: Chem. Eur. J. **10**, 4831 (2004)
36. Jiang, X.-J., Lo, P.-C., Yeung, S.-L., Fong, W.-P., Ng, D.K.P.: Chem. Commun. **46**, 3188 (2010)
37. Jiang, X.-J., Lo, P.-C., Tsang, Y.-M., Yeung, S.-L., Fong, W.-P., Ng, D.K.P.: Chem. Eur. J. **16**, 4777 (2010)
38. Jori, G.: J. Photochem. Photobiol. A **62**, 371 (1992)
39. Jori, G.: EPA Newslett. **60**, 12 (1997)
40. Li, X.-Y., Ng, A.C.H., Ng, D.K.P.: Macromolecules **33**, 2119 (2000)
41. Minchin, R.F., Raso, A., Martin, R.L., Ilett, K.F.: Eur. J. Biochem. **200**, 457 (1991)
42. Shen, H.M., Shi, C.Y., Shen, Y., Ong, C.N.: Free Radical Biol. Med. **21**, 139 (1996)
43. Oleinick, N.L., Morris, R.L., Belichenko, I.: Photochem. Photobiol. Sci. **1**, 1 (2002)
44. Vermes, I., Haanen, C., Steffens-Nakken, H., Reutelingsperger, C.J.: Immunol. Methods **184**, 39 (1995)

Chapter 4
A Redox-Responsive Silicon(IV) Phthalocyanine for Targeted Photodynamic Therapy

4.1 Introduction

Photodynamic therapy (PDT) is a promising therapeutic modality for cancer relying on the in situ generation of cytotoxic singlet oxygen ($^1O_2$) by activation of a photosensitizer with light [2, 10, 31]. By controlling how the light and the photosensitizer are delivered to tumor tissues, a certain degree of selectivity can be achieved. Compared to other treatment modalities, directed light delivery already confers high specificity to PDT because the distant body organs are unaffected and spared from singlet oxygen damage. Among the various strategies that have been explored to enhance the specificity of photosensitizers (Sect. 1.3 in Chap. 1), activatable photosensitizers have received considerable attention [22]. Upon interactions with various tumor-associated stimuli, such as the acidic environment of tumors, [13, 14, 24] cancer-related proteases [3, 4, 21, 30, 33], and mRNAs [5], the photosensitizing ability of these photosensitizers can be triggered, which offers a new level of selectivity for therapeutic applications. Disulfide linkages are also commonly used for the construction of activatable agents which can be cleaved by biological reducing agents such as glutathione (GSH). GSH is the most abundant cellular thiol and a major reducing agent in various biochemical processes [25]. The intracellular GSH concentration (ca. 10 mM) is known to be substantially higher than the extracellular levels (ca. 2 μM), which provides a mechanism for selective intracellular release [12]. The GSH concentrations are also elevated by as much as two-fold in tumor tissues as compared with normal tissues, which also offers a control of tumor selectivity of drugs [1, 8, 16]. A substantial number of disulfide-linked systems have been prepared and used for drug delivery and controlled release [6, 7, 15, 17, 32], and as fluorescent probes for thiols [20, 34] and protein transduction [19] in living cells. Recently, a disulfide-linked polymeric delivery system for photosensitizers has also been reported, in which the photosensitizing molecules of mesochlorin e_6 are linked to a *N*-(2-hydroxypropyl) methacrylamide copolymer backbone [9]. In the presence of the reducing agent dithiothreitol (DTT), the conjugate shows a time-dependent reductive cleavage with a concomitant increase in singlet oxygen quantum yield. It also exhibits faster

J. T. F. Lau, *Towards Dual and Targeted Cancer Therapy with Novel Phthalocyanine-based Photosensitizers*, Springer Theses,
DOI: 10.1007/978-3-319-00708-3_4,

release kinetics and a higher cytotoxicity in SKOV-3 human ovarian carcinoma cells as compared to the analogue with a proteolytically cleavable spacer. As part of our continuing interest in the development of efficient and selective photosensitizers for PDT, we have designed a novel ferrocenyl-substituted silicon(IV) phthalocyanine linked with a disulfide linkage. The preparation and basic photophysical properties of this compound, as well as the effect of the reductive stimulus on its in vitro properties are described in this chapter.

4.2 Results and Discussion

4.2.1 Preparation and Characterization

Scheme 4.1 shows the preparation of the redox-responsive silicon(IV) phthalocyanine and its non-cleavable analogue. The preparation starts with a modified Vilsmeier reaction of ferrocene (**4.1**) with *N*,*N*-dimethylformamide (DMF) and phosphoryl chloride ($POCl_3$) in chloroform to give ferrocenecarboxyaldehyde (**4.2**) [27]. It underwent a base-catalyzed Claisen-Schmidt condensation with *p*-hydroxyacetophenone (**4.3**) to afford 3-ferrocenyl-1-(*p*-hydroxyphenyl)-prop-2-en-1-one (**4.4**) [35], which was then further reacted with ethyl bromoacetate (**4.5**) in the presence of anhydrous potassium carbonate in refluxing acetone to give compound **4.6**. This compound was then hydrolyzed with NaOH in acetone to obtain compound **4.7**. Treatment of **4.7** with 2-hydroxyethyl disulfide (**4.8a**) or 1,6-hexanediol (**4.8b**) in the presence of *N*,*N*′-dicyclohexylcarbodiimide (DCC), 4-(dimethylamino) pyridine (DMAP), and 1-hydroxybenzotriazole (HOBt) gave the corresponding alcohols **4.9a** and **4.9b**, respectively. Further nucleophilic substitution of the readily available silicon(IV) phthalocyanine dichloride (**4.10**) with alcohol **4.9a** or **4.9b** and pyridine in toluene afforded the redox-responsive phthalocyanine **4.11a** and the non-cleavable analogue **4.11b**, respectively. Attempts to use a stronger base such as NaH or potassium carbonate were not successful during the preparation of these phthalocyanines. The reaction turned to a brownish black mixture immediately upon addition of these bases. These phthalocyanines are soluble in common organic solvents. Considering the fact that **4.10** is completely insoluble in water as well as many organic solvents, it is conspicuous that the presence of these axial ligands can greatly enhance the hydrophilicity of the phthalocyanine core. These compounds were purified readily by neutral alumina column chromatography, followed by recrystallization from a mixture of $CHCl_3$ and ethanol. For comparison, the non-ferrocene-containing phthalocyanine **4.12** was also prepared by typical axial substitution of **4.10** with alcohol **4.8a** (Scheme 4.2).

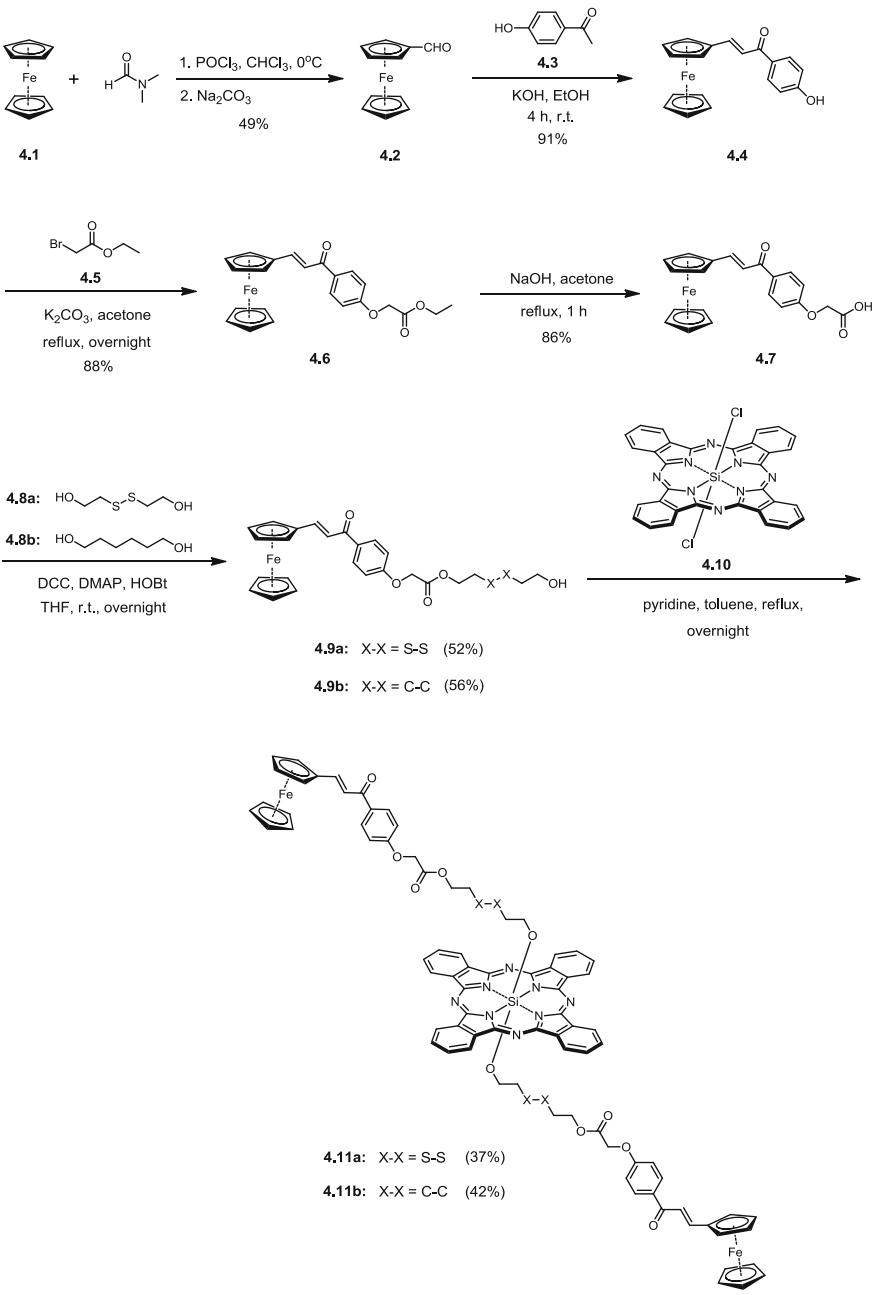

Scheme 4.1 Synthesis of the redox-responsive phthalocyanine **4.11a** and the non-cleavable analogue **4.11b**

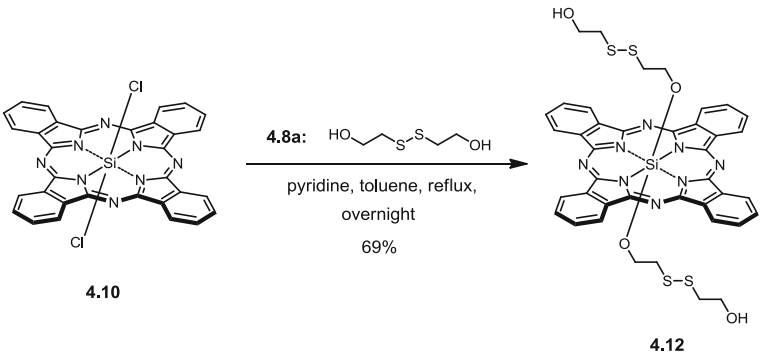

Scheme 4.2 Synthesis of silicon phthalocyanine **4.12**

4.2.2 Electronic Absorption and Photophysical Properties

The electronic absorption spectra of **4.11a**, **4.11b**, and **4.12** in DMF were typical for non-aggregated phthalocyanines (Fig. 4.1a–c). They showed a B-band at 353–355 nm, an intense and sharp Q-band at 674–676 nm, together with two vibronic bands at 608 and 642–646 nm (Table 4.1). The ferrocene-appended phthalocyanines **4.11a** and **4.11b** showed two additional bands at 330–332 and 494–498 nm due to the absorptions of the ferrocenyl π-conjugated system. It is supported by comparing the spectra with that of **4.9a**, which displays two absorption peaks at 311 and 489 nm in DMF (Fig. 4.1d). Upon excitation at 610 nm, these phthalocyanines showed a fluorescence emission at 684–688 nm. It can be seen in Table 4.1 that the fluorescence quantum yields of **4.11a** and **4.11b** ($\Phi_F = 0.04-0.05$) are exceptionally low as compared with that of **4.12** ($\Phi_F = 0.28$) relative to the unsubstituted zinc(II) phthalocyanine (ZnPc) in DMF ($\Phi_F = 0.28$) [28] It is likely that the ferrocenyl moieties quench the singlet excited state of the phthalocyanine core by photoinduced electron transfer (PET). In fact, similar phenomenon has been reported for related ferrocene-porphyrinic conjugates in which the fluorescence of porphyrin is quenched as a result of PET from the ferrocenyl moiety [11, 18, 26, 29].

To evaluate the photosensitizing efficiency of the phthalocyanines, their singlet oxygen quantum yields (Φ_Δ) were determined by a steady-state method with 1, 3-diphenylisobenzofuran (DPBF) as the scavenger in DMF. The changes in concentration of the quencher were monitored spectroscopically at 411 nm with time (Fig. 4.2), from which the values of Φ_Δ could be determined by the method described previously [23]. All these phthalocyanines could generate singlet oxygen ($\Phi_\Delta = 0.13-0.34$), but the efficiency is lower than that of ZnPc ($\Phi_\Delta = 0.56$) (Table 4.1) [23]. The relatively low singlet oxygen quantum yields of **4.11a** and **4.11b** as compared with that of **4.12** may also be attributed to the quenching effect induced by the ferrocenyl moieties, which disfavors intersystem crossing and eventually the formation of singlet oxygen.

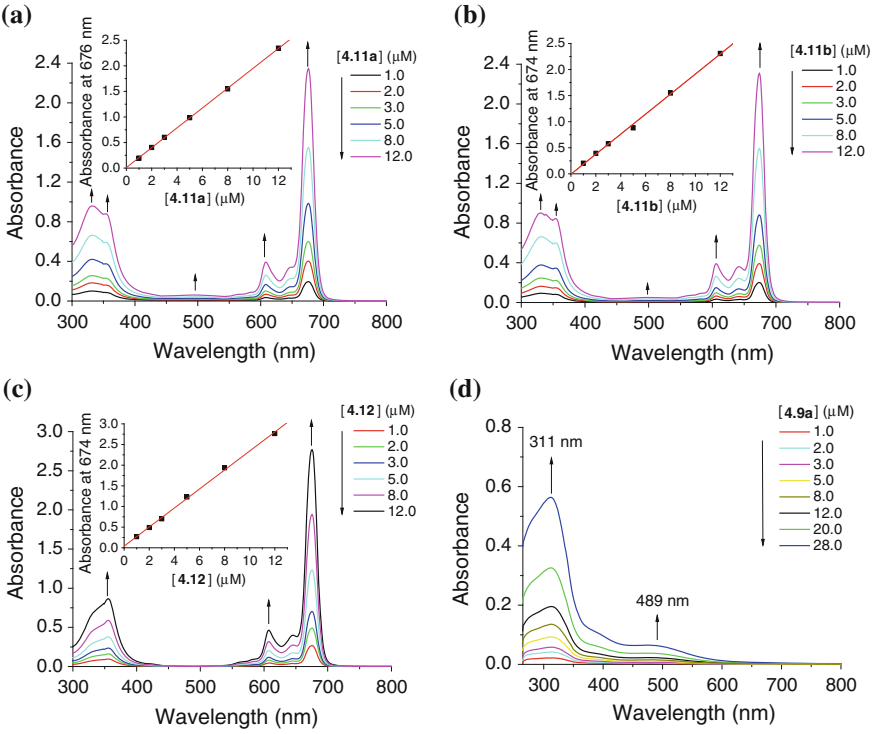

Fig. 4.1 Electronic absorption spectra of (**a**) **4.11a** (**b**) **4.11b** (**c**) **4.12**, and (**d**) **4.9a** in DMF in different concentrations. The insets of spectra (**a**) to (**c**) plot the Q-band absorbance versus the concentration of the phthalocyanine, and the line represents the best-fitted straight line

Table 4.1 Electronic absorption and photophysical data for **4.11a**, **4.11b**, and **4.12** in DMF

Compound	λ_{max} (nm) (log ε)	λ_{em}(nm)[a]	Φ^{b}_{F}	Φ^{c}_{Δ}
4.11a	332 (4.90), 353 (4.86), 494 (3.67), 608 (4.51), 646 (4.44), 676 (5.29)	688	0.04	0.17
4.11b	330 (4.88), 353 (4.85), 498 (3.63), 608 (4.51), 642 (4.48), 674 (5.28)	684	0.05	0.13
4.12	355 (4.85), 608 (4.58), 645 (4.52), 674 (5.36)	687	0.28	0.34

[a] Excited at 610 nm. [b] Using ZnPc in DMF as the reference ($\Phi_F = 0.28$). [c] Using ZnPc as the reference ($\Phi_\Delta = 0.56$ in DMF)

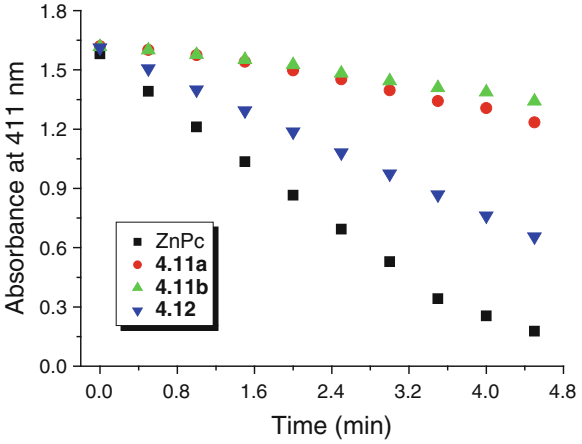

Fig. 4.2 Comparison of the rates of decay of DPBF (initial concentration = 70 μM) sensitized by **4.11a**, **4.11b**, **4.12**, and ZnPc (all at 3 μM) in DMF as shown by the decrease in the absorbance at 411 nm

In order to better mimic the aggregation behavior of the phthalocyanines in the biological environment, we also recorded their electronic absorption and fluorescence spectra in the Roswell Park Memorial Institute (RPMI) 1640 culture medium with 0.5 % Cremophor EL (Fig. 4.3). As shown in Fig. 4.3a, the phthalocyanines display sharp and intense Q-bands which indicate that they are essentially non-aggregated in the culture medium. Due to the quenching effect induced by the ferrocenyl moieties, phthalocyanines **4.11a** and **4.11b** show relatively weaker fluorescence intensities as compared with **4.12** in the medium (Fig. 4.3b).

To demonstrate the redox-responsive properties of **4.11a**, its fluorescence response to DTT was also investigated. Figure 4.4 shows the time-dependent changes in fluorescence spectra of **4.11a** and **4.11b** in different concentrations of DTT in phosphate buffered saline (PBS). Figure 4.5 summarizes the time-

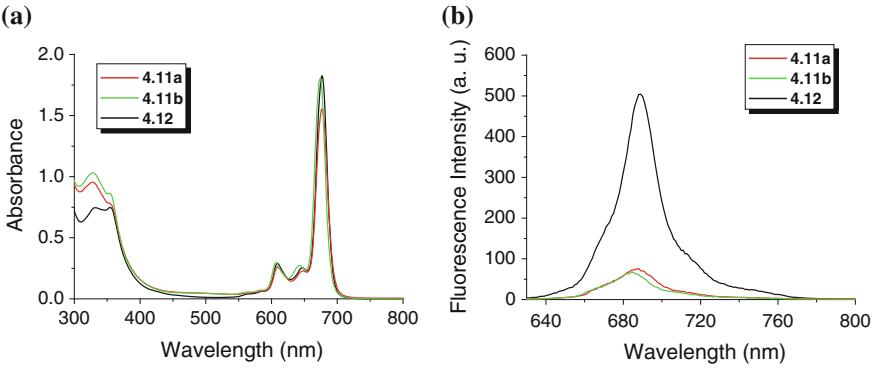

Fig. 4.3 (**a**) Electronic absorption and (**b**) Fluorescence spectra (λ_{ex} = 610 nm) of **4.11a**, **4.11b**, and **4.12** in the RPMI culture medium with 0.5 % Cremophor EL (all at 8 μM)

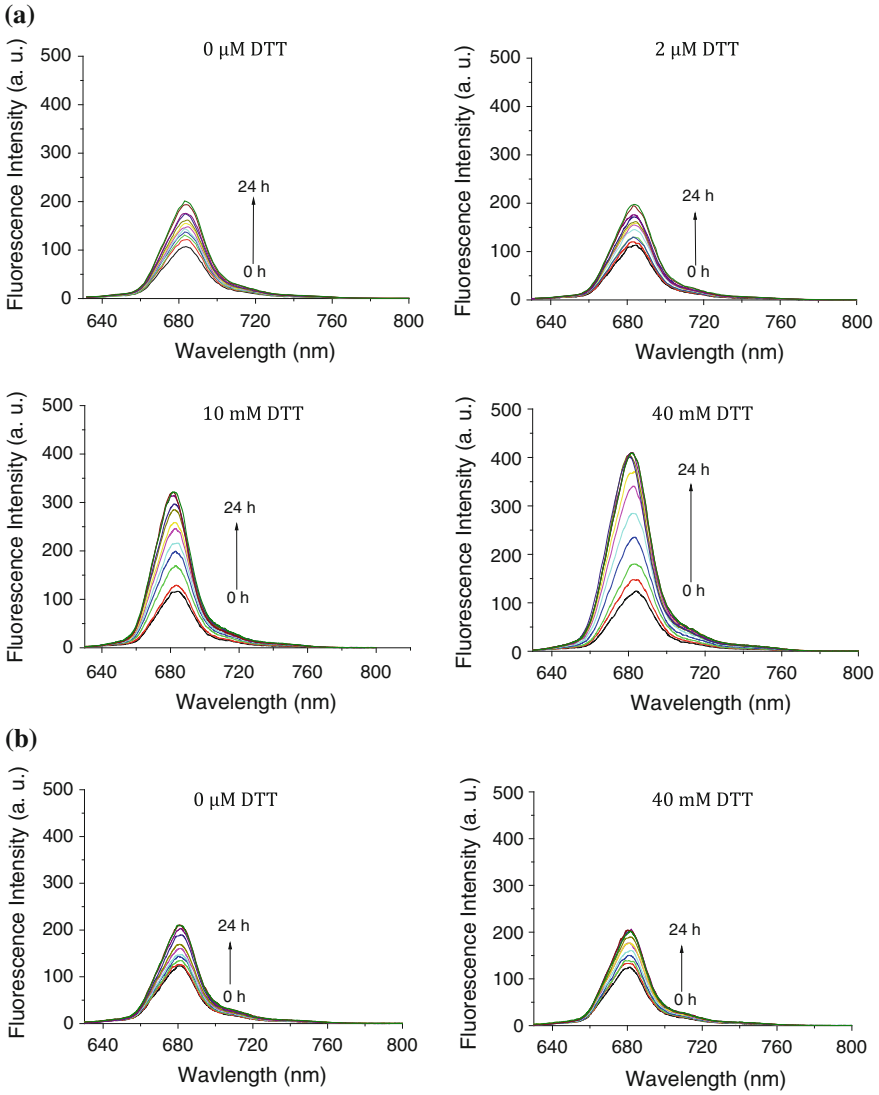

Fig. 4.4 Changes in fluorescence spectra ($\lambda_{ex} = 610$ nm) of (**a**) **4.11a** and (**b**) **4.11b** (both at 4 μM) with time upon exposure to different concentrations of DTT in PBS with 0.5 % Cremophor EL

dependent changes in fluorescence intensities of **4.11a** and **4.11b** upon exposure to different concentrations of DTT in PBS. Upon addition of 10–40 mM DTT, the fluorescence intensity of **4.11a** increases significantly within the first 6 h whereas the fluorescence intensity increases slightly in the presence of 0–2 μM DTT. The increase in fluorescence intensity results from the cleavage of disulfide linkers, hence releasing the ferrocenyl moieties and preventing the reductive quenching.

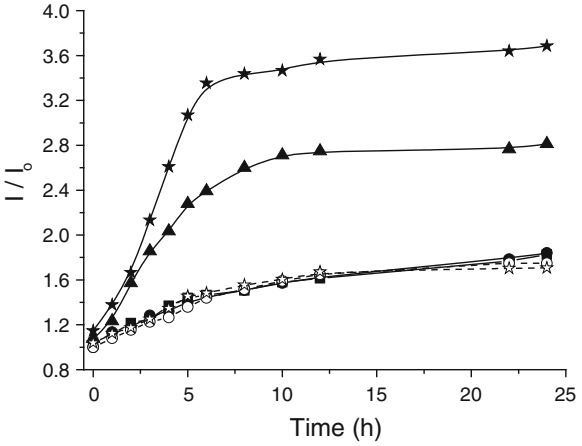

Fig. 4.5 Changes in fluorescence intensities of **4.11a** (*closed symbols*) and **4.11b** (*open symbols*) upon exposure to 0 μM (*circles*), 2 μM (*squares*), 10 mM (*triangles*), and 40 mM (*stars*) of DTT in PBS with 0.5 % Cremophor

For the non-cleavable analogue **4.11b**, no significant fluorescence enhancement was observed even in the presence of 40 mM DTT.

In order to examine the aggregation behavior of these phthalocyanines during the kinetic study, their respective Q-band was monitored over 24 h. As shown in Fig. 4.6, the Q-band remains relatively sharp and intense for both **4.11a** and **4.11b**, indicating that aggregation behavior of these phthalocyanines was not altered before and after the cleavage of the disulfide bonds in a reducing environment. As a result, the fluorescence enhancement could be attributed to the relaxation of the quenching effect upon reductive cleavage of the disulfide bonds rather than the changes in the aggregation behavior of the phthalocyanines.

DTT-mediated production of singlet oxygen was also investigated. Figure 4.7 compares the rates of decay of DPBF sensitized by **4.11a**, **4.11b**, and **4.12** upon exposure to different concentrations of DTT for 24 h in PBS solution. All these phthalocyanines could not induce singlet oxygen generation without illumination even in the presence of 10 mM DTT. At 2 μM DTT, which was used to mimic the extracellular reducing environment (e.g. plasma), **4.11a** could slightly produce singlet oxygen upon illumination. However, upon exposure to a higher concentration of DTT (5–10 mM), which mimics the intracellular reducing environment, the singlet oxygen production efficiency of **4.11a** increased remarkably. The enhancement in singlet oxygen generation could be ascribed to the reductive cleavage of the disulfide bonds, resulting in restoration of the photosensitizing property. By contrast, such an increase was not observed for **4.11b** even in the presence of 10 mM DTT for 24 h. The singlet oxygen generation efficiencies of **4.11a**, **4.11b**, and **4.12**, as reflected by the slope of the best-fit straight line fitted to the decay curve, are summarized in Table 4.2 for comparison. The greater the value of the slope represents the higher singlet oxygen generation efficiency. It is worth-noting that the singlet oxygen generation efficiency of **4.11a** is comparable to that of **4.12** in the presence of 10 mM DTT for 24 h. These results indicate that the free ferrocenyl moieties generated after the disulfide bond cleavage do not

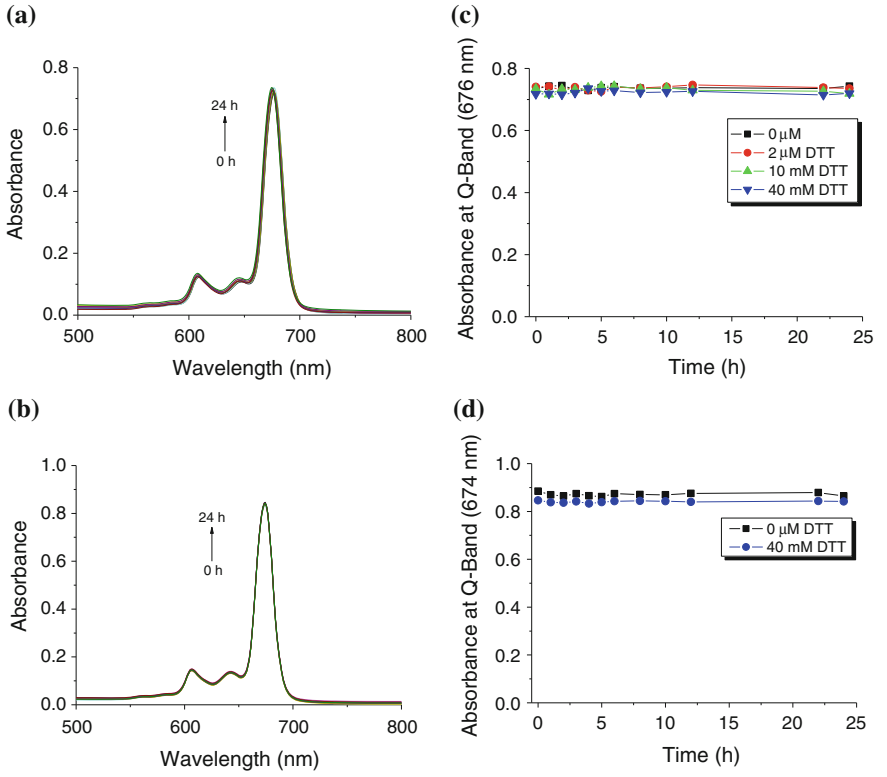

Fig. 4.6 Changes in absorption spectra of (**a**) **4.11a** and (**b**) **4.11b** (both at 4 μM) upon exposure to 40 mM DTT in PBS with 0.5 % Cremophor EL with time. The changes in Q-band absorbance upon exposure to 0–40 mM DTT with time are shown in (**c**) and (**d**) for **4.11a** and **4.11b**, respectively

Table 4.2 Summary of the slope values of the best-fitted straight line of the DPBF decay curves of **4.11a**, **4.11b**, and **4.12** upon exposure to different concentrations of DTT for 24 h with and without illumination

[DTT]	|Slope| (min^{-1})					
	With light			In dark		
	4.11a	**4.11b**	**4.12**	**4.11a**	**4.11b**	**4.12**
0 μM	0.020	0.016	–	–	–	–
2 μM	0.021	–	–	–	–	–
5 mM	0.096	–	–	–	–	–
10 mM	0.114	0.022	0.120	0.002	0.002	0.002

significantly affect the production of singlet oxygen. By attaching the ferrocenyl moieties to the phthalocyanine core, the fluorescence emission and singlet oxygen production of phthalocyanine are greatly reduced.

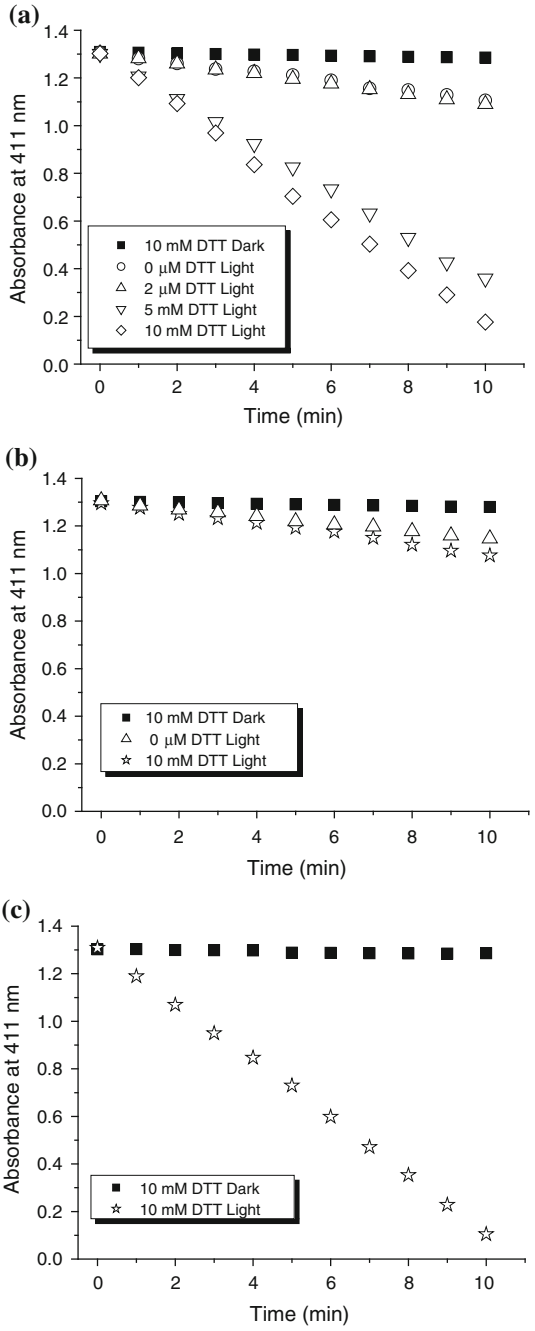

Fig. 4.7 Comparison of the rates of decay of DPBF (initial concentration = 70 μM) sensitized by (**a**) **4.11a**, (**b**) **4.11b**, and (**c**) **4.12** (all at 4 μM) upon exposure to different concentrations of DTT for 24 h in the presence of light (*open symbols*) ($\lambda > 610$ nm) in PBS with 0.5 % Cremophor EL. The corresponding dark control is shown as closed symbols

4.2.3 In Vitro Photodynamic Activities

The therapeutic efficacy of all these compounds was also investigated against MCF-7 human breast cancer cells. Figure 4.8 shows the dose-dependent curves of phthalocyanines **4.11a**, **4.11b**, **4.12**, and ferrocenyl compound **4.9a** with different concentrations of DTT in the absence and presence of light. The data for both 6 h and 24 h drug incubation are shown. It can be seen that all these compounds are non-cytotoxic in the absence of light regardless of the concentration of DTT and the incubation time. In the absence of DTT (Fig. 4.8a and b), phthalocyanines **4.11a** and **4.11b** exhibit similar photocytotoxicity, while the photocytotoxicity of **4.12** is relatively higher, which may be attributed to the absence of the ferrocenyl moieties. The ferrocenyl compound **4.9a** does not show any cytotoxicity up to a concentration of 1 mM (data not shown). To mimic the reducing environment of tumor, MCF-7 cells were first pretreated with DTT (2 μM or 4 mM) for 1 h, prior to incubation with the phthalocyanine solutions. In general, the photodynamic activity of these compounds remains virtually unchanged in the presence of 2 μM DTT (Fig. 4.8c and d). However, in the presence of 4 mM DTT, the photocytotoxicity of **4.11a**, but not **4.11b** and **4.12**, is significantly increased (Fig. 4.8e and f). Table 4.3 lists their corresponding IC_{50} values. It can be seen that the IC_{50} values of **4.11a** decrease by 2.0–2.5 fold upon addition of 4 mM DTT for both 6 h and 24 h incubation. The values are comparable to those of **4.12** under the same experimental conditions ($IC_{50} = 76$ nM for 6 h incubation and 50 nM for 24 h incubation). These results demonstrate that phthalocyanine **4.11a** is a promising photosensitizer of which the in vitro photodynamic activity can be greatly enhanced in a reducing environment as in tumor cells.

To further investigate the reductive cleavage of **4.11a** at the cellular level, its cellular uptake was examined by confocal laser scanning microscopy. MCF-7 cells were treated with different concentrations of DTT for 1 h, prior to incubation with the phthalocyanine solutions. In Fig. 4.9a, it can be seen that the MCF-7 cells, after being treated with **4.11a**, show strong intracellular fluorescence in the presence of 4 mM DTT, while the fluorescence is hardly observed in the cases of 0–2 μM DTT. As revealed by the images, there is no significant enhancement in fluorescence intensity for the non-cleavable analogue **4.11b** even in the presence of 4 mM DTT. The average relative fluorescence intensity per cell of these compounds was also measured and is compared in Fig. 4.9b. It is clear that the intracellular fluorescence intensity of **4.11a** is about 9-fold higher than that of **4.11b** at high concentration of DTT (4 mM). These results further demonstrate that the increase in fluorescence intensity is a result of the cleavage of the disulfide bonds of **4.11a** in the reducing environment.

To reveal the subcellular localization of **4.11a** after cleavage of the disulfide bonds, MCF-7 cells were stained with ER-Tracker, LysoTracker DND 26, or MitoTracker Green FM, which are specific fluorescence dyes for endoplasmic reticulum, lysosomes, and mitochondria, respectively, together with **4.11a**. As shown in Fig. 4.10, the fluorescence caused by the ER-Tracker (excited at 488 nm,

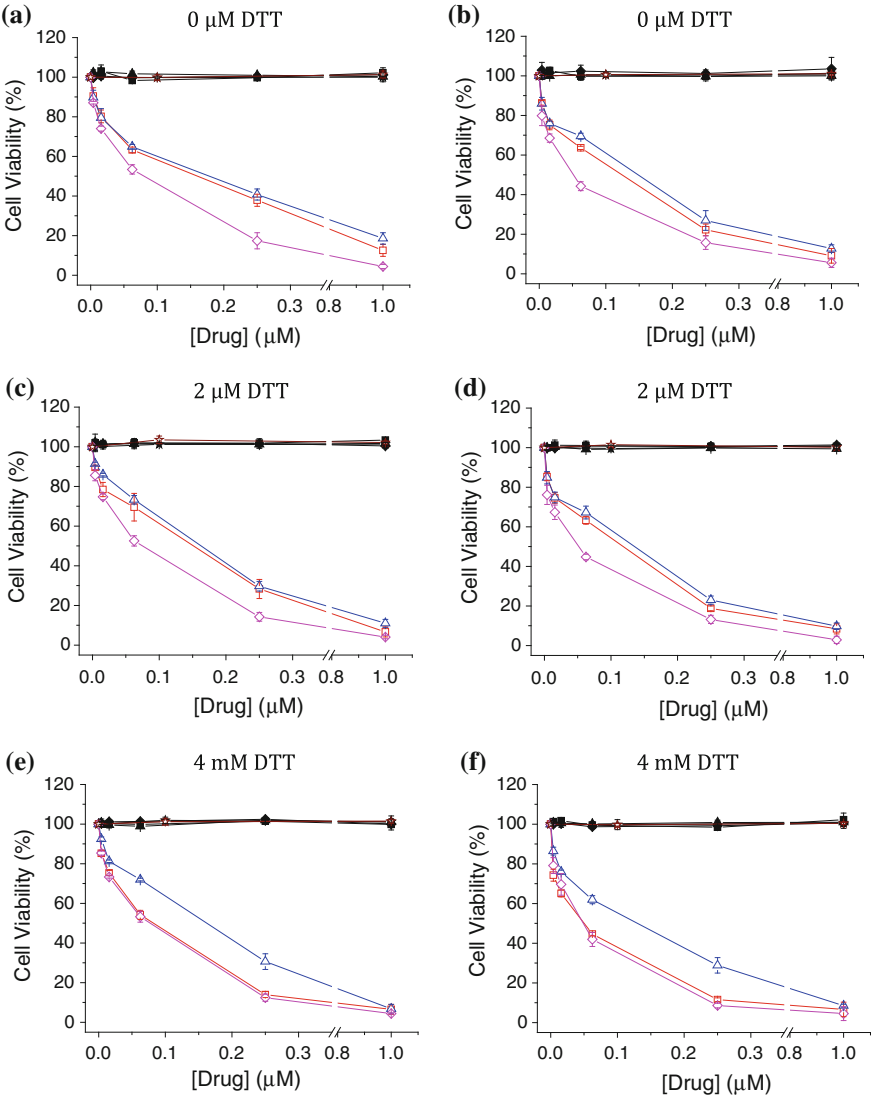

Fig. 4.8 Cytotoxic effects of **4.11a** (*squares*), **4.11b** (*triangles*), **4.12** (*rhombus*), and **4.9a** (*stars*) on MCF-7 cells pre-treated with different concentrations of DTT, prior to drug incubation for 6 h (**a**, **c**, and **e**) and 24 h (**b**, **d**, and **f**) in the absence (*closed symbols*) and presence (*open symbols*) of light ($\lambda > 610$ nm, 40 mW cm^{-2}, 48 J cm^{-2}). Data are expressed as mean value ± standard error of the mean (S.E.M.) of three independent experiments, each performed in quadruplicate

monitored at 510–560 nm) can superimpose with the fluorescence caused by **4.11a** after the disulfide bond cleavage (excited at 633 nm, monitored at 650–760 nm). This observation suggests that the photosensitizing fragment of **4.11a** can selectively localize in the endoplasmic reticulum of the cells. The very similar

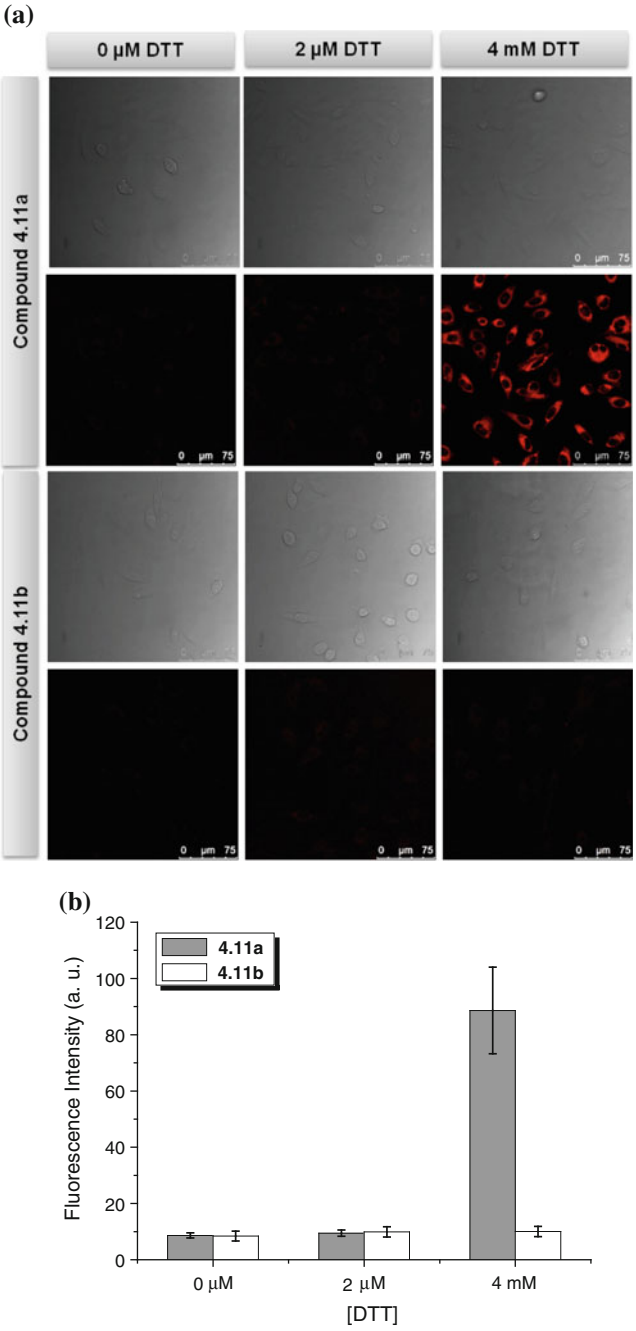

Fig. 4.9 (**a**) Confocal fluorescence images of MCF-7 cells pretreated with different concentrations of DTT, prior to incubation with **4.11a** or **4.11b** (both at 1 μM) for 24 h (*lower rows*). The corresponding bright field images are shown in the upper rows. (**b**) Comparison of the intracellular fluorescence intensity of **4.11a** and **4.11b** in the presence of various concentrations of DTT. Data are expressed as mean value ± standard deviation (S.D.) (number of cells = 30)

Table 4.3 Comparison of the IC_{50} values of **4.11a**, **4.11b**, and **4.12** against MCF-7 cells after 6 and 24 h incubation

	IC^{d}_{50} (nM)					
	6 h Drug Incubation			24 h Drug Incubation		
	0 μM DTT	2 μM DTT	4 mM DTT	0 μM DTT	2 μM DTT	4 mM DTT
4.11a	160	150	81	124	119	50
4.11b	179	162	163	149	135	130
4.12	80	75	76	52	51	50

[d] Defined as the dye concentration required to kill 50 % of the cells

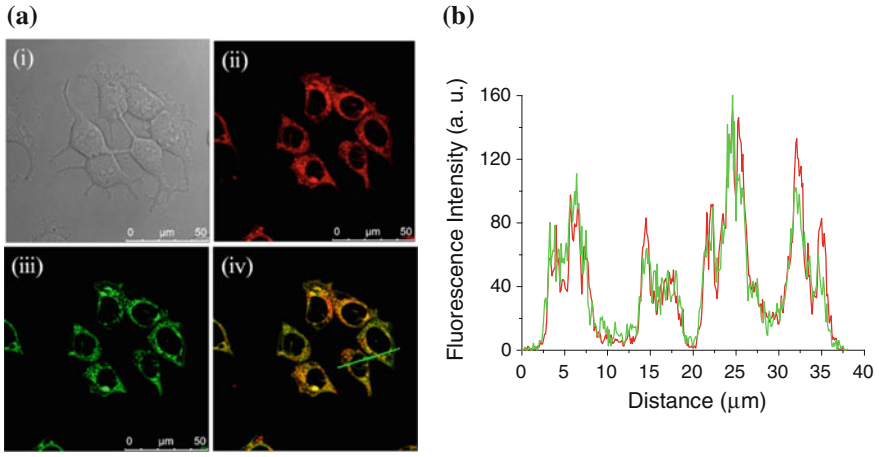

Fig. 4.10 (**a**) Visualization of (*i*) the bright field image, intracellular fluorescence of MCF-7 cells (pretreated with 4 mM DTT) using filter sets specific for (*ii*) **4.11a** (1 μM; in *red*) and (*iii*) ER-Tracker (in *green*), and (*iv*) the corresponding superimposed image. Figure (**b**) shows the fluorescence intensity profiles of **4.11a** (*red*) and ER-Tracker (*green*) traced along the *green line* in (**a**)(**iv**)

fluorescence intensity line profiles of **4.11a** and ER-Tracker traced along the green line in Fig. 4.10a (iv) further confirms the result. By contrast, the fluorescence images of **4.11a** could not overlap with the images of the MitoTracker and LysoTracker (Fig. 4.11), indicating that **4.11a** could not localize in the mitochondria or lysosomes of the MCF-7 cells after reductive disulfide bond cleavage.

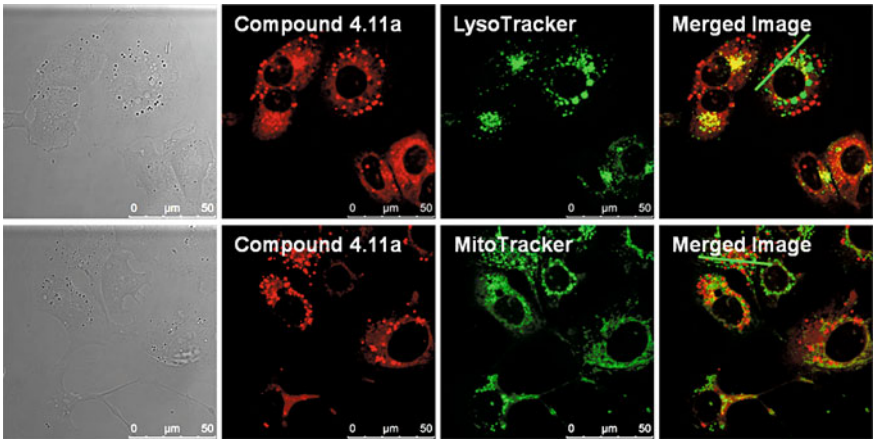

Fig. 4.11 Visualization of intracellular fluorescence of MCF-7 cells (pretreated with 4 mM DTT) using filter sets specific for **4.11a** (1 μM; in *red*, column 2) and LysoTracker or MitoTracker (in *green*, column 3). The corresponding superimposed and bright field images are given in columns 4 and 1, respectively

4.3 Summary

In summary, we have prepared a redox-responsive silicon(IV) phthalocyanine as potential photosensitizer for targeted PDT. In response to a DTT in millimolar range, which mimics the intracellular reducing environment of tumor cells, the fluorescence intensity, singlet oxygen generation efficiency, and photocytotoxicity of **4.11a** are significantly enhanced as a result of the cleavage of the disulfide bonds, thus restoring its fluorescence and photosensitizing property. As revealed by confocal microscopy, the photosensitizing fragment of **4.11a** can selectively accumulate in the endoplasmic reticulum of the MCF-7 cells. By replacing the ferrocenyl moiety with other ferrocene-containing anticancer drugs, it is envisaged that the resulting conjugates can exhibit targeted dual therapeutic effects. This further investigation is certainly worth-promising.

References

1. Blair, S.L., Heerdt, P., Sacher, S., Abolhoda, A., Hochwald, S., Cheng, H., Burt, M.: Cancer Res. **57**, 152 (1997)
2. Brown, S.B., Brown, E.A., Walker, I.: Lancet Oncol. **5**, 497 (2004)
3. Chen, J., Liu, T.W.B., Lo, P.-C., Wilson, B.C., Zheng, G.: Bioconjugate Chem. **20**, 1836 (2009)
4. Chen, J., Stefflova, K., Niedre, M.J., Wilson, B.C., Chance, B., Glickson, J.D., Zheng, G.J.: Am. Chem. Soc. **126**, 11450 (2004)

5. Chen, J., Lovell, J.F., Lo, P.-C., Stefflova, K., Niedre, M., Wilson, B.C., Zheng, G.: Photochem. Photobiol. Sci. **7**, 775 (2008)
6. Chen, J., Chen, S., Zhao, X., Kuznetsova, L.V., Wong, S.S., Ojima, I.J.: Am. Chem. Soc. **130**, 16778 (2008)
7. Chen, S., Zhao, X., Chen, J., Chen, J., Kuznetsova, L., Wong, S.S., Ojima, I.: Bioconjugate Chem. **21**, 979 (2010)
8. Cook, J.A., Pass, H.I., Iype, S.N., Friedman, N., Degraff, W., Russo, A., Mitchell, J.B.: Cancer Res. **51**, 4287 (1991)
9. Cuchelkar, V., Kopečková, P., Kopeček, J.: Macromol. Biosci. **8**, 375 (2008)
10. Dolmans, D.E.J.G.J., Fukumura, D., Jain, R.K.: Nat. Rev. Cancer **3**, 380 (2003)
11. Giasson, R., Lee, E.J., Zhao, X., Wrighton, M.S.J.: Phys. Chem. **97**, 2596 (1993)
12. Hong, R., Han, G., Fernández, J.M., Kim, B.-J., Forbes, N.S., Rotello, V.M.J.: Am. Chem. Soc. **128**, 1078 (2006)
13. Jiang, X.-J., Lo, P.-C., Yeung, S.-L., Fong, W.-P., Ng, D.K.P.: Chem. Commun. **46**, 3188 (2010)
14. Jiang, X.-J., Lo, P.-C., Tsang, Y.-M., Yeung, S.-L., Fong, W.-P., Ng, D.K.P.: Chem. Eur. J. **16**, 4777 (2010)
15. Jones, L.R., Goun, E.A., Shinde, R., Rothbard, J.B., Contag, C.H., Wender, P.A.J.: Am. Chem. Soc. **128**, 6526 (2006)
16. Kosower, N.S., Kosower, E.M.: Int. Rev. Cytol. **54**, 109 (1978)
17. Kuai, R., Yuan, W., Qin, Y., Chen, H., Tang, J., Yuan, M., Zhang, Z., He, Q.: Mol. Pharmaceutics **7**, 1816 (2010)
18. Lakshmi, V., Santosh, G., Ravikanth, M.J.: Organomet. Chem. **696**, 925 (2011)
19. Lee, Y.-J., Datta, S., Pellois, J.-P.J.: Am. Chem. Soc. **130**, 2398 (2008)
20. Lee, J.H., Lim, C.S., Tian, Y.S., Han, J.H., Cho, B.R.J.: Am. Chem. Soc. **132**, 1216 (2010)
21. Lo, P.-C., Chen, J., Stefflova, K., Warren, M.S., Navab, R., Bandarchi, B., Mullins, S., Tsao, M., Cheng, J.D., Zheng, G.J.: Med. Chem. **52**, 358 (2009)
22. Lovell, J.F., Liu, T.W.B., Chen, J., Zheng, G.: Chem. Rev. **110**, 2839 (2010)
23. Maree, M. D., Kuznetsova, N., Nyokong, T. J. Photochem. Photobiol. A **140**, 117 (2001)
24. McDonnell, S.O., Hall, M.J., Allen, L.T., Byrne, A., Gallagher, W.M., O'Shea, D.F.J.: Am. Chem. Soc. **127**, 16360 (2005)
25. Meister, A., Anderson, M.E.: Annu. Rev. Biochem. **52**, 711 (1983)
26. Poon, K.-W., Yan, Y., Li, X-y, Ng, D.K.P.: Organometallics **18**, 3528 (1999)
27. Sato, M., Kono, H., Shiga, M., Motoyama, I., Hata, K.: Bull. Chem. Soc. Jpn. **41**, 252 (1968)
28. Scalise, I., Durantini, E.N.: Bioorg. Med. Chem. **13**, 3037 (2005)
29. Shetti, V.S., Ravikanth, M.: Eur. J. Org. Chem. **3**, 494 (2010)
30. Stefflova, K., Chen, J., Marotta, D., Zheng, G.J.: Med. Chem. **49**, 3850 (2006)
31. Wilson, B.C., Patterson, M.S.: Phys. Med. Biol. **53**, R61 (2008)
32. Zheng, Z.-B., Zhu, G., Tak, H., Joseph, E., Eiseman, J.L., Creighton, D.J.: Bioconjugate Chem. **16**, 598 (2005)
33. Zheng, G., Chen, J., Stefflova, K., Jarvi, M., Li, H., Wilson, B.C.: Proc. Natl. Acad. Sci. U.S.A. **104**, 8989 (2007)
34. Zhu, B., Zhang, X., Li, Y., Wang, P., Zhang, H., Zhuang, X.: Chem. Commun. **46**, 5710 (2010)
35. Zsoldos-Mády, V., Csámpai, A., Szabó, R., Mészáros-Alapi, E., Pásztor, J., Hudecz, F., Sohár, P.: ChemMedChem **1**, 1119 (2006)

Chapter 5
A Dual pH- and Redox-Responsive Phthalocyanine-Based Photosensitizer for Targeted Photodynamic Therapy

5.1 Introduction

As mentioned in Chap. 1 (Sect. 1.3.2), different cancer-related stimuli have been explored to "turn on" the activatable photosensitizers with a view to controlling their photodynamic actions. One of the unique features of tumors is their highly reducing environment as compared to normal tissues due to an elevated level of glutathione (GSH) [4, 6, 15]. In Chap. 4, we have described a redox-responsive silicon(IV) phthalocyanine and evaluated the effect of the reductive stimulus on its photophysical properties and in vitro photodynamic activity. In response to a reducing condition analogous to tumor environment, it shows a significant enhancement in fluorescence intensity, singlet oxygen generation efficiency, and photocytotoxicity as a result of reductive cleavage of the disulfide bonds. Another special characteristic of tumors is their relatively low pH in the extracellular region (ca. 6.8) compared with that around normal tissues (ca. 7.3) [11, 27]. The pH-dependent behavior of several classes of photosensitizers, such as porphyrins [7–9, 19], chlorins [7–9, 19, 20, 24, 25], chalcogenopyrylium dyes [3], and phenylene vinylenes [1], has been briefly examined. Recently, we have reported a series of pH-responsive silicon(IV) phthalocyanines substituted with amino moieties in which their photosensitizing properties are greatly enhanced at lower pH, mainly due to protonation of the amino groups which inhibits the intramolecular photo-induced electron transfer (PET) process [14, 16].

The aforementioned examples have vividly demonstrated the use of a single stimulus for photosensitizer activation. In fact, another promising approach is to use two stimuli for the activation of photosensitizer in which the photosensitizer can be fully turned on only when it is exposed to two stimuli concurrently. To this end, Akkaya et al. have reported a boron dipyrromethene (BODIPY)-based activatable photosensitizer in which it exhibits about 6-fold increase in singlet oxygen generation at low pH and high concentration of sodium ion, but no increase in either low pH or high concentration of sodium ion [21]. In addition, dual pH- and redox-sensitive micelles [5] and microcapsules [10] for pinpointed intracellular delivery of anticancer drugs have also been developed. The anticancer drugs are

J. T. F. Lau, *Towards Dual and Targeted Cancer Therapy with Novel Phthalocyanine-based Photosensitizers*, Springer Theses,
DOI: 10.1007/978-3-319-00708-3_5,

effectively released due to the carrier's susceptible nature to both intracellular reduction and low pH conditions after internalization by tumor cells.

As an extension of our work described in Chap. 4, we have designed a novel dual pH- and redox-responsive phthalocyanine-based activatable photosensitizer. The preparation and basic photophysical properties of this compound, as well as the effect of the pH and reducing stimulus on its in vitro properties are described in this chapter.

5.2 Results and Discussion

5.2.1 Molecular Design, Synthesis, and Characterization

In order to confer a redox-responsive property to the phthalocyanine, the ferrocenyl-chalcone ligand **4.9a** (see Chap. 4) was introduced to one of the axial positions. To further incorporate a pH-responsive property to the same phthalocyanine, another ferrocenyl ligand **5.8** was conjugated to the macrocycle through an acid-labile hydrazone linker, which can be selectively cleaved under acidic conditions with pH ranging from 5 to 6 [2]. It is anticipated that the photosensitizing property of the phthalocyanine is inhibited by the ferrocenyl moieties when they are in close proximity. However, when it is exposed to a highly reducing and acidic environment as in the tumor tissues, the disulfide and hydrazone linkers of this compound are expected to be cleaved favorably, thus restoring the photosensitizing property.

Scheme 5.1 shows the synthesis of the acid-labile ferrocenyl carbonyl hydrazone ligand **5.8**. Starting with the commercially available 3,5-dihydroxybenzoic acid (**5.1**), it was first esterificated to methyl 3,5-dihydroxybenzoate (**5.2**) with the aid of a catalytic amount of H_2SO_4 and methanol [26]. It was then reduced by lithium aluminium hydride ($LiAlH_4$) in anhydrous tetrahydrofuran (THF) to give 3, 5-dihydroxybenzyl alcohol (**5.3**) [17]. One equiv. of ethyl bromoacetate (**4.5**) was allowed to react with 1 equiv. of alcohol **5.3** in the presence of anhydrous potassium carbonate and acetone to afford the monosubstituted product **5.4**. To enhance the solubility and reduce the aggregation tendency of the phthalocyanine before and after cleavage of both disulfide and hydrazone linkers, a triethylene glycol monomethyl ether chain was introduced by treating **5.4** with tosylate **5.5** [22] to give compound **5.6**. Treatment of hydrazine hydrate with ester **5.6** in ethanol gave hydrazine **5.7** in good yield, which further reacted with ferrocenecarboyaldehyde (**4.2**) in refluxing ethanol to give the ferrocenylcarbonylhydrazone ligand **5.8**.

Scheme 5.2 shows the synthetic route for the preparation of the unsymmetrical phthalocyanine **5.9**. The readily available silicon(IV) phthalocyanine dichloride (**4.10**) was first refluxed with alcohol **4.9a** in the presence of excess pyridine in toluene for 2 h, prior to the addition of ferrocenylcarbonylhydrazone **5.8**. The reaction mixture was continued to reflux for another 4 h to give the unsymmetrical phthalocyanine **5.9** in 15 % yield. Apart from the unsymmetrical phthalocyanine

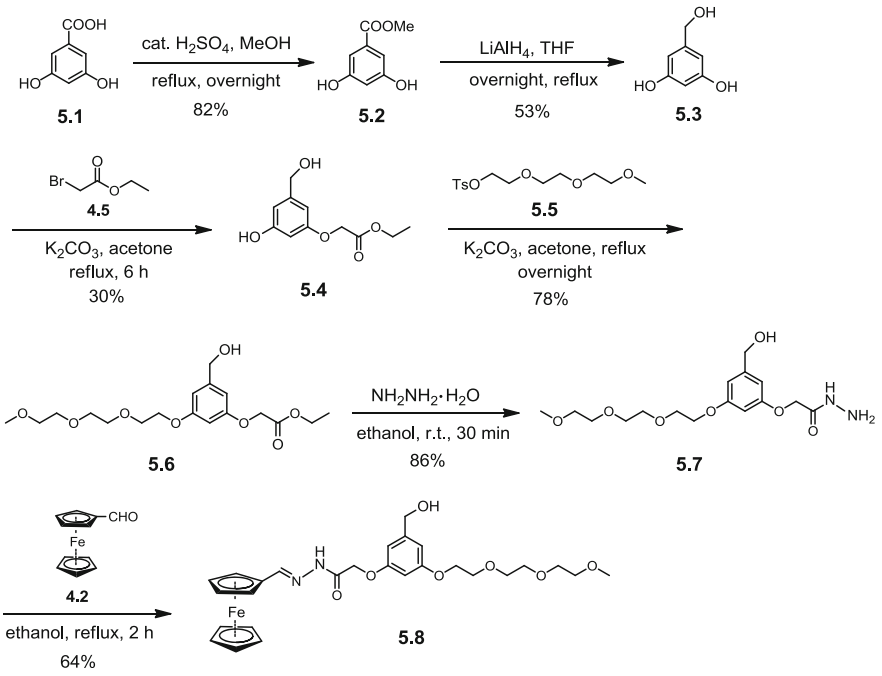

Scheme 5.1 Synthesis of ferrocenylcarbonylhydrazone **5.8**

5.9, a considerable amount of the symmetrical phthalocyanine **5.10** was also isolated in 43 % yield. In view of the potential pH-responsive property of this compound, we also included it in the following study. This compound was also prepared by treating ferrocenylcarbonylhydrazone **5.8** with phthalocyanine **4.10** under a similar reaction condition (Scheme 5.3). As expected, the reaction led to a higher yield (79 %) of **5.10**.

All the new compounds were fully characterized with various spectroscopic methods. Figure 5.1 shows the ^{1}H NMR spectrum of **5.9** in $CDCl_3$. It shows two AA′BB′ downfield multiplets at δ 9.61–9.63 and 8.33–8.35 (8H each), which are assigned to the phthalocyanine α- and β-ring protons, respectively. For the ferrocenyl-chalcone unit, H_a and H_b resonate as two separate triplets at δ −1.77 and −0.38, respectively. These signals appear at very upfield positions due to the shielding effect of the phthalocyanine ring. With reference to the ^{1}H NMR spectrum of symmetrical phthalocyanine **4.11a** (see Appendix 24) and the ^{1}H−^{1}H COSY spectrum of **5.9** (see Appendix 32 for the full spectrum), the signals for H_c and H_d are masked by the signal of residual water in $CDCl_3$ and the multiplets at δ 3.43–3.62, respectively. The four sets of doublets in between δ 6.81 and 7.91 correspond to the aromatic (H_f and H_g) and vinyl protons (H_h and H_i) of the ligand. As revealed by the coupling constants (J), the signals resonated at δ 7.08 and 7.73 are due to the vinyl protons (J = 15.2 and 15.6 Hz, respectively), whereas the signals at δ 6.81 and 7.91 correspond to the aromatic protons (J = 8.8 Hz). This assignment was further supported by

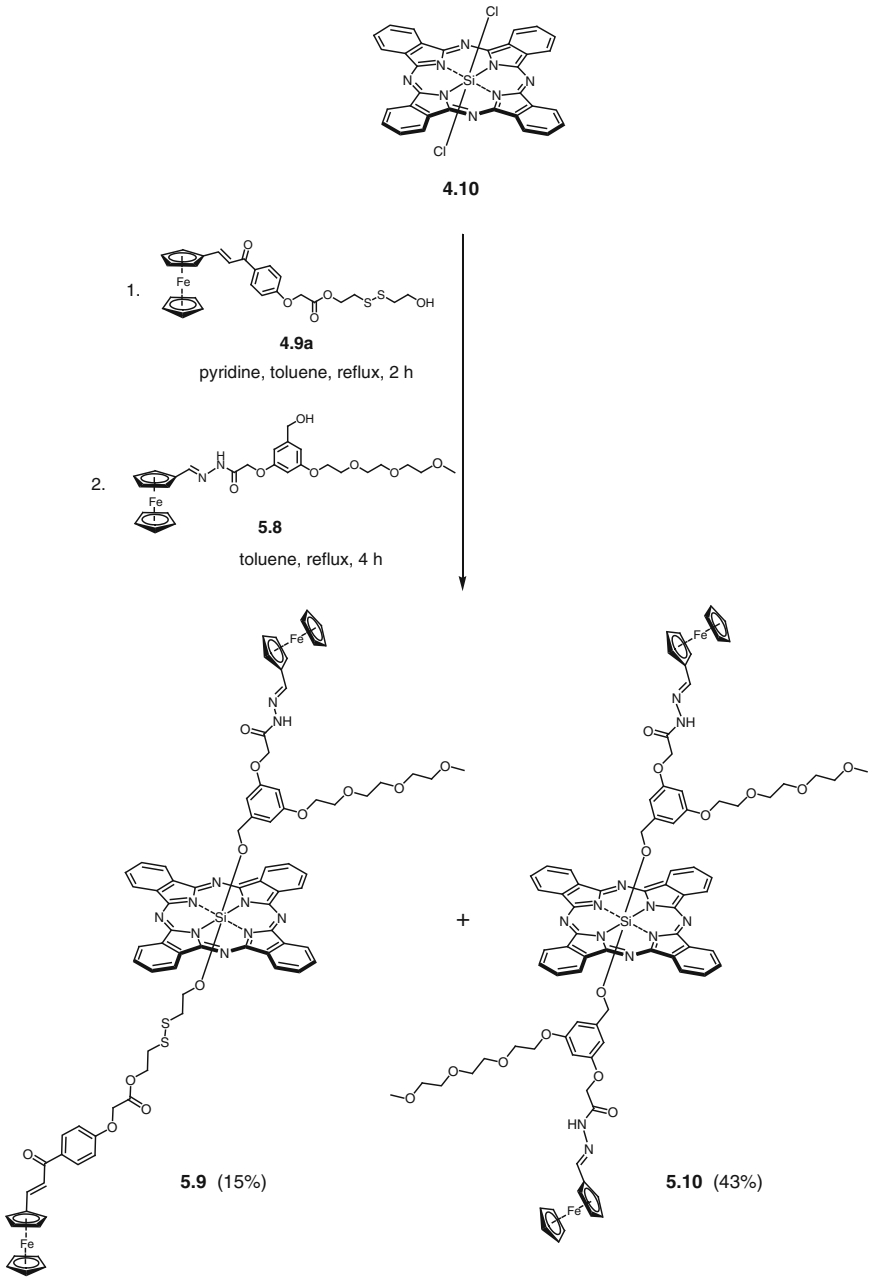

Scheme 5.2 Synthesis of silicon(IV) phthalocyanines **5.9** and **5.10**

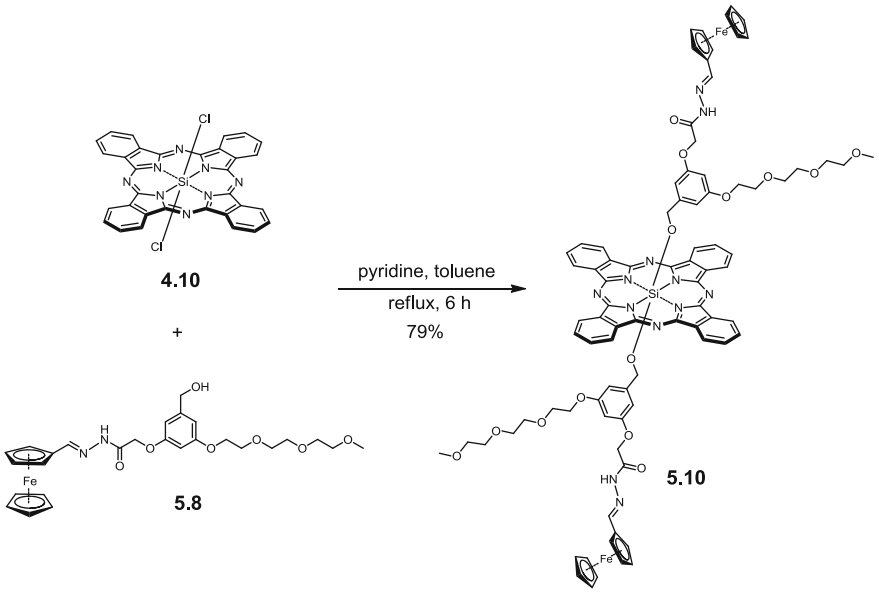

Scheme 5.3 Synthesis of silicon(IV) phthalocyanine **5.10**

the ^{1}H−^{1}H COSY spectrum in which two sets of correlated signals are observed (Fig. 5.2a). By taking reference to the ^{1}H NMR spectrum of **4.11a**, the singlet (2H) at δ 4.39 can be assigned to H_e. Since H_e does not couple with any nearby protons, it resonates as an isolated signal in the ^{1}H–^{1}H COSY spectrum (Fig. 5.2b). For the ferrocenylcarbonylhydrazone unit, the signal for H_1 is shifted upfield as a singlet at δ −0.70 due to the phthalocyanine ring current effect. Similarly, aromatic protons H_2, H_3, and H_4 are also shifted upfield. The strong singlet (3H) at δ 3.36 and the multiplets at δ 3.43–3.62 (14H, of which 2H belong to H_d) are assigned to the methyl and methylene protons of the triethylene glycol chain, respectively. The three distinct singlets at δ 3.83, 8.00, and 8.74 can be unambiguously assigned to the methylene proton H_5, imine proton H_7, and amide proton H_6, respectively, with reference to the ^{1}H NMR spectrum of **5.10** (see Appendix 33). As the two ferrocene units of **5.9** locate at two different electronic environments, it is expected that each of them resonates as two sets of signals with three singlets in a ratio of 2:2:5, which is typical for a monosubstituted ferrocene. The assignment is also confirmed by two sets of correlated signals as shown in the ^{1}H−^{1}H COSY spectrum (Fig. 5.2b).

5.2.2 Electronic Absorption and Photophysical Properties

Figure 5.3 shows the electronic absorption spectra of phthalocyanines **5.9** and **5.10** in DMF. These spectra are typical for non-aggregated phthalocyanines with a B-band at 354 nm, an intense and sharp Q-band at 677–678 nm, together with two

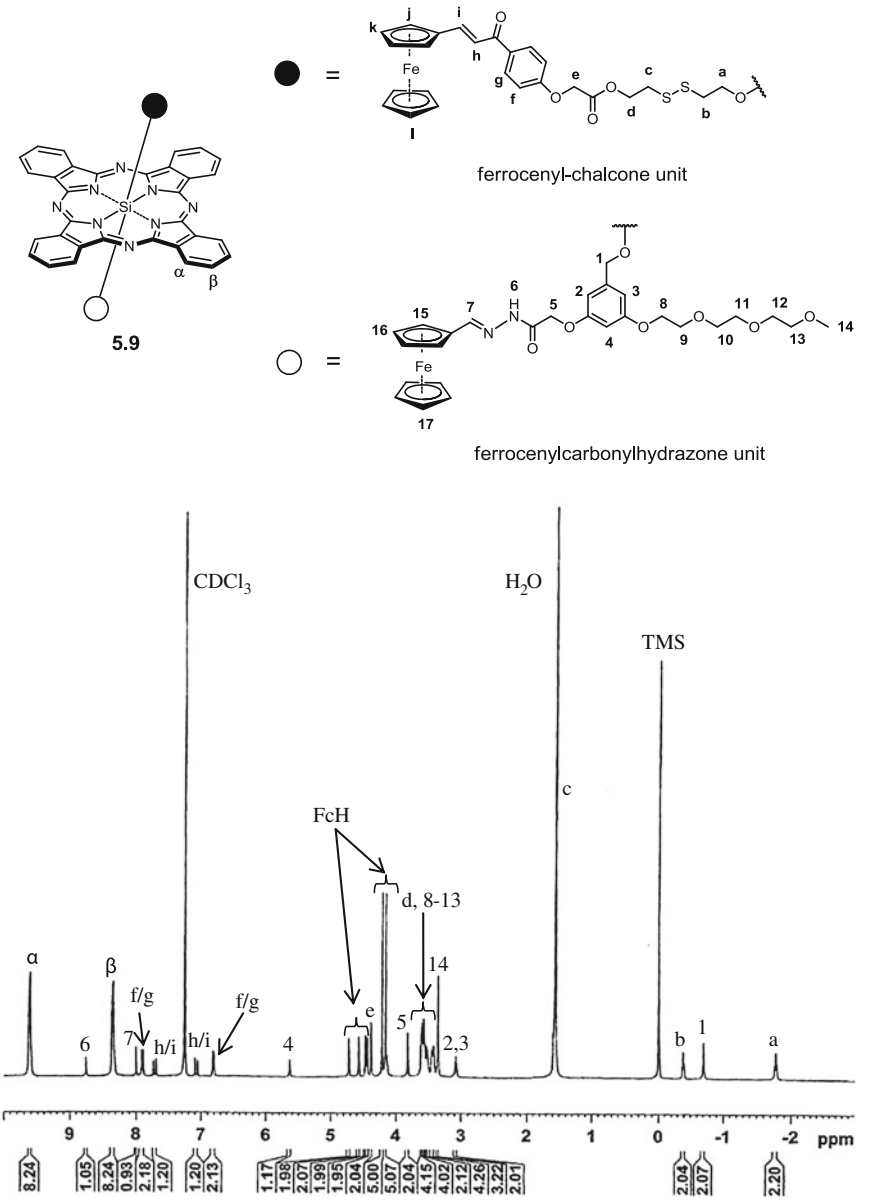

Fig. 5.1 ^{1}H NMR spectrum of **5.9** in $CDCl_3$

vibronic bands at 608–611 and 646–647 nm (Table 5.1). For the unsymmetrical phthalocyanine **5.9**, two additional bands at 330 and 496 nm, probably due to the absorption of the π-conjugated ferrocenyl-chalcone system, were also recorded. In fact, a similar phenomenon has been observed for phthalocyanines **4.11a** and **4.11b**

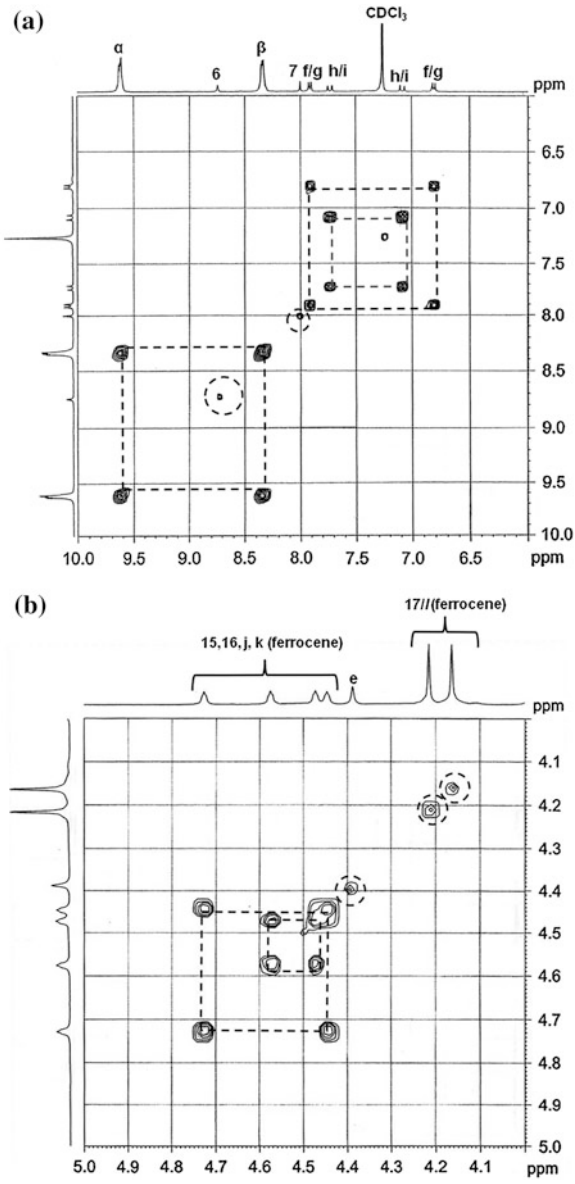

Fig. 5.2 $^{1}H-^{1}H$ COSY spectrum of **5.9** in $CDCl_3$. (*Dotted squares* and *circles* denote correlated and isolated signals, respectively.)

as described in Chap. 4. Upon excitation at 610 nm, these phthalocyanines showed a fluorescence emission at 687–688 nm. Due to the quenching effect of the singlet excited state of the phthalocyanines by the ferrocenyl moieties, they displayed relatively low fluorescence quantum yields ($\Phi_F = 0.03$-0.05) relative to unsubstituted zinc(II) phthalocyanine (ZnPc) in DMF ($\Phi_F = 0.28$) (Table 5.1) [23]. These values are comparable to the values for **4.11a** and **4.11b** (see Table 4.1).

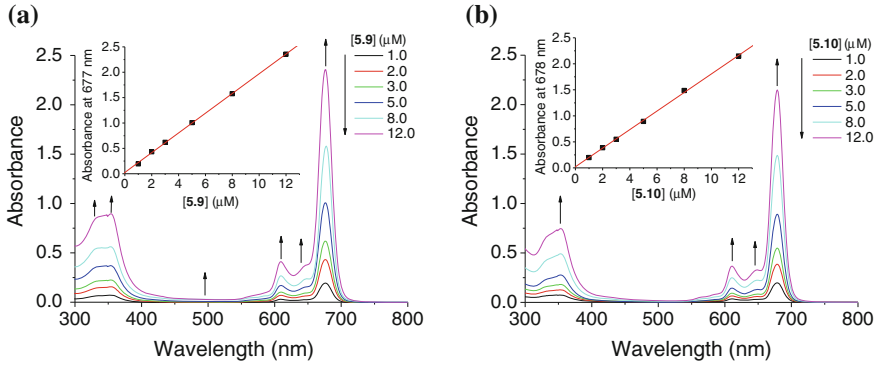

Fig. 5.3 Electronic absorption spectra of (**a**) **5.9** and (**b**) **5.10** in different concentrations in DMF. The inset plots the Q-band absorbance versus the concentration of the phthalocyanine, and the line represents the best-fitted straight line

To evaluate the photosensitizing efficiency of phthalocyanines **5.9** and **5.10**, their singlet oxygen quantum yields (Φ_Δ) were determined by a steady-state method with 1,3-diphenylisobenzofuran (DPBF) as the scavenger in DMF. The changes in concentration of the quencher were monitored spectroscopically at 411 nm with time (Fig. 5.4), from which the values of Φ_Δ could be determined by the method described previously [18]. Both phthalocyanines could generate singlet oxygen ($\Phi_\Delta = 0.07-0.10$), but the efficiency was much lower than that of ZnPc ($\Phi_\Delta = 0.56$) (Table 5.1) [18]. The relatively low singlet oxygen quantum yields of **5.9** and **5.10** may also be attributed to the quenching effect by the ferrocenyl moieties, which disfavor intersystem crossing and eventually the formation of singlet oxygen. A similar phenomenon has also been observed for **4.11a** and **4.11b** as described in Chap. 4.

In order to gain a better understanding on the aggregation behavior of the phthalocyanines in the biological environment, their electronic absorption and fluorescence spectra were also recorded in the Roswell Park Memorial Institute (RPMI) 1640 culture medium with 0.5 % Cremophor EL. As shown in Fig. 5.5a, both phthalocyanines display a sharp and intense Q-band, indicating that they are essentially non-aggregated in the culture medium. Their corresponding fluorescence spectra in the same condition are shown in Fig. 5.5b. To demonstrate the quenching effect exerted by the ferrocenyl moieties, the spectra of **4.11a** and **4.12** are also included for comparison. Among these four compounds, **4.12** shows the greatest fluorescence intensity since the two ferrocenyl moieties are absent in this compound. As expected, the three ferrocenyl phthalocyanines **4.11a**, **5.9**, and **5.10** show very weak fluorescence intensity due to the quenching effect, particularly for **5.10**, which has the shortest separation between two the quencher and the phthalocyanine ring.

Table 5.1 Electronic absorption and photophysical data for **5.9** and **5.10** in DMF

Compound	λ_{max} (nm) (log ε)	λ_{em}(nm)[a]	Φ^{b}_{F}	Φ^{c}_{Δ}
5.9	330 (4.84), 354 (4.86), 496 (3.47), 608 (4.53), 646 (4.49), 677 (5.29)	687	0.05	0.10
5.10	354 (4.79), 611 (4.48), 647 (4.43), 678 (5.25)	688	0.03	0.07

[a] Excited at 610 nm. [b] Using ZnPc in DMF as the reference ($\Phi_F = 0.28$). [c] Using ZnPc as the reference ($\Phi_\Delta = 0.56$ in DMF)

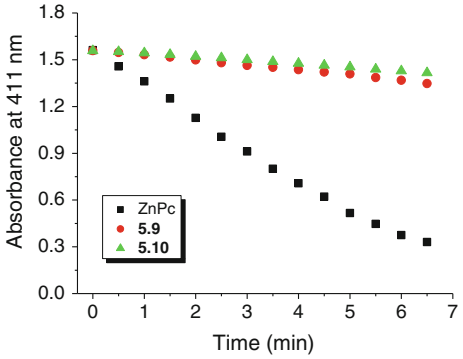

Fig. 5.4 Comparison of the rates of decay of DPBF (initial concentration = 70 μM) sensitized by **5.9**, **5.10**, and **ZnPc** (all at 3 μM) in DMF as shown by the decrease in the absorbance at 411 nm

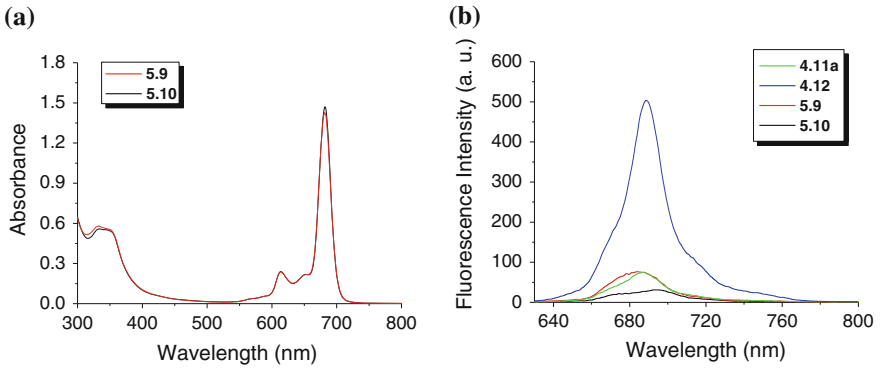

Fig. 5.5 (**a**) Electronic absorption spectra of **5.9** and **5.10** in the RPMI culture medium with 0.5 % Cremophor EL (both at 8 μM). The fluorescence spectra ($\lambda_{ex} = 610$ nm) of **4.11a**, **4.12**, **5.9**, and **5.10** under the same conditions are shown in (**b**)

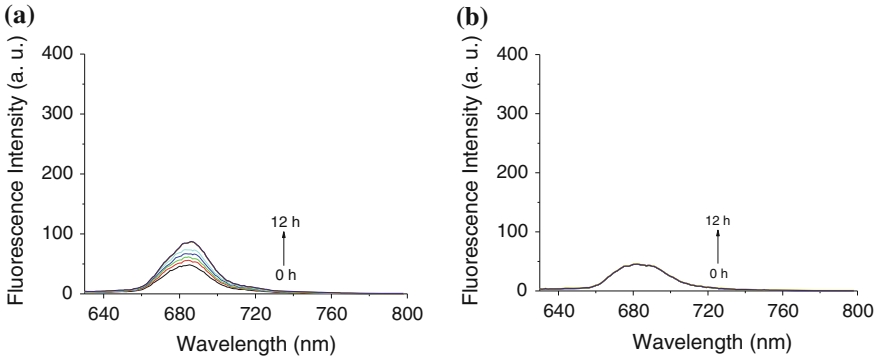

Fig. 5.6 Changes in fluorescence spectra ($\lambda_{ex} = 610$ nm) of (**a**) **5.9** and (**b**) **5.10** (both at 4 μM) in the presence of 10 mM DTT in PBS with 0.5 % Cremophor EL with time

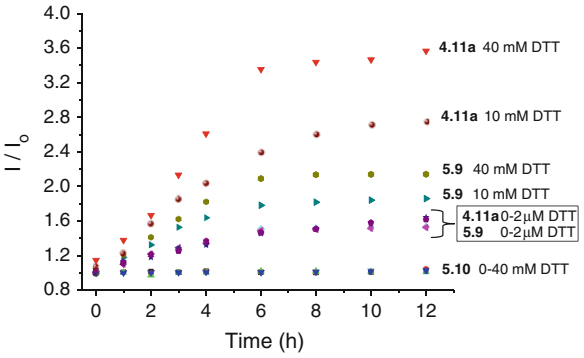

Fig. 5.7 Changes in fluorescence intensities of **4.11a**, **5.9**, and **5.10** (all at 4 μM) toward different concentrations of DTT in PBS with 0.5 % Cremophor with time

5.2.3 pH- and Redox-Responsive Properties

To investigate the pH- and redox-responsive properties of these phthalocyanines, their fluorescence response toward different concentrations of dithiothreitol (DTT), and different pH in phosphate buffered saline (PBS) was first studied. For comparison, the response of the redox-sensitive phthalocyanine **4.11a** and the non-cleavable control **4.11b** is also included.

5.2.3.1 Fluorescence Response to DTT

The redox-responsive properties of **4.11a**, **5.9**, and **5.10** were evaluated by monitoring their changes in fluorescence intensity with different DTT concentrations against time. In Chap. 4, we have reported the time-dependent changes in fluorescence spectra of **4.11a** and **4.11b** at different concentrations of DTT in PBS (Fig. 4.4). In the present investigation, we have also performed a similar study to

examine the effect of DTT on the fluorescence intensities of **5.9** and **5.10.** Figure 5.6 shows the time-dependent changes in fluorescence intensities of **5.9** and **5.10** in PBS with 10 mM DTT for exemplification. Figure 5.7 summarizes the time-dependent changes in fluorescence intensities of all the phthalocyanines upon exposure to different concentrations of DTT in PBS. It can be seen that phthalocyanine **4.11a** shows the greatest enhancement in fluorescence intensity in the presence of 10 or 40 mM DTT as a result of the disulfide bond cleavage. As expected, compound **5.10** shows negligible changes in fluorescence intensity as the acid-labile hydrazone linkers are not responsive to a reducing stimulus. For the unsymmetrical phthalocyanine **5.9**, it shows moderate fluorescence enhancement in the presence of 10 or 40 mM DTT. The moderate increase in fluorescence intensity is attributed to the cleavage of the disulfide bond, thus releasing one ferrocenyl moiety. Since the singlet excited state is still partially quenched by the ferrocenylcarbonylhydrazone moiety, the fluorescence intensity enhancement was not as significant as **4.11a** under the same experimental condition. Upon addition of 2 μM DTT, which mimics the extracellular environment, the fluorescence intensities of both **4.11a** and **5.9** only increase slightly.

In order to examine the aggregation behavior of these phthalocyanines during the kinetic study, their respective Q-band was monitored over 12 h. As shown in Fig. 5.8, the Q-bands remained relatively sharp and intense, suggesting that the phthalocyanine fragment formed after cleavage of the disulfide bond of **5.9** and compound **5.10** are essentially non-aggregated throughout the study.

5.2.3.2 Fluorescence Response to pH

The effect of pH on the fluorescence emission of **4.11a**, **5.9**, and **5.10** was also examined. Figure 5.9 shows the time-dependent changes in fluorescence spectra of **5.10** in PBS at pH 4.5, 6.0, and 7.4, which were used to mimic the tumor lysosomal compartment, tumor interstitial environment, and extracellular environment of normal tissues, respectively. It can be seen that the fluorescence increases to a greater extent at lower pH. Figure 5.10 summarizes the corresponding time-dependent changes in fluorescence intensities of **4.11a**, **5.9**, and **5.10** in PBS at the above pH values. For compound **5.10**, there are no significant changes in the fluorescence intensity over 12 h at pH 7.4, while its fluorescence intensity increases significantly at pH 4.5 and 6.0. The enhancement of fluorescence intensities at pH 4.5 and 6.0 is attributed to the hydrolytic cleavage of the hydrazone bond, thus releasing the ferrocenyl moieties and inhibiting the quenching effect. The fluorescence intensity of **5.10** increases by about 6-fold when the pH decreases from 7.4 to 4.5. For the unsymmetrical phthalocyanine **5.9**, it shows moderate increase in fluorescence intensity at pH 4.5 and 6.0 due to the release of only one ferrocenyl moiety. As the singlet excited state of the phthalocyanine is still partially quenched by the remaining ferrocenyl-chalcone moiety after cleavage of the hydrazone bond, the fluorescence intensity enhancement is not as drastic as **5.10** under the same experimental condition. For compound **4.11a**,

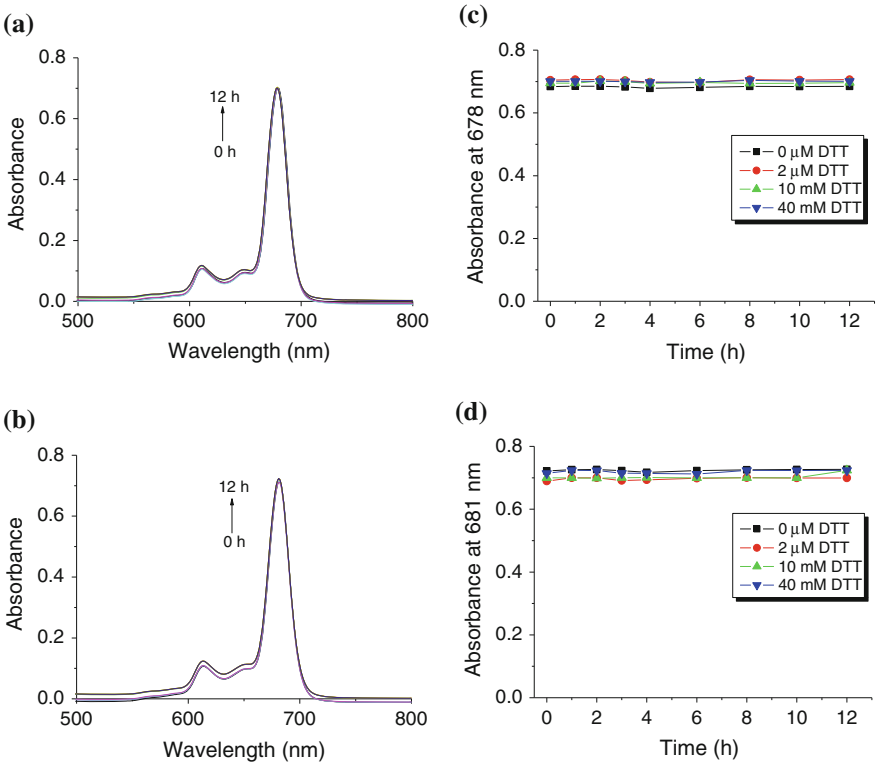

Fig. 5.8 Changes in absorption spectra of (**a**) **5.9** and (**b**) **5.10** (both at 4 μM) upon exposure to 40 mM DTT in PBS with 0.5 % Cremophor EL with time. The changes in Q-band absorbance upon exposure to 0-40 mM DTT with time are shown in (**c**) and (**d**) for **5.9** and **5.10**, respectively

which does not possess any pH-responsive linkages, no significant fluorescence enhancement was observed at pH 4.5 to 7.4. Similarly, the Q-band of these compounds remained sharp and intense during the 12-hour kinetic study (data not shown). The results suggest that these compounds or their phthalocyanine fragments are essentially non-aggregated throughout the study.

5.2.3.3 Fluorescence Response to DTT and pH

We proceeded to examine the time-dependent changes of fluorescence intensities of **4.11a**, **4.11b**, **5.9**, and **5.10** in PBS at pH 6.0 or 7.4 in the presence of 2 μM or 10 mM DTT (Fig. 5.11). For the redox-responsive phthalocyanine **4.11a**, enhancement in fluorescence intensity was observed in a higher DTT concentration (10 mM) and was independent of the change in pH (Fig. 5.11a). By contrast, the fluorescence enhancement of the pH-responsive analogue **5.10** was observed when the pH was changed from 7.4 to 6.0 regardless the concentration of DTT

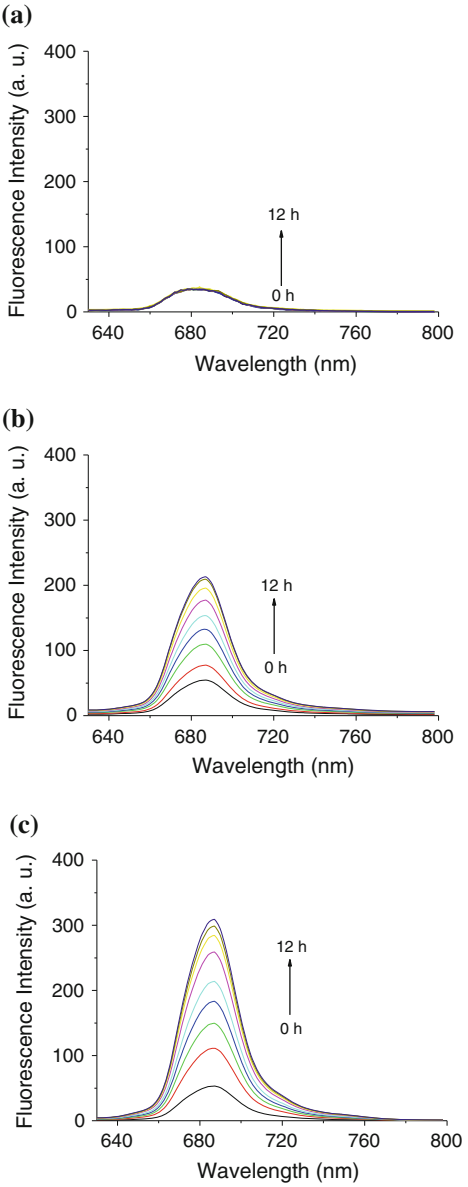

Fig. 5.9 Changes in fluorescence spectra ($\lambda_{ex} = 610$ nm) of **5.10** (4 μM) in PBS (with 0.5 % Cremophor) at different pH (4.5, 6.0, and 7.4) with time

(Fig. 5.11d). For the unsymmetrical phthalocyanine **5.9**, the fluorescence enhancement was most significant when it was exposed to pH 6.0 and 10 mM DTT, while the response was comparatively less significant at either low pH or high DTT concentration. The fluorescence increase was minimal at pH 7.4 and 2 μM DTT (Fig. 5.11c). These observations suggest that both the disulfide and hydrazone linkages of **5.9** are cleaved in the presence of 10 mM DTT at pH 6.0,

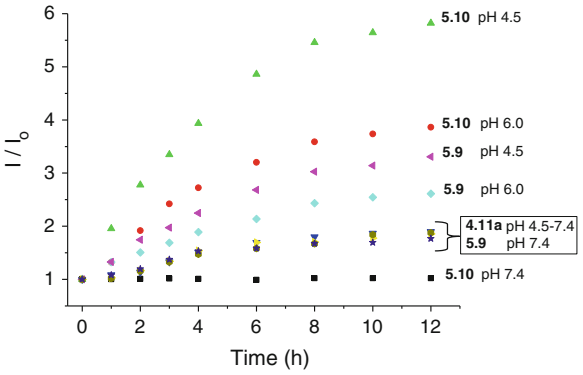

Fig. 5.10 Changes in fluorescence intensities of **4.11a**, **5.9**, and **5.10** (all at 4 μM) in PBS (with 0.5 % Cremophor) at different pH (4.5, 6.0, and 7.4) with time

releasing the two ferrocenyl moieties, thereby minimizing the quenching effect and restoring the fluorescence intensity. As expected, for the non-cleavable control **4.11b**, there were negligible changes in fluorescence intensities at all these conditions (Fig. 5.11b). As revealed by the sharp and intense Q-band of these phthalocyanines (data not shown), these compounds and their fragments remained essentially non-aggregated throughout the kinetic study.

5.2.3.4 Effect of DTT on Singlet Oxygen Production

Apart from fluorescence response, the effects of DTT and pH on the efficiency of singlet oxygen generation of **5.9** and **5.10** in PBS were also studied. For comparison, the response of **4.11a** was also included. Figure 5.12 compares the rates of decay of DPBF sensitized by **4.11a**, **5.9**, and **5.10** upon exposure to different concentrations of DTT for 8 h in PBS. All these phthalocyanines could not induce singlet oxygen generation in the dark even in the presence of 10 mM DTT (data not shown). Upon illumination and at 2 μM DTT, which was used to mimic the extracellular reducing environment, all these phthalocyanines could produce a small amount of singlet oxygen. In the presence of 10 mM DTT, which mimics the intracellular reducing environment, the singlet oxygen production efficiency of **4.11a** and **5.9** increased remarkably. The enhancement in singlet oxygen generation could be ascribed to the reductive cleavage of the disulfide bonds, resulting in restoration of the photosensitizing property. Since **5.9** still contains the ferrocenylcarbonylhydrazone moiety after cleavage of the disulfide bond, the singlet oxygen generation efficiency of **5.9** is lower than that of **4.11a**. For **5.10**, which does not contain disulfide linkages, the singlet oxygen production was minimal even in the presence of 10 mM DTT.

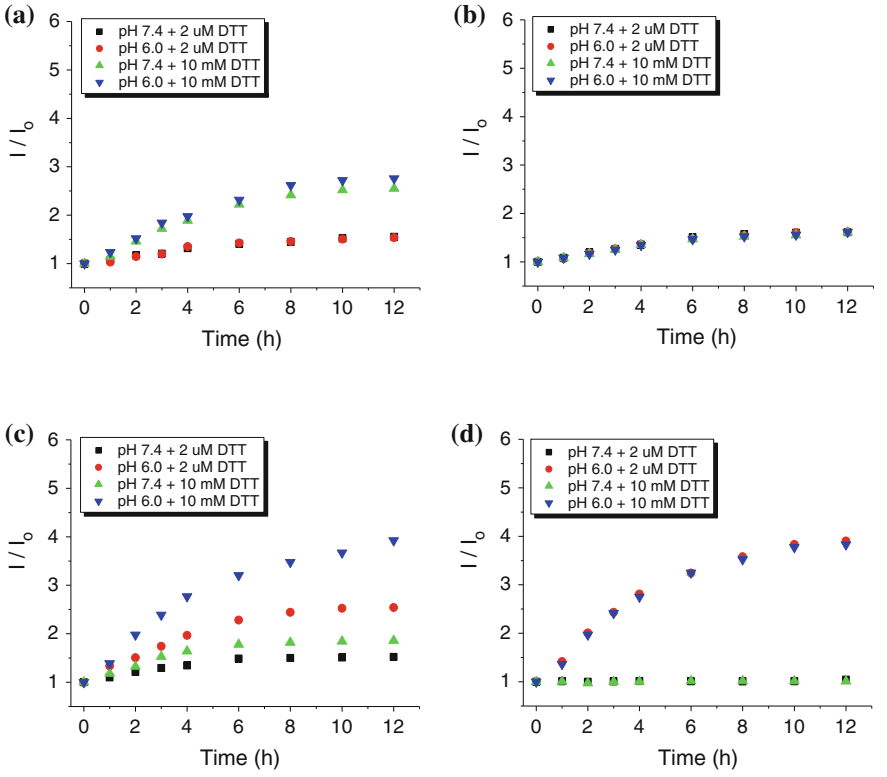

Fig. 5.11 Time-dependent changes in fluorescence intensities of (**a**) **4.11a**, (**b**) **4.11b**, (**c**) **5.9**, and (**d**) **5.10** (all at 4 μM) in PBS (with 0.5 % Cremophor) at pH 6.0 or 7.4 and in the presence of 2 μM or 10 mM DTT

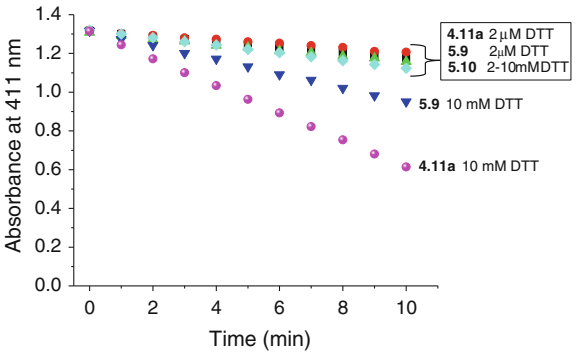

Fig. 5.12 Comparison of the rates of decay of DPBF (initial concentration = 70 μM) sensitized by **4.11a**, **5.9**, and **5.10** (all at 4 μM) upon exposure to different concentrations of DTT for 8 h in PBS with 0.5 % Cremophor EL

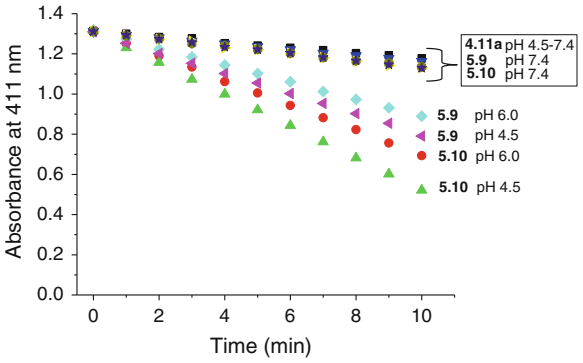

Fig. 5.13 Comparison of the rates of decay of DPBF (initial concentration = 70 μM) sensitized by **4.11a**, **5.9**, and **5.10** (all at 4 μM) in PBS with 0.5 % Cremophor EL at different pH (4.5, 6.0, and 7.4) for 8 h in the presence of light ($\lambda > 610$ nm)

5.2.3.5 Effect of pH on Singlet Oxygen Production

The effects of pH on the production of singlet oxygen of these phthalocyanines were also examined. Figure 5.13 compares the rates of decay of DPBF induced by these phthalocyanines in PBS at different pH (4.5, 6.0, and 7.4) for 8 h. In the absence of light, all these phthalocyanines could not sensitize the production of singlet oxygen (data not shown). At pH 7.4, they could slightly produce singlet oxygen upon illumination. Under a mildly acidic condition (pH 6.0), both **5.9** and **5.10** showed an increase in the production of singlet oxygen. The singlet oxygen generation efficiency was further enhanced when the pH was decreased to 4.5. Such an increase in singlet oxygen generation could be attributed to the hydrolysis of the hydrazone linkers under acidic conditions, thus releasing the ferrocenyl moieties and reducing the quenching effect. Since **5.9** still contains a ferrocenyl-chalcone moiety after cleavage of the hydrazone bond, its singlet oxygen generation efficiency is lower than that of **5.10** at the same pH. As expected, the control **4.11a** is not responsive to pH due to the absence of acid-labile linkages. These results demonstrate that compound **5.10** is also a promising tumor-selective photosensitizer as it exhibits remarkably different fluorescence emission and singlet oxygen generation properties at pH 4.5, 6.0, and 7.4, which are the general pH environments for tumor lysosomal compartments, tumor interstitium, and normal tissues, respectively [11, 12, 27].

5.2.3.6 Effect of DTT and pH on Singlet Oxygen Production

To show the effects of pH and DTT on the singlet oxygen generation efficiency of these compounds, we also compared the rates of decay of DPBF induced by these phthalocyanine in PBS at pH 6.0 or 7.4 and in the presence of 2 μM or 10 mM DTT for 8 h (Fig. 5.14). In the absence of light, these phthalocyanines could not produce singlet oxygen (data not shown). Upon illumination, these phthalocyanines exhibited different extent of singlet oxygen generation efficiency. For the redox-responsive phthalocyanine **4.11a**, the singlet oxygen generation efficiency was increased only

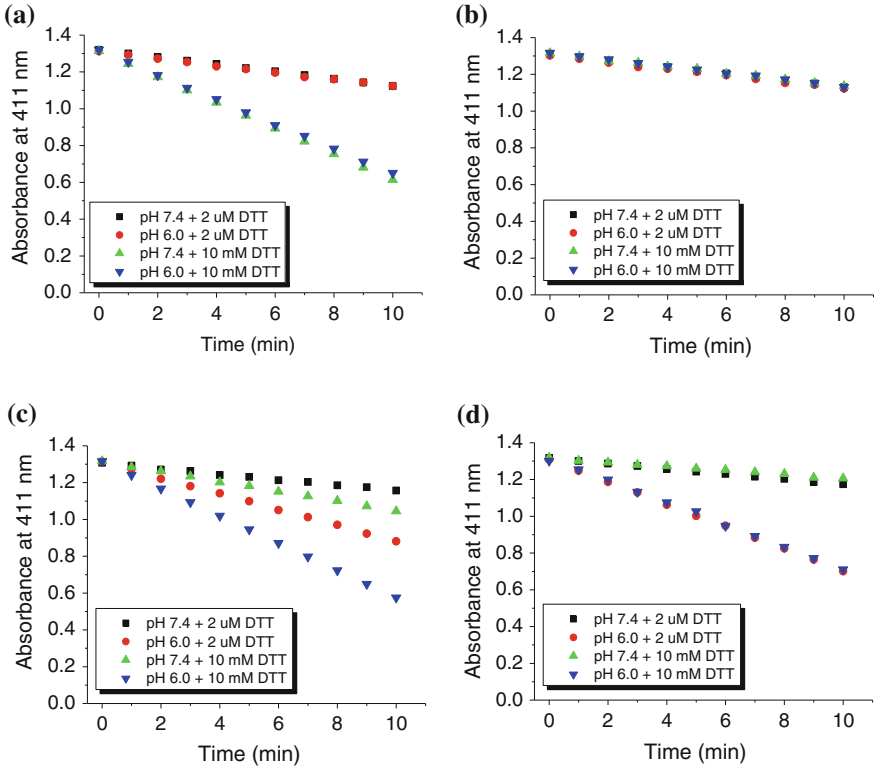

Fig. 5.14 Comparison of the rates of decay of DPBF (initial concentration = 70 μM) sensitized by (**a**) **4.11a**, (**b**) **4.11b**, (**c**) **5.9**, and (**d**) **5.10** (all at 4 μM) in PBS with 0.5 % Cremophor EL at different pH (6.0 and 7.4) for 8 h in the presence of light ($\lambda > 610$ nm)

when the DTT concentration was increased from 2 μM to 10 mM (Fig. 5.14a). On the other hand, the singlet oxygen generation efficiency of the pH-responsive derivative **5.10** increased only when the pH decreased from 7.4 to 6.0 (Fig. 5.14d). For the unsymmetrical phthalocyanine **5.9**, the production of singlet oxygen was the greatest at pH 6.0 and in the presence of 10 mM DTT, while the efficiency was comparatively lower at either low pH or high DTT concentration (Fig. 5.14c). As expected, the non-cleavable control **4.11b** could not cause any singlet oxygen generation enhancement under all these conditions (Fig. 5.14b).

5.2.4 In Vitro Photodynamic Activities

The pH- and redox-dependent fluorescence emission of unsymmetrical phthalocyanine **5.9** at the cellular level was also examined. In this study, MCF-7 human breast cancer cells were first pretreated with different concentrations of DTT

(0–4 mM) for 1 h, followed by incubation with the ionophore nigericin at two different pH (5.0 or 7.4) for 30 min. Nigericin is an H^+/K^+ antiporter, which enables the electroneutral transport of extracellular H^+ ions in exchange for intracellular K^+ ions, and can equilibrate the intracellular and extracellular pH [13, 28]. After the cells were treated with **5.9** (1 μM) for a further 1 h, the corresponding fluorescence images of the cells were captured with a confocal microscope (Fig. 5.15a), and the intracellular fluorescence intensities were determined (Fig. 5.15b). As shown in Fig. 5.15, very weak fluorescence was observed when the cells were exposed to 0–2 μM DTT at pH 7.4. However, the fluorescence intensity increased by about 3-fold when the DTT concentration was increased to 4 mM. This can be attributed to the cleavage of the disulfide bond and the separation of the ferrocenyl-chalcone moiety from the phthalocyanine partially relieved the quenching effect, leading to an enhancement in intracellular fluorescence intensity. At pH 5.0, the cells showed moderate intracellular fluorescence in the presence of 0–2 μM DTT due to the cleavage of the acid-labile linker and the release of ferrocenyl moiety. The intracellular fluorescence under this condition was stronger when compared with that exposed to 4 mM DTT at pH 7.4. It is likely that after the cleavage of the acid-labile hydrazone linker, the quenching effect induced by the remaining disulfide-linked ferrocene is not as efficient as the hydrazone-linked ferrocene due to the longer distance between the phthalocyanine ring and the ferrocenyl moiety, and hence relatively higher fluorescence intensity was observed. The fluorescence intensity was particularly strong when the cells were exposed to 4 mM DTT at pH 5.0, under which both disulfide and hydrazone linkages are cleaved, rendering the compound to be fully "turned on". Considering the fact that these conditions are analogous to the reducing and low pH environment as in the tumor, the results suggest that **5.9** is a potential dual pH- and redox-responsive photosensitizer for targeted PDT.

The pH-dependent fluorescence emission of **5.10** was also investigated. The MCF-7 cells were first incubated with nigericin at three different pH environments (5.0, 6.0, or 7.4) for 30 min, followed by incubation with **5.10** for 1 h. As shown in Fig. 5.16, the intracellular fluorescence intensities are much stronger at pH 5.0 and 6.0 than that at pH 7.4 (by about 9- to 10-fold). On the basis that the general pH environments for tumors and normal tissues fall in this region (from 6.0 to 7.4) [11, 27], the results suggest that compound **5.10** is also a promising pH-controlled photosensitizer for targeted PDT.

The photodynamic activities of phthalocyanines **5.9** and **5.10** were also evaluated against MCF-7 cells. To demonstrate the effect of reducing stimulus on the cytotoxicity, the cells were pretreated with DTT (2 μM or 4 mM) for 1 h, prior to incubation with the phthalocyanine solutions for 6 h. Figure 5.17 shows the dose-dependent survival curves for these two compounds with different concentrations of DTT in the absence and presence of light. Both compounds are essentially non-cytotoxic in the absence of light regardless of the concentration of DTT, but exhibit high photocytotoxicity. The IC_{50} values are summarized in Table 5.2. In the presence of light, the photocytotoxicity of **5.9** remains nearly unchanged in the absence and presence of 2 μM DTT. However, the antiproliferative effect is

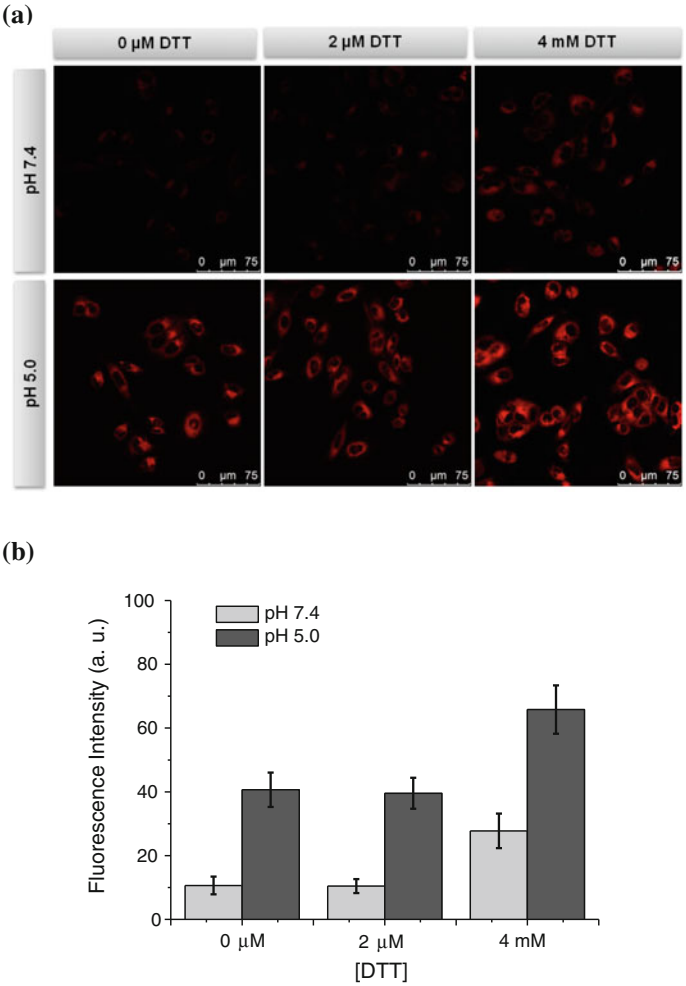

Fig. 5.15 (**a**) Fluorescence images of MCF-7 cells after incubation with 0–4 mM DTT for 1 h and then with nigericin (at pH 5.0 or 7.4) for 30 min, followed by incubation with **5.9** (1 μM) for 1 h. (**b**) Comparison of the relative intracellular fluorescence intensity of **5.9** at different DTT concentrations and pH values. Data are expressed as mean value ± standard deviation (S.D.) (number of cells = 30)

greatly enhanced when the DTT concentration is increased to 4 mM with IC_{50} value as low as 64 nm. The enhancement in photocytotoxicity can be attributed to the cleavage of the disulfide bond, thus releasing one ferrocenyl moiety and partially relieving the quenching effect. Compound **5.10** is highly potent with IC_{50} values in the range of 73–75 nM. It can be seen that its photocytotoxicity is independent of the concentrations of DTT.

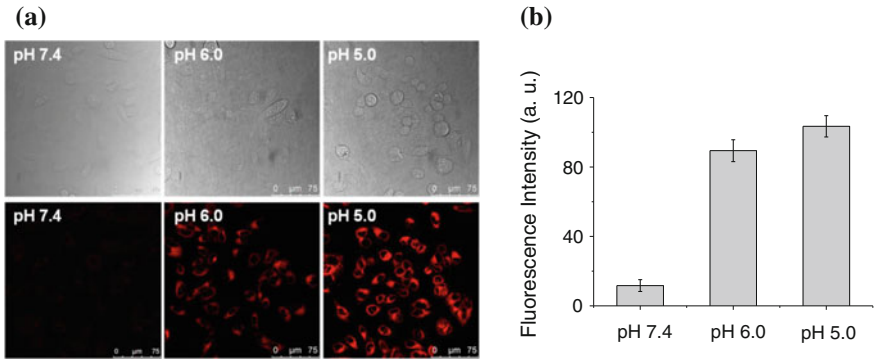

Fig. 5.16 (**a**) Fluorescence images of MCF-7 cells after incubation with a nigericin solution (25 μM) at pH 5.0, 6.0, or 7.4 for 30 min, followed by incubation with **5.10** (1 μM) for 1 h. The corresponding bright field images are shown in the upper row. (**b**) Comparison of the relative intracellular fluorescence intensity of **5.10** in the presence of nigericin at different pH values. Data are expressed as mean value ± S.D. (number of cells = 30)

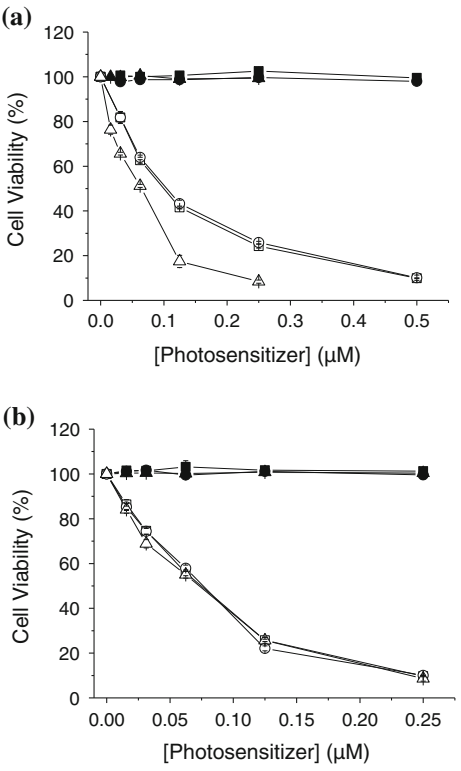

Fig. 5.17 Cytotoxic effects of (**a**) **5.9** and (**b**) **5.10** on MCF-7 cells pretreated with 0 μM (*squares*), 2 μM (*circles*), and 4 mM (*triangles*) DTT, prior to drug incubation for 6 h in the absence (*closed symbols*) and presence (*open symbols*) of light ($\lambda > 610$ nm, 40 mW cm^{-2}, 48 J cm^{-2}). Data are expressed as mean value ± standard error of the mean (S.E.M.) of three independent experiments, each performed in quadruplicate

Table 5.2 IC_{50} values for phthalocyanines **5.9** and **5.10** on MCF-7 cells

Compound	IC_{50} (nM)		
	0 μM DTT	2 μM DTT	4 mM DTT
5.9	100	105	64
5.10	75	76	73

The pH-dependent photocytotoxicity study of **5.9** and **5.10** against MCF-7 cells was not performed. Based on our previous results, most of the cells were killed when they were maintained in an acidic medium (e.g. pH = 6.5) for 2–3 h even in the absence of the phthalocyanines. Therefore, the study could not give any meaningful and conclusive results.

5.3 Summary

In summary, we have prepared and characterized a dual pH- and redox-responsive silicon(IV) phthalocyanine **5.9.** The fluorescence intensity and singlet oxygen generation efficiency of this compound are enhanced in a slightly acidic condition or in the presence of DTT (4 mM). The enhancement is particularly significant when the compound is exposed to an environment at low pH value and with a high level of DTT, which is analogous to the acidic and reducing environment found in tumor tissues. In addition, we have also described a pH-responsive silicon(IV) phthalocyanine **5.10**, which also shows pH-dependent properties in fluorescence emission and singlet oxygen generation. In the pH range of ca. 5–7, which can differentiate the environments for tumors and normal tissues, it shows stronger fluorescence emission and behaves as a more efficient singlet oxygen generator at lower pH. These pH- and/or redox-responsive properties render compounds **5.9** and **5.10** highly promising tumor-selective photosensitizers for targeted PDT.

References

1. Arnbjerg, J., Johnsen, M., Nielsen, C.B., Jørgensen, M., Ogilby, P.R.J.: Phys. Chem. A **111**, 4573 (2007)
2. Bae, Y., Fukushima, S., Harada, A., Kataoka, K.: Angew. Chem. Int. Ed. **42**, 4640 (2003)
3. Bellnier, D.A., Young, D.N., Detty, M.R., Camacho, S.H., Oseroff, A.R.: Photochem. Photobiol. **70**, 630 (1999)
4. Blair, S.L., Heerdt, P., Sacher, S., Abolhoda, A., Hochwald, S., Cheng, H., Burt, M.: Cancer Res. **57**, 152 (1997)
5. Chen, J., Qiu, X., Ouyang, J., Kong, J., Zhong, W., Xing, M.M.Q.: Biomacromolecules **12**, 3601 (2011)
6. Cook, J.A., Pass, H.I., Iype, S.N., Friedman, N., Degraff, W., Russo, A., Mitchell, J.B.: Cancer Res. **51**, 4287 (1991)

7. Cunderliková, B., Bjørklund, E.G., Pettersen, E.O., Moan, J.: Photochem. Photobiol. **74**, 246 (2001)
8. Cunderliková, B., Moan, J., Sjaastad, I.: Cancer Lett. **222**, 39 (2005)
9. Friberg, E.G., Cunderliková, B., Pettersen, E.O., Moan, J.: Cancer Lett. **195**, 73 (2003)
10. Gao, L., Fei, J., Zhao, J., Cui, W., Cui, Y., Li, J.: Chem. Eur. J. **18**, 3185 (2012)
11. Gerweck, L.E.: Drug Resist. Updates **3**, 49 (2000)
12. Gerweck, L.E., Seetharaman, K.: Cancer Res. **56**, 1194 (1996)
13. Jähde, E., Glüsenkamp, K.-H., Rajewsky, M.F.: Cancer Chemother. Pharmacol. **27**, 440 (1991)
14. Jiang, X.-J., Lo, P.-C., Yeung, S.-L., Fong, W.-P., Ng, D.K.P.: Chem. Commun. **46**, 3188 (2010)
15. Kosower, N.S., Kosower, E.M.: Int. Rev. Cytol. **54**, 109 (1978)
16. Lo, P.-C., Huang, J.-D., Cheng, D.Y.Y., Chan, E.Y.M., Fong, W.-P., Ko, W.-H., Ng, D.K.P.: Chem. Eur. J. **10**, 4831 (2004)
17. Loim, N.M., Kelbyscheva, E.S.: Russ. Chem. Bull. **53**, 2080 (2004)
18. Maree, M.D.; Kuznetsova, N.; Nyokong, T. J. Photochem. Photobiol., A **2001**, *140*, 117
19. Moan, J., Smedshammer, L., Christensen, T.: Cancer Lett. **9**, 327 (1980)
20. Mojzisova, H., Bonneau, S., Vever-Bizet, C., Brault, D.: Biochim. Biophys. Acta **1768**, 2748 (2007)
21. Ozlem, S., Akkaya, E.U.J.: Am. Chem. Soc. **131**, 48 (2009)
22. Pawar, G.M., Bantu, B., Weckesse, J., Blechert, S., Wurst, K., Buchmeiser, M.R.: Dalton Trans. **41**, 9043 (2009)
23. Scalise, I., Durantini, E.N.: Bioorg. Med. Chem. **13**, 3037 (2005)
24. Sharma, M., Dube, A., Bansal, H., Gupta, P.K.: Photochem. Photobiol. Sci. **3**, 231 (2004)
25. Sharma, M.; Sahu, K.; Dube, A.; Gupta, P.K. J. Photochem. Photobiol., B **2005**, *81*, 107
26. Sivakumar, S., Reddy, M.L.P., Cowley, A.H., Butorac, R.R.: Inorg. Chem. **50**, 4882 (2011)
27. Stubbs, M.; McSheehy, P.M.J.; Griffiths, J.R.; Bashford, C.L. Mol. Med. Today **2000**, 6
28. Varnes, M.E.; Bayne, M.T.; Bright, G.R. Photochem. Photobiol.**1996**, *64*, 853

Chapter 6
Conclusion and Future Outlook

Research related to targeting photosensitizers to cancerous tissues has been an area of increasing interest in photodynamic therapy (PDT) over the past decade. This thesis seeks to explore different approaches to develop phthalocyanine-based photosensitizers toward dual and targeted PDT, with a view to improving their specific delivery to cancerous tissues and efficiency in PDT. These strategies include conjugation to a platinum-based anticancer drug, vectorization by polyamines, and the development of activatable photosensitizers that can only be activated upon exposure to tumor-associated redox and/or pH conditions. The molecular design, synthesis, electronic, and photophysical properties as well as the in vitro photodynamic activities of these phthalocyanines are discussed and examined. Some promising results have been obtained and indicated that these methods are potentially useful for dual and targeted PDT. Although phthalocyanines have been extensively studied in various technological avenues, such as materials science, optoelectronics, catalysis, and nanotechnology, their applications in biomedicine is still relatively little studied. With the advancement in the discovery of tumor-targeting ligands such as peptides and monoclonal antibodies, as well as the facile synthesis of functionalized phthalocyanines, there is a great potential for further development of phthalocyanines as smart and efficient photosensitizers for dual and targeted PDT. It is hoped that this thesis can provide the grounding and stimulate further exploration in this important area.

J. T. F. Lau, *Towards Dual and Targeted Cancer Therapy with Novel Phthalocyanine-based Photosensitizers*, Springer Theses,
DOI: 10.1007/978-3-319-00708-3_6,

Chapter 7
Experimental Section

7.1 General

Experimental details regarding the purification of solvents, instrumentation, spectroscopic, and photophysical measurements, as well as in vitro studies followed the general procedures as described in Sects. 7.1.1–7.1.9 unless otherwise specified.

7.1.1 Materials and Methods

N,*N*-dimethylformamide (DMF) and *n*-pentanol were distilled under reduced pressure from barium oxide and sodium, respectively. Pyridine, dichloromethane, and acetonitrile were distilled from calcium hydride under nitrogen. Tetrahydrofuran (THF) and toluene were distilled from sodium benzophenone ketyl and sodium, respectively, under nitrogen prior to use. All the other solvents were of analytical reagent grade and used without further purification. All non-aqueous reactions were performed under an atmosphere of nitrogen. All reactions were monitored by thin layer chromatography (TLC) performed on Merck precoated silica gel $60F_{254}$ plates, and the compounds were visualized by irradiation with UV light and/or by treatment with a spray of 5 % w/v dodecamolybdophosphoric acid in ethanol followed by a brief heating. Chromatographic purifications were performed on silica gel (Macherey–Nagel, 230–400 mesh) columns with the indicated eluents. Gel permeation chromatography was carried out on Bio-Rad Bio-Beads S-X1 beads (200–400 mesh).

^{1}H and $^{13}C\{^{1}H\}$ NMR spectra were recorded on a Bruker Avance III 400 spectrometer (^{1}H, 400 MHz; ^{13}C, 100.6 MHz) in deuterated solvents. Spectra were referenced internally using the residual solvent (^{1}H: δ 7.26 for $CDCl_3$, δ 2.49 for DMSO-d_6, δ 4.79 for D_2O, δ 2.05 for acetone-d_6, and δ 7.22 for pyridine-d_5 for the most upfield signal) or solvent (^{13}C: δ 77.0 for $CDCl_3$, δ 39.5 for DMSO-d_6, δ 29.8 for acetone-d_6, and δ 150.4 for pyridine-d_5 for the most downfield signal)

J. T. F. Lau, *Towards Dual and Targeted Cancer Therapy with Novel Phthalocyanine-based Photosensitizers*, Springer Theses,
DOI: 10.1007/978-3-319-00708-3_7, © Springer International Publishing Switzerland 2013

resonances relative to $SiMe_4$. Electrospray ionization (ESI) mass spectra were measured on a Thermo Finnigan MAT 95 XL mass spectrometer. Elemental analyses were performed by Medac Ltd., Brunel Science Center, U. K.

7.1.2 Photophysical Measurements

UV-Vis and steady-state fluorescence spectra were taken on a Cary 5G UV-Vis-NIR spectrophotometer and a Hitachi F-7000 spectrofluorometer, respectively.

Determination of Fluorescence Quantum Yields in DMF

Fluorescence quantum yields [$\Phi_{F\ (\text{sample})}$] were determined by the equation [1]:

$$\Phi_{F(\text{sample})} = \left(\frac{F_{\text{sample}}}{F_{\text{ref}}}\right)\left(\frac{A_{\text{ref}}}{A_{\text{sample}}}\right)\left(\frac{\eta_{\text{sample}}}{\eta_{\text{ref}}}\right)^2 \Phi_{F(\text{ref})}$$

where F, A, and η are the measured fluorescence (area under emission peak), the absorbance at the excitation position (610 nm), and the refractive index of the solvent, respectively. Unsubstituted zinc(II) phthalocyanine (ZnPc) in DMF was used as the reference [$\Phi_{\text{F (ref)}} = 0.28$] [2]. To minimize reabsorption of radiation by the ground state species, the emission spectra were obtained in very dilute solutions of which the absorbance at 610 nm was less than 0.05.

Determination of Singlet Oxygen Quantum Yields in DMF

Singlet oxygen quantum yields (Φ_Δ) were measured in DMF by a steady-state method described by Nyokong and coworkers with some modifications [3]. A mixture of 1,3-diphenylisobenzofuran (DPBF; 70 μM) and the phthalocyanines (3 μM), without saturation with air or oxygen, was illuminated with red light coming from a 100 W halogen lamp after passing through a water tank for cooling and a color glass filter (Newport, cut-on at 610 nm). The decay of DPBF at 411 nm was monitored with time. The singlet oxygen quantum yields of the phthalocyanines (Φ_Δ) were obtained by using the following equation:

$$\Phi_\Delta = \Phi_{\Delta(\text{ZnPc})} \times \frac{W \times I_{\text{abs(ZnPc)}}}{W_{\text{ZnPc}} \times I_{\text{abs}}}$$

where I_{abs} and $I_{\text{abs(ZnPc)}}$ are the rates of light absorption by the phthalocyanines and ZnPc, respectively. The photobleaching of DPBF by the phthalocyanines and ZnPc denoted as W and W_{ZnPc} were determined as the slopes of their corresponding DPBF decay curves under the same conditions. The singlet oxygen quantum yields of the phthalocyanines were correlated with ZnPc in DMF as a reference [$\Phi_{\Delta(\text{ZnPc})} = 0.56$].

7.1.3 Cell Lines and Culture Conditions

The HT29 human colon adenocarcinoma cells (ATCC, cat. no. HTB-38) were maintained in Dulbecco's modified Eagle's medium (DMEM; Invitrogen, cat. no. 10313-021) supplemented with fetal calf serum (10 %), penicillin–streptomycin (100 units mL^{-1} and 100 μg mL^{-1}, respectively), L-glutamine (2 mM), and transferrin (10 μg mL^{-1}). The B16 melanoma (ATCC, cat. no. CRL-6475), Chinese Hamster Ovary (CHO; ATCC, cat. no. CCL-61), and MCF-7 human breast cancer cells (ATCC, cat. no. HTB-22) were maintained Roswell Park Memorial Institute (RPMI) 1640 medium (Invitrogen, cat. no. 23400-021) supplemented with fetal calf serum (10 %), sodium pyruvate (1 mM), and penicillin–streptomycin (100 units mL^{-1} and 100 μg mL^{-1}, respectively).

7.1.4 Photocytotoxicity Assay

Approximately 3×10^4 cells per well in the culture medium were inoculated in 96-multiwell plates and incubated overnight at 37 °C in a humidified 5 % CO_2 atmosphere. The cells, after being rinsed with phosphate buffered saline (PBS), were incubated with 100 μL of the drug solutions for 2 h at 37 °C under 5 % CO_2. The cells were then rinsed again with PBS and re-fed with 100 μL of the culture medium before illuminated at ambient temperature. The light source consisted of a 300 W halogen lamp, a water tank for cooling, and a color glass filter (Newport) cut-on 610 nm. The fluence rate ($\lambda > 610$ nm) was 40 mW cm^{-2}. An illumination of 20 min led to a totally fluence of 48 J cm^{-2}. Cell viability was determined by means of the colorimetric MTT assay [4]. After illumination, the cells were incubated at 37 °C under 5 % CO_2 overnight. An MTT (Sigma) solution in PBS (3 mg mL^{-1}, 50 μL) was added to each well followed by incubation for 2 h under the same environment. A solution of sodium dodecyl sulfate (SDS; Sigma, 10 % by weight, 50 μL) was then added to each well. The plate was incubated in an oven at 60 °C for 30 min and then 80 μL of *iso*-propanol was added to each well. The plate was agitated on a Bio-Rad microplate reader at ambient temperature for 10 s before the absorbance at 540 nm of each well was taken. The average absorbance of the blank wells, which did not contain the cells, was subtracted from the readings of the other wells. The cell viability was then determined by the equation:

$$\% \text{ Viability} = \left[\sum (A_i / A_{\text{control}} \times 100)\right] / n$$

where A_i is the absorbance of the ith data ($i = 1, 2, \ldots, n$), A_{control} is the average absorbance of the control wells, in which the phthalocyanine was absent, and n (= 4) is the number of data points.

7.1.5 ROS Measurements

ROS production was determined by using 2′,7′-dichlorodihydrofluorescein diacetate (DCFDA; Molecular Probes) as the probe. Approximately 3×10^4 cells per well in the culture medium was inoculated in a 96-multiwell plate for 24 h before photodynamic treatment. After the cells were incubated with different concentrations of the drugs (2-fold dilution from 2 μM) for 2 h in darkness, the cells were rinsed with PBS before 100 μL of DCFDA (10 μM in PBS) was added to each well. The mixture was incubated at 37 °C under 5 % CO_2 for 30 min in darkness, followed by illumination for 20 min at ambient temperature using a halogen lamp light source as described in Sect. 7.1.4. Fluorescence measurements were made in a fluorescence plate reader (TECAN Polarion) with a 485 nm excitation filter and a 535 nm emission filter set at a gain of 60.

7.1.6 Intracellular Fluorescence Studies

For the detection of intracellular fluorescence intensity of the phthalocyanines, approximately 6×10^4 cells in the culture medium (2 mL) were seeded on a coverslip and incubated overnight at 37 °C under 5 % CO_2. The medium was removed and then the cells were incubated with phthalocyanine dilutions in the medium (2 mL) for 2 h under the same conditions. The cells were then rinsed with PBS twice, and then viewed with a Leica SP5 confocal laser scanning microscope equipped with a 633 nm helium–neon laser. The emission signals from 650 to 760 nm were collected and the images were digitized and analyzed by Leica Application Suite Advanced Fluorescence Software. The intracellular fluorescence intensities (for a total of 30 cells in each sample) were also determined.

7.1.7 Cellular Uptake Determined by an Extraction Method

Approximately 2×10^6 cells in the culture medium (2 mL) were seeded on a Petri dish (diameter = 35 mm). After incubation at 37 °C under 5 % CO_2 overnight, the medium was removed and the cells were rinsed with PBS (2 mL). The cells were then incubated with phthalocyanine dilutions in the medium (2 mL) for 2 h under the same conditions. The medium was removed and the cells were rinsed with PBS (2 mL) and then harvested by 0.25 % trypsin–EDTA (Invitrogen, 0.5 mL). The trypsin was then quenched with the medium (0.5 mL). The solution was transferred to centrifuge tubes and centrifuged at 2,400 rpm for 5 min. The cell pellet was then washed with PBS (1 mL) and the suspension was centrifuged again. After removing the PBS, the cells were lysed with DMF (1 mL). The mixture was sonicated for 20 min and then centrifuged again. The supernatants

were transferred for UV-Vis spectroscopic measurements. The Q-band absorbance of the phthalocyanines was compared with the respective calibration curves to give the uptake concentrations. Each experiment was repeated for three times.

7.1.8 Subcellular Localization Studies

About 6×10^4 cells in the culture medium (2 mL) were seeded on a coverslip and incubated overnight at 37 °C under 5 % CO_2. The medium was then removed. The cells were incubated with phthalocyanine dilutions in the medium (2 mL) for 2 h under the same conditions. For the study using LysoTracker, LysoTracker Green DND-26 (Molecular Probes; 2 μM in culture medium) was then added, and the cells were incubated under these conditions for a further 10 min. For the study using MitoTracker, the cells were incubated with MitoTracker Green FM (Invitrogen; 0.25 μM in culture medium) for 10 min. For the study using ER-Tracker, the cells were incubated with ER-Tracker Green (Invitrogen; 0.2 μM in culture medium) for 20 min. For the study using SYTO-16, the cells were incubated with SYTO-16 (Invitrogen; 0.5 μM in culture medium) for 10 min. For all the cases, the cells were then rinsed with PBS and viewed with a Leica SP5 confocal laser scanning microscope equipped with a 488 nm argon laser and a 633 nm helium–neon laser. All the Trackers were excited at 488 nm and monitored at 500–570 nm, while the phthalocyanines were excited at 633 nm and monitored at 650–760 nm. The images were digitized and analyzed by Leica Application Suite Advanced Fluorescence Software. The subcellular localization of the phthalocyanines was revealed by comparing the intracellular fluorescence images caused by the Trackers and the dyes.

7.1.9 Flow Cytometric Studies

Approximately 6×10^5 cells in the medium (2 mL) were seeded on a Petri dish (diameter = 35 mm) and incubated for 24 h at 37 °C under 5 % CO_2. For **2.11**, **2.14**, and **2.17**, the HT29 cells were treated with the respective concentrations of these compounds as mentioned in Table 2.3, while the B16 or CHO cells were treated with different concentrations of **3.10d** as described in Table 3.3. The cells were then incubated under the same conditions for 2 h. The cells were rinsed thrice with PBS and refilled with 2 mL of the culture medium before being illuminated at ambient temperature using a halogen lamp light source as described in Sect. 7.1.4. After incubation for 24 h, the cells were rinsed with PBS and then harvested by 0.25 % trypsin–EDTA (Invitrogen, 0.5 mL). The trypsin was quenched with the medium (0.5 mL) and the mixture was centrifuged at 2,400 rpm for 5 min at room temperature. The pellet was then washed again by PBS and then subject to centrifugation. The cells were suspended in 1 mL of binding buffer (10 mM HEPES,

140 mM NaCl and 25 mM $CaCl_2$, pH = 7.4) containing annexin V-GFP (5 μL) and PI (2 μg mL^{-1}). After incubation in darkness for 15 min at room temperature, the signals of annexin V-GFP and PI were measured by a BD FACSCanto flow cytometer (Becton–Dickinson) with 10^4 cells counted in each sample. Both annexin V-GFP and PI were excited by a 488 nm argon laser. The emitted fluorescence was monitored at 500–560 nm for annexin V-GFP and at >670 nm for PI. The data collected were analyzed by using WinMDI 2.9.

7.2 Experiments Described in Chapter 2

7.2.1 Synthesis

Preparation of 2-[2-[2-(Tetrahydropyranyloxy)ethoxy]ethoxy]ethanol (2.2) [5]

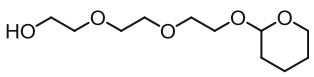

A mixture of triethylene glycol (**2.1**; 51.65 g, 343.94 mmol), 3,4-dihydropyran (31.83 g, 378.39 mmol), and concentrated HCl (10 drops) was stirred at room temperature for 24 h. The reaction was then quenched with an aqueous solution of $NaHCO_3$ (100 mL). The aqueous layer was extracted with CH_2Cl_2 (200 mL × 3). The combined organic layers were dried over anhydrous Na_2SO_4 and concentrated. The crude product was then purified by silica-gel column chromatography using ethyl acetate/MeOH (9:1 v/v) as the eluent. The product was obtained as a colorless oil (56.37 g, 70 % yield). R_f [ethyl acetate/MeOH (9:1 v/v)] = 0.54. ^1H NMR ($CDCl_3$): δ = 4.62–4.64 (m, 1 H, THP-CH), 3.84–3.85 (m, 2 H), 3.71–3.75 (m, 2 H), 3.66–3.70 (m, 6 H), 3.60–3.65 (m, 3 H), 3.47–3.52 (m, 1 H), 1.79–1.86 (m, 1 H, THP), 1.68–1.76 (m, 1 H, THP), 1.50–1.64 (m, 4 H, THP).

Preparation of Compound 2.3 [5]

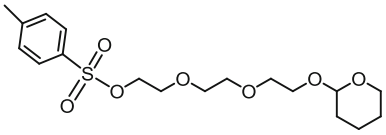

A mixture of 2-[2-[2-(tetrahydropyranyloxy)ethoxy]ethoxy]ethanol (**2.2**; 14.88 g, 63.55 mmol), tosyl chloride (TsCl; 18.17 g, 95.31 mmol), and pyridine (7.7 mL, 95.20 mmol) was stirred in CH_2Cl_2 (80 mL) under an inert atmosphere for 24 h. The mixture was washed with 10 % HCl solution (v/v, 100 mL) and then with water (100 mL × 3). The organic layer was dried over anhydrous Na_2SO_4 and concentrated. The residue was subject to silica-gel column chromatography

using diethyl ether as the eluent. The product was obtained as a colorless oil (12.83 g, 52 % yield). R_f (diethyl ether) = 0.69. ^{1}H NMR ($CDCl_3$): δ = 7.80 (d, J = 8.4 Hz, 2 H, ArH), 7.34 (d, J = 8.0 Hz, 2 H, ArH), 4.60–4.64 (m, 1 H, THP-CH), 4.12–4.17 (m, 2 H), 3.82–3.89 (m, 2 H), 3.57–3.73 (m, 8 H), 3.47–3.52 (m, 2 H), 2.44 (s, 3 H, CH_3), 1.79–1.85 (m, 1 H, THP), 1.68–1.75 (m, 1 H, THP), 1.49–1.62 (m, 4 H, THP).

Preparation of 1-Iodo-8-(tetrahydro-2H-pyran-2-yloxy)-3,6-dioxaoctane (2.4) [6]

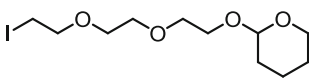

Sodium iodide (10.00 g, 66.72 mmol) was added to a solution of **2.3** (5.18 g, 13.35 mmol) in acetone (100 mL). The mixture was brought to reflux for 24 h. The inorganic salt was removed by suction filtration and the filtrate was concentrated under reduced pressure. The residue was then redissolved in ethyl acetate (100 mL) and this solution was washed with saturated sodium thiosulfate solution (100 mL × 2) and water (100 mL × 1). The organic layer was dried over anhydrous Na_2SO_4 and concentrated. The crude product was subject to silica-gel column chromatography using ethyl acetate/hexane (9:1 v/v) as the eluent to afford the product as a colorless oil (4.36 g, 95 % yield). R_f [ethyl acetate/hexane (9:1 v/v)] = 0.54. ^{1}H NMR ($CDCl_3$): δ = 4.63 (t, J = 3.2 Hz, 1 H, THP-CH), 3.84–3.90 (m, 2 H), 3.73–3.79 (m, 4 H), 3.67–3.70 (m, 4 H), 3.60–3.64 (m, 1 H), 3.48–3.52 (m, 1 H), 3.26–3.29 (m, 2 H, -CH_2I), 1.79–1.86 (m, 1 H, THP), 1.69–1.76 (m, 1 H, THP), 1.50–1.64 (m, 4 H, THP).

Preparation of Compound 2.5

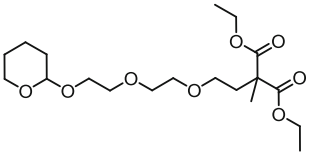

Diethyl methylmalonate (4.00 g, 22.96 mmol) was added to a slurry suspension of NaH (0.83 g, 34.58 mmol) in DMF (30 mL) at 0 °C under a nitrogen atmosphere. A solution of **2.4** (7.90 g, 22.95 mmol) in DMF (30 mL) was then added in dropwise to the reaction mixture. The mixture was heated at 60 °C overnight, then the solvent was evaporated under reduced pressure. The residue was then subject to silica-gel column chromatography using ethyl acetate/hexane (9:1 v/v) as the eluent to obtain the product as a yellow oily liquid (4.83 g, 54 % yield). R_f [ethyl acetate/hexane (9:1 v/v)] = 0.42. ^{1}H NMR ($CDCl_3$): δ = 4.62 (t, J = 4.0 Hz, 1 H, CH), 4.16 (dq, J = 2.0, 7.2 Hz, 4 H, CH_2), 3.83–3.89 (m, 2 H, CH_2), 3.47–3.67 (m, 10 H, CH_2), 2.18 (t, J = 6.4 Hz, 2 H, CH_2), 1.67–1.87 (m, 3 H, CH and CH_2),

1.48–1.63 (m, 3 H, CH and CH_2), 1.43 (s, 3 H, CH_3), 1.24 (t, $J = 7.2$ Hz, 6 H, CH_3). $^{13}C\{^1H\}$ NMR ($CDCl_3$): $\delta = 172.1$, 98.9, 70.5 (two overlapping signals), 70.2, 67.2, 66.6, 62.2, 61.2, 52.0, 35.0, 30.5, 25.4, 20.0, 19.5, 14.0. MS (ESI): *m/z* 413 (100 %, $[M + Na]^+$). HRMS (ESI): *m/z* calcd for $C_{19}H_{34}NaO_8$ $[M + Na]^+$: 413.2146; found: 413.2145.

Preparation of Compound 2.6

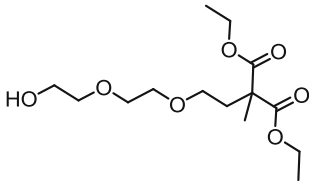

Concentrated sulfuric acid (5 drops) was added to a solution of **2.5** (1.08 g, 2.77 mmol) in ethanol (10 mL). The mixture was stirred at room temperature for 3 h, then it was neutralized with an aqueous solution of $NaHCO_3$. The solvent was evaporated under reduced pressure, then the residue was redissolved in diethyl ether. The insoluble material was removed by filtration. The filtrate was evaporated to give a pale yellow oil (0.62 g, 73 % yield). ^1H NMR ($CDCl_3$): $\delta = 4.16$ (dq, $J = 2.8$, 7.2 Hz, 4 H, CH_2), 3.72 (t, $J = 4.0$ Hz, 2 H, CH_2), 3.52–3.61 (m, 8 H, CH_2), 2.19 (t, $J = 6.4$ Hz, 2 H, CH_2), 1.43 (s, 3 H, CH_3), 1.23 (t, $J = 7.2$ Hz, 6 H, CH_3). $^{13}C\{^1H\}$ NMR ($CDCl_3$): $\delta = 172.2$, 72.4, 70.3, 70.2, 67.1, 61.8, 61.3, 51.9, 35.0, 19.9, 14.0. MS (ESI): *m/z* 329 (100 %, $[M + Na]^+$). HRMS (ESI): *m/z* calcd for $C_{14}H_{26}NaO_7$ $[M + Na]^+$: 329.1571; found: 329.1580.

Preparation of Phthalonitrile 2.7

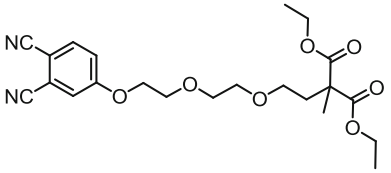

A mixture of **2.6** (0.58 g, 1.89 mmol), 4-nitrophthalonitrile (0.16 g, 0.92 mmol), and anhydrous K_2CO_3 (0.38 g, 2.75 mmol) in DMF (20 mL) was stirred at 110 °C under nitrogen for 24 h. The solvent was removed at 60 °C under reduced pressure. The residue was mixed with H_2O (50 mL), then it was extracted with $CHCl_3$ (50 mL × 3). The combined organic layers was dried over anhydrous Na_2SO_4 and concentrated in vacuo. The crude product was subject to silica-gel column chromatography using hexane/ethyl acetate (1:1 v/v) as the eluent to afford the product as a pale yellow oil (0.21 g, 53 % yield). R_f [hexane/ethyl acetate (1:1 v/v)] = 0.29. ^1H NMR ($CDCl_3$): $\delta = 7.70$ (d, $J = 8.8$ Hz, 1 H, ArH), 7.31 (d, $J = 2.8$ Hz, 1 H, ArH), 7.23 (dd, $J = 2.8$, 8.8 Hz, 1 H, ArH), 4.22 (t,

$J = 4.8$ Hz, 2 H, CH_2), 4.16 (dq, $J = 2.4$, 7.2 Hz, 4 H, CH_2), 3.85–3.89 (m, 2 H, CH_2), 3.64–3.69 (m, 2 H, CH_2), 3.47–3.59 (m, 4 H, CH_2), 2.18 (t, $J = 6.4$ Hz, 2 H), 1.42 (s, 3 H, CH_3), 1.23 (t, $J = 7.2$ Hz, 6 H, CH_3). $^{13}C\{^1H\}$ NMR ($CDCl_3$): $\delta = 172.1$, 162.0, 135.2, 119.8, 119.5, 117.4, 115.6, 115.2, 107.4, 70.9, 70.2, 69.1, 68.6, 67.3, 61.2, 51.9, 35.0, 20.0, 14.0. MS (ESI): *m/z* 455 (100 %, $[M + Na]^+$). HRMS (ESI): *m/z* calcd for $C_{22}H_{28}N_2NaO_7$ $[M + Na]^+$: 455.1789; found: 455.1800.

Preparation of Phthalocyanine 2.8

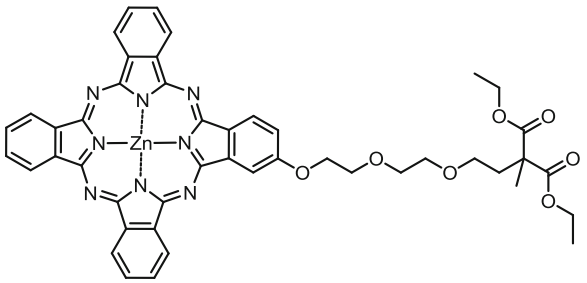

A mixture of **2.7** (0.53 g, 1.23 mmol), 1,2-dicyanobenzene (1.42 g, 11.08 mmol), and $Zn(OAc)_2 \bullet 2H_2O$ (0.81 g, 3.69 mmol) in *n*-pentanol (25 mL) was heated to 100 °C, then a small amount of 1,8-diazabicyclo[5.4.0]undec-7ene (DBU; 1 mL) was added. The mixture was stirred at 140–150 °C for 24 h. After cooling, the volatiles were removed under reduced pressure. The residue was dissolved in $CHCl_3$ (150 mL), then part of the ZnPc formed was removed by filtration. The filtrate was collected and evaporated to dryness in vacuo. The residue was purified by silica-gel column chromatography using $CHCl_3$ and then $CHCl_3$/MeOH (100:1 v/v) as the eluents. The crude product was purified by size exclusion chromatography with Bio-Beads S-X1 beads using THF as the eluent. The product was then further purified by recrystallization from a mixture of THF and hexane to give a green solid (0.19 g, 18 % yield). ^1H NMR ($CDCl_3$ with a trace amount of pyridine-d_5): $\delta = 8.92$–9.10 (m, 6 H, Pc-H_α), 8.71 (d, $J = 8.0$ Hz, 1 H, Pc-H_α), 8.24 (s, 1 H, Pc-H_α), 7.89–8.01 (m, 6 H, Pc-H_β), 7.42 (d, $J = 8.0$ Hz, 1 H, Pc-H_β), 4.57 (vt, $J = 4.4$ Hz, 2 H, CH_2), 4.16–4.23 (m, 6 H, CH_2), 3.91 (t, $J = 4.4$ Hz, 2 H, CH_2), 3.74 (t, $J = 4.4$ Hz, 2 H, CH_2), 3.66 (t, $J = 6.8$ Hz, 2 H, CH_2), 2.30 (t, $J = 6.8$ Hz, 2 H, CH_2), 1.50 (*s*, 3 H, CH_3), 1.25 (t, $J = 7.2$ Hz, 6 H, CH_3). $^{13}C\{^1H\}$ NMR ($CDCl_3$ with a trace amount of pyridine-d_5): $\delta = 172.1$, 160.1, 153.0, 152.9, 152.7, 152.6, 152.3, 152.2, 139.8, 138.1, 138.0, 137.9, 137.7, 131.2, 128.6, 128.5, 128.4, 128.3, 123.1, 122.2, 122.1, 122.0, 117.9, 104.8, 70.9, 70.4, 69.9, 67.9, 67.3, 61.2, 52.0, 35.1, 20.0, 14.0 (some of the aromatic signals were overlapped). MS (ESI): an isotopic cluster peaking at *m/z* 881 (80 %, $[M + H]^+$). HRMS (ESI): *m/z* calcd for $C_{46}H_{41}N_8O_7Zn$ $[M + H]^+$: 881.2384; found: 881.2391.

Preparation of Phthalocyanine 2.9

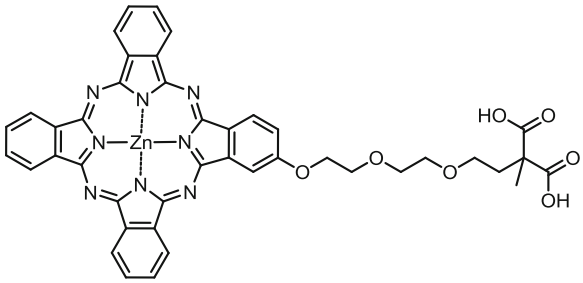

A mixture of **2.8** (0.15 g, 0.17 mmol), 5 M NaOH (0.3 mL, 1.5 mmol), and acetone (20 mL) was heated under reflux for 2 h. The volatiles were removed under reduced pressure. The green residue was washed thoroughly with acetone, then redissolved in water and acidified with 3 M HCl until pH = 4. The green precipitate was washed thoroughly with water and ethanol, then dried in vacuo (0.11 g, 78 % yield). ^{1}H NMR (DMSO-d_6 with a trace amount of pyridine-d_5): δ = 9.25–9.34 (m, 6 H, Pc-H$_\alpha$), 9.05 (d, J = 8.0 Hz, 1 H, Pc-H$_\alpha$), 8.65 (d, J = 2.0 Hz, 1 H, Pc-H$_\alpha$), 8.17–8.23 (m, 6 H, Pc-H$_\beta$), 7.69 (dd, J = 2.0, 8.0 Hz, 1 H, Pc-H$_\beta$), 4.66 (vt, J = 4.4 Hz, 2 H, CH$_2$), 4.08 (vt, J = 4.4 Hz, 2 H, CH$_2$), 3.80 (t, J = 4.4 Hz, 2 H, CH$_2$), 3.64 (t, J = 4.4 Hz, 2 H, CH$_2$), 3.53 (t, J = 7.2 Hz, 2 H, CH$_2$), 2.08 (t, J = 7.2 Hz, 2 H, CH$_2$), 1.35 (s, 3 H, CH$_3$) ^{13}C{^{1}H} NMR (DMSO-d_6 with a trace amount of pyridine-d_5): δ = 174.3, 160.3, 152.8, 152.6, 152.4, 152.2, 152.1, 139.9, 138.0, 137.8, 137.7, 130.9, 129.2, 129.0, 123.2, 122.4, 122.2, 117.9, 105.4, 70.4, 70.0, 69.5, 68.1, 67.4, 51.2, 35.5, 20.9 (some of the aromatic signals were overlapped). MS (ESI): isotopic clusters peaking at m/z 780 (100 %, [M − CO$_2$]$^+$) and 824 (35 %, M$^+$). HRMS (ESI): m/z calcd for $C_{42}H_{32}N_8O_7Zn$ [M]$^+$: 824.1680; found: 824.1654. Anal. calcd for $C_{42}H_{32}N_8O_7Zn$: C, 61.06; H, 3.90; N, 13.56. Found: C, 60.81; H, 3.56; N, 13.27.

Preparation of *Trans*-(d,l)-1,2-diaminocyclohexanedinitratoplatinum(II) (2.10) [7]

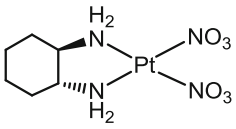

A solution of *trans*-(d,l)-1,2-diaminocyclohexanedichloroplatinum(II) complex (**2.16**; 0.99 g, 2.60 mmol) and $AgNO_3$ (0.88 g, 5.18 mmol) in H_2O (30 mL) was vigorously stirred at 60 °C for 1 h and then at room temperature overnight. The mixture was then filtered through a fine sintered glass funnel to remove the AgCl formed and the filtrate was evaporated to dryness at 60 °C in vacuo to obtain the product as a yellow solid (0.87 g, 77 % yield). ^{1}H NMR (D_2O): δ = 2.35–2.38 (m,

2 H), 2.00–2.04 (*d*, $J = 13.2$ Hz, 2 H), 1.53–1.55 (m, 2 H), 1.24–1.32 (m, 2 H), 1.09–1.17 (m, 2 H).

Preparation of Phthalocyanine 2.11

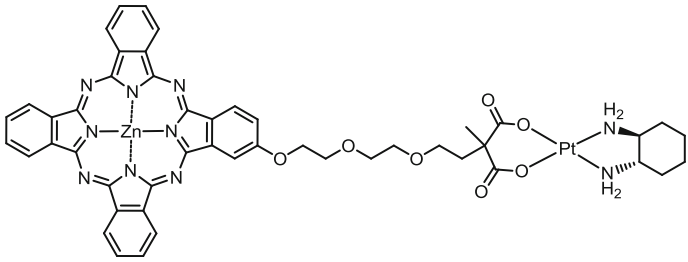

Phthalocyanine **2.9** (0.25 g, 0.30 mmol) was dissolved in water (50 mL) containing 5 M NaOH (0.15 mL, 0.75 mmol). It was then added to a solution of **2.10** (0.13 g, 0.30 mmol) in water (30 mL). The mixture was heated at 70 °C for 48 h. The resulting blue precipitate was filtered and washed thoroughly with water and ethanol. The crude product was then subject to flash silica-gel column chromatography using DMF as the eluent. The product was further purified by recrystallization from a mixture of DMF and ethanol to afford a blue solid (0.12 g, 35 % yield). R_f (DMF) = 0.65. ^{1}H NMR (DMSO-d_6 with a trace amount of pyridine-d_5): $\delta = 9.38$–9.44 (m, 6 H, Pc-H$_\alpha$), 9.24 (d, $J = 8.4$ Hz, 1 H, Pc-H$_\alpha$), 8.87 (d, $J = 2.0$ Hz, 1 H, Pc-H$_\alpha$), 8.21–8.24 (m, 6 H, Pc-H$_\beta$), 7.77 (dd, $J = 2.0$, 8.4 Hz, 1 H, Pc-H$_\beta$), 4.67 (vt, $J = 4.4$ Hz, 2 H, CH_2), 4.04 (vt, $J = 4.4$ Hz, 2 H, CH_2), 3.75 (t, $J = 4.4$ Hz, 2 H, CH_2), 3.61 (t, $J = 4.4$ Hz, 2 H, CH_2), 3.53 (t, $J = 7.2$ Hz, 2 H, CH_2), 2.34 (br s, 2 H, CH_2), 1.88–1.97 (m, 4 H, CH_2), 1.49 (br s, 2 H, CH_2), 1.16–1.37 (m, 5 H, CH_2 and CH_3), 0.98–1.05 (m, 2 H, CH_2). The ^{13}C{^{1}H} NMR spectrum could not be obtained due to its low solubility in common organic solvents. MS (ESI): an isotopic cluster peaking at *m/z* 1133 (38 %, $[M + H]^+$). HRMS (ESI): *m/z* calcd for $C_{48}H_{45}N_{10}O_7PtZn$ $[M + H]^+$: 1133.2404; found: 1133.2415. Anal. calcd for $C_{48}H_{44}N_{10}O_7PtZn$: C, 50.87; H, 3.91; N, 12.35. Found: C, 50.50; H, 3.63; N, 11.95.

Preparation of 4-(3,6,9-Trioxadecyloxy)phthalonitrile (2.13) [8]

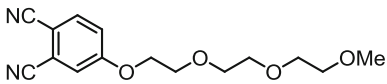

A mixture of triethylene glycol monomethyl ether (**2.12**; 4.63 g, 28.20 mmol), 4-nitrophthalonitrile (2.44 g, 14.09 mmol), and anhydrous K_2CO_3 (5.84 g, 42.25 mmol) in DMF (30 mL) was stirred at 80 °C under an inert atmosphere for 24 h. The solvent was evaporated at 60 °C under reduced pressure, then the residue was redissolved in H_2O (100 mL). The solution was extracted with $CHCl_3$

(100 mL × 3). The combined organic layers were dried over anhydrous Na_2SO_4 and concentrated. The crude product was subject to silica-gel column chromatography using hexane/ethyl acetate (1:1 v/v) as the eluent to afford the product as a white solid (2.37 g, 58 % yield). R_f [hexane/ethyl acetate (1:1 v/v)] = 0.48. ^{1}H NMR ($CDCl_3$): δ = 7.70 (d, J = 8.8 Hz, 1 H, ArH), 7.31 (s, 1 H, ArH), 7.23 (dd, J = 2.0, 9.2 Hz, 1 H, ArH), 4.23 (t, J = 4.4 Hz, 2 H, Ph-OCH_2), 3.89 (t, J = 4.8 Hz, 2 H, CH_2), 3.71–3.72 (m, 2 H, CH_2), 3.63–3.68 (m, 4 H), 3.55 (t, J = 4.8 Hz, 2 H, CH_2), 3.38 (s, 3 H, CH_3).

Preparation of Phthalocyanine 2.14

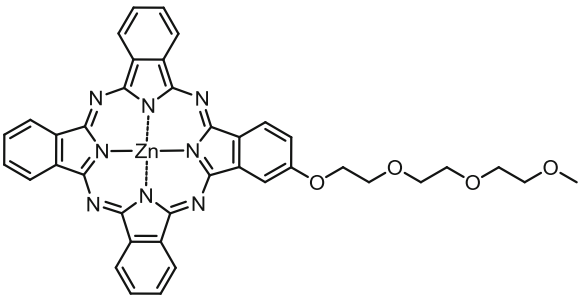

A mixture of 1,2-dicyanobenzene (2.06 g, 16.08 mmol), 4-(3,6,9-trioxadecyloxy)phthalonitrile (**2.13**; 0.52 g, 1.79 mmol), and $Zn(OAc)_2$•$2H_2O$ (1.18 g, 5.38 mmol) in *n*-pentanol (20 mL) was heated to 100 °C, then a small amount of DBU (1 mL) was added. The mixture was stirred at 140–150 °C for 24 h. After a brief cooling, the volatiles were removed under reduced pressure. The residue was dissolved in $CHCl_3$ (150 mL), then filtered to remove part of the ZnPc formed. The filtrate was collected and evaporated to dryness in vacuo. The residue was purified by silica-gel column chromatography using $CHCl_3$ and then $CHCl_3$/MeOH (100:1 v/v) as the eluents. The crude product was purified by size exclusion chromatography using THF as the eluent followed by recrystallization from a mixture of $CHCl_3$ and hexane to give a green solid (0.32 g, 24 % yield). ^{1}H NMR ($CDCl_3$ with a trace amount of pyridine-d_5): δ = 9.05–9.10 (m, 3 H, Pc-H_α), 9.01 (d, J = 7.2 Hz, 1 H, Pc-H_α), 8.95 (d, J = 6.4 Hz, 1 H, Pc-H_α), 8.90 (d, J = 6.8 Hz, 1 H, Pc-H_α), 8.68 (d, J = 8.0 Hz, 1 H, Pc-H_α), 8.20 (d, J = 2.0 Hz, 1 H, Pc-H_α), 7.88–8.01 (m, 6 H, Pc-H_β), 7.39 (dd, J = 2.0, 8.0 Hz, 1 H, Pc-H_β), 4.57 (vt, J = 4.4 Hz, 2 H, CH_2), 4.19 (vt, J = 4.4 Hz, 2 H, CH_2), 3.97–3.99 (m, 2 H, CH_2), 3.85–3.87 (m, 2 H, CH_2), 3.77–3.79 (m, 2 H, CH_2), 3.64–3.66 (m, 2 H, CH_2), 3.42 (s, 3 H, CH_3). ^{13}C{^{1}H} NMR ($CDCl_3$ with a trace amount of pyridine-d_5): δ = 160.2, 153.2, 152.9, 152.8, 152.5, 139.9, 138.1, 138.0, 137.8, 131.3, 128.7, 128.5, 123.2, 122.3, 118.1, 105.1, 71.9, 71.0, 70.8, 70.6, 70.0, 68.0, 59.0 (some of the aromatic signals were overlapped). MS (ESI): an isotopic cluster peaking at *m*/*z* 738 (100 %, M^+). HRMS (ESI): *m*/*z* calcd for $C_{39}H_{30}N_8O_4Zn$ $[M]^+$:

738.1676; found: 738.1674. Anal. calcd for $C_{39}H_{30}N_8O_4Zn$: C, 63.29; H, 4.09; N, 15.13. Found: C, 63.52; H, 4.35; N, 14.75.

Preparation of *Trans*-(d,l)-1,2-diaminocyclohexanedichloroplatinum(II) (2.16) [7]

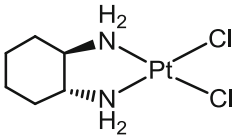

Trans-(d,l)-1,2-diaminocyclohexane (**2.15**; 0.82 g, 7.18 mmol) was dissolved in H_2O (25 mL) containing potassium tetrachloroplatinate(II) (2.98 g, 7.18 mmol). The mixture was stirred at room temperature for 16 h. The yellow precipitate formed was then filtered and washed thoroughly with water, methanol, and diethyl ether (2.18 g, 80 % yield). ^{1}H NMR (DMSO-d_6): $\delta = 2.35$ (br s, 2 H), 1.88–1.97 (m, 2 H), 1.50–1.51 (m, 2 H), 1.29–1.36 (m, 2 H), 0.96–1.07 (m, 2 H).

Preparation of *Trans*-(d,l)-1,2-diaminocyclohexanemalonatoplatinum(II) (2.17) [7]

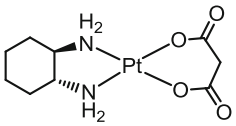

A solution of malonic acid (0.25 g, 2.40 mmol) in water (15 mL) was made alkaline (pH = 5–6) with 2 M KOH. It was then added to a solution of *trans*-(d,l)-1,2-diaminocyclohexanedinitratoplatinum(II) (**2.10**; 0.52 g, 1.20 mmol) in water (30 mL). The mixture was stirred at 60 °C for 1 h and then at room temperature for 24 h. The white precipitate formed was filtered and washed thoroughly with water, methanol, and diethyl ether (0.37 g, 76 % yield). ^{1}H NMR (DMSO-d_6): $\delta = 2.05$ (br s, 2 H), 1.78–1.81 (m, 2 H), 1.43–1.45 (m, 2 H), 1.18–1.20 (m, 2 H), 0.96–1.01 (m, 2 H).

7.2.2 Photocytotoxicity Assay

Compounds **2.11**, **2.14**, and **2.17** were first dissolved in DMF to give 10 mM solutions, which were diluted to 1 mM with the culture medium (with 0.5 % Cremophor EL). They were then further diluted with the culture medium to appropriate concentrations. The remaining steps are the same as described in Sect. 7.1.4.

7.2.3 Intracellular Fluorescence Studies

The HT29 cells were incubated with phthalocyanine **2.11** or **2.14** (5 μM, 2 mL) in the medium for 2 h at 37 °C under 5 % CO_2 before being viewed with a confocal laser scanning microscope.

7.2.4 Cellular Uptake Determined by an Extraction Method

The HT29 cells were incubated with phthalocyanine **2.11** or **2.14** (5 μM, 2 mL) in the medium for 2 h at 37 °C under 5 % CO_2. The remaining steps are the same as described in Sect. 7.1.7. The absorbance at 672 nm for both **2.11** and **2.14** were compared with the respective calibration curves to give the uptake concentrations.

7.2.5 Subcellular Localization Studies

The HT29 cells were incubated with a solution of **2.11** in the medium (5 μM, 2 mL) for 2 h at 37 °C under 5 % CO_2 prior to the treatment with LysoTracker, MitoTracker, ER-Tracker, or SYTO-16 as described in Sect. 7.1.8.

7.3 Experiments Described in Chapter 3

7.3.1 Synthesis

Preparation of *N*-(*tert*-Butoxycarbonyl)-2-aminoethanol (3.2a) [9]

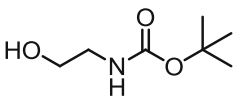

A solution of 2-aminoethanol (**3.1a**; 8.65 g, 141.62 mmol) in MeOH/triethylamine (7:1 v/v, 150 mL) was stirred at 0 °C for 10 min under an inert atmosphere. A solution of di-*tert*-butyl dicarbonate (46.36 g, 212.42 mmol) in MeOH (150 mL) was then added slowly over 30 min. The mixture was stirred at 0 °C for 1 h, and then at room temperature for 24 h. The solvent was removed under reduced pressure. The oily residue was redissolved in CH_2Cl_2 (300 mL) and washed with water (300 mL × 3). The organic layer was then dried over anhydrous Na_2SO_4 and concentrated to give the product as a colorless oil (19.17 g,

84 % yield). ^{1}H NMR ($CDCl_3$): $\delta = 3.69$ (t, $J = 5.2$ Hz, 2 H, CH_2), 3.28 (t, $J = 5.2$ Hz, 2 H, CH_2), 1.44 (s, 9 H, CH_3).

Preparation of *N*,*N*'-Bis(*tert*-butoxycarbonyl)-2-[(2-aminoethyl)amino]ethanol (3.2b) [9]

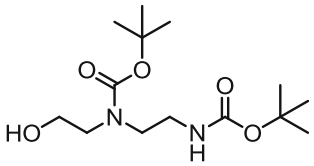

According to the procedure for **3.2a**, 2-(2-aminoethylamino)ethanol (**3.1b**; 9.65 g, 92.65 mmol) was treated with di-*tert*-butyl dicarbonate (50.55 g, 213.62 mmol) in MeOH/triethylamine (7:1 v/v, 150 mL) to give the product as a colorless oil (24.24 g, 86 % yield). ^{1}H NMR ($CDCl_3$): $\delta = 3.72$ (br s, 2 H, CH_2), 3.36 (br s, 4 H, CH_2), 3.30 (br s, 4 H, CH_2), 1.46 (s, 9 H, CH_3), 1.43 (s, 9 H, CH_3).

Preparation of *N*-(*tert*-Butoxycarbonyl)-3-amino-1-propanol (3.4a) [9]

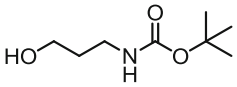

According to the procedure for **3.2a**, 3-amino-1-propanol (**3.3a**; 5.21 g, 69.36 mmol) was treated with di-*tert*-butyl dicarbonate (22.71 g, 104.05 mmol) in MeOH/triethylamine (7:1 v/v, 100 mL) to give the product as a colorless oil (10.45 g, 86 % yield). ^{1}H NMR ($CDCl_3$): $\delta = 3.69$–3.72 (m, 2 H, CH_2), 3.27–3.31 (m, 2 H, CH_2), 1.67 (br s, 2 H, CH_2), 1.45 (s, 9 H, CH_3).

Preparation of *N*-(*tert*-Butoxycarbonyl)-4-amino-1-butanol (3.4b) [9]

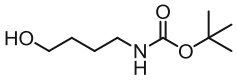

According to the procedure for **3.2a**, 4-amino-1-butanol (**3.3b**; 6.43 g, 72.13 mmol) was treated with di-*tert*-butyl dicarbonate (23.61 g, 108.18 mmol) in MeOH/triethylamine (7:1 v/v, 100 mL) to give the product as a colorless oil (11.19 g, 82 % yield). ^{1}H NMR ($CDCl_3$): $\delta = 3.60$–3.69 (m, 2 H, CH_2), 3.08–3.19 (m, 2 H, CH_2), 1.51–1.61 (m, 4 H, CH_2), 1.44 (s, 9 H, CH_3).

Preparation of Methanesulfonic Acid 3-*tert*-Butoxycarbonylaminopropyl Ester (3.5a) [9]

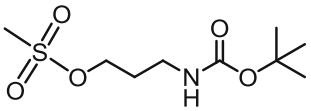

To a solution of *N*-(*tert*-butoxycarbonyl)-3-amino-1-propanol (**3.4a**; 3.03 g, 17.30 mmol) and triethylamine (12 mL, 86.33 mmol) in CH_2Cl_2 (100 mL) at 0 °C, methanesulfonyl chloride (MsCl; 3.96 g, 34.57 mmol) was added dropwise over 30 min under an inert atmosphere. The reaction mixture was stirred at 0 °C for 1 h and was then gradually warmed to room temperature. It was stirred at this temperature for 24 h under an inert atmosphere. The mixture was then cooled to 0 °C, and 4 M NaOH solution (20 mL) was added slowly. The organic phase was separated and washed with water (100 mL × 3). It was then dried over anhydrous Na_2SO_4 and concentrated to give the product as a colorless oil (3.85 g, 88 % yield). ^{1}H NMR ($CDCl_3$): $\delta = 4.29$ (t, $J = 6.0$ Hz, 2 H, OCH_2), 3.26 (q, $J = 6.0$ Hz, 2 H, CH_2), 3.02 (s, 3 H, CH_3), 1.93 (t, $J = 6.0$ Hz, 2 H, CH_2) 1.43 (s, 9 H, CH_3).

Preparation of Methanesulfonic Acid 4-*tert*-Butoxycarbonylaminobutyl Ester (3.5b) [9]

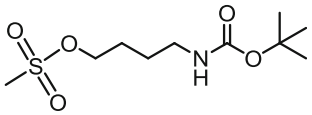

According to the procedure for **3.5a**, *N*-(*tert*-butoxycarbonyl)-4-amino-1-butanol (**3.4b**; 3.87 g, 20.46 mmol) was treated with triethylamine (14 mL, 100.72 mmol) and MsCl (4.68 g, 40.86 mmol) in CH_2Cl_2 (100 mL) to afford the product as a colorless oil (4.53 g, 83 % yield). ^{1}H NMR ($CDCl_3$): $\delta = 4.24$ (t, $J = 6.4$ Hz, 2 H, OCH_2), 3.14–3.18 (m, 2 H, CH_2), 3.01 (s, 3 H, CH_3), 1.76–1.80 (m, 2 H, CH_2), 1.58–1.62 (m, 2 H, CH_2), 1.43 (s, 9 H, CH_3).

Preparation of [3-(3-Hydroxypropylamino)propyl]carbamic Acid *tert*-Butyl Ester (3.6a) [9]

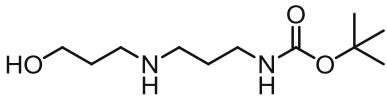

A mixture of methanesulfonic acid 3-*tert*-butoxycarbonylaminopropyl ester (**3.5a**; 3.86 g, 15.25 mmol) and 3-amino-1-propanol (**3.3a**; 11.45 g, 152.44 mmol) in acetonitrile (20 mL) was heated at 75 °C overnight under an inert atmosphere.

The volatiles were evaporated under reduced pressure. The residue was redissolved in CH_2Cl_2 (50 mL) and the solution was washed with saturated aqueous Na_2CO_3 solution (50 mL × 3). The organic layer was separated, dried over anhydrous Na_2SO_4 and concentrated. The crude product was subject to silica-gel column chromatography using $CHCl_3$/MeOH (10:1 v/v) as the eluent to afford the product as a pale yellow oily liquid (2.48 g, 70 % yield). R_f [$CHCl_3$/MeOH (10:1 v/v)] = 0.16. ^{1}H NMR ($CDCl_3$): δ = 3.82 (t, J = 5.6 Hz, 2 H, OCH_2), 3.19–3.21 (m, 2 H, CH_2), 2.90 (t, J = 5.6 Hz, 2 H, CH_2), 2.71 (t, J = 6.8 Hz, 2 H, CH_2), 1.70–1.76 (m, 4 H), 1.44 (s, 9 H, CH_3).

Preparation of [4-(4-Hydroxybutylamino)butyl]carbamic Acid *tert*-Butyl Ester (3.6b) [9]

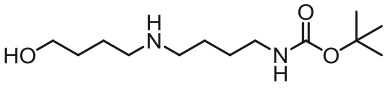

According to the procedure for **3.6a**, methanesulfonic acid 4-*tert*-butoxycarbonylaminobutyl ester (**3.5b**; 3.23 g, 12.09 mmol) was treated with 4-amino-1-butanol (**3.3b**; 10.78 g, 120.93 mmol) in acetonitrile (20 mL) to give the product as a pale yellow oily liquid (2.01 g, 64 % yield). R_f [$CHCl_3$/MeOH (10:1 v/v)] = 0.17. ^{1}H NMR ($CDCl_3$): δ = 3.54–3.57 (m, 2 H, OCH_2), 3.10 (br s, 2 H, CH_2), 2.60–2.65 (m, 4 H, CH_2), 1.58–1.70 (m, 4 H, CH_2), 1.53 (br s, 4 H, CH_2), 1.45 (s, 9 H, CH_3).

Preparation of (3-*tert*-Butoxycarbonylaminopropyl)-(3-hydroxypropyl)carbamic Acid *tert*-Butyl Ester (3.7a) [9]

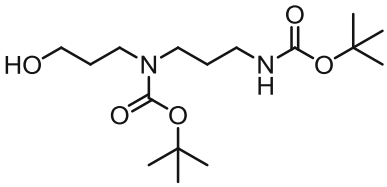

According to the procedure for **3.2a**, [3-(3-hydroxypropylamino)propyl]carbamic acid *tert*-butyl ester (**3.6a**; 7.27 g, 31.31 mmol) was treated with di-*tert*-butyl dicarbonate (10.25 g, 46.96 mmol) in MeOH/triethylamine (7:1 v/v, 150 mL) to afford the product as a pale yellow oily liquid (8.53 g, 82 % yield). ^{1}H NMR ($CDCl_3$): δ = 3.50 (br s, 2 H, OCH_2), 3.31–3.16 (m, 4 H), 3.06 (vt, J = 5.8 Hz, 2 H, CH_2), 1.64–1.68 (m, 4 H), 1.42 (s, 9 H, CH_3), 1.39 (s, 9 H, CH_3).

Preparation of (4-*tert*-Butoxycarbonylaminobutyl)-(4-hydroxybutyl)carbamic Acid *tert*-Butyl Ester (3.7b) [9]

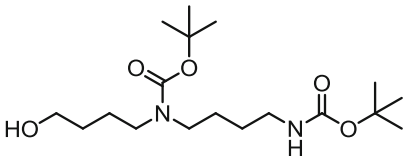

According to the procedure for **3.2a**, [4-(4-hydroxybutylamino)butyl]carbamic acid *tert*-butyl ester (**3.6b**; 6.28 g, 24.13 mmol) was treated with di-*tert*-butyl dicarbonate (7.90 g, 36.20 mmol) in MeOH/triethylamine (7:1 v/v, 150 mL) to give the product as a pale yellow oily liquid (7.39 g, 85 % yield). ^{1}H NMR ($CDCl_3$): $\delta = 3.64$ (br s, 2 H, OCH_2), 3.10–3.18 (m, 6 H, CH_2), 1.51–1.59 (m, 8 H, CH_2), 1.43 (s, 18 H, CH_3).

Preparation of Phthalonitrile 3.8a

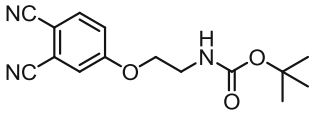

A mixture of 4-nitrophthalonitrile (2.37 g, 13.69 mmol), *N*-(*tert*-butoxycarbonyl)-2-aminoethanol (**3.2a**; 4.41 g, 27.37 mmol), and anhydrous K_2CO_3 (9.46 g, 68.45 mmol) in DMF (20 mL) was heated at 80 °C under an inert atmosphere for 48 h. The volatiles were evaporated under reduced pressure at 60 °C. The crude product was mixed with water (50 mL) and the mixture was extracted with $CHCl_3$ (50 mL × 3). The organic layers were combined, dried over anhydrous Na_2SO_4, and concentrated under reduced pressure. The residue was subject to silica-gel column chromatography using first CH_2Cl_2 and then with CH_2Cl_2/MeOH (100:1 v/v) as the eluents to give the product as a pale yellow oily liquid (2.67 g, 68 % yield). R_f [CH_2Cl_2/MeOH (100:1 v/v)] = 0.20. ^{1}H NMR ($CDCl_3$): $\delta = 7.72$ (d, $J = 8.8$ Hz, 1 H, ArH), 7.26 (s, 1 H, ArH), 7.20 (d, $J = 8.8$ Hz, 1 H, ArH), 4.11 (vt, $J = 4.8$ Hz, 2 H, CH_2), 3.57 (vt, $J = 5.2$ Hz, 2 H, CH_2), 1.45 (s, 9 H, CH_3). ^{13}C{^{1}H} NMR ($CDCl_3$): $\delta = 161.6$, 155.7, 135.2, 119.7, 119.1, 117.1, 115.5, 115.1, 107.2, 79.6, 68.1, 39.4, 28.1. HRMS (ESI): *m/z* calcd for $C_{15}H_{17}N_3NaO_3$ $[M + Na]^+$: 310.1162; found: 310.1156.

Preparation of Phthalonitrile 3.8b

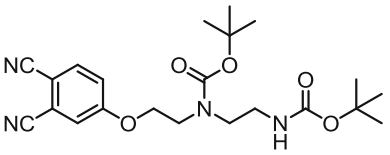

According to the procedure for **3.8a**, *N*,*N*'-bis(*tert*-butoxycarbonyl)-2-[(2-aminoethyl)amino]ethanol (**3.2b**; 10.96 g, 36.03 mmol) was treated with 4-nitrophthalonitrile (3.12 g, 18.02 mmol) and anhydrous K_2CO_3 (12.45 g, 90.08 mmol) in DMF (20 mL) to give the product as a pale yellow oily liquid (4.88 g, 63 % yield). R_f [CH_2Cl_2/MeOH (100:1 v/v)] = 0.22. ^{1}H NMR (acetone-d_6): δ = 7.98 (d, J = 8.8 Hz, 1 H, ArH), 7.69 (s, 1 H, ArH), 7.51 (d, J = 8.8 Hz, 1 H, ArH), 4.34–4.39 (m, 2 H, CH_2), 3.67–3.71 (m, 2 H, CH_2), 3.41 (t, J = 6.4 Hz, 2 H, CH_2), 3.27 (vt, J = 6.4 Hz, 2 H, CH_2), 1.45 (s, 9 H, CH_3), 1.40 (s, 9 H, CH_3). ^{13}C{^{1}H} NMR (acetone-d_6): δ = 162.9, 156.7, 155.9, 136.4, 120.7, 120.6, 117.8, 116.6, 116.2, 107.6, 80.1, 78.7, 68.5, 48.3, 47.6, 39.9, 28.6, 28.5. HRMS (ESI): *m*/*z* calcd for $C_{22}H_{30}N_4NaO_5$ [M + Na]$^+$: 453.2108; found: 453.2110.

Preparation of Phthalonitrile 3.8c

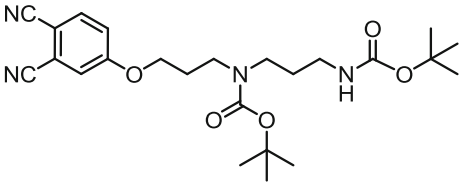

According to the procedure for **3.8a**, (3-*tert*-butoxycarbonylaminopropyl)-(3-hydroxypropyl)carbamic acid *tert*-butyl ester (**3.7a**; 13.40 g, 40.33 mmol) was treated with 4-nitrophthalonitrile (3.49 g, 20.16 mmol) and anhydrous K_2CO_3 (13.93 g, 100.79 mmol) in DMF (20 mL) to give the product as a pale yellow oily liquid (5.54 g, 60 % yield). R_f [CH_2Cl_2/MeOH (100:1 v/v)] = 0.23. ^{1}H NMR ($CDCl_3$): δ = 7.71 (d, J = 8.8 Hz, 1 H, ArH), 7.25 (s, 1 H, ArH), 7.18 (d, J = 8.8 Hz, 1 H, ArH), 4.06 (t, J = 6.0 Hz, 2 H, CH_2), 3.36 (br s, 2 H, CH_2), 3.27 (br s, 2 H, CH_2), 3.11 (br s, 2 H, CH_2), 2.06 (t, J = 6 Hz, 2 H, CH_2), 1.69 (br s, 2 H, CH_2) 1.44 (s, 18 H, CH_3). ^{13}C{^{1}H} NMR ($CDCl_3$): δ = 161.7, 155.8, 155.3, 135.0, 119.4, 119.1, 117.0, 115.5, 115.0, 106.8, 79.6, 78.7, 66.8, 66.5, 44.5, 43.8, 43.5, 37.2, 28.1 (two overlapping signals). HRMS (ESI): *m*/*z* calcd for $C_{24}H_{34}N_4NaO_5$ [M + Na]$^+$: 481.2421; found: 481.2424.

Preparation of Phthalonitrile 3.8d

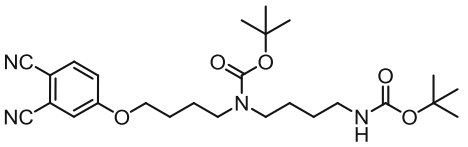

According to the procedure for **3.8a**, (4-*tert*-butoxycarbonylaminobutyl)- (4-hydroxybutyl)carbamic acid *tert*-butyl ester (**3.7b**; 14.06 g, 39.03 mmol) was treated with 4-nitrophthalonitrile (3.38 g, 19.52 mmol) and anhydrous K_2CO_3 (13.49 g, 97.61 mmol) in DMF (20 mL) to give the product as a pale yellow oily liquid (6.07 g, 64 % yield). R_f [CH_2Cl_2/MeOH (100:1 v/v)] = 0.22. ^{1}H NMR ($CDCl_3$): δ = 7.70 (d, J = 8.8 Hz, 1 H, ArH), 7.25 (s, 1 H, ArH), 7.18 (d, J = 8.4 Hz, 1 H, ArH), 4.06 (t, J = 6.0 Hz, 2 H, CH_2), 3.11–3.23 (m, 6 H), 1.77–1.82 (m, 2 H, CH_2), 1.66–1.71 (m, 2 H, CH_2), 1.50–1.62 (m, 4 H, CH_2), 1.44 (s, 9 H, CH_3), 1.43 (s, 9 H, CH_3). ^{13}C{^{1}H} NMR ($CDCl_3$): δ = 162.0, 155.9, 155.5, 135.1, 119.5, 119.3, 117.3, 115.6, 115.2, 106.9, 79.3, 79.0, 68.8, 46.6, 46.1, 40.1, 28.4, 28.3, 27.4, 26.0, 25.8, 25.5. HRMS (ESI): m/z calcd for $C_{26}H_{38}N_4NaO_5$ [M + Na]$^+$: 509.2734; found: 509.2741.

Preparation of Phthalocyanine 3.9a

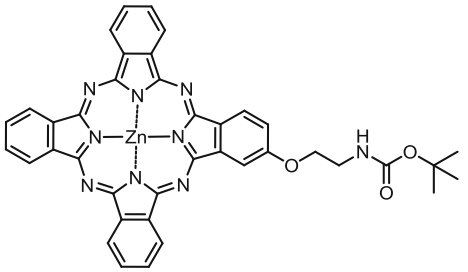

A mixture of phthalonitrile **3.8a** (0.69 g, 3.98 mmol), 1,2-dicyanobenzene (4.59 g, 35.82 mmol), and $Zn(OAc)_2$•$2H_2O$ (2.62 g, 11.94 mmol) in *n*-pentanol (30 mL) was heated to 100 °C, then a small amount of DBU (1 mL) was added. The mixture was stirred at 140–150 °C overnight. After a brief cooling, the volatiles were removed under reduced pressure at 80 °C. The residue was dissolved in $CHCl_3$ (150 mL) and then filtered to remove part of the ZnPc formed. The filtrate was collected and evaporated to dryness in vacuo. The residue was purified by silica-gel column chromatography using $CHCl_3$ and then with $CHCl_3$/MeOH (100:1 v/v) as the eluents. The crude product was purified by size exclusion chromatography using THF as the eluent. The product was further purified by recrystallization from a mixture of THF and hexane to obtain the pure product as a shiny purplish blue solid (0.53 g, 18 % yield). ^{1}H NMR ($CDCl_3$ with a trace amount of pyridine-d_5): δ = 9.14–9.22 (m, 3 H, Pc-H$_\alpha$), 9.00–9.02 (m, 1 H, Pc-H$_\alpha$), 8.88–8.89 (m, 1 H, Pc-H$_\alpha$), 8.82 (d, J = 7.6 Hz, 1 H, Pc-H$_\alpha$), 8.35 (d,

$J = 8.0$ Hz, 1 H, Pc-H_α), 7.83–8.07 (m, 7 H, 1 Pc-H_α and 6 Pc-H_β), 7.04 (d, $J = 8.0$ Hz, 1 H, Pc-H_β), 4.28–4.33 (m, 2 H, OCH_2), 3.82–3.88 (m, 2 H, CH_2), 1.61 (s, 9 H, CH_3). $^{13}C\{^1H\}$ NMR ($CDCl_3$, with a trace amount of pyridine-d_5): $\delta = 159.3$, 152.7, 152.6, 152.5, 152.2, 152.1, 152.0, 151.5, 139.2, 138.1, 138.0, 137.9, 137.7, 137.5, 130.7, 128.5, 122.9, 122.5, 122.2, 122.0, 121.8, 117.0, 104.3, 79.5, 67.4, 37.7, 28.5. HRMS (ESI): *m/z* calcd for $C_{39}H_{30}N_9O_3Zn$ $[M + H]^+$: 736.1758; found: 736.1771. Anal. calcd for $C_{39}H_{29}N_9O_3Zn$: C, 63.55; H, 3.97; N, 17.09. Found: C, 63.25; H, 3.91; N, 16.76.

Preparation of Phthalocyanine 3.9b

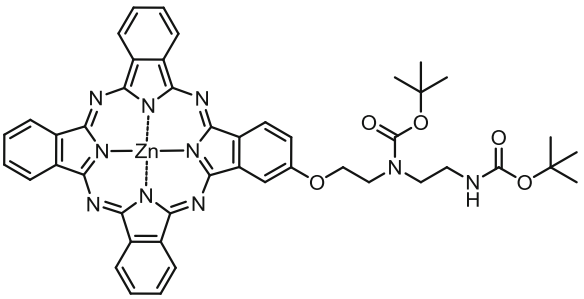

According to the procedure for **3.9a**, a mixture of phthalonitrile **3.8b** (0.46 g, 1.07 mmol), 1,2-dicyanobenzene (1.23 g, 9.60 mmol), and $Zn(OAc)_2 \bullet 2H_2O$ (0.70 g, 3.19 mmol) with a small amount of DBU (1 mL) was heated in *n*-pentanol (30 mL) to afford the product as a shiny purplish blue solid (0.14 g, 15 % yield). ^1H NMR ($CDCl_3$, with a trace amount of pyridine-d_5): $\delta = 9.15$–9.28 (m, 6 H, Pc-H_α), 8.83–8.90 (m, 1 H, Pc-H_α), 8.40 (s, 1 H, Pc-H_α), 8.03–8.08 (m, 6 H, Pc-H_β), 7.45 (br s, 1 H, Pc-H_β), 4.58 (br s, 2 H, OCH_2), 3.90 (br s, 2 H, CH_2), 3.67 (br s, 2 H, CH_2), 3.51 (br s, 2 H, CH_2), 1.55 (s, 9 H, CH_3), 1.49 (s, 9 H, CH_3). $^{13}C\{^1H\}$ NMR ($CDCl_3$ with a trace amount of pyridine-d_5): $\delta = 159.6$, 152.8, 152.6, 152.3, 152.2, 151.9, 139.6, 138.0, 137.9, 137.7, 131.1, 130.9, 128.5, 122.7, 122.2, 122.1, 122.0, 117.5, 104.6, 80.2, 67.2, 48.9, 47.7, 39.7, 28.4. HRMS (ESI): *m/z* calcd for $C_{46}H_{43}N_{10}O_5Zn$ $[M + H]^+$: 879.2704; found: 879.2697. Anal. calcd for $C_{46}H_{42}N_{10}O_5Zn$: C, 62.76; H, 4.81; N, 15.91. Found: C, 62.42; H, 4.81; N, 15.86.

Preparation of Phthalocyanine 3.9c

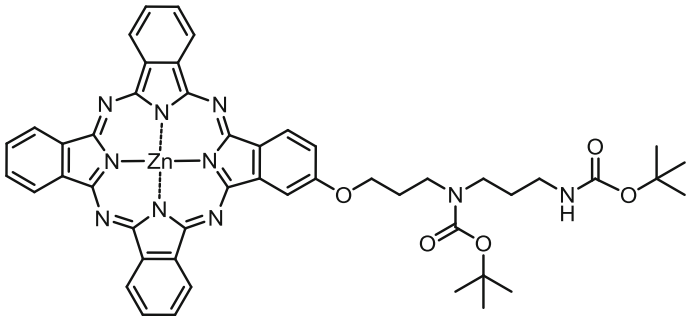

According to the procedure for **3.9a**, a mixture of phthalonitrile **3.8c** (0.52 g, 1.13 mmol), 1,2-dicyanobenzene (1.30 g, 10.15 mmol), and $Zn(OAc)_2 \bullet 2H_2O$ (0.74 g, 3.37 mmol) with a small amount of DBU (1 mL) was heated in *n*-pentanol (30 mL) to afford the product as a shiny purplish blue solid (0.20 g, 20 % yield). ^1H NMR ($CDCl_3$ with a trace amount of pyridine-d_5): $\delta = 8.94$–9.08 (m, 6 H, Pc-H_α), 8.68 (d, $J = 7.2$ Hz, 1 H, Pc-H_α), 8.15 (br s, 1 H, Pc-H_α), 7.88–7.99 (m, 6 H, Pc-H_β), 7.34 (br s, 1 H, Pc-H_β), 4.35 (br s, 2 H, OCH_2), 3.59 (br s, 2 H, CH_2), 3.47 (br s, 2 H, CH_2), 3.22 (br s, 2 H, CH_2), 2.30 (br s, 2 H, CH_2), 1.82 (br s, 2 H, CH_2), 1.57 (s, 9 H, CH_3), 1.45 (s, 9 H, CH_3). $^{13}C\{^1H\}$ NMR ($CDCl_3$, with a trace amount of pyridine-d_5): $\delta = 160.1$, 153.1, 153.0, 152.9, 152.7, 152.4, 152.3, 139.9, 138.1 (two overlapping signals), 138.0, 137.8, 131.2, 128.6, 128.5, 128.3, 122.7, 122.2 (two overlapping signals), 122.1, 117.7, 104.7, 79.8, 65.8, 44.4, 44.0, 43.8, 37.4, 28.5, 28.4, 22.3. HRMS (ESI): *m/z* calcd for $C_{48}H_{47}N_{10}O_5Zn$ $[M + H]^+$: 907.3017; found: 907.3016. Anal. calcd for $C_{48}H_{46}N_{10}O_5Zn$: C, 63.47; H, 5.10; N, 15.41. Found: C, 63.73; H, 5.30; N, 15.77.

Preparation of Phthalocyanine 3.9d

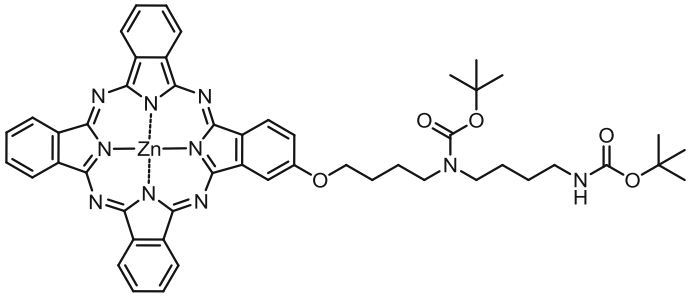

According to the procedure for **3.9a**, a mixture of phthalonitrile **3.8d** (0.43 g, 0.88 mmol), 1,2-dicyanobenzene (1.01 g, 7.88 mmol), and $Zn(OAc)_2 \bullet 2H_2O$ (0.58 g, 2.64 mmol) with a small amount of DBU (1 mL) was heated in *n*-pentanol

(30 mL) to afford the product as a shiny purplish blue solid (0.13 g, 16 % yield). ^{1}H NMR ($CDCl_3$ with a trace amount of pyridine-d_5): δ = 9.23–9.32 (m, 6 H, Pc-H$_\alpha$), 9.04 (d, J = 8.4 Hz, 1 H, Pc-H$_\alpha$), 8.59 (s, 1 H, Pc-H$_\alpha$), 8.00–8.08 (m, 6 H, Pc-H$_\beta$), 7.53–7.55 (m, 1 H, Pc-H$_\beta$), 4.46 (t, J = 6.4 Hz, 2 H, OCH_2), 3.39 (br s, 2 H, CH_2), 3.33 (br s, 2 H, CH_2), 3.17 (br s, 2 H, CH_2), 2.05 (t, J = 6.4 Hz, 2 H, CH_2), 1.93–1.95 (m, 2 H, CH_2), 1.78–1.82 (m, 2 H, CH_2), 1.61–1.62 (m, 2 H, CH_2), 1.51 (s, 9 H, CH_3), 1.41 (s, 9 H, CH_3). ^{13}C{^{1}H} NMR ($CDCl_3$, with a trace amount of pyridine-d_5): δ = 160.5, 153.3, 153.0, 152.8, 152.6, 152.4, 140.1, 138.1, 138.0, 137.9, 131.2, 128.7, 128.6, 128.4, 122.3, 122.1, 117.9, 105.1, 79.3, 68.2, 47.0, 46.8, 40.3, 28.5, 28.4, 27.5, 27.0, 25.7, 25.3. HRMS (ESI): m/z calcd for $C_{50}H_{51}N_{10}O_5Zn$ $[M + H]^+$: 935.3330; found: 935.3323. Anal. calcd for $C_{50}H_{50}N_{10}O_5Zn$: C, 64.13; H, 5.38; N, 14.95. Found: C, 63.92; H, 5.08; N, 14.62.

Preparation of Phthalocyanine 3.10a

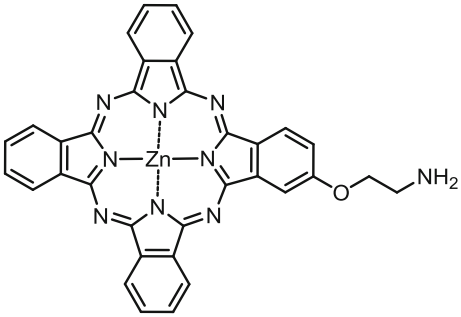

Phthalocyanine **3.9a** (0.14 g, 0.19 mmol) was dissolved in a mixture of trifluoroacetic acid (TFA)/CH_2Cl_2 (1:1 v/v, 10 mL). The reaction was stirred at room temperature for 2 h under an inert atmosphere. The solvent was removed under reduced pressure. The residue was dissolved in water (30 mL), and the mixture was neutralized by adding 2 M NaOH until pH = 8. The blue precipitate was filtered and washed thoroughly with water, acetone, and ether. The product was obtained as a blue solid (0.10 g, 86 % yield). ^{1}H NMR (pyridine-d_5): δ = 9.50–9.67 (m, 6 H, Pc-H$_\alpha$), 9.33–9.39 (m, 1 H, Pc-H$_\alpha$), 9.03 (s, 1 H, Pc-H$_\alpha$), 8.12–8.22 (m, 6 H, Pc-H$_\beta$), 7.76 (t, J = 8.4 Hz, 1 H, Pc-H$_\beta$), 4.76 (t, J = 6.0 Hz, 1 H), 4.59 (br s, 1 H), 4.43 (t, J = 6.4 Hz, 1 H), 4.14–4.18 (m, 1 H). ^{13}C{^{1}H} NMR (pyridine-d_5): δ = 161.5, 154.7, 154.6, 154.4, 154.2, 154.1, 154.0, 153.9, 153.8, 141.4, 140.1, 139.5 (two overlapping signals), 139.4 (two overlapping signals), 139.2, 132.7, 130.1 (two overlapping signals), 130.0 (two overlapping signals), 129.9, 129.4, 119.0, 107.0, 69.0, 38.8. HRMS (ESI): m/z calcd for $C_{34}H_{22}N_9OZn$ $[M + H]^+$: 636.1233; found: 636.1236. Anal. calcd for $C_{34}H_{21}N_9OZn$: C, 64.11; H, 3.32; N, 16.79. Found: C, 63.72; H, 3.02; N, 19.58.

Preparation of Phthalocyanine 3.10b

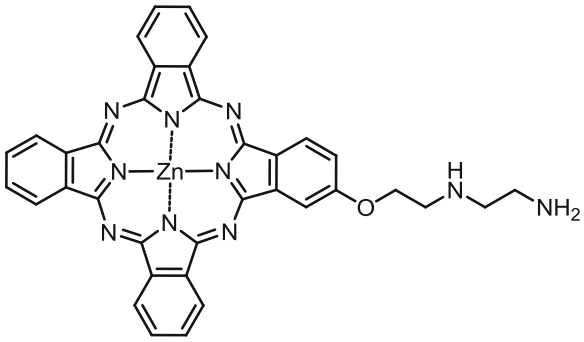

According to the procedure for **3.10a**, phthalocyanine **3.9b** (0.18 g, 0.20 mmol) was stirred in a mixture of TFA/CH_2Cl_2 (1:1 v/v, 10 mL) to give the product as a blue solid (0.12 g, 88 % yield). ^{1}H NMR (pyridine-d_5): δ = 9.66–9.76 (m, 6 H, Pc-H$_\alpha$), 9.53 (d, J = 8.4 Hz, 1 H, Pc-H$_\alpha$), 9.23 (s, 1 H, Pc-H$_\alpha$), 8.19–8.29 (m, 6 H, Pc-H$_\beta$), 7.87 (d, J = 6.8 Hz, 1 H, Pc-H$_\beta$), 4.64 (t, J = 5.6 Hz, 2 H, CH_2), 3.70 (t, J = 6.4 Hz, 2 H, CH_2), 3.31 (t, J = 5.6 Hz, 2 H, CH_2), 2.88 (br s, 2 H, CH_2). ^{13}C{^{1}H} NMR (pyridine-d_5): δ = 162.1, 155.1, 154.9, 154.4, 154.3, 154.1, 141.7, 140.7, 139.6, 139.5, 139.4, 132.7, 130.3, 130.1, 130.0, 119.2, 107.2, 69.6, 52.9, 49.6, 42.4. HRMS (ESI): m/z calcd for $C_{36}H_{27}N_{10}OZn$ $[M + H]^+$: 679.1655; found: 679.1673. Anal. calcd for $C_{36}H_{26}N_{10}OZn$: C, 63.58; H, 3.85; N, 20.59. Found: C, 63.33; H, 3.70; N, 20.34.

Preparation of Phthalocyanine 3.10c

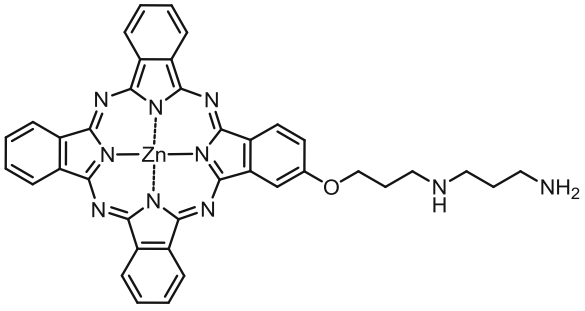

According to the procedure for **3.10a**, phthalocyanine **3.9c** (0.20 g, 0.22 mmol) was stirred in a mixture of TFA/CH_2Cl_2 (1:1 v/v, 10 mL) to give the product as a blue solid (0.13 g, 84 % yield). ^{1}H NMR (pyridine-d_5): δ = 9.44–9.59 (m, 6 H, Pc-H$_\alpha$), 9.28 (d, J = 8.4 Hz, 1 H, Pc-H$_\alpha$), 8.89 (s, 1 H, Pc-H$_\alpha$), 8.08–8.21 (m, 6 H, Pc-H$_\beta$), 7.71 (d, J = 8.0 Hz, 1 H, Pc-H$_\beta$), 4.41 (br s, 2 H, OCH_2), 2.71 (br s, 2 H, CH_2), 2.33 (br s, 2 H, CH_2), 2.06 (t, J = 5.6 Hz, 2 H, CH_2) 1.76 (br s, 2 H, CH_2), 1.03 (br

s, 2 H, CH_2). $^{13}C\{^1H\}$ NMR (pyridine-d_5): δ = 162.0, 154.8, 154.6, 154.3, 154.2, 154.1, 154.0, 153.7, 153.6, 153.3, 141.5, 140.1, 139.6, 139.5 (two overlapping signals), 139.4, 139.2, 132.4, 130.0, 129.8, 129.7, 129.5, 118.9, 106.9, 67.8, 48.7, 47.4, 40.5, 30.9, 30.1. HRMS (ESI): *m/z* calcd for $C_{38}H_{31}N_{10}OZn$ $[M + H]^+$: 707.1968; found: 707.1949. Anal. calcd for $C_{38}H_{30}N_{10}OZn$: C, 64.46; H, 4.27; N, 19.77. Found: C, 64.23; H, 4.12; N, 19.55.

Preparation of Phthalocyanine 3.10d

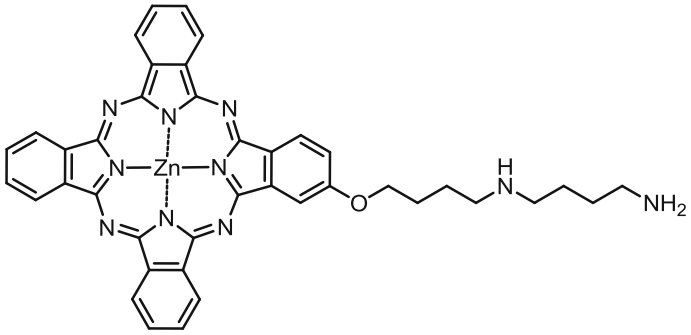

According to the procedure for **3.10a**, phthalocyanine **3.9d** (0.16 g, 0.17 mmol) was stirred in a mixture of TFA/CH_2Cl_2 (1:1 v/v, 10 mL) to give the product as a blue solid (0.10 g, 83 % yield). ^1H NMR (pyridine-d_5): δ = 9.48–9.63 (m, 6 H, Pc-H_α), 9.35 (d, J = 8.0 Hz, 1 H, Pc-H_α), 8.99 (s, 1 H, Pc-H_α), 8.09–8.21 (m, 6 H, Pc-H_β), 7.79 (d, J = 8.4 Hz, 1 H, Pc-H_β), 4.45 (t, J = 6.4 Hz, 2 H, OCH_2), 2.69 (t, J = 6.8 Hz, 2 H, CH_2), 2.48 (t, J = 6.8 Hz, 2 H, CH_2), 2.08–2.13 (m, 4 H, CH_2), 1.82 (t, J = 6.8 Hz, 2 H, CH_2), 1.29–1.35 (m, 2 H, CH_2), 1.14 (t, J = 6.8 Hz, 2 H, CH_2). $^{13}C\{^1H\}$ NMR (pyridine-d_5): δ = 162.2, 155.0, 154.8, 154.4 (two overlapping signals), 154.2 (two overlapping signals), 153.9, 153.8, 153.2, 141.6, 140.1, 139.6, 139.5 (three overlapping signals), 139.3, 132.5, 130.1 (two overlapping signals), 130.0, 129.8, 129.5, 119.1, 107.1, 69.5, 50.5, 42.3, 35.5, 28.4, 28.2, 27.6, 21.9. HRMS (ESI): *m/z* calcd for $C_{40}H_{35}N_{10}OZn$ $[M + H]^+$: 735.2281; found: 735.2263. Anal. calcd for $C_{40}H_{34}N_{10}OZn$: C, 65.26; H, 4.66; N, 19.02. Found: C, 65.53; H, 4.72; N, 19.35.

7.3.2 Photocytotoxicity Assay

Cytotoxicity of Phthalocyanines 3.10a-d on B16 and CHO Cells

All the phthalocyanines were first dissolved in DMF to give 1.6 mM solutions which were then diluted to 80 μM with the culture medium (with 0.5 % Cremophor EL). The solutions were further diluted with the culture medium to appropriate concentrations. The remaining steps are the same as described in Sect. 7.1.4.

Cytotoxicity of Spermidine on B16 and CHO Cells

Spermidine was dissolved in deionized water to give a 1 M stock solution, which was diluted with the culture medium to give a 100 mM spermidine solution. This solution was adjusted to pH = 7.4 with aqueous HCl or NaOH solution. This solution was filtered with a 0.22 μm filter and then diluted with the culture medium to give 0.05, 0.5, and 5 mM solutions. The remaining steps are the same as described in Sect. 7.1.4.

7.3.3 Effect of Spermidine on the Cellular Uptake

The spermidine stock solution was prepared as mentioned in Sect. 7.3.2. For the competitive cellular uptake experiments, the solution was diluted with the culture medium to give 0.1, 1, and 10 mM solutions.

Approximately 2×10^6 B16 or CHO cells in the culture medium (2 mL) were seeded on a Petri dish (diameter = 35 mm). Following overnight incubation at 37 °C under 5 % CO_2, the medium was removed and the cells were rinsed with PBS (2 mL). They were then incubated with the phthalocyanine dilution in the medium (16 μM, 1 mL) and the above spermidine solutions (1 mL) for 2 h under the same conditions. For the control, the culture medium (1 mL) instead of the spermidine solution was added. The remaining steps are the same as described in Sect. 7.1.7. The absorbance at 673 nm for **3.10a**, 672 nm for **3.10b**, 674 nm for **3.10c**, and 673 nm for **3.10d** were compared with the respective calibration curves to give the uptake concentrations.

7.3.4 Intracellular Fluorescence Studies

The B16 or CHO cells were incubated with phthalocyanines **3.10a-d** (2 μM, 2 mL) in the medium for 2 h at 37 °C under 5 % CO_2 before being viewed with a confocal laser scanning microscope.

7.3.5 Subcellular Localization Studies

The B16 or CHO cells were incubated with a solution of **3.10d** in the medium (2 μM, 2 mL) for 2 h at 37 °C under 5 % CO_2 prior to the treatment with LysoTracker, MitoTracker, or ER-Tracker as described in Sect. 7.1.8.

7.4 Experiments Described in Chapter 4

7.4.1 Synthesis

Preparation of Ferrocenecarboxyaldehyde (4.2) [10]

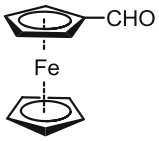

DMF (1.75 mL, 22.62 mmol) was added to a solution of ferrocene (**4.1**; 2.18 g, 11.72 mmol) in $CHCl_3$ (9 mL). The resulting mixture was stirred in an ice water bath under an inert atmosphere for 10 min. Phosphoryl chloride (4 mL, 42.9 mmol) was added dropwise to the mixture over about 30 min. After addition, the mixture was heated at 60 °C overnight. The volatiles were evaporated under reduced pressure and the residue was poured into ice water (50 mL). The precipitate formed, which was mainly the unreacted ferrocene, was filtered off. The filtrate, which was an aqueous solution of the Vilsmeier complex {[Fc-$CH = N^+(CH_3)_2$]Cl^-}, was neutralized by adding sodium carbonate powder until pH = 7. The mixture was then extracted with ether (100 mL × 3). The combined organic layers were dried with anhydrous Na_2SO_4 and concentrated under reduced pressure. The product was obtained as a reddish brown solid (1.22 g, 49 % yield). ^{1}H NMR ($CDCl_3$): $\delta = 9.96$ (s, 1 H, CHO), 4.80 (t, $J = 1.6$ Hz, 2 H), 4.60 (t, $J = 1.6$ Hz, 2 H), 4.28 (s, 5 H).

Preparation of 3-Ferrocenyl-1-(*p*-hydroxyphenyl)-prop-2-en-1-one (4.4) [11]

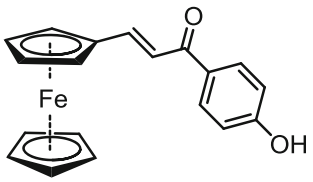

To a stirred mixture of ferrocenecarboxyaldehyde (**4.2**; 4.98 g, 23.3 mmol) and *p*-hydroxyacetopheone (**4.3**; 3.31 g, 24.31 mmol) in ethanol (30 mL), aqueous KOH solution (40 % w/w, 15 mL) was added dropwise. The mixture was continued to stir for 4 h at room temperature. The dark red solution was cooled in refrigerator at ca. −4 °C overnight. Chilled concentrated HCl was added dropwise to the mixture until pH = 7. The purple precipitate was filtered and washed thoroughly with water. The crude product was recrystallized from methanol to afford a shiny purple solid (7.00 g, 91 % yield). ^{1}H NMR ($CDCl_3$): $\delta = 7.96$ (d, $J = 8.4$ Hz, 2 H, ArH), 7.74 (d, $J = 15.2$ Hz, 1 H, CH = CH), 7.13 (d,

$J = 15.2$ Hz, 1 H, CH = CH), 6.92 (d, $J = 8.4$ Hz, 2 H), 4.59 (t, $J = 1.8$ Hz, 2 H, FcH), 4.47 (t, $J = 1.8$ Hz, 2 H, FcH), 4.18 (s, 5 H, FcH).

Preparation of Compound 4.6

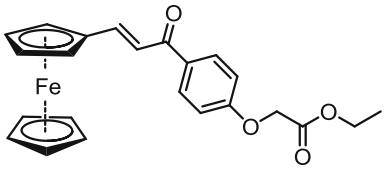

A mixture of 3-ferrocenyl-1-(*p*-hydroxyphenyl)-prop-2-en-1-one (**4.4**; 7.10 g, 21.37 mmol), ethyl bromoacetate (**4.5**; 7.14 g, 42.75 mmol), and anhydrous K_2CO_3 (8.86 g, 64.11 mmol) in acetone (100 mL) was heated under reflux overnight. The volatiles were evaporated under reduced pressure, then the residue was redissolved in water (200 mL). The mixture was then extracted with $CHCl_3$ (100 mL × 3) and the combined organic layers were dried with anhydrous Na_2SO_4 and concentrated in vacuo. The crude product was then purified by silica-gel column chromatography using $CHCl_3$/ethyl acetate (10:1 v/v) as the eluent. It was finally recrystallized from $CHCl_3$/hexane to afford a reddish brown solid (7.86 g, 88 % yield). R_f [$CHCl_3$/ethyl acetate (10:1 v/v)] = 0.90. ^{1}H NMR ($CDCl_3$): $\delta = 8.00$ (d, $J = 8.8$ Hz, 2 H, ArH), 7.74 (d, $J = 15.2$ Hz, 1 H, CH = CH), 7.12 (d, $J = 15.2$ Hz, 1 H, CH = CH), 6.98 (d, $J = 8.8$ Hz, 2 H, ArH), 4.70 (s, 2 H, CH_2), 4.59 (t, $J = 1.6$ Hz, 2 H, FcH), 4.48 (t, $J = 1.6$ Hz, 2 H, FcH), 4.29 (q, $J = 7.2$ Hz, 2 H, CH_2), 4.18 (s, 5 H, FcH), 1.31 (t, $J = 7.2$ Hz, 3 H, CH_3). ^{13}C{^{1}H} NMR ($CDCl_3$): $\delta = 188.1$, 168.3, 161.1, 146.1, 132.3, 130.6, 118.7, 114.3, 79.3, 71.3, 69.8, 68.9, 65.2, 61.6, 14.1. MS (ESI): an isotopic cluster peaking at $m/z = 418$ (100 %, $[M]^+$). HRMS (ESI): m/z calcd for $C_{23}H_{22}FeO_4$ $[M]^+$: 418.0862; found: 418.0862. Anal. calcd for $C_{23}H_{22}FeO_4$: C, 66.05; H, 5.30. Found: C, 65.94; H, 4.94.

Preparation of Compound 4.7

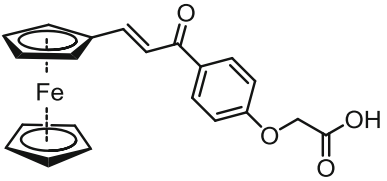

A mixture of **4.6** (7.26 g, 17.36 mmol), 5 M NaOH (31 mL, 155.0 mmol), and acetone (50 mL) was heated under reflux for 1 h. The volatiles were evaporated under reduced pressure. The residue was redissolved in water and acidified with 3 M HCl until pH = 4. The reddish orange precipitate formed was washed thoroughly with water and dried under reduced pressure at 60 °C (5.81 g, 86 % yield).

^{1}H NMR (acetone-d_6): $\delta = 8.08$ (d, $J = 8.8$ Hz, 2 H, ArH), 7.69 (d, $J = 15.2$ Hz, 1 H, CH = CH), 7.41 (d, $J = 15.2$ Hz, 1 H, CH = CH), 7.08 (d, $J = 8.8$ Hz, 2 H, ArH), 4.85 (s, 2 H, CH_2), 4.78 (t, $J = 1.6$ Hz, 2 H, FcH), 4.50 (t, $J = 1.6$ Hz, 2 H, FcH), 4.20 (s, 5 H, FcH). ^{13}C{^{1}H} NMR (acetone-d_6): $\delta = 187.5$, 169.7, 162.5, 145.9, 133.0, 131.3, 119.8, 115.3, 80.6, 71.9, 70.5, 69.9, 65.3. MS (ESI): an isotopic cluster peaking at $m/z = 390$ (100 %, $[M]^+$). HRMS (ESI): m/z calcd for $C_{21}H_{18}FeO_4$ $[M]^+$: 390.0549; found: 390.0550. Anal. calcd for $C_{21}H_{18}FeO_4$: C, 64.64; H, 4.65. Found: C, 64.39; H, 4.34.

Preparation of Compound 4.9a

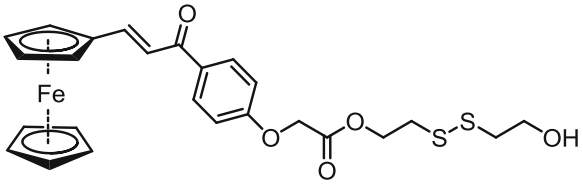

A mixture of **4.7** (0.53 g, 1.36 mmol), 2-hydroxyethyl disulfide (**4.8a**; 0.42 g, 2.72 mmol), *N*,*N*'-dicyclohexylcarbodiimide (DCC; 0.33 g, 1.60 mmol), 4-(dimethylamino)pyridine (DMAP; 0.05 g, 0.41 mmol), and 1-hydroxybenzotriazole (HOBt; 0.22 g, 1.63 mmol) in THF (20 mL) was stirred at room temperature under an inert atmosphere overnight. The volatiles were evaporated under reduced pressure. The residue was purified by silica-gel column chromatography using $CHCl_3$/MeOH (4:1 v/v) as the eluent. The crude product was redissolved in a minimum amount of $CHCl_3$. The white solid of dicyclohexylurea (DCU) formed was filtered off. This process was repeated for several times until there was no white solid left. The product was obtained as a reddish brown oily liquid (0.37 g, 52 % yield). R_f [$CHCl_3$/MeOH (4:1 v/v)] = 0.50. ^{1}H NMR ($CDCl_3$): $\delta = 7.99$ (d, $J = 8.8$ Hz, 2 H, ArH), 7.74 (d, $J = 15.6$ Hz, 1 H, CH = CH), 7.12 (d, $J = 15.6$ Hz, 1 H, CH = CH), 6.99 (d, $J = 8.8$ Hz, 2 H, ArH), 4.74 (s, 2 H, CH_2), 4.59 (t, $J = 1.6$ Hz, 2 H, FcH), 4.51, (t, $J = 6.4$ Hz, 2 H, CH_2) 4.48 (t, $J = 1.6$ Hz, 2 H, FcH), 4.18 (s, 5 H, FcH), 3.88 (q, $J = 6.0$ Hz, 2 H, CH_2), 2.96 (t, $J = 6.4$ Hz, 2 H, CH_2), 2.88 (t, $J = 6.0$ Hz, 2 H, CH_2). ^{13}C{^{1}H} NMR ($CDCl_3$): $\delta = 188.1$, 168.2, 161.0, 146.3, 132.4, 130.6, 118.7, 114.3, 79.2, 71.3, 69.7, 68.9, 65.0, 63.2, 41.5, 36.7, 33.9. MS (ESI): an isotopic cluster peaking at $m/z = 526$ (98 %, $[M]^+$). HRMS (ESI): m/z calcd for $C_{25}H_{26}FeO_5S_2$ $[M]^+$: 526.0566; found: 526.0578.

Preparation of Compound 4.9b

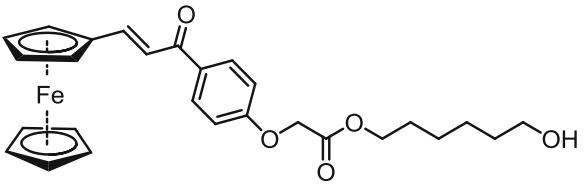

According to the procedure for **4.9a, 4.7** (0.51 g, 1.31 mmol) was treated with 1,6-hexanediol (**4.8b**; 0.31 g, 2.62 mmol), DCC (0.32 g, 1.55 mmol), DMAP (0.05 g, 0.41 mmol), and HOBt (0.21 g, 1.55 mmol) in THF (20 mL) to give the product as a reddish brown oily liquid (0.36 g, 56 % yield). R_f [$CHCl_3$/MeOH (4:1 v/v)] = 0.49. ^{1}H NMR ($CDCl_3$): δ = 7.99 (d, J = 8.8 Hz, 2 H, ArH), 7.74 (d, J = 15.2 Hz, 1 H, CH = CH), 7.12 (d, J = 15.2 Hz, 1 H, CH = CH), 6.98 (d, J = 8.8 Hz, 2 H, ArH), 4.72 (s, 2 H, CH_2), 4.59 (t, J = 1.6 Hz, 2 H, FcH), 4.48 (t, J = 1.6 Hz, 2 H, FcH), 4.22 (t, J = 6.4 Hz, 2 H, CH_2), 4.18 (s, 5 H, FcH), 3.61 (q, J = 6.4 Hz, 2 H, CH_2), 1.64–1.72 (m, 2 H, CH_2), 1.53 (t, J = 6.8 Hz, 2 H, CH_2), 1.34–1.41 (m, 4 H, CH_2). ^{13}C{^{1}H} NMR ($CDCl_3$): δ = 188.2, 168.5, 161.2, 146.3, 132.4, 130.6, 118.8, 114.3, 79.3, 71.3, 69.8, 69.0, 65.5, 65.2, 62.7, 32.6, 28.5, 25.6, 25.3. MS (ESI): an isotopic cluster peaking at m/z = 491 (100 %, $[M + H]^+$). HRMS (ESI): m/z calcd for $C_{27}H_{31}FeO_5$ $[M + H]^+$: 491.1515; found: 491.1507.

Preparation of Compound 4.11a

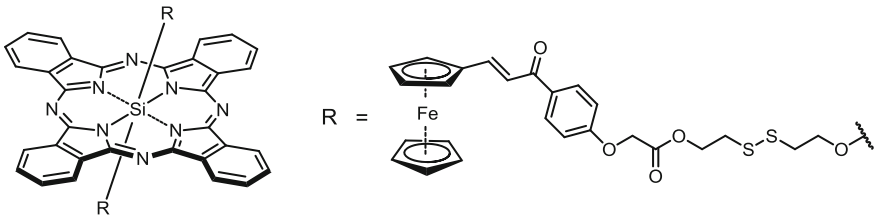

A mixture of silicon(IV) phthalocyanine dichloride (**4.10**; 0.23 g, 0.38 mmol), **4.9a** (0.50 g, 0.95 mmol), and pyridine (1 mL, 12.4 mmol) in toluene (20 mL) was heated under reflux overnight. After evaporating the solvent in vacuo, the residue was chromatographed on a neutral alumina column with $CHCl_3$ as the eluent. The crude product was recrystallized from $CHCl_3$/EtOH to afford the product as a shiny dark blue solid (0.22 g, 37 % yield). ^{1}H NMR ($CDCl_3$): δ = 9.63–9.66 (m, 8 H, Pc-H_α), 8.33–8.36 (m, 8 H, Pc-H_β), 7.92 (d, J = 8.8 Hz, 4 H, ArH), 7.73 (d, J = 15.2 Hz, 2 H, CH = CH), 7.09 (d, J = 15.2 Hz, 2 H, CH = CH), 6.82 (d, J = 8.8 Hz, 4 H, ArH), 4.58 (t, J = 1.6 Hz, 4 H, FcH), 4.48 (t, J = 1.6 Hz, 4 H, FcH), 4.40 (s, 4 H, CH_2), 4.17 (s, 10 H, FcH), 3.58 (t, J = 6.4 Hz, 4 H, CH_2), 1.59 (t, J = 6.4 Hz, 4 H, CH_2), -0.38 (t, J = 6.4 Hz, 4 H, CH_2), -1.77 (t, J = 6.4 Hz, 4 H, CH_2). ^{13}C{^{1}H} NMR ($CDCl_3$): δ = 188.0, 167.7,

160.9, 149.4, 146.1, 135.9, 132.3, 131.0, 130.5, 123.7, 118.8, 114.3, 79.3, 71.3, 69.8, 68.9, 64.7, 62.5, 53.8, 38.8, 35.9. MS (ESI): an isotopic cluster peaking at *m/z* = 1592 (13 %, $[M + H]^+$), 1065 (28 %, $[M\text{-}C_{25}H_{25}O_5S_2Fe]^+$). HRMS (ESI): *m/z* calcd for $C_{82}H_{66}Fe_2N_8O_{10}S_4Si$ $[M]^+$: 1591.2276; found: 1591.2266. Anal. calcd for $C_{82}H_{66}Fe_2N_8O_{10}S_4Si$: C, 61.89; H, 4.18; N, 7.04. Found: C, 62.22; H, 4.26; N, 7.29.

Preparation of Compound 4.11b

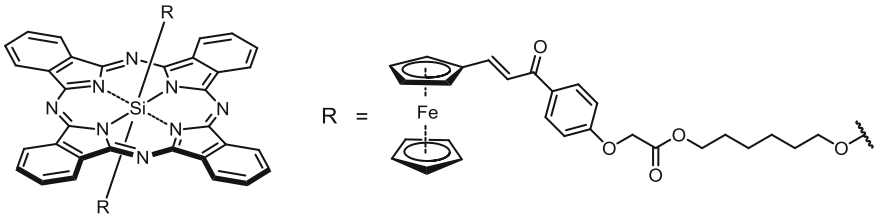

According to procedure **4.11a, 4.10** (0.33 g, 0.54 mmol) was treated with **4.9b** (0.66 g, 1.35 mmol) and pyridine (1 mL, 12.4 mmol) in toluene (20 mL) to give the product as a shiny dark blue solid (0.34 g, 42 % yield). ^{1}H NMR ($CDCl_3$): δ = 9.62–9.64 (m, 8 H, Pc-H_α), 8.32–8.34 (m, 8 H, Pc-H_β), 7.90 (d, J = 8.8 Hz, 4 H, ArH), 7.70 (d, J = 15.2 Hz, 2 H, CH = CH), 7.04 (d, J = 15.2 Hz, 2 H, CH = CH), 6.85 (d, J = 8.8 Hz, 4 H, ArH), 4.55 (s, 4 H, CH_2), 4.47 (s, 4 H, FcH), 4.46 (s, 4 H, FcH), 4.14 (s, 10 H, FcH), 3.51 (t, J = 6.8 Hz, 4 H, CH_2), 0.54 (p, J = 7.2, 4 H, CH_2), -0.48 (p, J = 7.2, 4 H, CH_2), −1.44 (p, J = 7.2, 4 H, CH_2), -1.63 (p, J = 6.8, 4 H, CH_2), -2.10 (t, J = 6.0 Hz, 4 H, CH_2). $^{13}C\{^1H\}$ NMR ($CDCl_3$): δ = 187.9, 168.0, 161.0, 149.2, 146.0, 135.9, 130.8, 130.5, 123.6, 118.7, 114.2, 79.2, 71.2, 70.0, 68.9, 68.4, 65.0, 64.9, 54.3, 28.7, 27.5, 23.6, 23.2. MS (ESI): an isotopic cluster peaking at *m/z* = 1029 (30 %, $[M\text{-}C_{25}H_{25}O_5S_2Fe]^+$). HRMS (ESI): *m/z* calcd for $C_{59}H_{45}FeN_8O_5Si$ $[M\text{-}C_{27}H_{29}FeO_5]^+$: 1029.2626; found: 1029.2611. Anal. calcd for $C_{86}H_{74}Fe_2N_8O_{10}Si$: C, 67.99; H, 4.91; N, 7.37. Found: C, 67.61; H, 4.59; N, 7.16.

Preparation of Compound 4.12

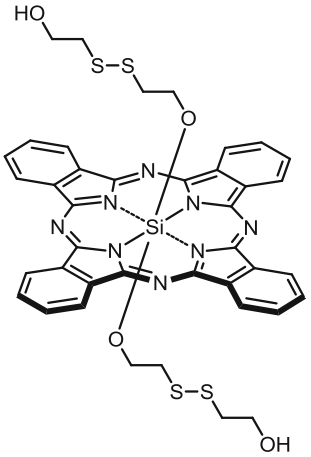

A mixture of **4.10** (0.26 g, 0.43 mmol), **4.8a** (0.33 g, 2.13 mmol), and pyridine (1 mL, 12.4 mmol) in toluene (20 mL) was heated under reflux overnight. The volatiles were evaporated in vacuo. The crude product was purified by silica-gel column chromatography using $CHCl_3$, followed by $CHCl_3$/MeOH (10:1 v/v) as the eluents. The product was obtained as a blue solid (0.25 g, 69 % yield). R_f [$CHCl_3$/MeOH (10:1 v/v)] = 0.24. ^{1}H NMR ($CDCl_3$): δ = 9.65–9.66 (m, 8 H, Pc-H_α), 8.36–8.38 (m, 8 H, Pc-H_β), 2.91 (q, J = 6.0 Hz, 4 H, CH_2), 1.48 (t, J = 6.0 Hz, 4 H, CH_2), -0.34 (t, J = 6.0 Hz, 4 H, CH_2), -1.76 (t, J = 6.0 Hz, 4 H, CH_2). ^{13}C{^{1}H} NMR (DMSO-d_6): δ = 149.3, 135.6, 132.3, 124.1, 60.0, 58.9, 54.6, 43.1. MS (ESI): m/z = 693 (100 %, [M-$C_4H_9O_2S_2$]$^+$). HRMS (ESI): m/z calcd for $C_{36}H_{25}N_8O_2S_2Si$ [M-$C_4H_9O_2S_2$]$^+$: 693.1306; found: 693.1309. Anal. calcd for $C_{40}H_{34}N_8O_4S_4Si$: C, 56.72; H, 4.05; N, 13.22. Found: C, 56.32; H, 3.98; N, 12.92.

7.4.2 Redox-Responsive Fluorescence Emission Studies

Fluorescence measurements were made in different concentrations of dithiothreitol (DTT) in PBS solution. First, the phthalocyanines were dissolved in DMF to give 1 mM solutions, which were diluted to 4 μM with PBS (with 0.5 % Cremophor EL). DTT was dissolved in deionized water to give a 1 M solution. A mixture of the phthalocyanine (4 μM) with DTT (2 μM, 10 mM, or 40 mM) or without DTT in PBS was prepared and stirred continuously at room temperature. Its fluorescence spectra (λ_{ex} = 610 nm, λ_{em} = 630–800 nm) at different time intervals.

7.4.3 Redox-Responsive Singlet Oxygen Generation Studies

For singlet oxygen generation measurements, DPBF was first dissolved in DMF to give a 10 mM solution. A mixture of phthalocyanine (4 μM) with DTT (2 μM, 5 mM, or 10 mM) or without DTT in PBS was stirred continuously at room temperature for 24 h. The above phthalocyanine solutions with or without DTT (3 mL) were mixed with the DPBF solution (10 mM, 21 μL). They were then illuminated with red light coming from a 100 W halogen lamp after passing through a water tank for cooling and a color glass filter (Newport, cut-on at 610 nm). The decay of DPBF at 411 nm was monitored with time.

7.4.4 Photocytotoxicity Assay

All the phthalocyanines were first dissolved in DMF to give 1.6 mM solutions, which were diluted to 80 μM with the culture medium (with 0.5 % Cremophor EL). For compound **4.9a**, it was dissolved in DMF to give a 100 mM solution, which was diluted to 10 mM with the culture medium (with 0.5 % Cremophor EL). They were then further diluted with the culture medium to appropriate concentrations.

DTT was dissolved in deionized water to give a 1 M stock solution. It was then further diluted with the culture medium to give 2 μM and 4 mM DTT solutions. Approximately, 3×10^4 cells per well in the culture medium were inoculated in 96-multiwell plates and incubated overnight at 37 °C in a humidified 5 % CO_2 atmosphere. The cells were rinsed with PBS and incubated with DTT (2 μM or 4 mM) or without DTT (100 μL) for 1 h under the same conditions. The cells, after being rinsed with PBS twice, were incubated with 100 μL of the above drug solutions for 6 h or 24 h at 37 °C under 5 % CO_2. The remaining steps are the same as described in Sect. 7.1.4.

7.4.5 Intracellular Fluorescence Studies

About 6×10^4 MCF-7 cells were seeded on a coverslip and incubated overnight at 37 °C under 5 % CO_2. The cells, after being rinsed with PBS, were incubated with DTT (2 μM or 4 mM) or without DTT (2 mL) for 1 h under the same conditions. The cells were rinsed with PBS twice and further incubated with **4.11a** or **4.11b** in the medium (1 μM, 2 mL) for 24 h under the same conditions. The remaining steps are the same as described in Sect. 7.1.6.

7.4.6 Subcellular Localization Studies

About 6×10^4 MCF-7 cells were seeded on a coverslip and incubated overnight at 37 °C under 5 % CO_2. The cells, after being rinsed with PBS, were incubated with DTT (4 mM, 2 mL) for 1 h under the same conditions. The cells were rinsed with PBS twice and then incubated with **4.11a** in the medium (1 μM, 2 mL) for 24 h under the same conditions. The cells were further treated with LysoTracker, MitoTracker, or ER-Tracker as described in Sect. 7.1.8 before being viewed with a confocal laser scanning microscope.

7.5 Experiments Described in Chapter 5

7.5.1 Synthesis

Preparation of Methyl 3,5-dihydroxybenzoate (5.2) [12]

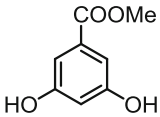

A mixture of 3,5-dihydroxybenzoic acid (**5.1**; 14.76 g, 95.77 mmol), concentrated H_2SO_4, (1.5 mL), and methanol (150 mL) was heated under reflux overnight. After evaporating the excess methanol, the resulting precipitate was washed thoroughly with ice cold water, filtered, and dried. The product was obtained as a white solid (13.22 g, 82 % yield). ^{1}H NMR ($CDCl_3$): $\delta = 7.09$ (s, 2 H, ArH), 6.65 (s, 1H, ArH), 3.88 (s, 3 H, -$COOCH_3$).

Preparation of 3,5-Dihydroxybenzyl Alcohol (5.3) [13]

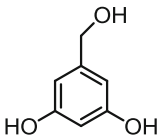

A solution of methyl 3,5-dihydroxybenzoate (**5.2**; 8.43 g, 50.13 mmol) in THF (100 mL) was added dropwise with stirring to a suspension of $LiAlH_4$ (5.71 g, 150.46 mmol) in THF (100 mL) at 0 °C. The reaction mixture was then brought to reflux. After 24 h, ice cold water was added dropwise to quench the reaction. The precipitate was then filtered and the resulting filtrate was neutralized with 7 % HCl to pH = 5. It was then extracted with ethyl acetate (100 mL × 5). The combined organic extracts were dried over anhydrous Na_2SO_4 and concentrated. The crude product was recrystallized from $CHCl_3$/MeOH to afford a white solid (3.72 g, 53 % yield). ^{1}H NMR (DMSO-d_6): $\delta = 9.04$ (s, 2 H, Ph-OH), 6.15 (s, 2 H, ArH),

6.03 (s, 1 H, ArH), 4.97 (t, $J = 5.6$ Hz, 1 H, -CH_2OH), 4.29 (d, $J = 5.6$ Hz, 2 H, -CH_2OH).

Preparation of Compound 5.4

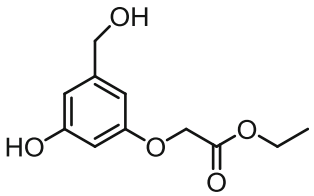

A mixture of 3,5-dihydroxybenzyl alcohol (**5.3**; 2.50 g, 17.84 mmol), ethyl bromoacetate (**4.5**; 2.98 g, 17.84 mmol), and anhydrous K_2CO_3 (2.47 g, 17.87 mmol) in acetone (10 mL) was heated under reflux for 6 h. The volatiles were evaporated under reduced pressure. The residue was redissolved in water, and the pH of the solution was adjusted to 5 with 3 M HCl. The mixture was then evaporated under reduced pressure at 80 °C. The residue was redissolved in THF and filtered to remove the inorganic salt. The crude product was then subject to silica-gel column chromatography using $CHCl_3$ and then $CHCl_3$/EtOH (50:1 v/v) as the eluents to afford the product as a pale yellow oily liquid (1.21 g, 30 % yield). R_f [$CHCl_3$/EtOH (10:1 v/v)] = 0.32. ^{1}H NMR ($CDCl_3$): $\delta = 6.39$ (s, 1 H, ArH), 6.33 (s, 1 H, ArH), 6.25 (s, 1 H, ArH). 4.48 (s, 2 H), 4.43 (s, 2 H), 4.21 (q, $J = 7.2$ Hz, 2 H, -OCH_2CH_3), 3.74 (s, 1 H, Ph-OH), 1.26 (t, $J = 7.2$ Hz, 3 H, -OCH_2CH_3). ^{13}C{^{1}H} NMR ($CDCl_3$): $\delta = 169.6$, 158.9, 157.4, 143.2, 107.6, 105.0, 101.5, 65.1, 64.6, 61.7, 14.0. HRMS (ESI): *m/z* calcd for $C_{11}H_{14}NaO_5$ $[M + Na]^+$: 249.0733; found: 249.0741.

Preparation of Toluene-4-sulfonic Acid 2-[2-(2-Methoxy-ethoxy)ethoxy]ethyl Ester (5.5) [14]

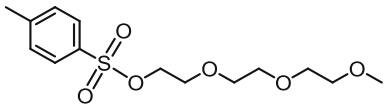

A mixture of triethylene glycol monomethyl ether (5.45 g, 33.19 mmol), tosyl chloride (6.96 g, 36.51 mmol), and pyridine (3 mL, 37.09 mmol) in CH_2Cl_2 (50 mL) was stirred at room temperature under an inert atmosphere for 24 h. The solution was successively washed with 1 M HCl (100 mL × 1), $NaHCO_3$ (100 mL × 1), and water (100 mL × 3). The organic layer was dried over anhydrous Na_2SO_4 and concentrated. The residue was subject to silica-gel column chromatography using $CHCl_3$ as the eluent. The product was obtained as a colorless oil (8.65 g, 82 % yield). R_f [$CHCl_3$/EtOH (50:1 v/v)] = 0.44. ^{1}H NMR ($CDCl_3$): $\delta = 7.80$ (d, $J = 8.0$ Hz, 2 H, ArH), 7.34 (d, $J = 8.0$ Hz, 2 H, ArH),

4.16 (t, $J = 4.8$ Hz, 2 H), 3.68 (t, $J = 4.8$ Hz, 2 H), 3.59–3.63 (m, 6 H), 3.52–3.54 (m, 2 H), 3.37 (s, 3 H, -OCH_3), 2.45 (s, 3 H, CH_3).

Preparation of Compound 5.6

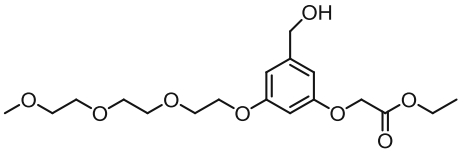

A mixture of compound **5.4** (0.80 g, 3.54 mmol), toluene-4-sulfonic acid 2-[2-(2-methoxy-ethoxy)ethoxy]ethyl ester (**5.5**; 1.24 g, 3.89 mmol), and anhydrous K_2CO_3 (1.47 g, 10.64 mmol) in acetone (20 mL) was heated under reflux overnight. The reaction mixture was then cooled to room temperature and filtered. The crude product was subject to silica-gel column chromatography using $CHCl_3$ and then $CHCl_3$/EtOH (50:1 v/v) as the eluents to afford the product as a colorless oily liquid (1.03 g, 78 % yield). R_f [$CHCl_3$/EtOH (50:1 v/v)] = 0.29. ^{1}H NMR ($CDCl_3$): $\delta = 6.58$ (s, 1 H, ArH), 6.51 (s, 1 H, ArH), 6.42 (s, 1 H, ArH). 4.61 (d, $J = 6.0$ Hz, 2 H, -CH_2OH), 4.59 (s, 2 H, -OCH_2COO-), 4.26 (q, $J = 7.2$ Hz, -OCH_2CH$_3$), 4.11 (t, $J = 4.8$ Hz, 2 H), 3.83 (t, $J = 4.8$ Hz, 2 H), 3.71–3.73 (m, 2 H), 3.63–3.68 (m, 4 H), 3.54 (t, $J = 4.4$ Hz, 2 H), 3.37 (s, 3 H, -OCH_3), 1.30 (t, $J = 7.2$ Hz, 3 H, -OCH_2CH_3). ^{13}C{^{1}H} NMR ($CDCl_3$): $\delta = 168.8$, 160.2, 159.1, 143.6, 106.3, 105.2, 101.1, 71.9, 70.8, 70.7, 70.5, 69.7, 67.6, 65.4, 65.1, 61.4, 59.0, 14.1. HRMS (ESI): *m/z* calcd for $C_{18}H_{28}NaO_8$ $[M + Na]^+$: 395.1676; found: 395.1676.

Preparation of Compound 5.7

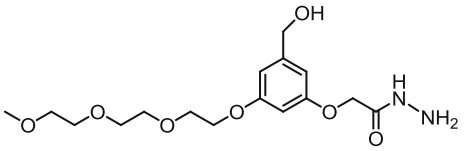

A mixture of hydrazine hydrate (80 %; 2 mL) and **5.6** (0.41 g, 1.10 mmol) in ethanol (2 mL) was stirred at room temperature for 30 min. The reaction mixture was then evaporated under reduced pressure at 60 °C. The product was obtained as a colorless oily liquid (0.34 g, 86 % yield). ^{1}H NMR ($CDCl_3$): $\delta = 7.90$ (br s, 1 H, -CON*H*NH_2), 6.57 (s, 1 H, ArH), 6.49 (s, 1 H, ArH), 6.35 (s, 1 H, ArH). 4.59 (s, 2 H), 4.48 (s, 2 H), 4.08 (t, $J = 4.4$ Hz, 2 H), 3.82 (t, $J = 4.4$ Hz, 2 H), 3.70–3.71 (m, 2 H), 3.62–3.67 (m, 4 H), 3.53 (t, $J = 4.0$ Hz, 2 H), 3.36 (s, 3 H, -OCH_3). ^{13}C{^{1}H} NMR ($CDCl_3$): $\delta = 168.4$, 160.2, 158.2, 144.1, 106.3, 105.1, 100.8, 71.8, 70.7, 70.6, 70.5, 69.6, 67.5, 66.8, 64.7, 59.0. HRMS (ESI): *m/z* calcd for $C_{16}H_{27}N_2O_7$ $[M + H]^+$: 359.1813; found: 359.1813.

Preparation of Ferrocenylcarbonylhydrazone 5.8

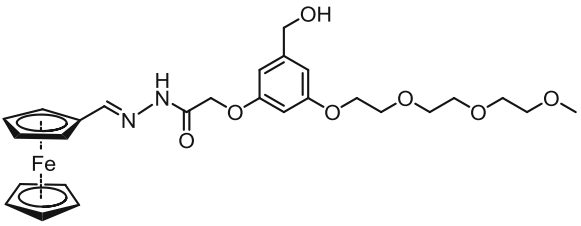

A mixture of ferrocenecarboxyaldehyde (**4.2**; 0.32 g, 1.50 mmol) and **5.7** (0.45 g, 1.26 mmol) in ethanol (10 mL) was heated under reflux for 2 h. The volatiles were evaporated under reduced pressure. The crude product was subject to silica-gel column chromatography using $CHCl_3$ and then $CHCl_3$/MeOH (50:1 v/v) as the eluents to afford an orange oily liquid (0.45 g, 64 % yield). R_f [$CHCl_3$/MeOH (10:1 v/v)] = 0.29. ^{1}H NMR ($CDCl_3$): δ = 9.27 (s, 1 H, -CON*H*N = CH-), 8.12 (s, 1 H, -CONHN = C*H*-), 6.63 (s, 1 H, ArH), 6.59 (s, 1 H, ArH), 6.46 (s, 1 H, ArH), 4.70 (s, 2 H, FcH), 4.65 (d, J = 5.6 Hz, 2 H, Ph-CH_2OH), 4.59 (s, 2 H, -OCH_2COO-), 4.42 (s, 2 H, FcH), 4.21 (s, 5 H, FcH), 4.13 (t, J = 4.8 Hz, 2 H), 3.85 (t, J = 4.8 Hz, 2 H), 3.73–3.74 (m, 2 H), 3.64–3.69 (m, 4 H), 3.54–3.56 (m, 2 H), 3.38 (s, 3 H, -OCH_3). ^{13}C{^{1}H} NMR ($CDCl_3$): δ = 163.8, 160.2, 158.2, 151.4, 144.3, 106.5, 105.3, 101.0, 77.9, 71.9, 70.7, 70.6, 70.4, 69.6, 69.3, 69.2, 68.3, 67.7, 67.6, 64.7, 58.9. HRMS (ESI): *m/z* calcd for $C_{27}H_{35}N_2O_7Fe$ $[M + H]^+$: 555.1788; found: 555.1784.

Preparation of Phthalocyanine 5.9

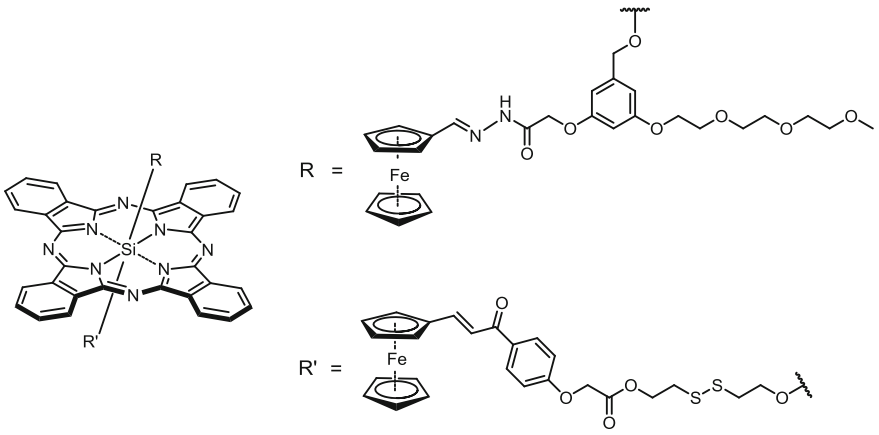

A mixture of silicon phthalocyanine dichloride (**4.10**; 0.12 g, 0.20 mmol), **4.9a** (0.13 g, 0.25 mmol), and pyridine (1 mL, 12.36 mmol) in toluene (10 mL) was heated under reflux for 2 h. To this reaction mixture, a solution of

ferrocenylcarbonylhydrazone **5.8** (0.13 g, 0.23 mmol) and pyridine (0.5 mL, 6.18 mmol) in toluene (10 mL) was added and the mixture was kept stirring under reflux for another 4 h. After evaporating the volatiles in vacuo, the crude product was filtered through a bed of Celite to remove the insoluble black solid. It was then subject to silica-gel column chromatography using $CHCl_3$ and then $CHCl_3$/MeOH (50:1 v/v) as the eluents. The two greenish-blue bands were collected separately and evaporated. The residues were recrystallized from $CHCl_3$/hexane to afford **5.9** (0.048 g, 15 % yield) and **5.10** (0.14 g, 43 % yield), both as a blue solid. R_f [$CHCl_3$/MeOH (10:1 v/v)] = 0.52 for **5.9** and 0.44 for **5.10**. ^{1}H NMR ($CDCl_3$): δ = 9.61–9.63 (m, 8 H, Pc-H$_\alpha$), 8.74 (s, 1 H, -CON*H*-), 8.33–8.35 (m, 8 H, Pc-H$_\beta$), 8.00 (s, 1 H, -N = C*H*Fc), 7.91 (d, J = 8.8 Hz, 2 H, ArH), 7.73 (d, J = 15.2 Hz, 1 H, CH = CH), 7.08 (d, J = 15.6 Hz, 1 H, CH = CH), 6.81 (d, J = 8.8 Hz, 2 H, ArH), 5.64 (s, 1 H, ArH), 4.73 (s, 2 H, FcH), 4.58 (s, 2 H, FcH), 4.47 (s, 2 H, FcH), 4.45 (s, 2 H, FcH), 4.39 (s, 2 H, -COOCH_2CO-), 4.22 (s, 5 H, FcH), 4.16 (s, 5 H, FcH), 3.83 (s, 2 H, -OCH_2CONH-), 3.61–3.62 (m, 4 H), 3.56–3.59 (m, 4 H), 3.52–3.54 (m, 2 H), 3.43–3.46 (m, 4 H), 3.36 (s, 3 H, -OCH$_3$), 3.09 (t, 2 H, J = 4.8 Hz, ArH), −0.38 (t, J = 6.0 Hz, 2 H, Pc-OCH$_2$CH_2SS-), -0.70 (s, 2 H, Pc-OCH_2Ph-), -1.77 (t, J = 6.0 Hz, 2 H, Pc-OCH_2CH$_2$SS-). ^{13}C{^{1}H} NMR ($CDCl_3$): δ = 187.3, 167.3, 163.5, 159.7, 157.8, 156.1, 150.4, 149.4, 146.1, 141.7, 135.9, 133.5, 131.1, 130.5, 123.7, 118.8, 114.3, 102.2, 100.2, 79.3, 71.9, 71.3, 70.8, 70.7, 70.6, 70.5, 69.8, 69.3, 69.0, 68.4, 66.6, 66.5, 64.7, 62.5, 59.1, 53.8, 38.7, 35.8. HRMS (ESI): *m/z* calcd for $C_{84}H_{75}Fe_2N_{10}O_{12}S_2Si$ $[M + H]^+$: 1620.3504; found: 1620.3507.

Preparation of Phthalocyanine 5.10

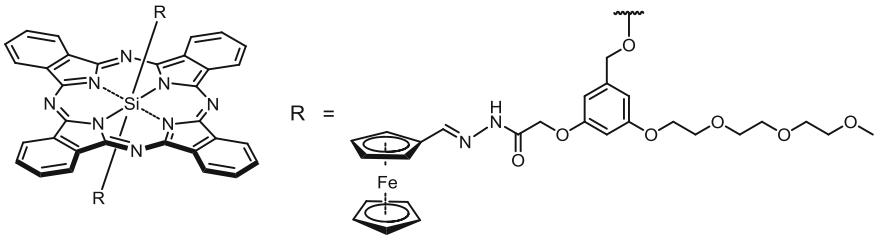

A mixture of **4.10** (0.063 g, 0.10 mmol), ferrocenylcarbonylhydrazone **5.8** (0.12 g, 0.22 mmol), and pyridine (1 mL, 12.36 mmol) in toluene (15 mL) was heated under reflux for 6 h. The volatiles were evaporated in vacuo. The crude product was filtered through a bed of Celite to remove the insoluble black solid. It was then subject to silica-gel column chromatography using $CHCl_3$ and then $CHCl_3$/MeOH (10:1 v/v) as the eluents. The residue was further purified by gel permeation chromatography using THF as the eluent. It was chromatographed again on silica-gel using $CHCl_3$ and then $CHCl_3$/MeOH (10:1 v/v) as the eluents. The residue was finally recrystallized from $CHCl_3$/hexane to afford the product as

a blue solid (0.13 g, 79 % yield). R_f [$CHCl_3$/MeOH (10:1 v/v)] = 0.43. ^{1}H NMR ($CDCl_3$): δ = 9.59–9.61 (m, 8 H, Pc-H$_\alpha$), 8.75 (s, 2 H, -CON*H*-), 8.33–8.35 (m, 8 H, Pc-H$_\beta$), 7.97 (s, 2 H, -N = C*H*Fc), 5.64 (s, 2 H, ArH), 4.72 (s, 4 H, FcH), 4.44 (s, 4 H, FcH), 4.21 (s, 10 H, FcH), 3.81 (s, 4 H, -OCH_2CONH-), 3.58–3.61 (m, 14 H), 3.52–3.53 (m, 4 H), 3.42–3.45 (m, 6 H), 3.36 (s, 6 H, -OCH_3), 3.06 (m, 4 H, ArH), −0.70 (s, 4 H, Pc-OCH_2-). ^{13}C{^{1}H} NMR ($CDCl_3$): δ = 163.2, 158.4, 156.2, 150.8, 149.4 (Pc), 142.1, 135.9 (Pc), 131.1 (Pc), 130.9, 123.6 (Pc), 102.2, 99.5, 71.9, 70.7, 70.6 (two overlapping signals), 70.5, 69.3, 68.3, 66.5, 66.2, 59.0, 58.1. HRMS (ESI): *m*/*z* calcd for $C_{86}H_{83}Fe_2N_{12}O_{14}Si$ $[M + H]^+$: 1648.4643; found: 1648.4640.

7.5.2 pH- and Redox-Responsive Fluorescence Emission Studies

First, all the phthalocyanines were dissolved in DMF to give 1 mM solutions, which were diluted to 4 μM with PBS at appropriate pH (with 0.5 % Cremophor EL). DTT was dissolved in deionized water to give a 1 M solution. To study the effect of DTT on the fluorescence intensity, a mixture of the phthalocyanine (4 μM) with DTT (2 μM, 10 mM, or 40 mM) or without DTT in PBS at pH 7.4 was prepared. To examine the effect of pH on the fluorescence intensity, the study was started readily after the phthalocyanine solution (1 mM in DMF) was diluted to 4 μM with PBS at different pH (4.5, 6.0, or 7.4). To study the effect of pH and DTT on the fluorescence intensity, a mixture of the phthalocyanine (4 μM) with DTT (2 μM or 10 mM) or without DTT in PBS at pH 6.0 or 7.4 was prepared. All these solutions were stirred continuously at room temperature during the kinetic study and the fluorescence spectra (λ_{ex} = 610 nm, λ_{em} = 630–800 nm) were recorded at different time intervals.

7.5.3 pH- and Redox-Responsive Singlet Oxygen Generation Studies

DPBF was dissolved in DMF to give a 10 mM solution. To study the effect of DTT on the singlet oxygen generation efficiency, a mixture of phthalocyanine (4 μM) with DTT (2 μM or 10 mM) in PBS at pH 7.4 was prepared. To examine the effect of pH, the study was carried out after the phthalocyanine solution (1 mM in DMF) was diluted to 4 μM with PBS at different pH (4.5, 6.0, or 7.4). To study the effect of pH and DTT, a mixture of the phthalocyanine (4 μM) with DTT (2 μM or 10 mM) in PBS at pH 6.0 or 7.4 was prepared. The above phthalocyanine solutions were stirred continuously at room temperature for 8 h. These solutions (3 mL) were mixed with DPBF solution (10 mM, 21 μL), followed by illumination with

red light coming from a 100 W halogen lamp after passing through a water tank for cooling and a color glass filter (Newport, cut-on at 610 nm). The decay of DPBF at 411 nm was monitored with time.

7.5.4 Intracellular Fluorescence Studies

About 6×10^4 MCF-7 cells were seeded on a coverslip and incubated overnight at 37 °C under 5 % CO_2. The medium was removed and rinsed with PBS. For **5.9**, the cells were first incubated with DTT (2 μM or 4 mM) or without DTT (2 mL) for 1 h under the same conditions. The cells were rinsed with PBS and then incubated with nigericin (Sigma) in PBS (25 μM, 2 mL) at different pH (5.0 or 7.4) for 30 min under the same conditions. The cells were then rinsed with PBS and incubated with a solution of **5.9** in the medium (1 μM, 2 mL) for 1 h under the same conditions. For **5.10**, the cells were incubated with nigericin in PBS (25 μM, 2 mL) at different pH (5.0, 6.0, or 7.4) for 30 min. They were then rinsed with PBS, followed by incubation with a solution of **5.10** in the medium (1 μM, 2 mL) for 1 h. The remaining steps are the same as described in Sect. 7.1.6.

References

1. Eaton, D.F.: Pure Appl. Chem. **60**, 1107 (1988)
2. Scalise, I., Durantini, E.N.: Bioorg. Med. Chem. **13**, 3037 (2005)
3. Maree, M.D., Kuznetsova, N., Nyokong, T.: J. Photochem. Photobiol., A **140**, 117 (2001)
4. MTT = 3-(4,5-dimethyl-2-thiazolyl)-2,5-diphenyl-2*H*-tetrazolium bromide. Tada H, Shiho O, Kuroshima K, Koyama M, Tsukamoto K (1986) J Immunol Methods **93**, 157
5. Richard, A., Bourel-Bonnet, L.: Chem. Eur. J. **11**, 7315 (2005)
6. Loiseau, F.A., Hill, A.M., Hii, K.K.: Tetrahedron **63**, 9947 (2007)
7. Wyrick, S.D., Chaney, S.G.J.: Labelled Compd. Radiopharm. **25**, 349 (1988)
8. Erdem, S.S., Nesterova, I.V., Soper, S.A., Hammer, R.P.J.: Org. Chem. **73**, 5003 (2008)
9. Kaur, N., Delcros, J.G., Martin, B., Phanstiel, O.J.: Med. Chem. **48**, 3832 (2005)
10. Sato, M., Kono, H., Shiga, M., Motoyama, I., Hata, K.: Bull. Chem. Soc. Jpn. **41**, 252 (1968)
11. Zsoldos-Mády, V., Csámpai, A., Szabó, R., Mészáros-Alapi, E., Pásztor, J., Hudecz, F., Sohár, P.: Chem. Med. Chem. **1**, 1119 (2006)
12. Sivakumar, S., Reddy, M.L.P., Cowley, A.H., Butorac, R.R.: Inorg. Chem. **50**, 4882 (2011)
13. Loim, N.M., Kelbyscheva, E.S.: Russ. Chem. Bull. **53**, 2080 (2004)
14. Pawar, G.M., Bantu, B., Weckesse, J., Blechert, S., Wurst, K., Buchmeiser, M.R.: Dalton Trans. **41**, 9043 (2009)

Appendices
^{1}H and $^{13}C\{^{1}H\}$ NMR Spectra

J. T. F. Lau, *Towards Dual and Targeted Cancer Therapy with Novel Phthalocyanine-based Photosensitizers*, Springer Theses,
DOI: 10.1007/978-3-319-00708-3, © Springer International Publishing Switzerland 2013

Appendix 1

^{1}H and $^{13}C\{^{1}H\}$ NMR spectra of compound **2.5** in $CDCl_3$

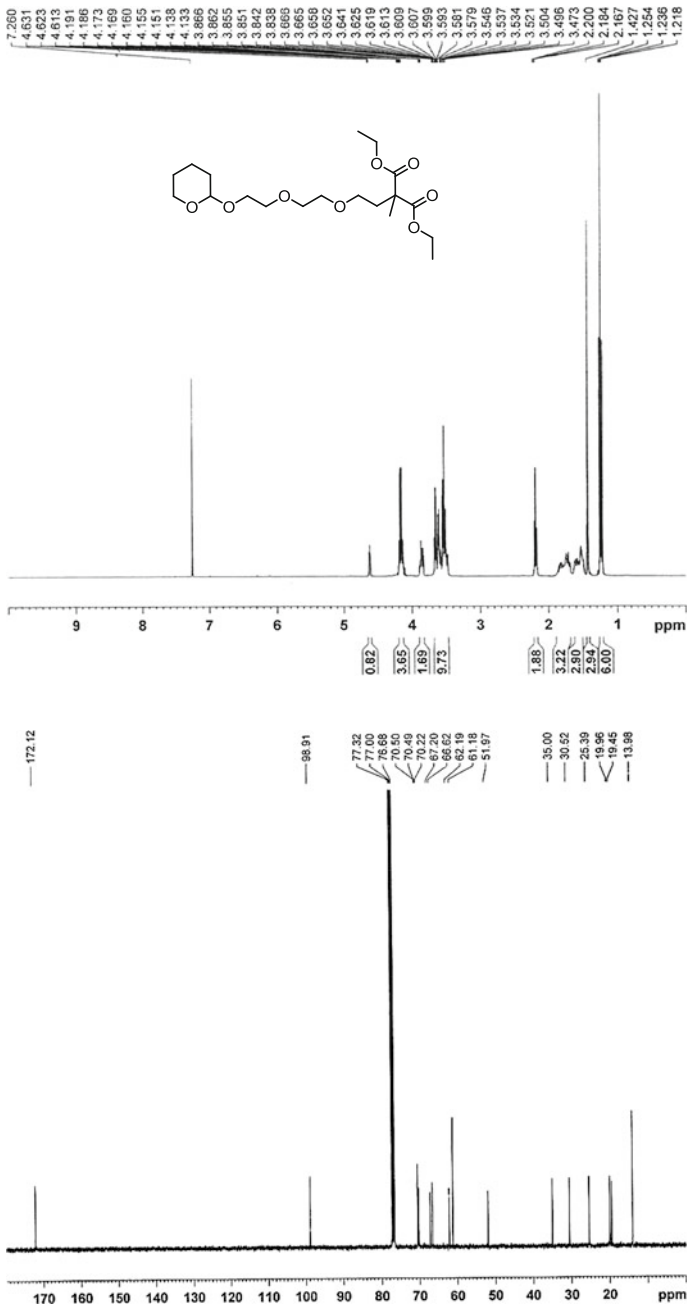

Appendix 2

^{1}H and $^{13}C\{^{1}H\}$ NMR spectra of compound **2.6** in $CDCl_3$

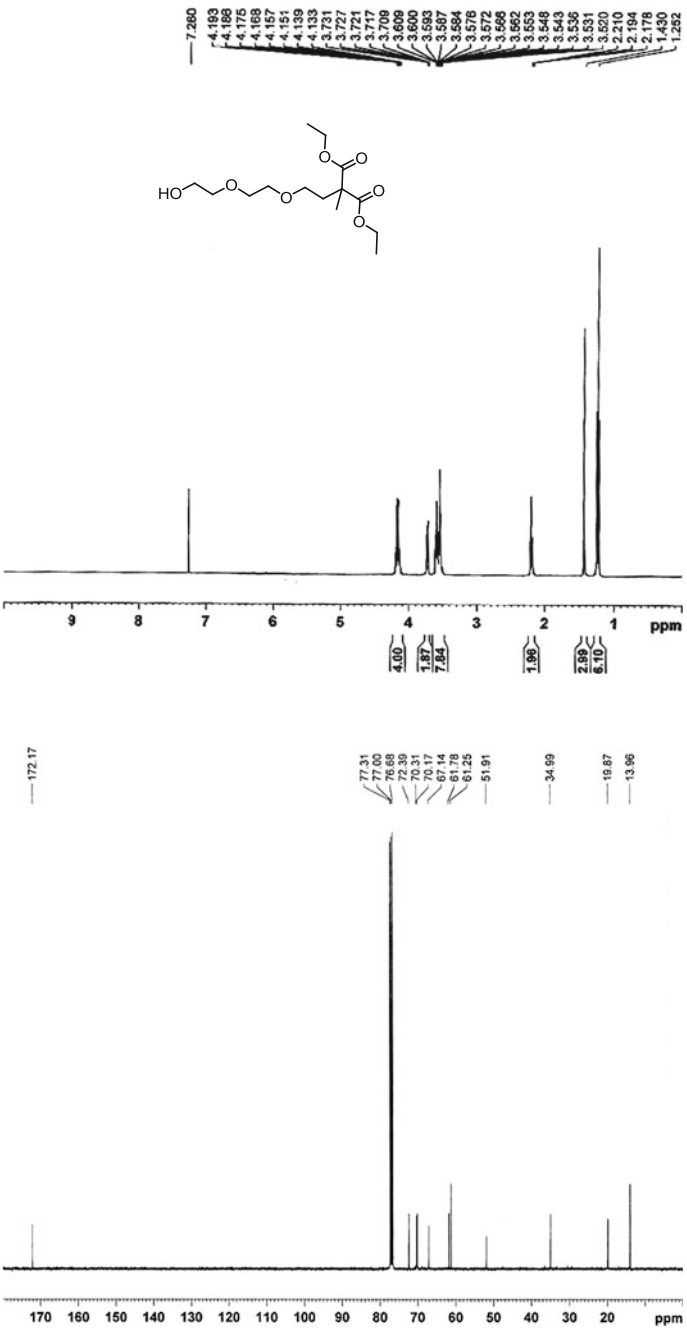

Appendix 3

^{1}H and $^{13}C\{^{1}H\}$ NMR spectra of compound **2.7** in $CDCl_3$

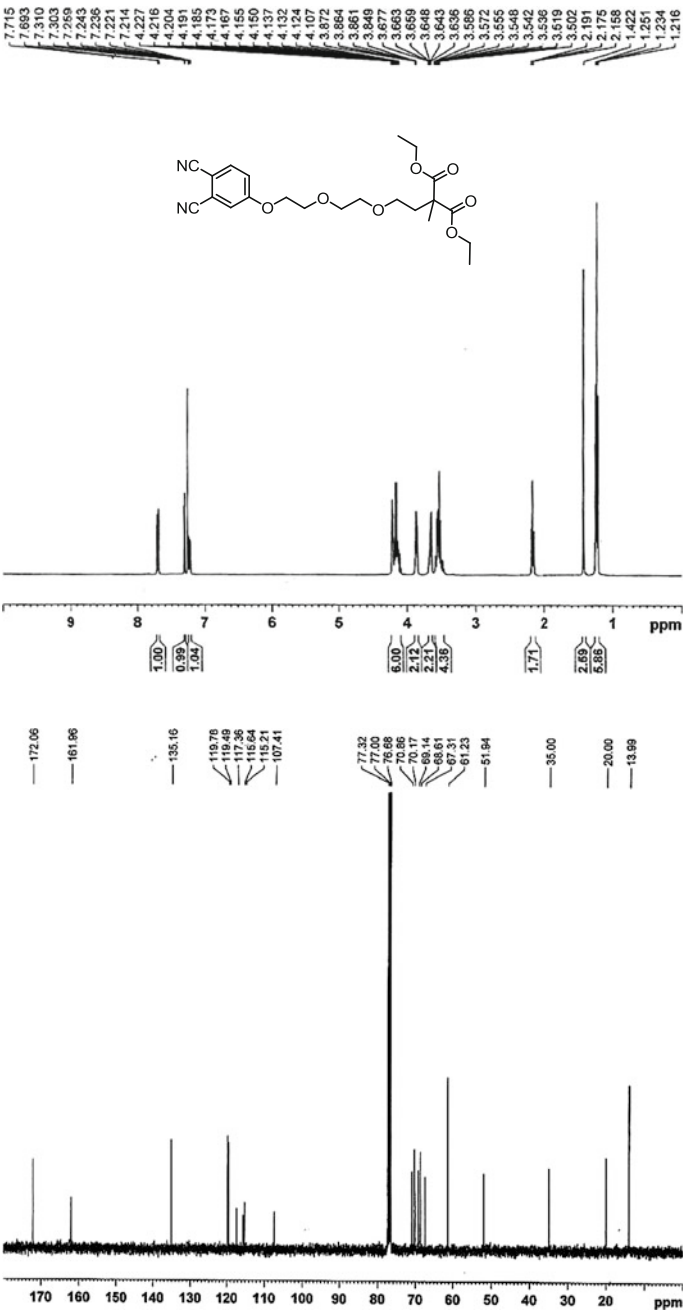

Appendix 4

^{1}H and $^{13}C\{^{1}H\}$ NMR spectra of compound **2.8** in $CDCl_3$ with a trace amount of pyridine-d_5

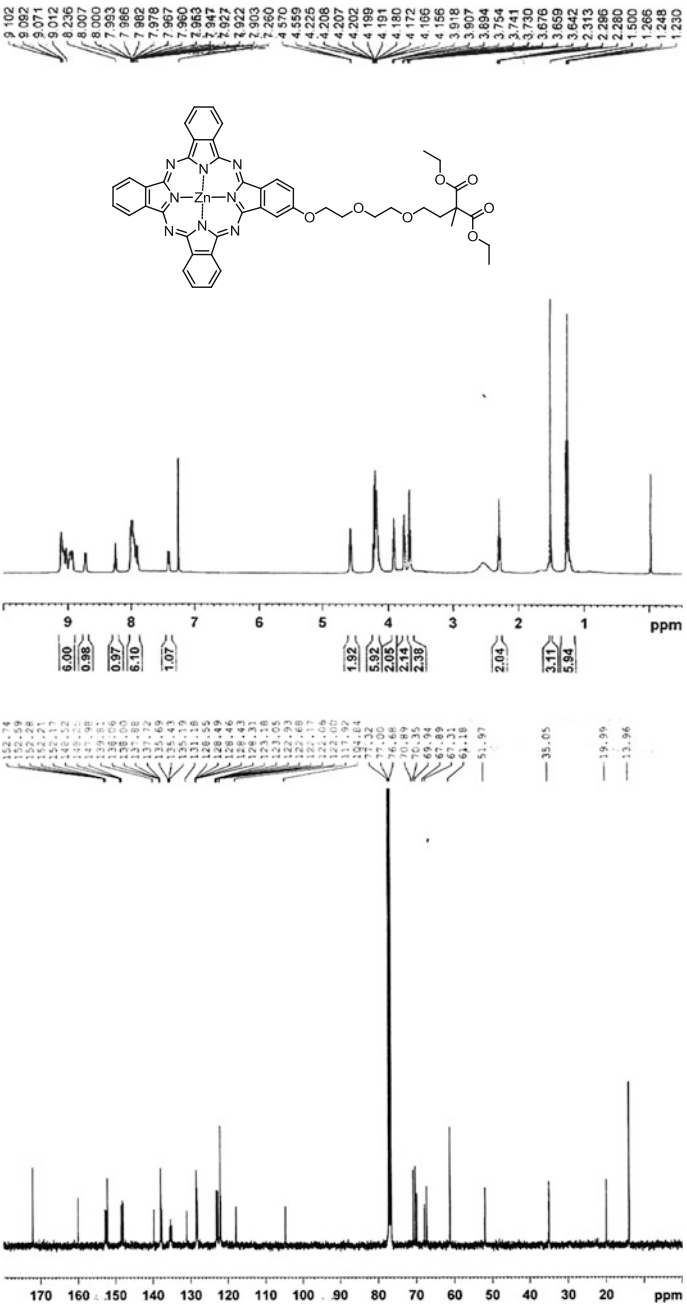

Appendix 5

^{1}H and $^{13}C\{^{1}H\}$ NMR spectra of compound **2.9** in DMSO-d_6 with a trace amount of pyridine-d_5

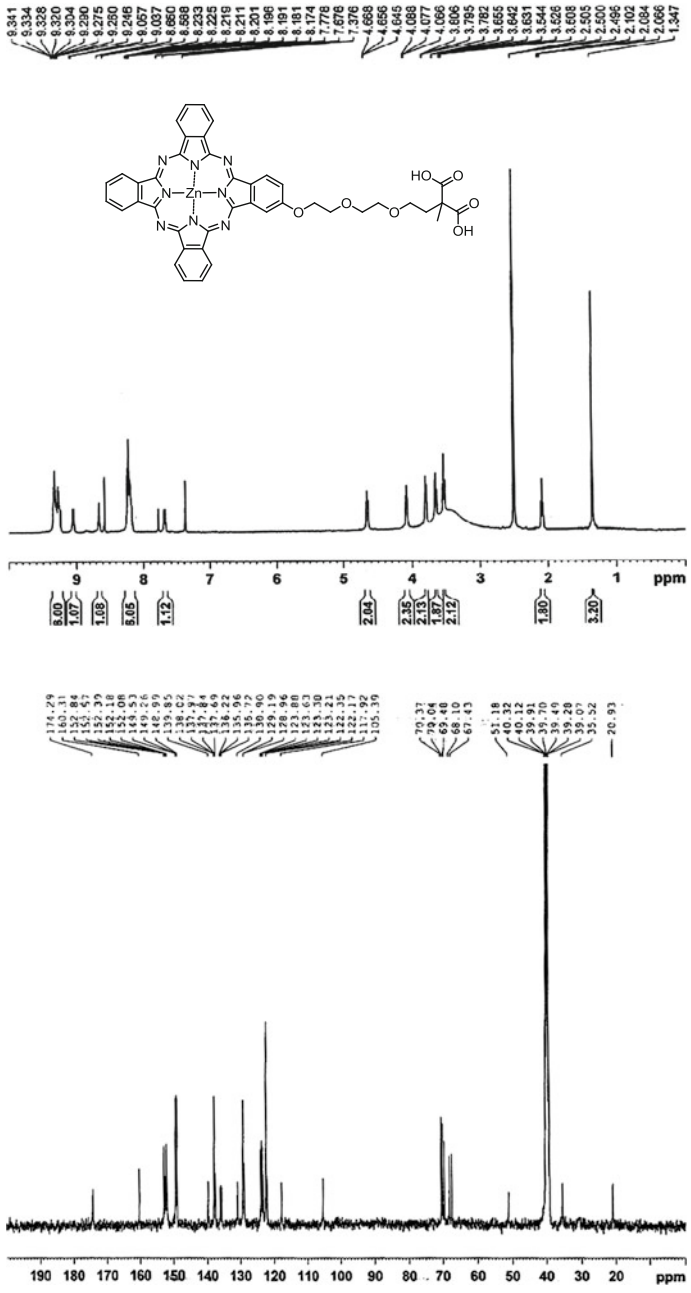

Appendix 6

^{1}H NMR spectrum of compound **2.11** in DMSO-d_6 with a trace amount of pyridine-d_5

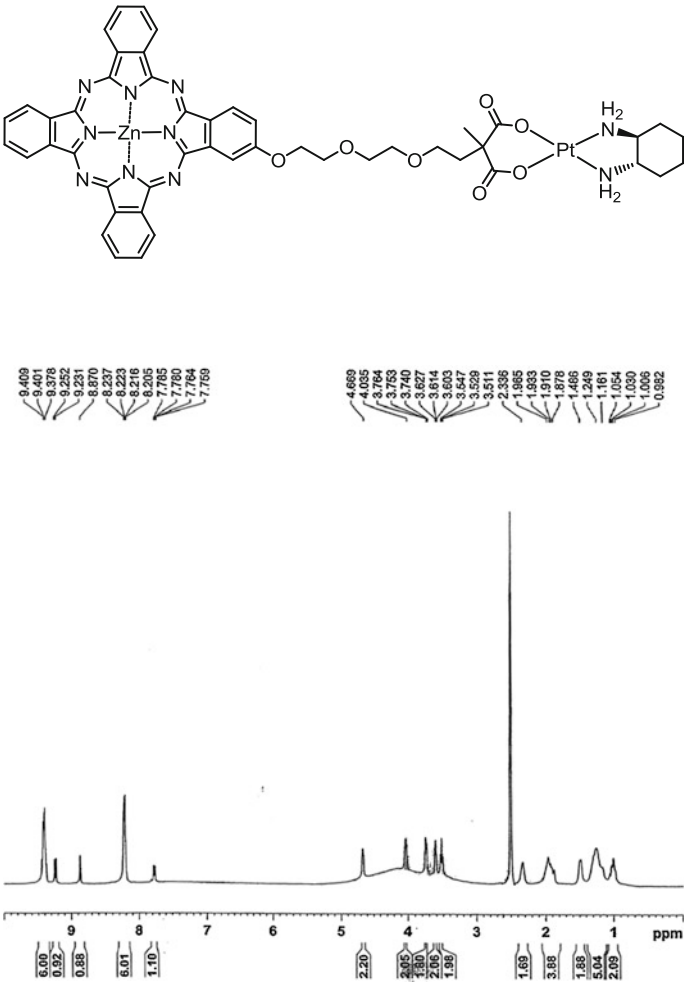

Appendix 7

^{1}H and $^{13}C\{^{1}H\}$ NMR spectra of compound **2.14** in $CDCl_3$ with a trace amount of pyridine-d_5

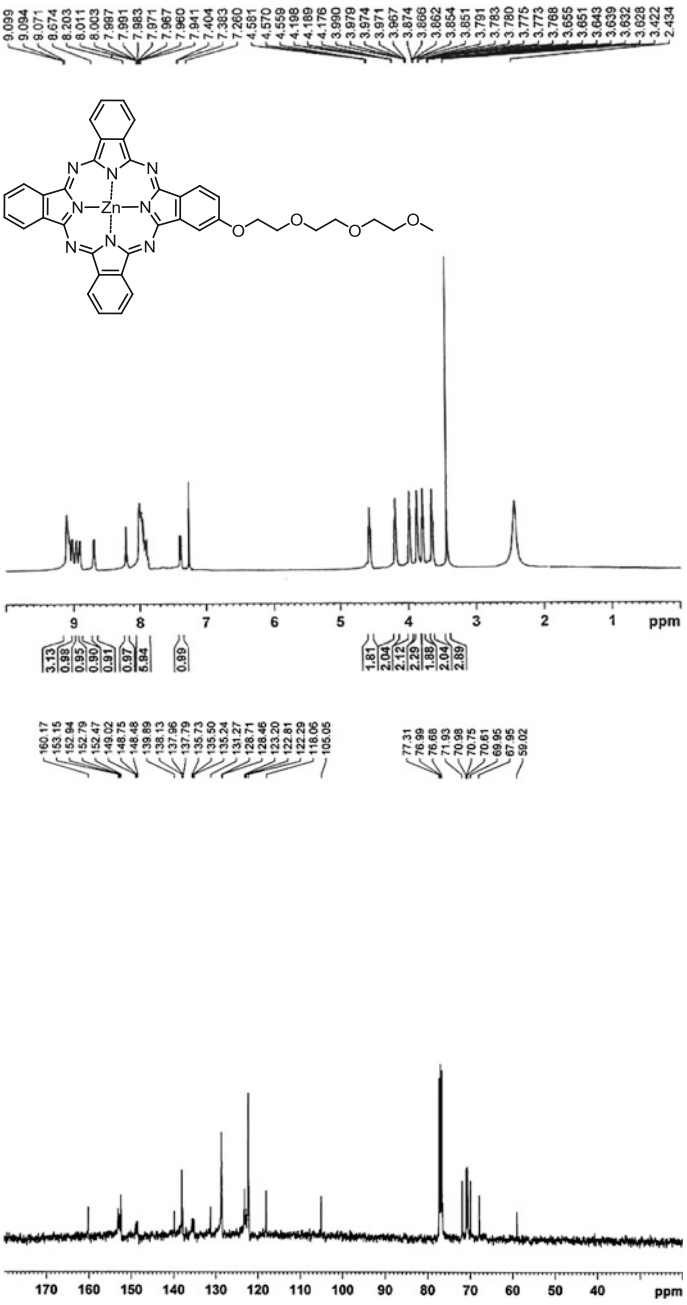

Appendix 8

^{1}H and $^{13}C\{^{1}H\}$ NMR spectra of compound **3.8a** in $CDCl_3$

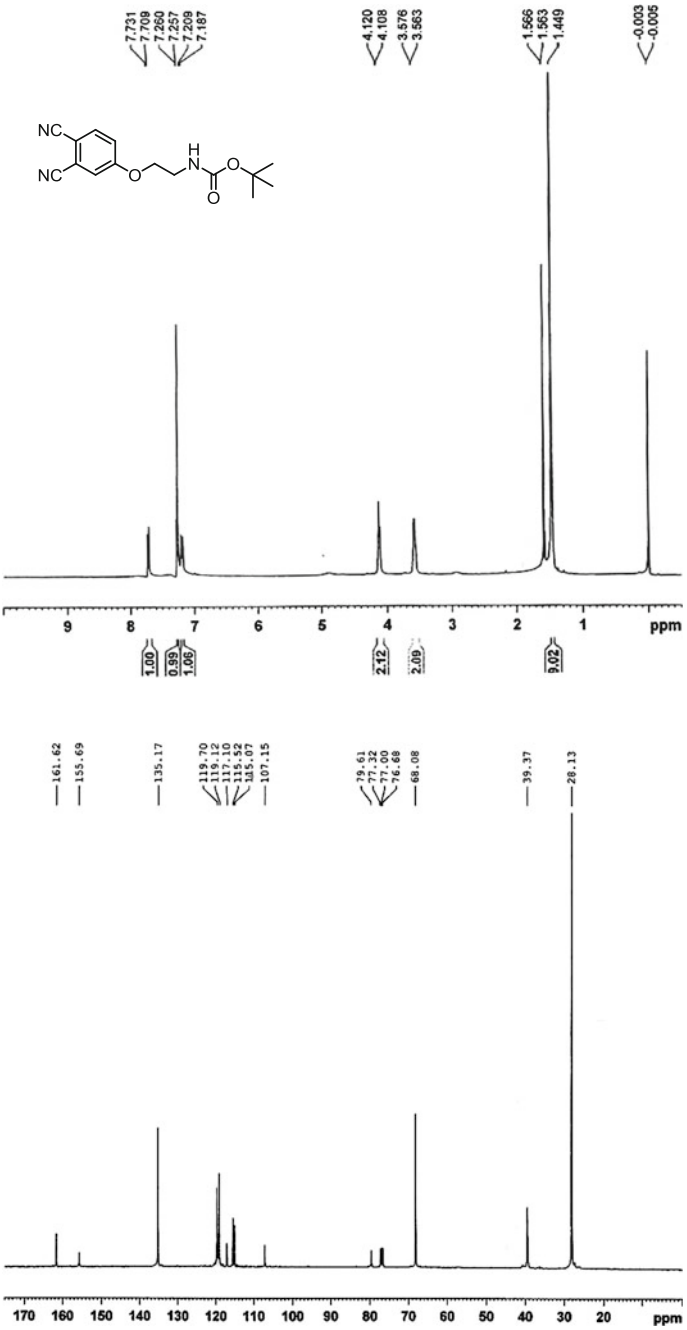

Appendix 9

^{1}H and $^{13}C\{^{1}H\}$ NMR spectra of compound **3.8b** in acetone-d_6

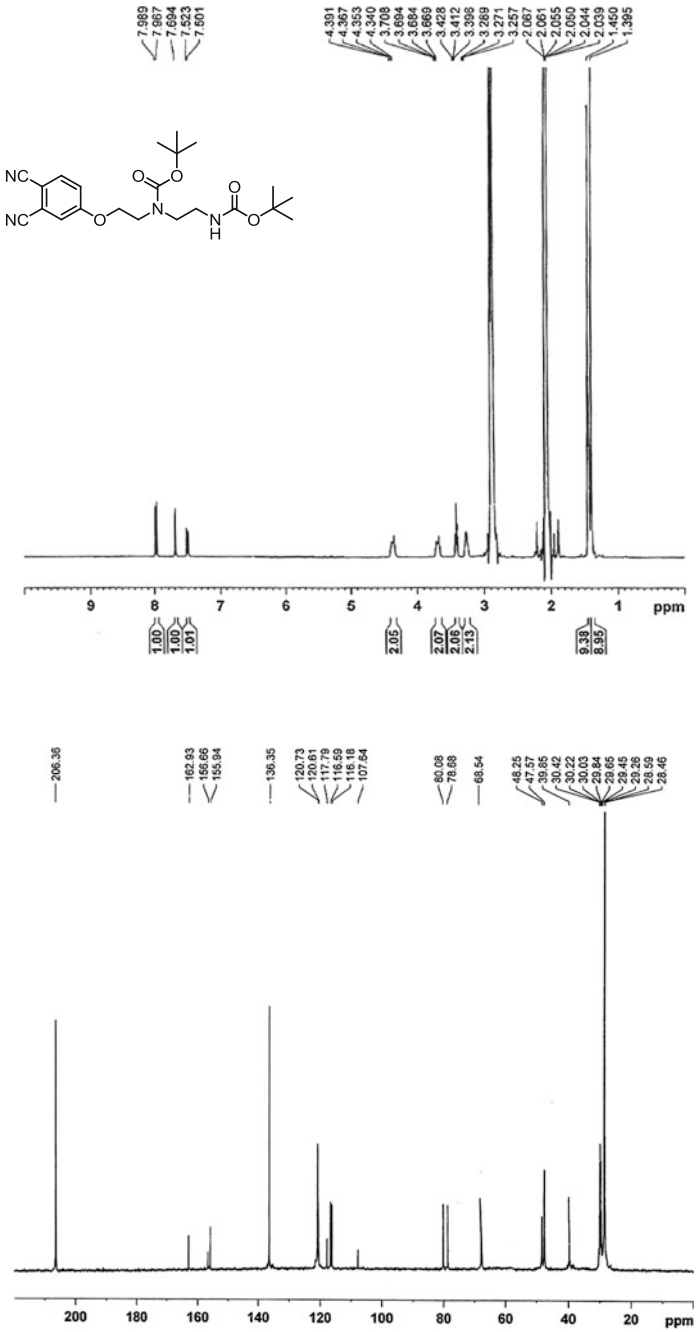

Appendix 10

^{1}H and $^{13}C\{^{1}H\}$ NMR spectra of compound **3.8c** in $CDCl_3$

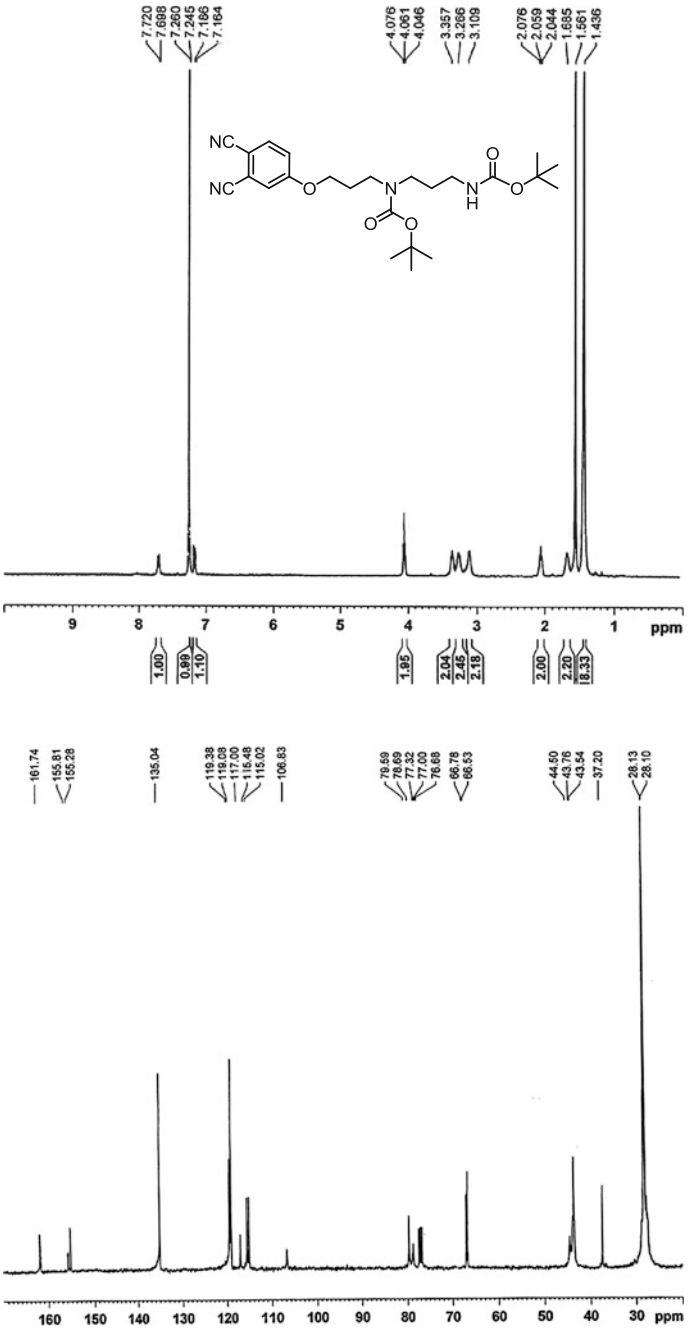

Appendix 11
^{1}H and $^{13}C\{^{1}H\}$ NMR spectra of compound **3.8d** in $CDCl_3$

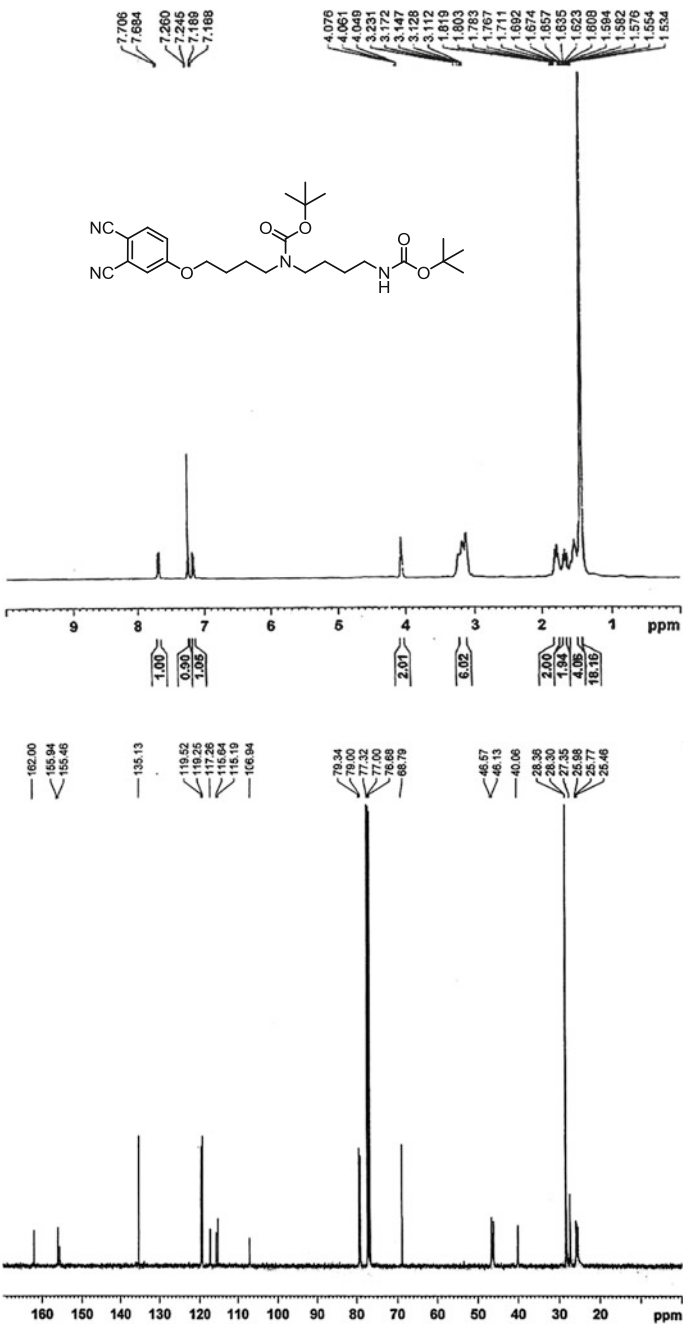

Appendix 12

^{1}H and $^{13}C\{^{1}H\}$ NMR spectra of compound **3.9a** in $CDCl_3$ with a trace amount of pyridine-d_5

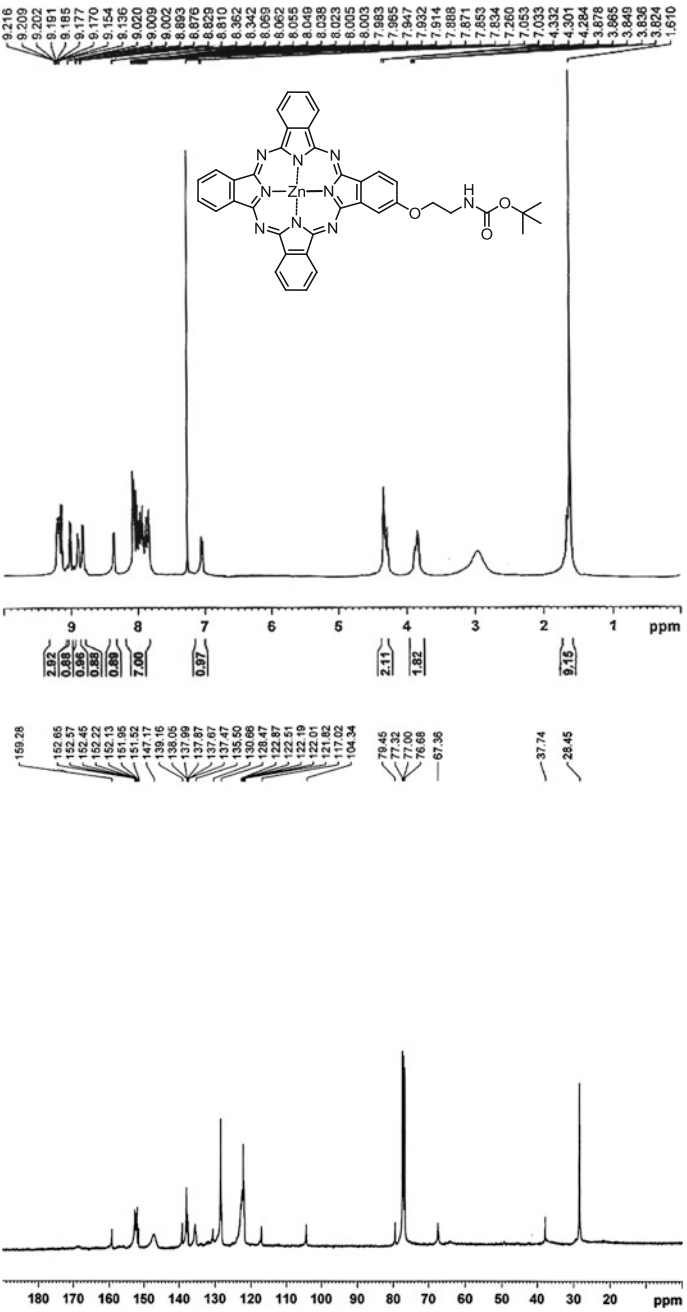

Appendix 13

^{1}H and $^{13}C\{^{1}H\}$ NMR spectra of compound **3.9b** in $CDCl_3$ with a trace amount of pyridine-d_5

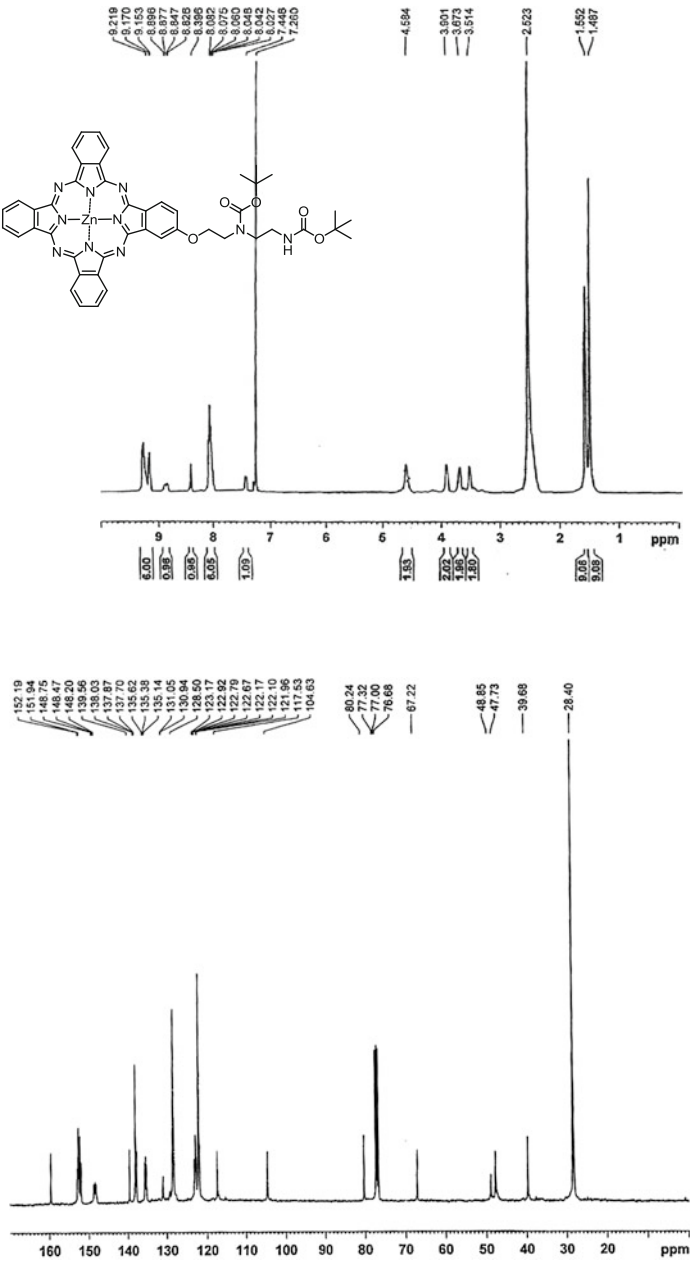

Appendix 14

^{1}H and $^{13}C\{^{1}H\}$ NMR spectra of compound **3.9c** in $CDCl_3$ with a trace amount of pyridine-d_5

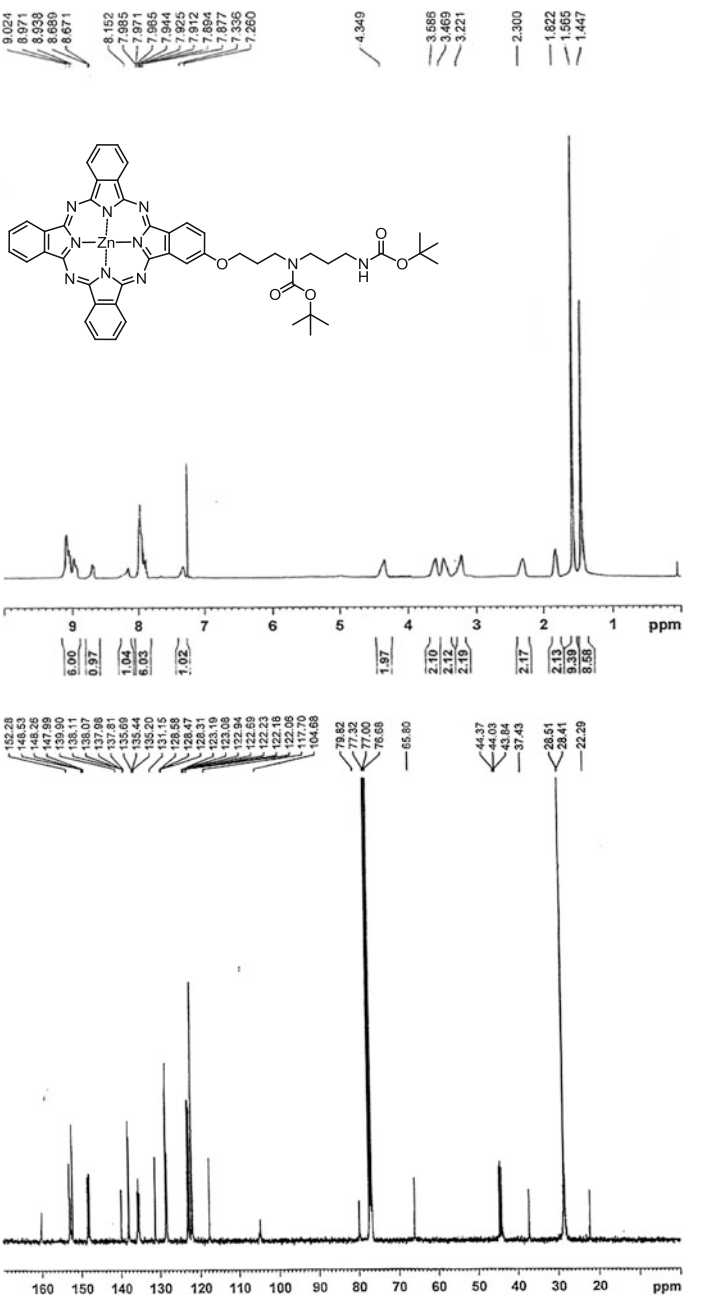

Appendix 15

^{1}H and $^{13}C\{^{1}H\}$ NMR spectra of compound **3.9d** in $CDCl_3$ with a trace amount of pyridine-d_5

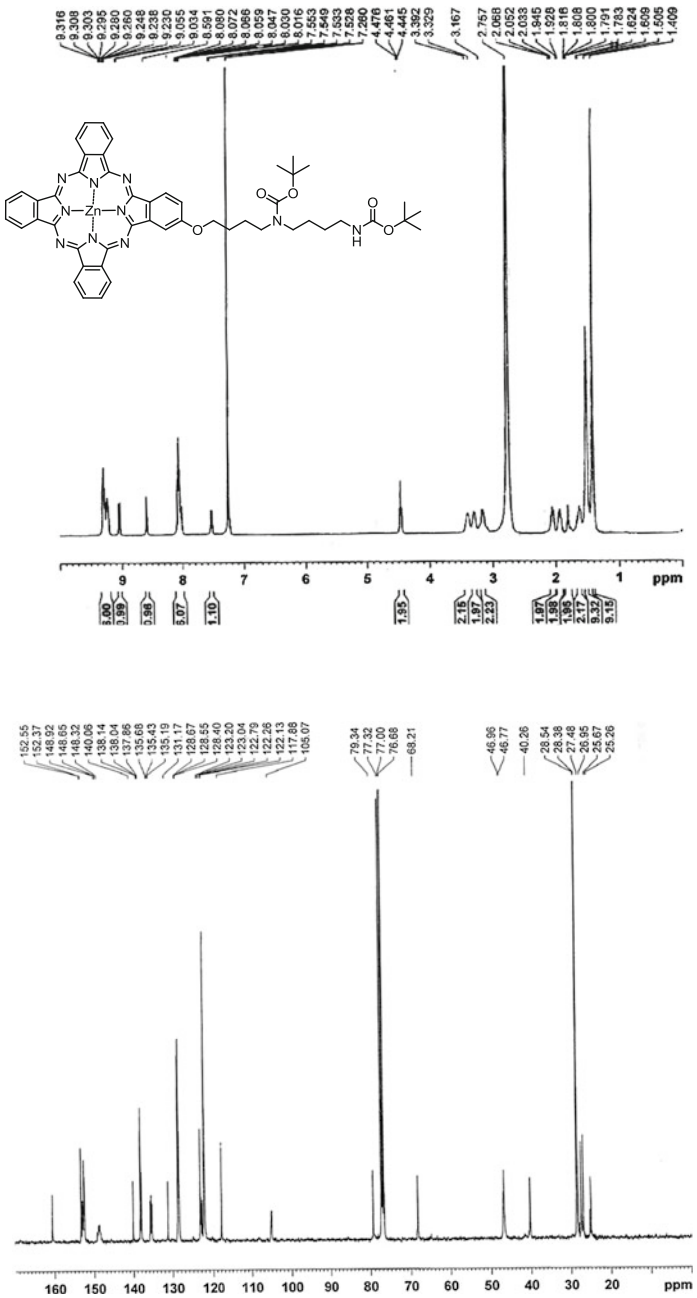

Appendix 16

^{1}H and $^{13}C\{^{1}H\}$ NMR spectra of compound **3.10a** in pyridine-d_5

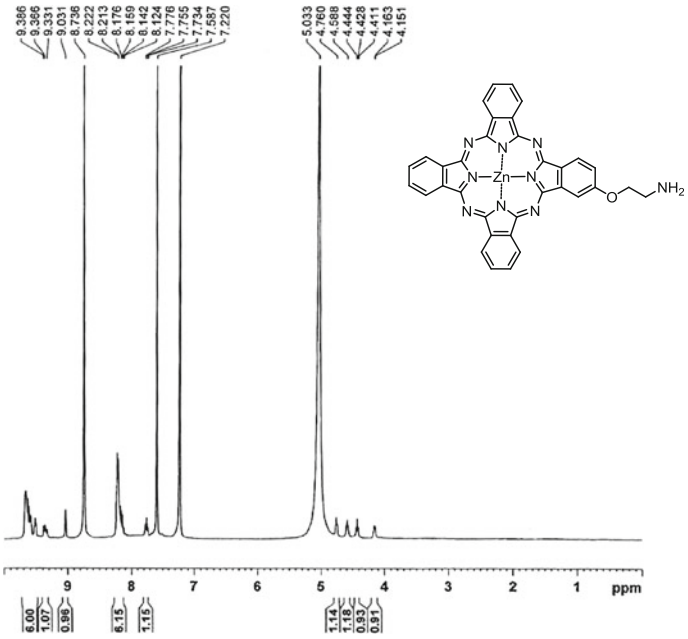

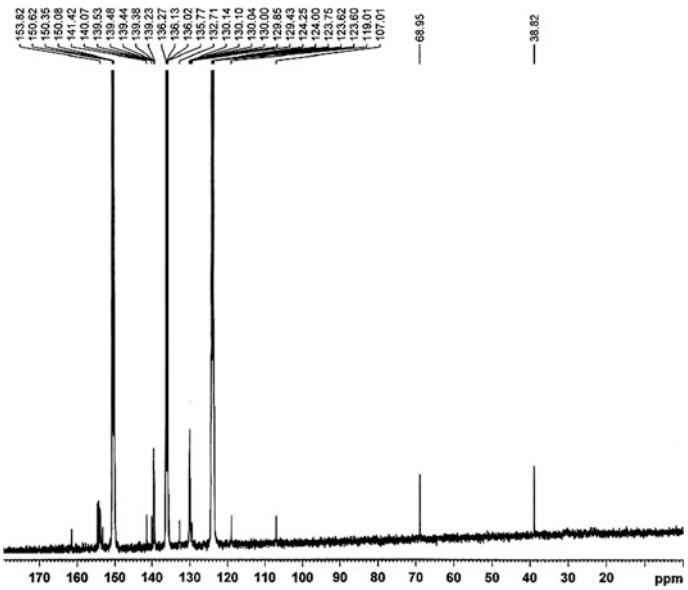

Appendix 17

^{1}H and $^{13}C\{^{1}H\}$ NMR spectra of compound **3.10b** in pyridine-d_5

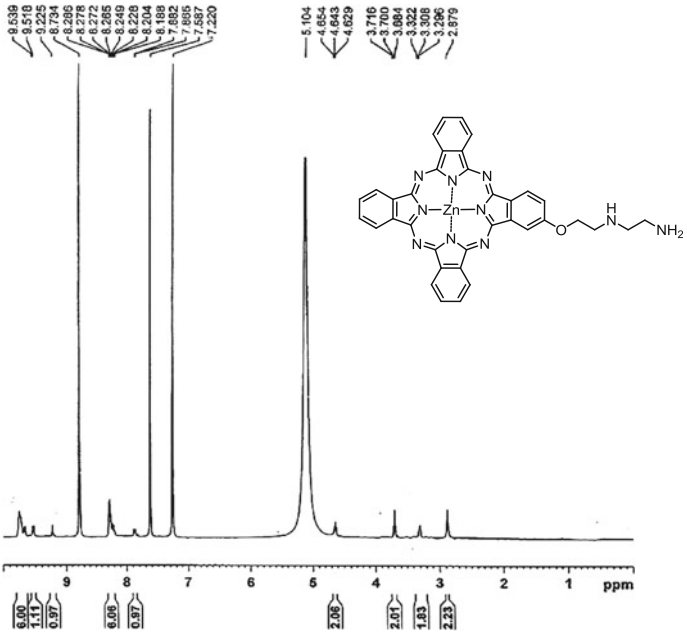

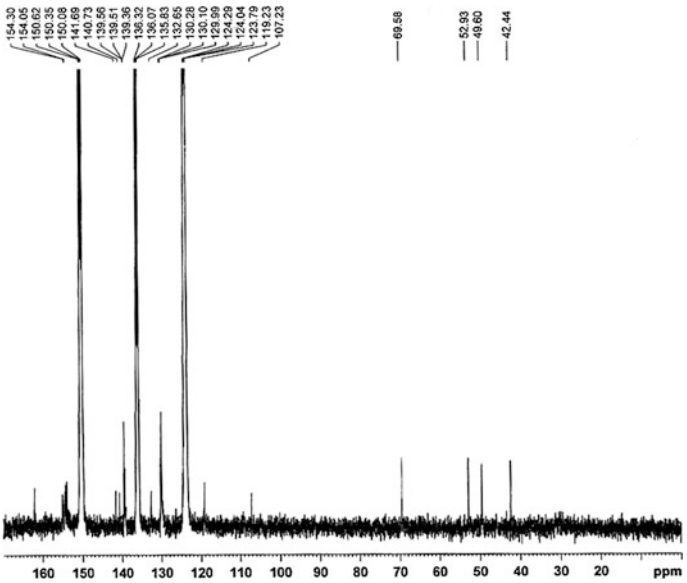

Appendix 18

^{1}H and $^{13}C\{^{1}H\}$ NMR spectra of compound **3.10c** in pyridine-d_5

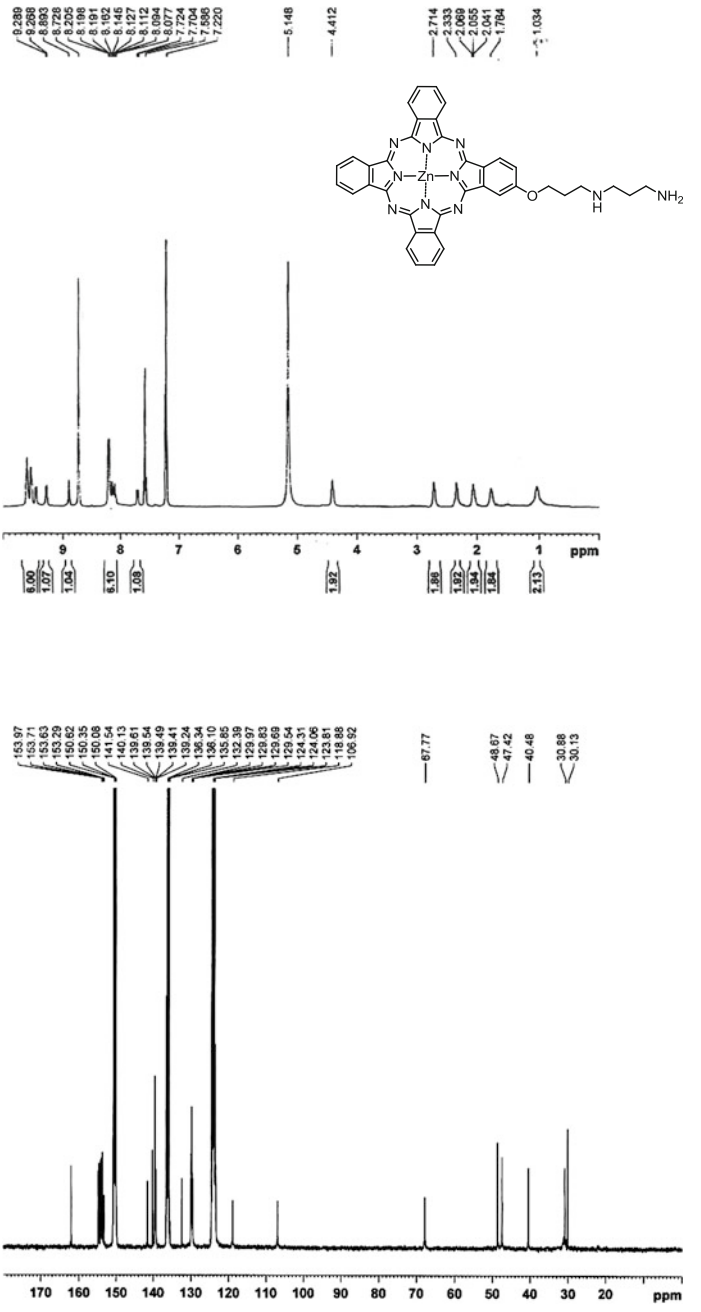

Appendix 19
^{1}H and $^{13}C\{^{1}H\}$ NMR spectra of compound **3.10d** in pyridine-d_5

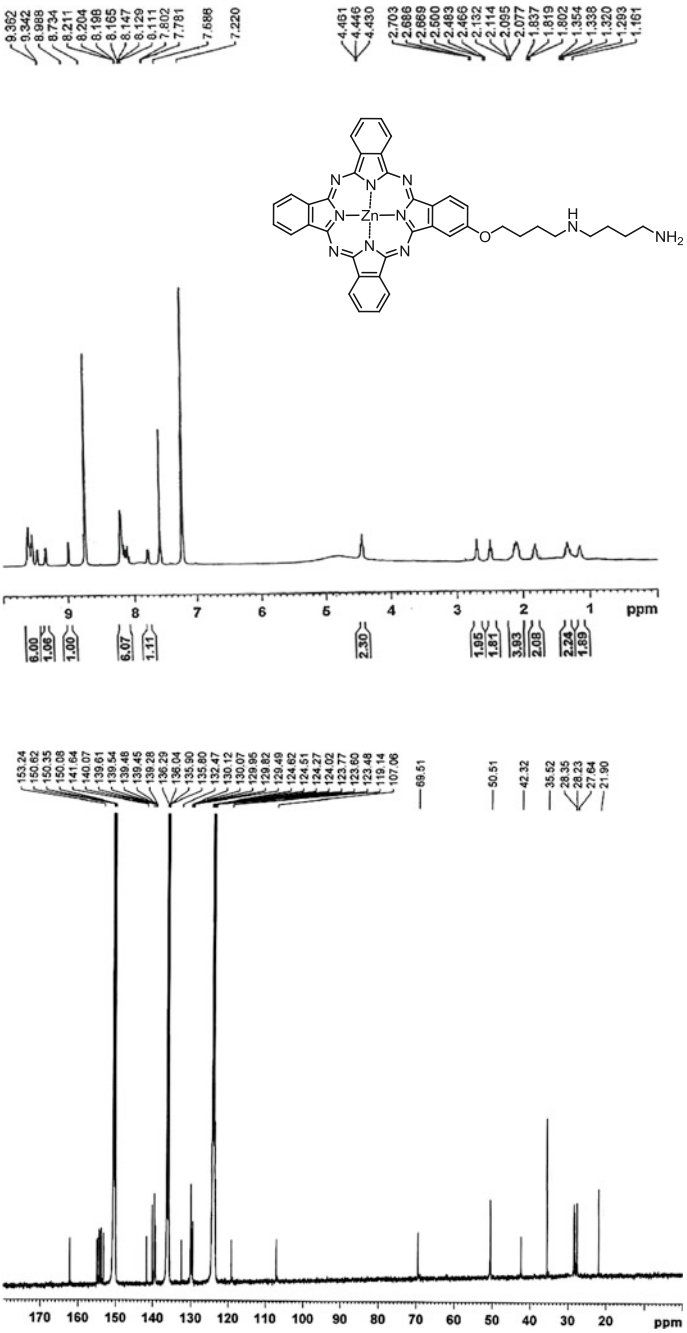

Appendix 20

^{1}H and $^{13}C\{^{1}H\}$ NMR spectra of compound **4.6** in $CDCl_3$

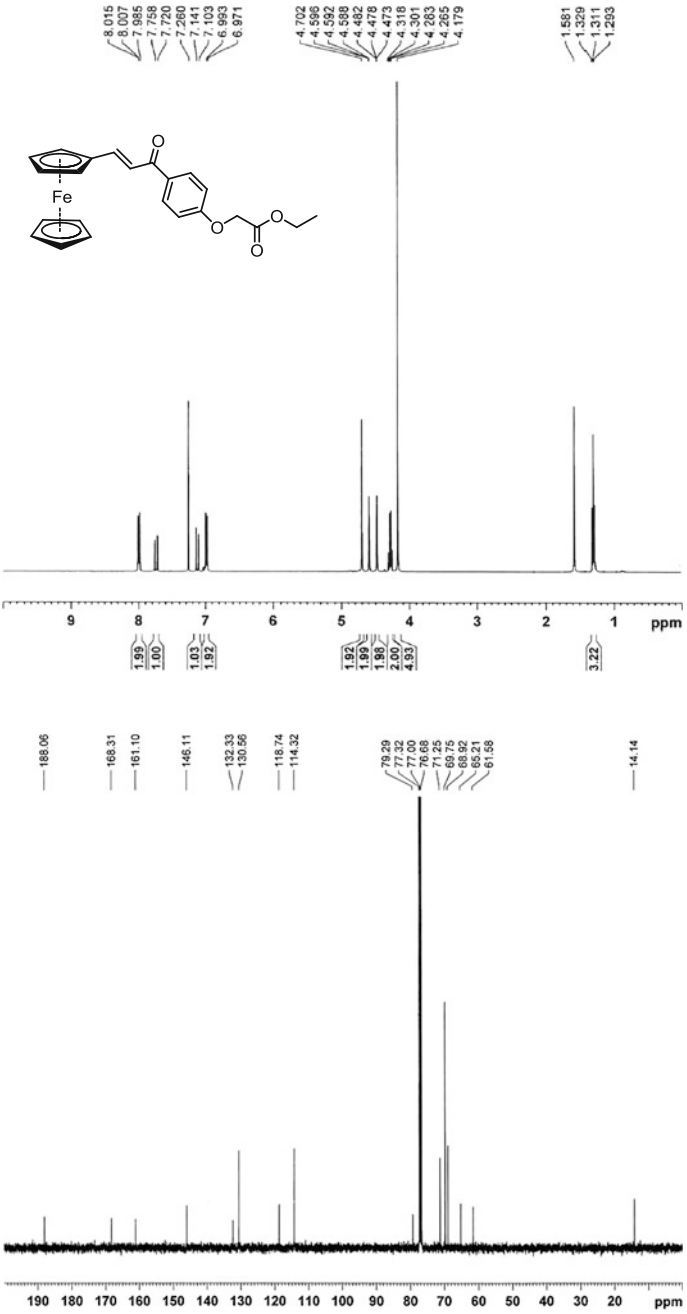

Appendix 21
^{1}H and $^{13}C\{^{1}H\}$ NMR spectra of compound **4.7** in acetone-d_6

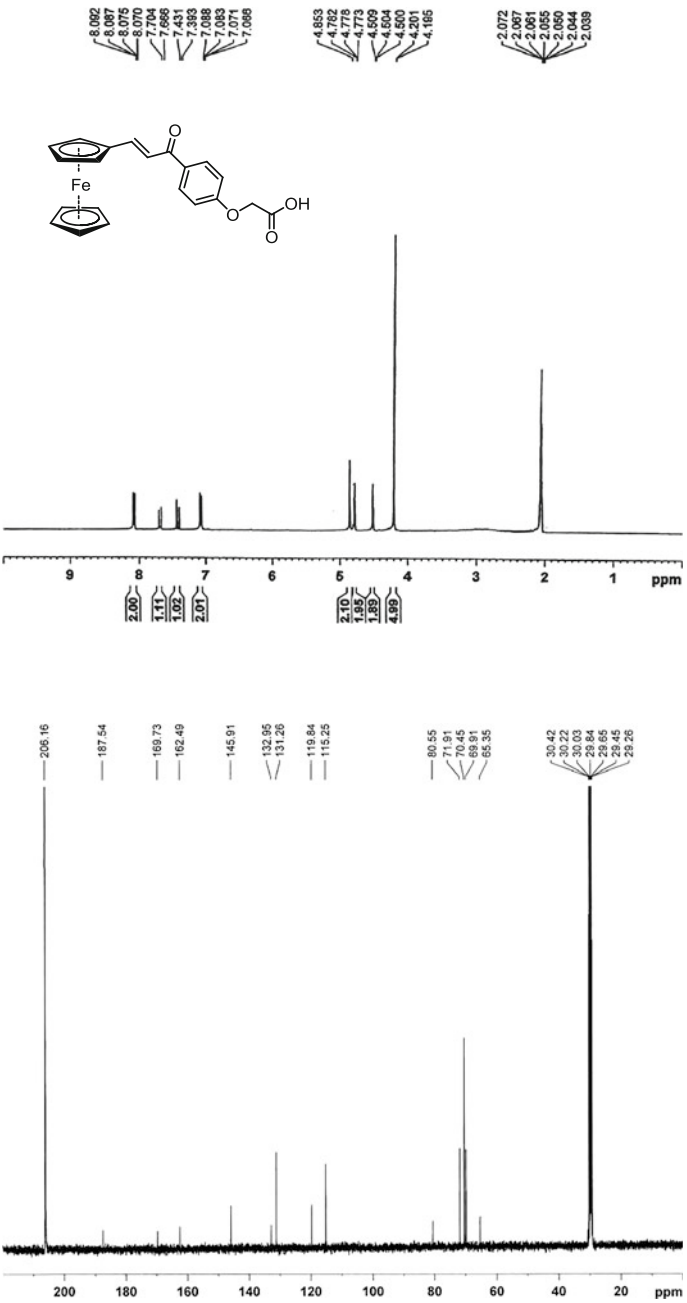

Appendix 22

^{1}H and $^{13}C\{^{1}H\}$ NMR spectra of compound **4.9a** in $CDCl_3$

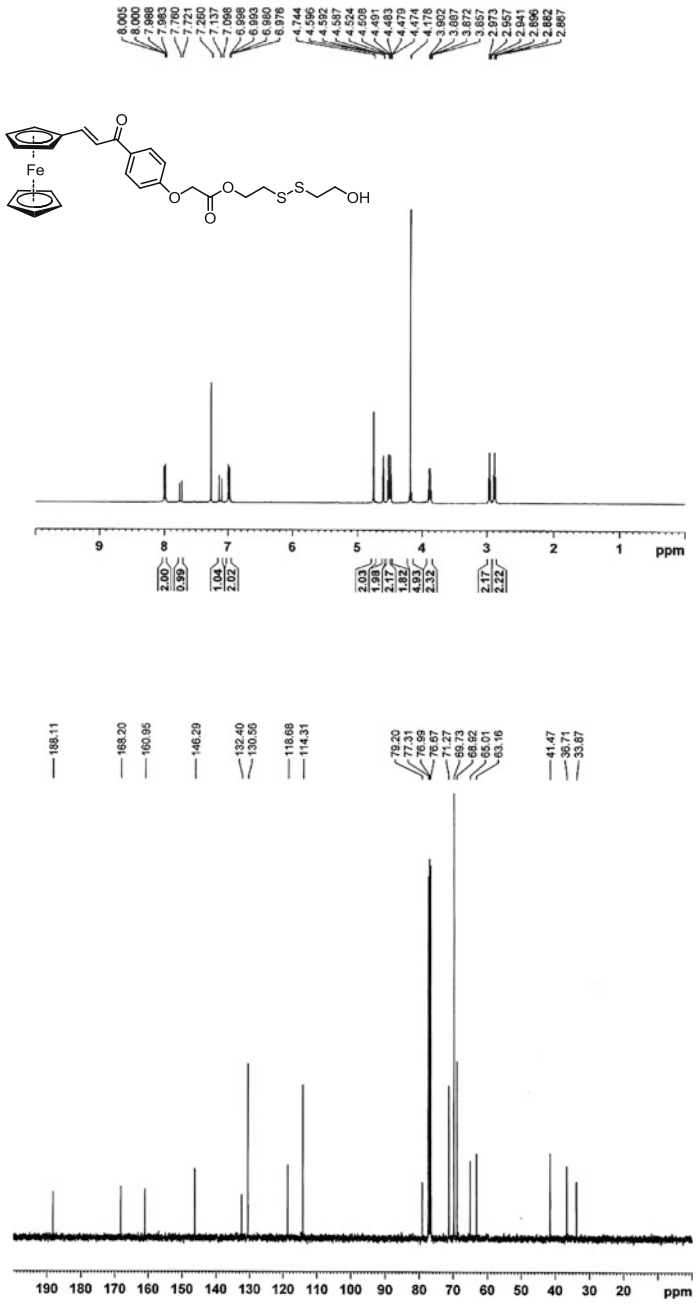

Appendix 23

^{1}H and $^{13}C\{^{1}H\}$ NMR spectra of compound **4.9b** in $CDCl_3$

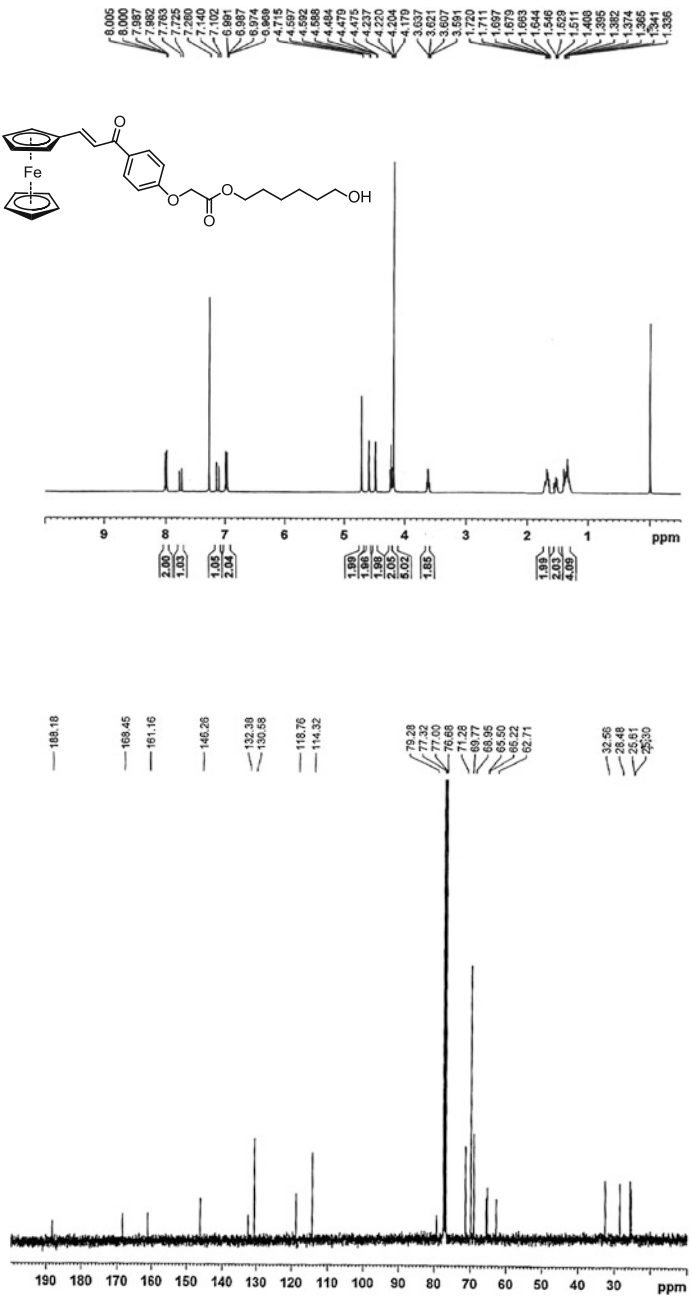

Appendix 24

^{1}H and $^{13}C\{^{1}H\}$ NMR spectra of compound **4.11a** in $CDCl_3$

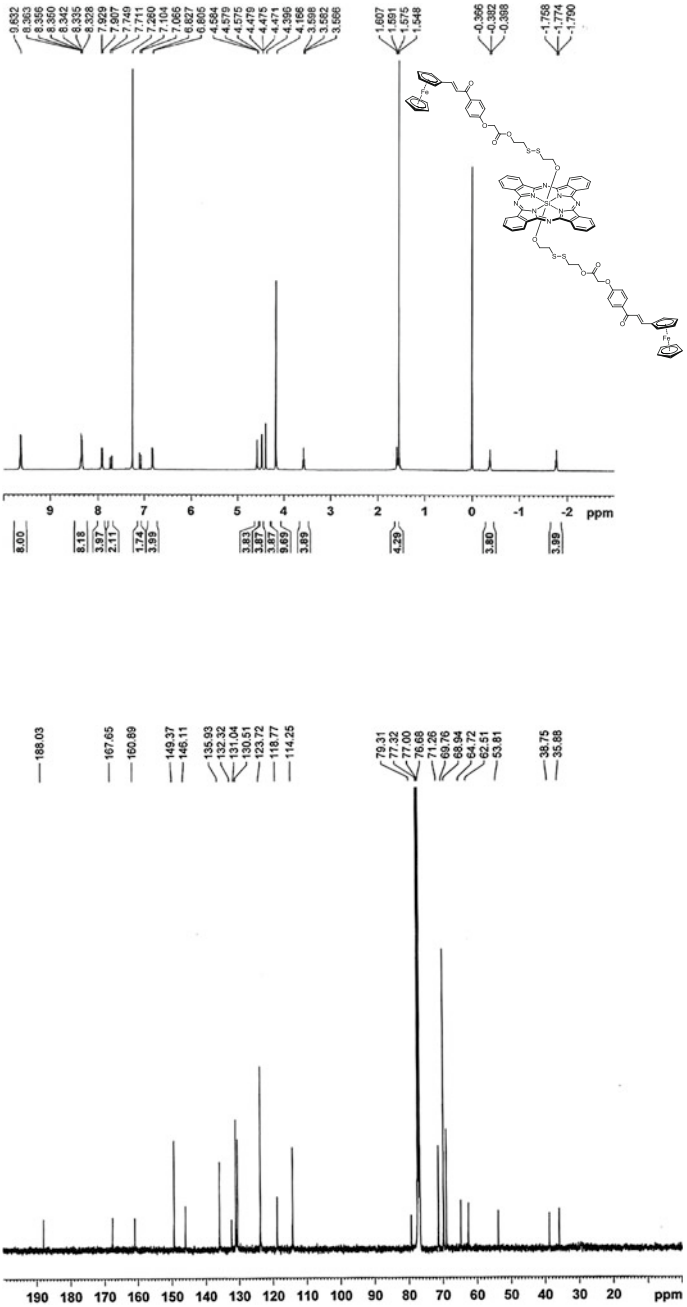

Appendix 25
^{1}H and $^{13}C\{^{1}H\}$ NMR spectra of compound **4.11b** in $CDCl_3$

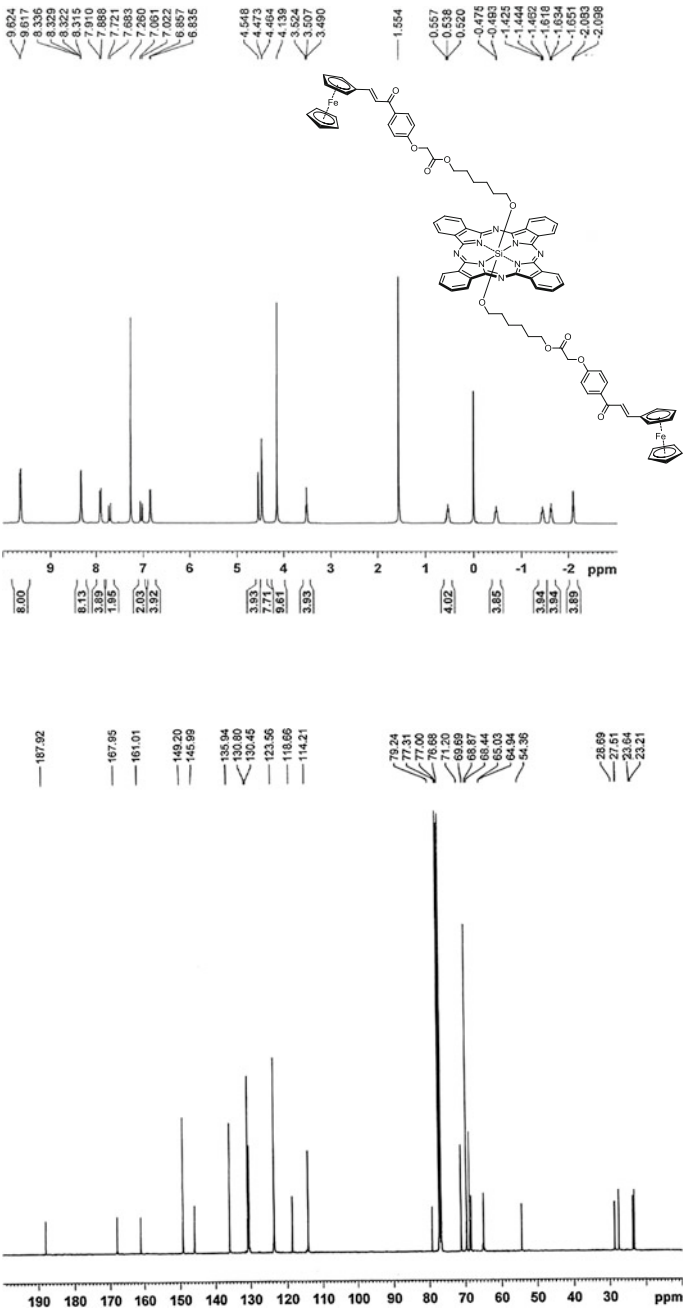

Appendix 26

^{1}H and $^{13}C\{^{1}H\}$ NMR spectra of compound **4.12** in $CDCl_3$ and DMSO-d_6, respectively.

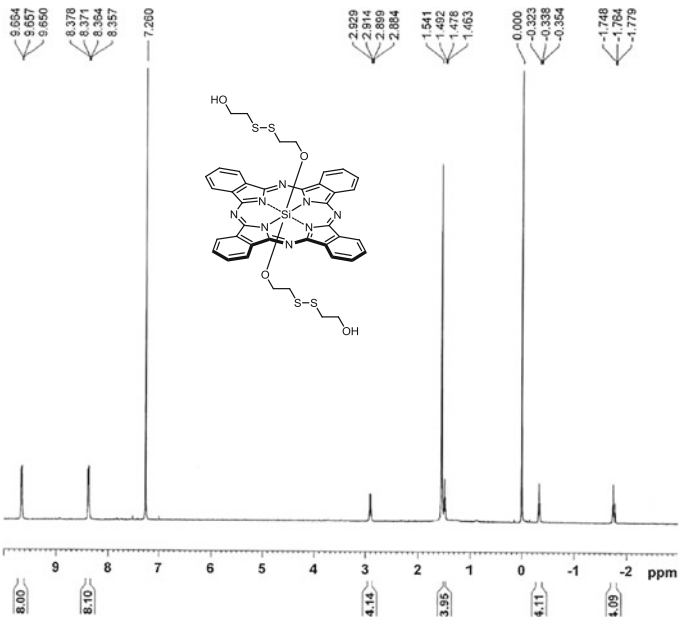

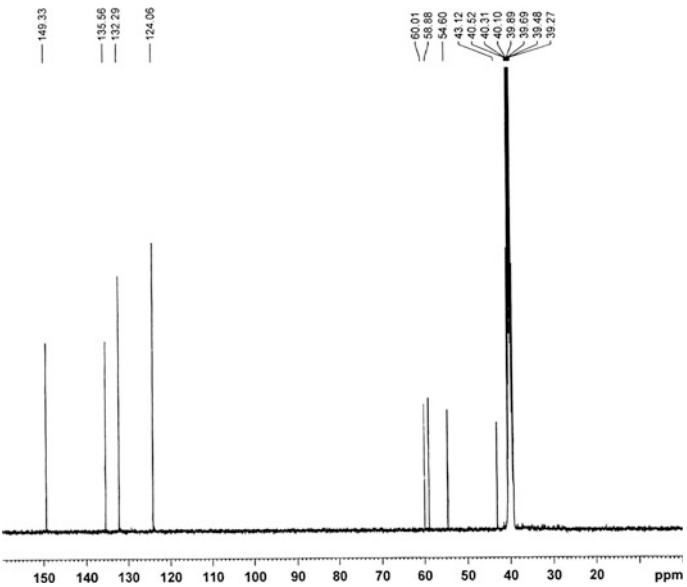

Appendix 27
^{1}H and $^{13}C\{^{1}H\}$ NMR spectra of compound **5.4** in $CDCl_3$

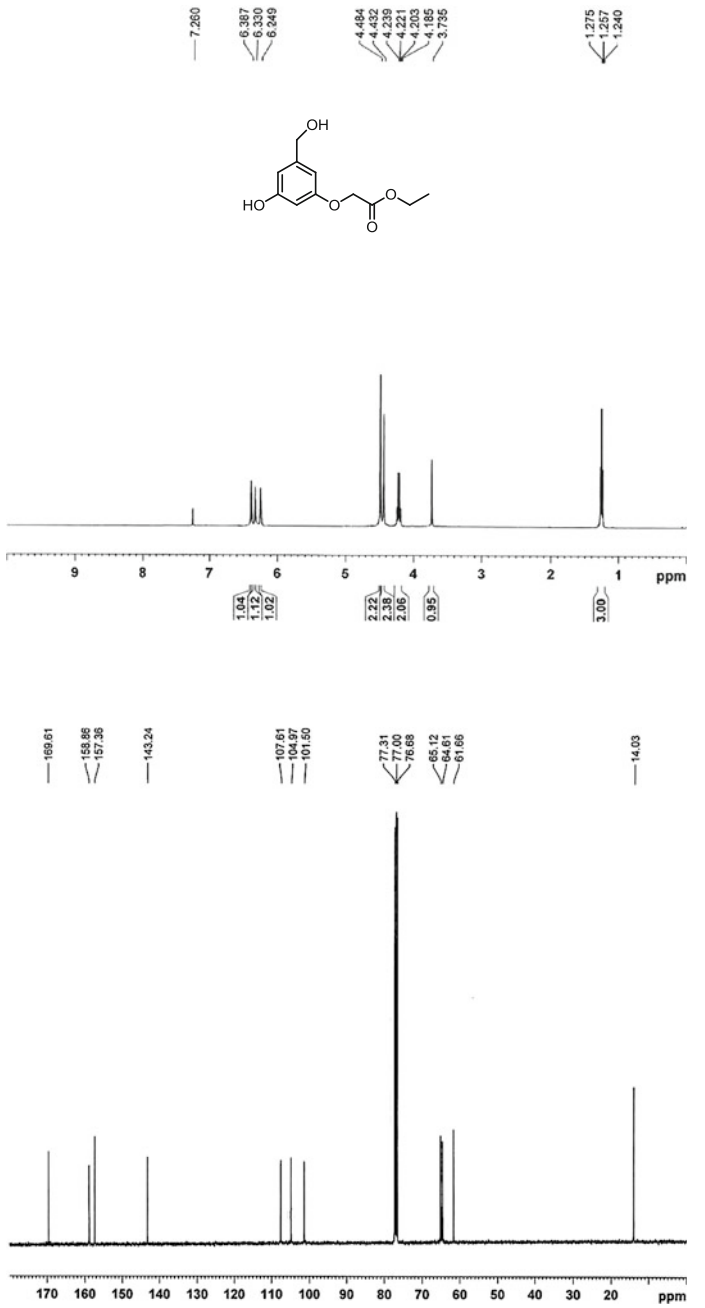

Appendix 28

^{1}H and $^{13}C\{^{1}H\}$ NMR spectra of compound **5.6** in $CDCl_3$

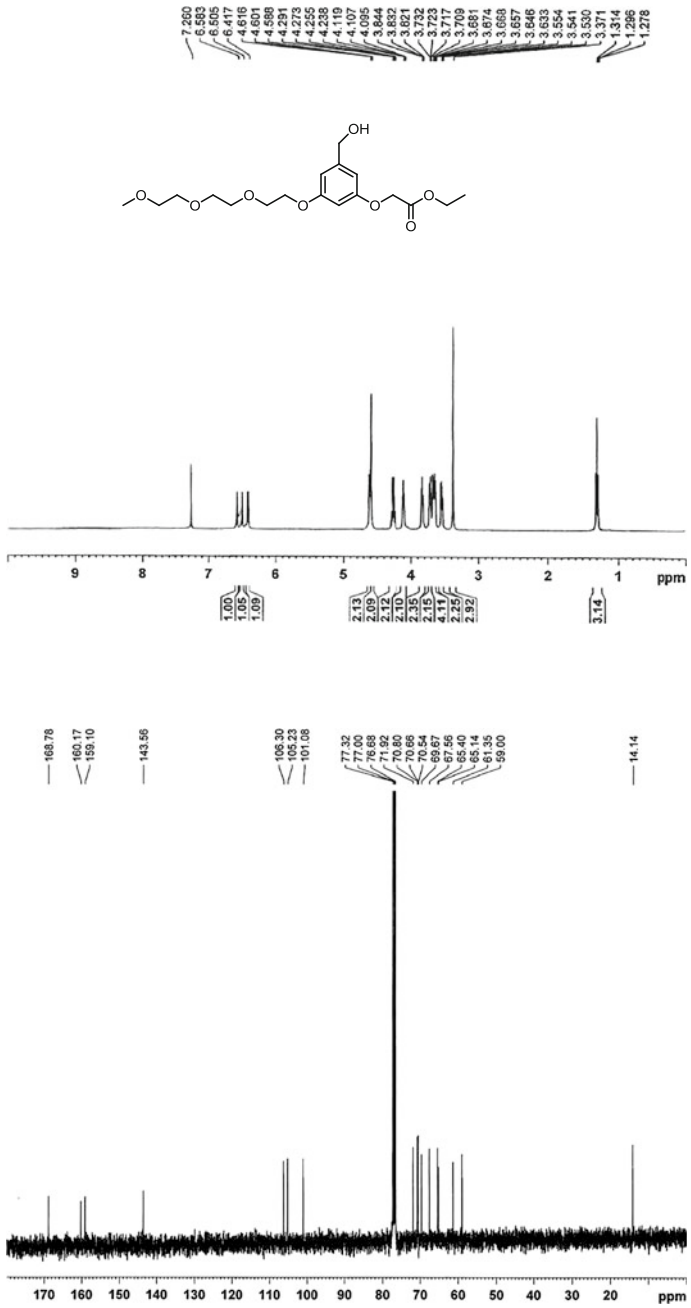

Appendix 29
^{1}H and $^{13}C\{^{1}H\}$ NMR spectra of compound **5.7** in $CDCl_3$

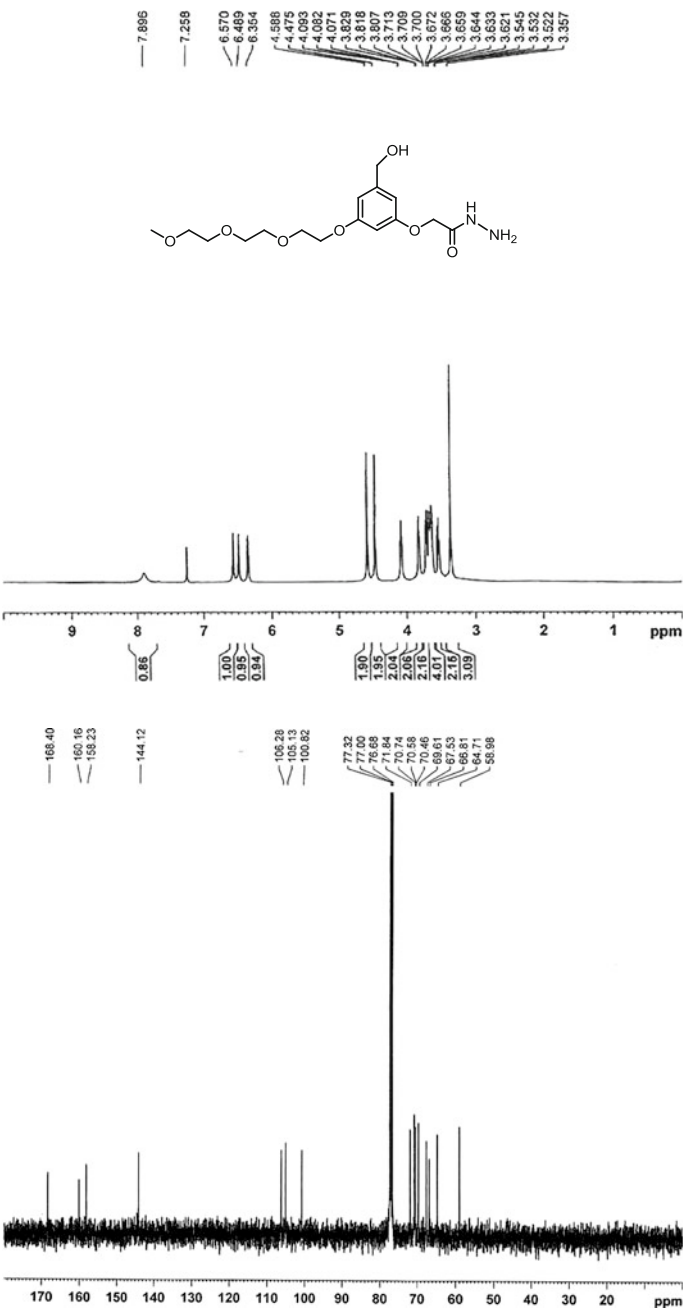

Appendix 30

^{1}H and $^{13}C\{^{1}H\}$ NMR spectra of compound **5.8** in $CDCl_3$

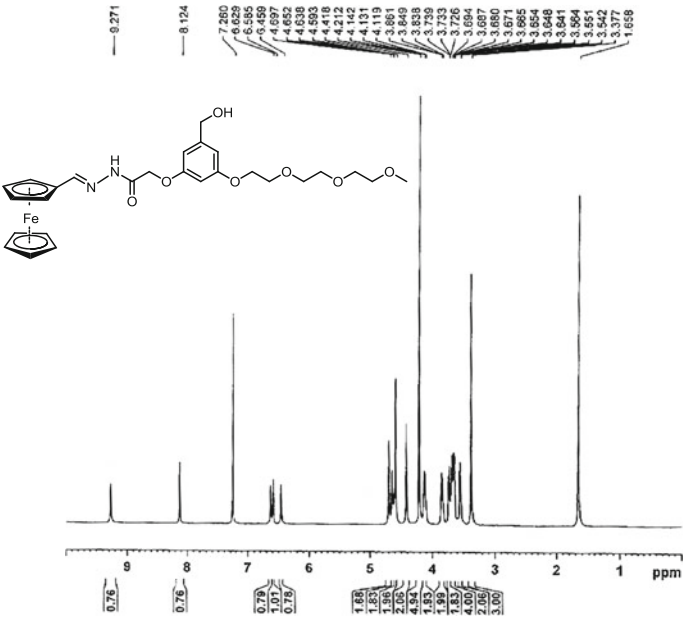

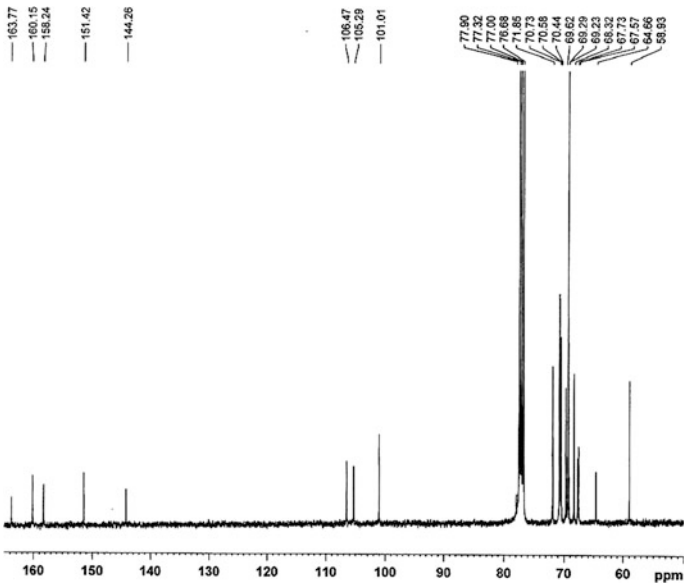

Appendix 31

^{1}H and $^{13}C\{^{1}H\}$ NMR spectra of compound **5.9** in $CDCl_3$

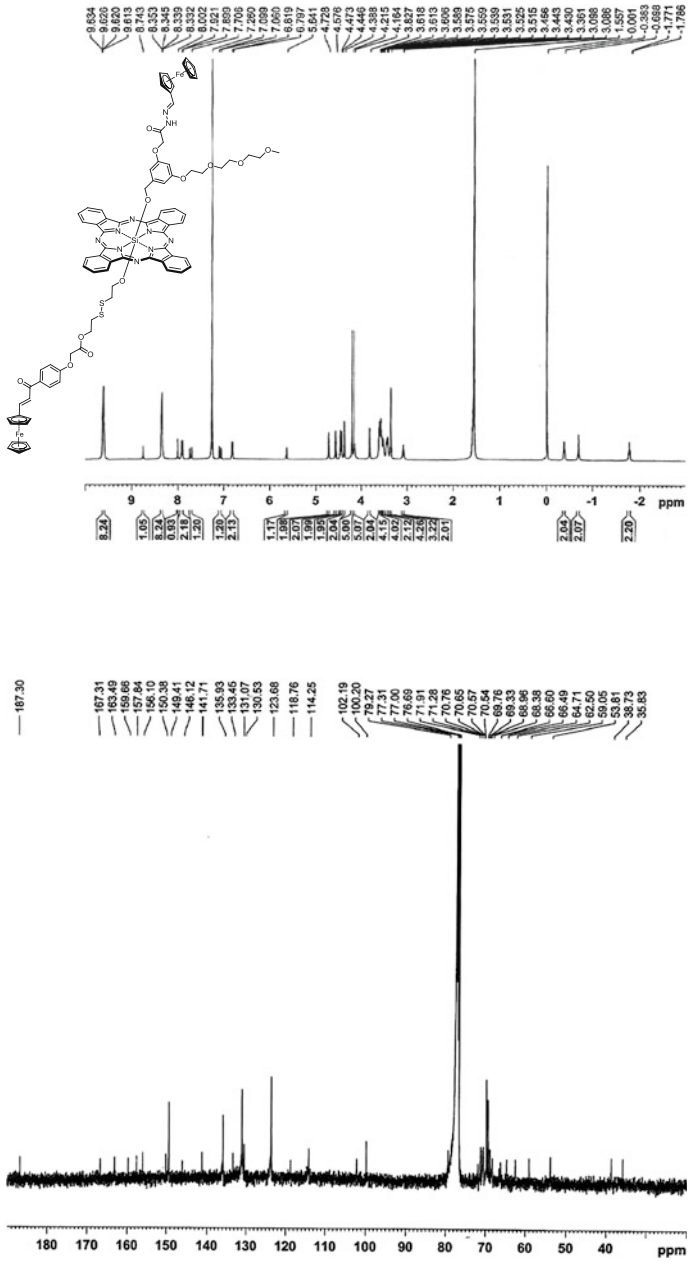

Appendix 32

^{1}H –^{1}H COSY spectrum of compound **5.9** in $CDCl_3$

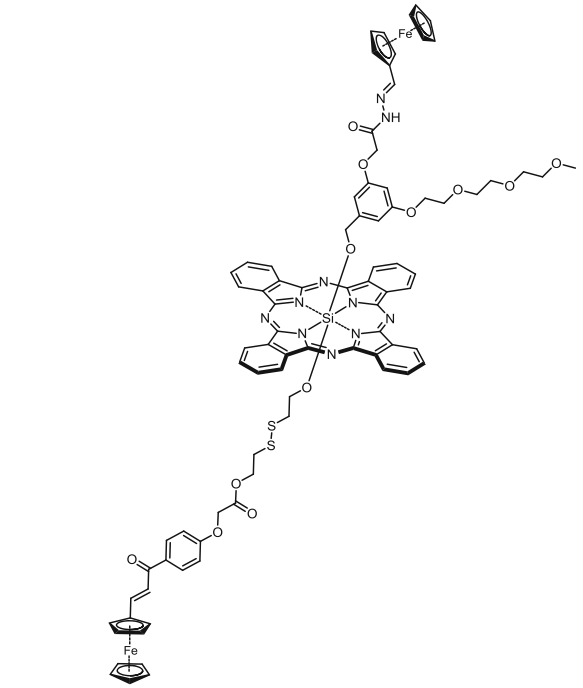

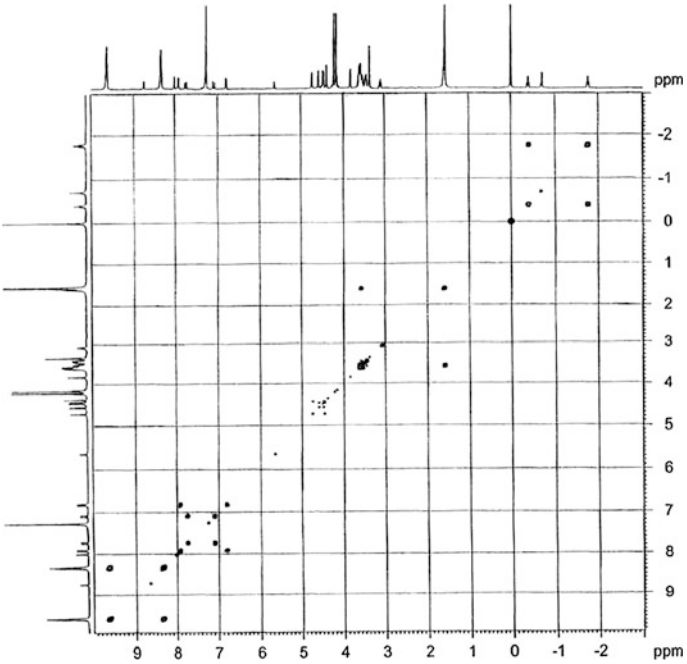

Appendix 33

^{1}H and $^{13}C\{^{1}H\}$ NMR spectra of compound **5.10** in $CDCl_3$